COMPUTATIONAL STUDY OF THE COMPLEXATION OF METAL ION PRECURSORS IN DENDRITIC POLYMERS

A Dissertation

by

FRANCISCO TARAZONA VASQUEZ

Submitted to the Office of Graduate Studies of
Texas A&M University
in partial fulfillment of the requirements for the degree of

DOCTOR OF PHILOSOPHY

December 2007

Major Subject: Chemical Engineering

COMPUTATIONAL STUDY OF THE COMPLEXATION OF METAL ION PRECURSORS IN DENDRITIC POLYMERS

A Dissertation

by

FRANCISCO TARAZONA VASQUEZ

Submitted to the Office of Graduate Studies of
Texas A&M University
in partial fulfillment of the requirements for the degree of

DOCTOR OF PHILOSOPHY

Approved by:

Chair of Committee,	Perla B. Balbuena
Committee Members,	Michael A. Bevan
	Hae-Kwon Jeong
	Marcetta Y. Darensbourg
Head of Department,	Michael Pishko

December 2007

Major Subject: Chemical Engineering

ABSTRACT

Computational Study of the Complexation of Metal Ion Precursors in Dendritic Polymers. (December 2007)

Francisco Tarazona Vasquez, B.S., Universidad Nacional de Ingeniería, Lima, Perú

Chair of Advisory Committee: Dr. Perla B. Balbuena

Metal ions are important for medical, environmental and catalytic applications. They are used as precursor molecules for the manufacture of metal nanocatalysts, which are promising materials for an array of biomedical, industrial, and technological applications.

Understanding the effect of the environment upon a metal ion-dendrimer system constitutes a step closer to the understanding of the liquid phase templated synthesis of metal nanoparticles. In this dissertation we have used computational techniques such as abinitio calculations and molecular dynamics (MD) simulations to investigate the complexation of Cu(II) and Pt(II) metal ions to a polyamidoamine (PAMAM) dendritic polymer from structural, thermodynamic, and kinetic viewpoints.

First, we analyze the local configuration of a low generation polyamidoamine dendrimer to understand the role of intramolecular interactions. Then, we examine the local configuration of dendrimer outer pockets in order to determine their capacity to encapsulate water within. Next, the complexation of Cu(II) with a small –OH terminated dendrimer in presence of solvent and counterions is investigated. This relatively simple system gives insight on how cationic species bind within a dendrimer.

The complexation of potassium tetrachloroplatinate, commonly used precursor salt in dendrimer templated synthesis of platinum and bimetallic platinum-containing nanoparticles, with PAMAM dendrimer has been the subject of several experimental reports. So we investigate the complexation of potassium tetrachloroplatinate within a dendrimer outer pocket in order to understand the effect of dendrimer branches, Pt(II) speciation, pH, solvent and counterions upon it. Our study shows that dendrimer

branches can improve the thermodynamics but can also preclude the kinetics by raising the energy barriers. Our study provides an explanation of why, where Pt(II) and how Pt(II) binds. We believe that these molecular level details, unaccessible to experimental techniques, can be a helpful contribution toward furthering our understanding of the complexation of Pt(II) and the starting point to study the next step of dendrimer templated synthesis, the reduction of Pt(II) into platinum nanoparticles inside pockets.

To two of my heroes: To my father Francisco, who exhorted me “the higher you rise, the humbler you ought to be” and to my mother Maxima, who with her tears and meekness has spoken more than any other person

ACKNOWLEDGEMENTS

I would like to express my sincere gratitude to Dr. Balbuena, my advisor, who had led me through these five years with professionalism. I am thankful for the opportunity she has given me to guest lecture in a few of her classes. I am grateful also for the opportunities she facilitated to promote interactions outside the lab. I can honestly say that Dr. Balbuena has been a positive and helpful influence in my professional and personal life; her patience and her passionate commitment to work are things I admire of her.

I would also like to thank the members of my dissertation committee, Dr. Michael Bevan, Dr. Hae-Kwon Jeong and Dr. Marcetta Darensbourg, for their willingness to serve on my committee and for their respect and kind attitude toward me.

Next, I would like to acknowledge the encouragement received from Dr. David Ford who believed that I could make a difference with this project. I am thankful also for the great insights obtained in my interactions with Dr. Richard Crooks, Dr. Bert Chandler and Dr. Keith J. Stevenson, among others, through my participation in the dendrimer minisimposiums held in San Antonio (2004), Austin (2005) and College Station (2006). These events have been an invaluable help in my research.

I am thankful for all the members of Dr. Balbuena's group. In particular, I want to thank Sergio for his friendship and gracious help in our discussions and interactions. Next, I would like to thank Dr. Alberto Martinez-Limia for our fruitful interactions and discussions while he was in Dr. Balbuena's group. I am also thankful to Diego Altomare and Dr. Eduardo Lamas for their help and support, especially in the first years of the PhD program. I am also thankful to Dr. Daniela Mainardi, Zhihui Gu, Zhao Jin, Dr. Yingchun Zhang, and Kevin Lamonte for the spirit of camaraderie present in the offices that we have shared together over the course of the last five years.

I would also like to thank the faculty and staff at the Artie McFerrin Department of Chemical Engineering. I want to thank especially Towanna Hubacek and Jeff Polasek for their enthusiastic service and support.

I would also like to thank Texas A&M University and the institutions that compose it. I am also grateful to the CTE and the Graduate Teaching Academy (GTA) for allowing me to explore teaching as a viable career. In particular I am indebted to Dr. Michael Stephenson for his willingness to become not only my mentor through the GTA mentorship program but for offering himself as a friend.

In the personal realm, I want to thank my family for their continual love and support. Thank you to Francisco and Maxima, my parents, for their example of hard work and commitment to a cause, and to Jenny and David, my siblings, for their encouragement.

Finally, I would also like to thank the institutions who have provided the monetary funds to make this project possible. This work has been supported by the National Science Foundation grant CTS-0103135 as well as by the Department of Energy grant DE-FG02-05ER15729. Supercomputer time granted by the National Energy Research Scientific Computing Center (NERSC), by the National Alliance for Supercomputing Applications, and by the DoD Major Shared Resource Centers (ARL MSRC and ASC MSRC) is gratefully acknowledged.

TABLE OF CONTENTS

CHAPTER Page

CHAPTER Page

CHAPTER Page

CHAPTER Page

LIST OF FIGURES

Page

Page

Page

Page

LIST OF TABLES

Page

Page

Page

Page

Page

Page

CHAPTER I
INTRODUCTION – METAL ION COMPLEXATION

1.1 Importance of metal ions in chemical processes

Life as we know it is not possible without the participation of metallic elements. In fact, at least seven metallic elements –iron, zinc, copper, manganese, magnesium, potassium and calcium- are considered essential for all known living organisms.[1] Even elements formerly thought of as poisons such as selenium and molybdenum -and possibly arsenic, nickel, silicon and vanadium- could also be included in the list of essential elements.[2]

Metal ions are essential for many brain functions. Although the molecular causes of neurodegenerative diseases remain unknown,[3] it has been suggested that mismanagement of metal ion homeostasis[4] coupled to protein misfolding[5] contribute significantly to their pathological progression. Therefore understanding the molecular details that underlie these phenomena and the factors that affect them (such as pH and metal complexation) holds potential to cure neurological diseases such as Alzheimer's or prion diseases.[5]

Metal ions have also found important applications as imaging agents provided that the proper chelating ligand (to ensure enough time to obtain a high-contrast image) and targeting ligand (a protein-binding moiety) to attach the metal ion to the right tissue be found. For instance, gadolinium as Gd(III)-BOPTA is used as a contrast agent for magnetic resonance imaging (MRI) whereas technetium is used as ^{99m}Tc-cardiolite (methoxy-isobutyl-isonitrile) for single-photon emission computed tomography (SPECT) of the heart.[2]

This dissertation follows the style of the *Journal of Physical Chemistry B.*

Metal ions can be complexed with multidentate ligands, immobilized in macroporous polymer and then used in metal ion mediated molecular recognition applications where the metal ion binds molecules reversibly. For that purpose, transition metal ion complexes with coordinatively unsaturated metal centers are chosen.[6,7] For instance it has been found that a macroporous polymer containing Cu(I),[6] a similar polymer containing a five-coordinate square-pyramidal Co(II) center[8,9] and a square-planar Co(II)-salen complex[10] are able to bind reversibly carbon monoxide, oxygen and nitrogen oxide respectively. Other molecular recognition applications include recognition of aminoacids, peptides, carbohydrates and small protein analogues.[11] Potential applications include chromatographic separation, chemosensors and biosensors and catalysis.[7,12]

Metal ions are also part of the structure of metalloproteins. These macromolecules constitute a third to a half of all known proteins[13] and play important roles in respiratory processes (e.g. hemoglobin and mioglobin), electron transport processes (e.g. citochromes and ferrodoxins), metal storage (e.g. ferritin),[1] nitrogen fixation (e.g. nitrogenase),[13] hydrolytic reactions and superoxide dismutation.[4]

Metalloenzymes are a subclass of metalloproteins[1] and are basically enzymes that contain active-site transition metal ions[4] that can exist in multiple oxidation states.[13] For instance it has been found that metal ions play important and multiple roles during the course of cleavage reactions in dinuclear[14] and trinuclear[15] zinc ion metalloenzymes.

The discovery of the functions of metal ions in metalloproteins opens the door to novel biomimetic and bioinspired synthesis of molecular architectures[4] and to potential nanomagnetic, conductivity or catalytic applications.[16] A few notable examples are the synthesis of mimics of superoxide dismutase and catalase to scavenge reactive oxygen species (ROS),[2] the synthesis of a tungstate layered double hydroxide (WO_4^{2-}LDH) that mimics a vanadium bromoperoxidase for highly selective electrophilic bromination[17] and the self-assembly of Cu(II) and Zn(II) inside artificial DNA duplexes with interesting metal sequence-dependent functions.[16]

1.2 Why understanding metal ion interactions with chelating ligands is important

Understanding interactions between metal ions and chelating ligands and their surrounding environment is important for environmental, medical, and catalytic applications.

For instance, understanding the interactions between thiodisuccinic acid and metal ions has enabled the development of a highly-selective chemical-modified electrode to detect electrochemically trace amounts of toxic heavy metal ions –such as Cd(II)- amidst competing ions.[18]

Selective complexation of metal ions with functionalized water-soluble metal-binding polymers in combination with ultrafiltration can be implemented for sequestration of metal species in water streams. Thus, it was found that thiourea functionalized polyethylenimine (PEI) had high affinity for toxic metal ions such as Hg, Pb, Cd and Cu.[19] On the other hand, amine terminated polyamidoamine (PAMAM) dendrimers have been found to have high affinity for Cu(II),[20-23] and Pb(II)[24] whereas benzoyl thiourea functionalized PAMAM dendrimers bound strongly Cu(II), Pb(II), Co(II), Ni(II), Zn(II) and Hg(II).[25] Potential applications for recovery of heavy metals from contaminated soils and industrial effluents are envisioned.

It was suggested that complexation of iron(II/III) ions with the uronic acids -or other residues- of the extracellular polymeric substances (EPS) of extremophilic bacteria -such as *Acidithiobacillus ferroxidans* and *Leptospirillum ferroxidans*- precede oxidative attack on sulfide ores. Therefore, understanding the structure and functions of the EPS in relation to iron(II/III) ions could lead to better control of biocorrosion of metals and bioleaching of metal sulfides containing precious metals, e.g. gold.[26]

Metal ion complex formation is central to the electrodeposition of composite materials by electrophoretic deposition (EPD) of organic polyelectrolytes and cathodic electrosynthesis of inorganic particles. For instance, PEI forms complexes with Zr salts,[27] Co(II),[28] Mn(II),[29] and Ni(II)[30] to yield PEI-metal oxide composites. And although high deposition rates, thicker films, enhanced cracking resistance and better adhesion of the coating on metal substrates have been observed, the simultaneous

occurrence of various reactions alongside the complex formation has hampered the understanding of the mechanism of deposition.

It has been acknowledged that studies on the structure and reactivity of metal complexes –such as the nature of the metal ion, its first and second coordination sphere[31]- will further understanding and aid in interpreting experiments performed with molecular imprinted transition metal ion catalysts.[12]

Similarly, further understanding of the structure and functions of metal ions in metalloproteins as well as the underlying mechanisms hold the potential for future applications for harnessing solar energy, synthesizing fertilizers and liquefying natural gas.[4]

In spite of important advances made in the field of medicinal bioinorganic chemistry, the synthesis of organ- and disease-specific molecules has not been achieved yet.[4] Thus, the theoretical understanding of metal-based therapeutic agents is needed in order to obtain specific guidelines to predict the effects of variation of the targeting ligand.[2]

Finally, complexation of metal ions with macromolecules is one of the most important methods available to produce metal nanoparticles.[32] Better understanding of the interactions between metal ions and polymer template will enable us to achieve control over the size of the nanoparticles.[33]

1.3 Relevance of molecular engineering in a nanotechnology age

Understanding and controlling the processes leading to nanomaterials (from which nanoparticles are a subset) is part of the vision of the National Nanotechnology Initiative (NNI) launched by the United States Government in 2001[34]:

> The vision of the National Nanotechnology Initiative (NNI) is a future in which the ability to understand and control matter on the nanoscale leads to a revolution in technology and industry.

As it can be inferred from this vision, the study of various molecular-level processes is necessary and will lead to a better understanding of these processes resulting in an array of products unthinkable in the past. Thus, a strong investment in molecular engineering is needed in order to bring into reality a technological nanorevolution.

Molecular engineering involves the design and manufacture of a new set of materials. Thus, a new interesting set of nanostructured materials can be obtained such as nanoparticles, nanotubes and nanocomposites to mention a few.

Nanoparticles range in size from approximately 1 nm to 100 nm. Harnessing their peculiar properties will result in promising applications such as data storage, medicinal imaging,[35] cancer therapeutics,[36] drug delivery systems,[37] orthopedic biomaterials,[38] in vitro diagnostics,[39] catalysis,[40,41] and electronics.[42]

Nanotubes are nanostructures that are rolled up in the form of small tubes. They look promising for applications such as storage of hydrogen for fuel-cell applications,[43] probes for scanning tunneling microscopy (STM),[44] molecular wires,[45] stronger light-weight materials,[46] electromechanical resonators,[47] and optical sensors.[48]

Nanocomposites are composites made out of two or more components where one of them is a nanomaterial in order to achieve superior properties to those of the individual components. Potential applications include carbon nanotube-elastomer nanocomposites as light-responsive actuators[49] and hydroxyapatite ceramic nanocomposites as strong bioactive load-bearing implants.[50,51]

Organic/inorganic polymer nanocomposites consist typically of an inorganic nanoparticle filler dispersed in an organic polymer matrix[52] and have found several applications that range from stiffer car bumpers to advanced optoelectronic devices.[53]

Dendrimer-encapsulated nanoparticles (DENs) are a particular type of polymer nanocomposite obtained by liquid-phase reduction of dendrimer-metal precursor ion complexes.[32] PAMAM dendrimer encapsulated nanoparticles[54] are currently studied for catalytic applications[55-58] because they in principle allow control of size, shape and composition of the nanocatalysts,[59] thus enabling an enhanced catalytic performance.[41,60]

Dendrimers are macromolecules composed of a core molecule, repetitive units (branches) stemming from a common point (branching point) in a dendrite-like manner and terminated with surface groups like $–NH_2$, -OH, etc. (See Figure 1.1)

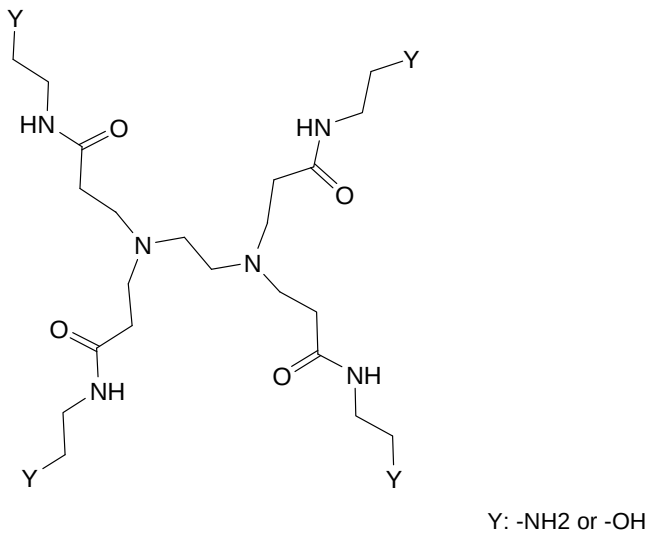

Figure 1.1 Polyamidoamine dendrimer of generation 0. Y: Surface group

1.4 Objectives of this project

As the formation of the metal-dendrimer ion complex is prior to its reduction into encapsulated nanoparticles, an understanding of the metal ion-dendrimer complexation stage is important. This has been furthered by experimental work. For instance, the binding of Cu(II) to dendrimer[20,21] and Pt(II) to dendrimer[55,61-63] have been investigated. However, a generalization across different metal ions has not been attempted and should be avoided because of the peculiarities of each dendrimer-metal ion system.

It should also be considered that some experimental techniques can not provide the information required for a particular system. The limitations of some techniques for a particular system may seem quite obvious. For instance, TEM and AFM techniques are designed to enable observation of metal clusters. However the limitations of other techniques may not be quite obvious. For instance, EXAFS has been used to discern

between binding to N and O atom sites even though the similarity between N and O scatterers has been recognized as a source of potential confusion.[55,64]

Thus, notwithstanding the valuable insights provided by experimental work, there is still a gap to cover, because all these experimental techniques can not look into the system at the atomic level. In this project we apply reliable computational techniques such as quantum mechanical (QM) and molecular dynamics (MD) calculations to conveniently and rationally thought models of metal-dendrimer ion complexes in order to obtain molecular-level detail of the metal-ion complexation of Cu(II) and particularly of Pt(II) in a dendritic polymer. Toward this goal, in this project we aim to investigate 1) guest-host interactions with the dendrimer as a host and water, counterions, metal complexes as guests 2) the effect of the pH on the structure of dendrimer as it relates to the complexation of metal ions 3) the effect of the host and the solvent on the complexation of metal ions.

As we acknowledge that our computational techniques can not substitute but complement the current experimental studies, another of our goals in this project is to explain the current experimental results. Therefore, we expect that the insights obtained in this project contribute not only to further our current understanding of the complexation of Cu(II) and particularly of Pt(II) in dendrimer templated synthesis of metal nanoparticles but also constitute an step forward toward the improvement of the dendrimer templated synthesis of metal nanoparticles.

Finally, our project aims also to inspire and promote the interaction between computational and experimental chemistry, as has been illustrated by previous studies.[65-69]

CHAPTER II
METHODOLOGY AND COMPUTATION/SIMULATION DETAILS

2.1 Overview

In the same way that physical processes and chemical reactions can be characterized by a set of experimental techniques, molecular modeling and subsequent characterization at the atomic level of processes and reactions can be done by several computational approaches depending on the properties one desires to calculate.

In this project, quantum-mechanical methods –particularly Density Functional Theory (DFT)- have been used mainly. Molecular Mechanics (MM) and Molecular Dynamics (MD) simulations have also been performed. In this section, these methods and the details of the simulation procedures are provided.

2.2 Quantum-mechanical simulations

Although recently developed force fields[70] are being used to study chemical reactions, –processes involving the breaking and formation of bonds- electronic structure methods such as ab-initio quantum-mechanical (QM) methods are generally the method of choice because of their parameter-free nature and their ability to better reproduce –in principle- ground state molecular properties. However QM calculations are limited to molecular systems with relatively small number of atoms because of their computational cost in terms of CPU time.[69]

QM calculations can be static or dynamic depending on whether sampling of the potential energy surface (PES) is done or not.[71] Static calculations are used to find stationary points (local minima and saddle-points) along the PES. On the other hand, dynamic QM calculations –or so-called ab-initio MD (AIMD) calculations such as Car Parrinello MD[72]- can in principle give information about dynamical features of chemical reactions. However their practical application is limited due to the small size (number of atoms) and time (normally in the order of tens of picoseconds) that can be handled.

Several types of QM static calculations can be performed. In this project we have used Gaussian 98[73] and Gaussian 03[74] to perform optimizations to stationary points (both to stable and saddle points) and calculations of the second derivative of the energy (frequency calculations) with respect to the nuclear positions.

Optimizations to a stable stationary point were done with the Berny algorithm[75] as implemented in Gaussian 98[73] and Gaussian 03;[74] optimizations to a saddle point were done with the Berny algorithm[75] as implemented in Gaussian 03.[74] Synchronous Transit-Guide Quasi-Newton (STQN)[76] was also used to find transition states. In the latter method a guess for the transition state is not required but only optimized structures for reactant and product.

Frequency calculations on the optimized structures were done in order to characterize the stationary points. Because the roots of the eigenvalues of the diagonalized Hessian matrix (second derivative of the energy) are the fundamental frequencies of the molecular system, the absence of imaginary frequencies reflect no negative eigenvalues and therefore the stationary point is a local minimum whereas the presence of n imaginary frequencies reveals n negative eigenvalues that correspond to an nth-order saddle point. Transition state structures correspond with first-order saddle points. It should be noticed also that frequency calculations make use of the harmonic approximation, namely that nuclear displacement in each one of the normal modes of the molecule resembles that of a simple harmonic oscillator.[77]

The electronic energies resulting from the optimization runs need to include a zero-point energy (ZPE) correction (because molecular vibration persists even at 0K, following the Heisenberg's principle) and thermal corrections to the enthalpy (including the effects of molecular translation, rotation and vibration) at 298.15 K and 1 atm of pressure.[77]

Before optimizations and frequency calculations can be done, a method and a basis set as well as proper convergence criteria need to be specified.

2.2.1 DFT calculations

The time-dependent Schrodinger equation (eqn 2.1) reduces to the time-independent Schrodinger equation by assuming the potential energy to be independent of time.

$$\left(-\frac{\hbar^2}{2m}\nabla^2 + V(\bar{r},t)\right)\psi(\bar{r},t) = i\hbar\frac{\partial\psi(\bar{r},t)}{\partial t} \qquad (2.1)$$

An exact solution to the time-dependent Schrodinger equation (TDSE) for molecular systems such as the ones studied in this project is not possible. One notable approximation to the TDSE is the Born-Oppenheimer approximation that by assuming that the electrons move in a field of fixed nuclei enables the independent solution of the electronic wavefunction.

Solutions for the electronic wavefunction can be obtained by a number of methods. One of the most popular methods is Hartree-Fock –also called Self-Consistent Field (SCF)- where the energy of the wavefunction is minimized in accordance to the variational principle. In this method, the Hartree-Fock orbitals are expressed as linear combination of basis functions. These basis functions are chosen to be a linear combination of Gaussian Type Orbitals (GTO) because their integration has lower computational cost that using Slater Type Orbitals (STO).

As it has been noticed,[77] the Hartree-Fock method does not take in account the instantaneous electron-electron interactions (i.e. electron correlation). The methods proposed in order to improve it are known as post-SCF methods, such as Configuration Interaction (CI), Moller-Plesset (MPx, x = 2-4) and Coupled Cluster (CC). These methods are restricted to small molecules because of their high demand of computer time and therefore were not used in this project.

Density Functional Theory (DFT) methods take in account electron correlation via general functionals (functions of a function) of the electron density.[77] DFT methods are based on the Hohenberg-Kohn theorem and do not attempt to solve the Schrodinger Equation for the molecular electronic wavefunction but rather solve for the electronic energy. However the relationship between electron density and electronic energy is not known and here is where a variety of DFT methods come into play.[78]

Current DFT methods partition the electronic energy into several terms:

$$E = E^T + E^V + E^J + E^{XC} \quad (2.2)$$

E^T is the kinetic energy term, E^V is the potential energy of nuclear-electron attraction and repulsion between pairs of nuclei, E^J is the electron-electron repulsion term, and E^{XC} is the exchange correlation term to account for the energy due to both antisymmetry of the wavefunction and dynamic correlation in the motions of individual electrons.[77]

A major problem in DFT is finding suitable functionals for the E^{XC} term. This term is usually partitioned into separate parts: the correlation functional and the exchange functional. Two common approximations to derive these two functionals are given by the Local Density Approximation (LDA) and the Generalized Gradient Approximation (GGA).

DFT provides a balance between accuracy and computational demand for the optimization of molecular systems. Its accuracy is superior to SCF methods and it is comparable with that of MP2 methods with a computational demand comparable to SCF methods.

Hybrid methods include exact exchange as part of their formulation. The exchange term of the hybrid functional is made of a mixture of exact exchange (e.g. Hartree-Fock) with DFT exchange and DFT correlation.[77] For instance, the exchange-correlation part of the B3LYP hybrid functional is given by the following equation:

$$E^{XC}_{B3LYP} = (1-a_0)E^X_{Slater} + a_0E^X_{HF} + a_x\Delta E^X_{Becke} + (1-a_c)E^C_{VWN3} + a_c(E^C_{LYP}) \quad (2.3)$$

where the first term is given by the X_α method proposed by Slater[79], the second term is given by Hartree-Fock exchange, the third term is given by Becke exchange,[80] the fourth term by Vosko, Wilk and Nusair (VWN)[81] correlation and the fifth term (LYP correlation) is given by Lee, Yang and Parr (LYP)[82] along with the parameters a_0, a_x and a_c that best reproduced a set of experimental atomic properties.[83]

As it has been mentioned before, a QM method requires orbitals in order to find the electronic wavefunction. It should be immediately clear that a full treatment of valence and core electrons as accomplished with the use of GTO for light atoms would not work

and be prohibitive for the handling of heavy atoms. Therefore, a different treatment of the valence electrons and the core electrons should be apparent. This is what Effective Core Potentials (ECP) do by describing the core electrons with an energy potential called pseudopotential. ECPs can also be designed to account for relativistic effects and thus can not only help to overcome computational limitations posed by a full-electron treatment of heavy atoms but actually give accurate results when modeling molecular systems involving transition metal atoms as done in this project.

Hartree-Fock and B3LYP were the methods of choice in this project along with Pople basis sets for light atoms and LANL2 basis set[84] in combination with its associated relativistic ECP for heavy atoms. Thus, the small Pople basis set 3-21G was used to optimize configurations for low generation PAMAM dendrimers (Chapter III) while the basis set 6-31g(d) was used for light atoms in Cu(II)-dendrimer system (Chapter IV). However, the presence of Cl^- called for the use of the basis set 6-31+g(d) in the Pt(II)-dendrimer systems (Chapters V-IX) because diffuse functions are required for the proper description of anionic systems.[77]

2.3 Classical molecular simulations

Unlike quantum mechanical calculations that have been used consistently in this project, classical molecular simulations were used only in Chapter IV. What follows is a brief account of the two methods that were used there.

2.3.1 Molecular Mechanics (MM)

Quantum mechanical effects are not considered in molecular mechanics (MM) methods. So, in principle larger molecular systems can be handled by resorting to this strategy. MM methods make use of simple mathematical functions called force fields that are designed to describe the potential energy of the molecular system which includes both non-bonded and bonded atomic interactions.[67]

Non-bonded interactions are those between atoms not linked by covalent bonds and include electrostatic interactions and van der Waals interactions. In order to model

electrostatic interactions with a Coulomb potential energy function, charges for the different molecules that compose the system are needed. For anions and cations, these charges are modeled as point charges, for water these charges are included in the explicit water model, and for the dendrimer, these charges are modeled with a charge distribution calculated by either charge scheme procedures[85] or as a result of quantum mechanical calculations. On the other hand, van dar Waals interactions are modeled with the Lennard-Jones potential with energy and length parameters determined for the force field being used.

Bonded interactions are those between atoms linked by covalent bonds. It should be clear that the modeling of these interactions presuppose an a priori knowledge of the existence of these bonds while assuming that they will not break during the course of the chemical reactions they may be involved in. Thus, the force fields are limited only to molecules for which a molecular structure is known. Simple force fields include at least three types of bonded interactions: harmonic bond stretching, harmonic bond angle bending and dihedral angle twisting. Additional complexity can be added, but it should be kept in mind that the more complex the force field, the more computationally demanding the simulation will be.

In this project, the atomic interactions were modeled with the universal force field (UFF)[86] –as implemented in Gaussian 03[74]- and the DREIDING force field[87] in the MM optimization and MD simulations respectively.

2.3.2 Molecular Dynamics (MD) simulations

Although in general MD simulations are not used to describe chemical reactions where breaking and formation of bonds occur, MD simulations are useful in the study of conformational dynamics, ion mobility and diffusion among other properties.[67]

Conventional molecular dynamic (MD) simulations require force fields to solve Newton's equations of motion[67] The Newtonian equation of motion for atom i is:

$$F_i = \frac{dp_i}{dt} \qquad (2.4)$$

Equation 2.4 shows that at a given time t, force F_i is being exerted over atom i and that p_i is its momentum. It is also known that the force F_i is a function of the gradient of potential energy –modeled with a force field- which in its turn depends on the position of atom i. On the other hand, the momentum is a function of the velocity of atom i which in its turn depends on the position of atom i with respect to its initial position. Therefore, it is apparent the connection between force fields and initial configuration. Thus, by solving Newton's equations of motion in an iterative fashion, new positions for atom i can be determined and the dynamic behavior of the system –structural fluctuations- observed over time and properties derived with statistical mechanics methods.

In order to obtain meaningful results, the molecular system is to be set up as closely as possible to the experimental conditions. In this project, for instance, periodic boundary conditions (PBC) were used to ensure that all simulated atoms were surrounded by neighboring atoms whether those neighbors are their images or not.[67] The turning on of PBC require the use of the Ewald summation method[88] to properly treat the long range electrostatics.

Solvent effect was addressed explicitly rather than implicitly. Thus, the SPC/E,[89] a rigid explicit water model was selected not only because of its ability to describe properly the liquid state, the coexistence curve, and critical properties of water but because rigid models are less costly in terms of CPU time than non-rigid models. The use of SPC/E requires the use of a special program called SHAKE[90,91] that controls the water bond lengths and the angle.

Finally, additional experimental conditions such as constant temperature and volume were addressed by using the NVT ensemble. The target temperature for the system was fixed to 300 K and the Nose-Hoover[92] thermostat was used. The DL_POLY_2[93] program was used to perform MD simulations.

CHAPTER III
PAMAM DENDRIMERS: LOW GENERATION DENDRIMERS AND DENDRIMER OUTER POCKETS*

3.1 Introduction

Dendrimers are macromolecules with a tree-like, highly-branched structure.[94,95] Dendrimers consist of a core molecule, repetitive units (branches) stemming from a common point (branching point) in a dendrite-like manner and terminated with surface groups like –NH2, -OH, etc. Dendrimers tend to adopt a spherical structure as the molecular weight increases.[96]

The following nomenclature is generally used to name a dendrimer: Gx-S, where G stands for 'generation', term closely related to x the number of 'layers' of branches (minus one) grown from the core molecule; and S that stands for the surface group. Thus, a G0-S dendrimer is the simplest and smallest dendrimer because it has a number of branches equal to the number of branching points which are four –because in this project the core molecule is ethylenediamine (EDA). Out of these branching points, a 'layer' of branches (eight branches) is grown resulting in G1-S. If another layer of branches is grown upon G1-S, then the resulting dendrimer will be G2-S whereas larger dendrimers can be obtained by repeating this procedure (See Figure 3.1).

Because of their peculiar chemical and geometrical structure that originate their dendritic encapsulation properties, dendrimers have recently generated a great deal of attention, for applications ranging from controlled fabrication of nanocatalysts to electronic devices with specific functions that take advantage of their energy-harvesting, and light emitting properties.[61,94-105] PAMAM dendrimers in particular have been used as

---

* Parts of sections 3.1, 3.2, 3.3.1 and 3.3.2 are reproduced in part with permission from Tarazona-Vasquez and Balbuena, *J. Phys. Chem. B* **2004**, *108*, 15982. Copyright 2004 American Chemical Society, and parts of sections 3.1., 3.2 and 3.3.3 are reproduced in part with permission from Tarazona-Vasquez and Balbuena, *J. Phys. Chem. A* **2007**, *111*, 932. Copyright 2007 American Chemical Society

template agents for several ions, metal atoms, and clusters, including Pt, Pd, Au, Ag, Cu.[61,98,103,104,106,107]

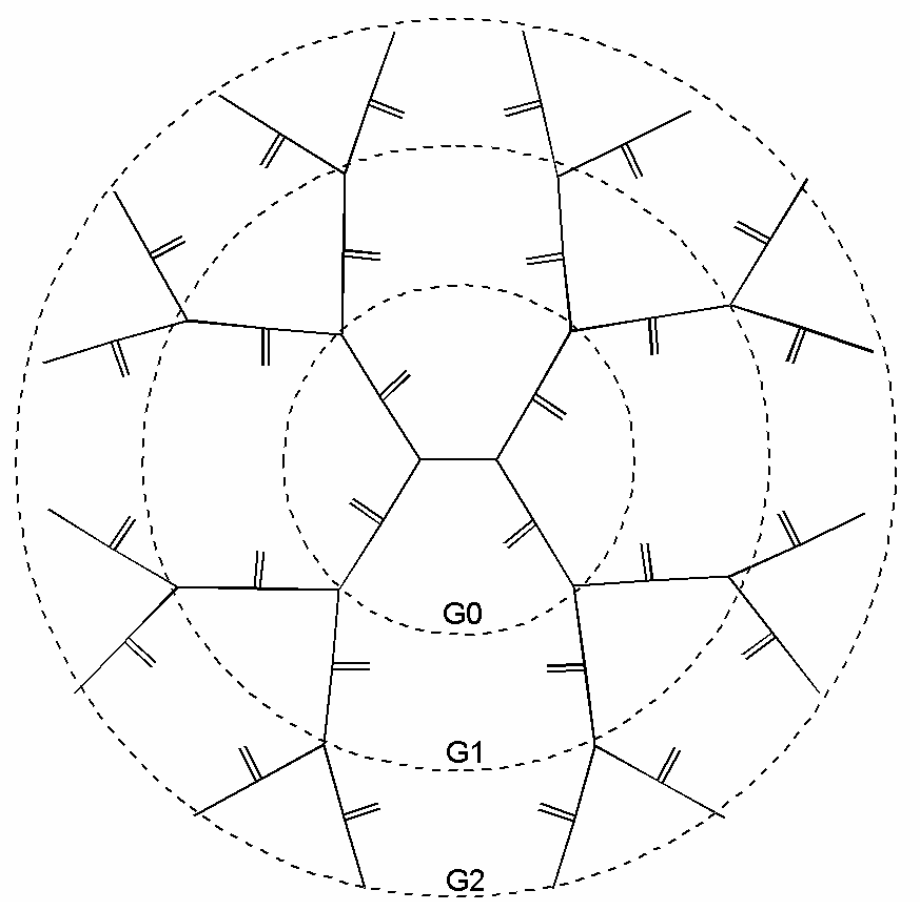

Figure 3.1. Schematics showing subgenerations G0, G1 and G2 in a G2 dendrimer. Notice subgeneration G0 (composed of ethylenediamine (EDA) and four branches contaning a secondary amide group), subgeneration G1 (obtained adding a 'layer' of eight branches upon subgeneration G0) and G2-dendrimer (resulting from adding a 'layer' of sixteen branches upon subgeneration G1)

The configuration of a PAMAM dendrimer is altered by the presence of the solvent and by pH as previously reported in experimental studies.[108] Experimentally it has been observed a progressive protonation of tertiary amine sites as pH was decreased. However at a given pH –around 3- protonation is total and further decreases in pH do not seem to

promote further protonation.[109] On the other hand, ions like Na^+ have been detected inside small dendrimers.[110] but neither *detailed* description of the binding between cations/anions/water molecules and dendrimer nor insights about the identity of those binding sites has been offered by experiments. Also, it is expected that cations and anions alter the configuration of a PAMAM dendrimer.

3.2 Methods

A systematic procedure for building and optimizing a PAMAM-G0-NH_2 (ethylenediamine, EDA-core) where building blocks (fragments of branches) were added sequentially –emulating the experimental synthesis methodologies[95]- was used. Initially, optimizations were performed at the HF/STO-3G method for an EDA molecule. Then, one by one, branches were added by replacing the four amine-terminal-hydrogen atoms and the resulting fragments optimized until obtaining the optimized complete dendrimer structure. Successive steps involved improving the basis set (HF/3-21G and HF-6-31G(d)) and incorporating electron correlation through DFT methods in order to properly describe various conformers both for G0-NH_2 and G0-OH. No constraints on the symmetry were applied. Mulliken population charges[111-113]of various local minima conformers was also analyzed. Energetics for the various conformers was calculated with both HF/6-31G(d) and B3LYP/6-31G(d)//HF/6-31G(d) levels of theory. These calculations were performed using the Gaussian 98 suite of programs.[73]

Although pH and solvent are expected to affect the conformation of a dendrimer in solution[114] its effect was not considered in the calculation of minimum energy PAMAM-G0-NH_2 and PAMAM-G0-OH. However, it was studied with outer pocket (See Figure 3.2) models though only for the –OH terminated pocket. Solvent effect was addressed by adding explicit water molecules inside the pocket rather than by treating it implicitly with a continuum because the dendrimer –and particularly outer pockets- is not surrounded by an environment of uniform dielectric constant. On the other hand, the effect of the pH was targeted by recognizing two distinct scenarios in an outer pocket: absence and presence of proton on tertiary amine N sites.

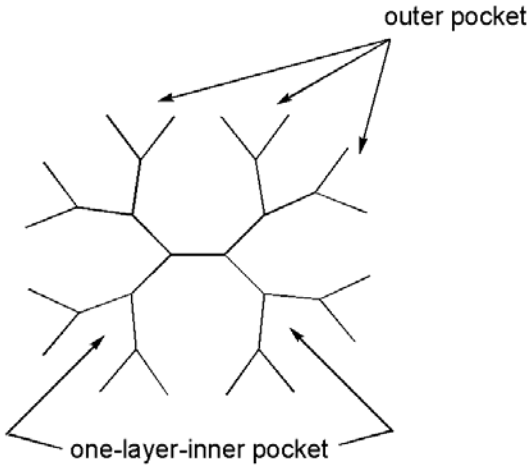

Figure 3.2. Pictorial representation of a G2 dendrimer illustrating the difference between outer pocket and one-layer-inner pocket. Outer pockets are the outermost pockets delimited by two branches. One-layer-inner pockets are also delimited by two branches but they are located closer to the core –center of the dendrimer

The dendrimer outer pocket is modeled with a 41-atom fragment. This fragment (DF41) -DF stands for "Dendrimer Fragment" whereas 41 is the number of atoms that make up the fragment- consist of two branches stemming out of one tertiary amine nitrogen with a dangling methyl group instead of the branch to which it should be attached to the dendrimer to complete the triple-coordination of nitrogen. DF41 was used to model an *unprotonated* pocket. Another fragment, DF41-H -made out of DF41 with a proton on top of its tertiary amine N- was used to model a tertiary-amine-N protonated pocket.

DFT was used to obtain minimum energy structures of unprotonated and protonated pockets. The B3LYP/6-31+g(d) method was used. The optimization of the geometries (bond length, angles) was followed by second derivative matrix calculations that provided estimates for the zero point energy (ZPE). The calculations were done with Gaussian 03[74]

3.3 Results and discussion

3.3.1 Low generation dendrimers: minimum energy conformers

Two types of conformers were found: one where the secondary amide group of one of the branches was in *cis* conformation, whereas all the others were in *trans* position (*tttc*), and another type where the four secondary amide groups were in *trans* position, designated as *tttt1*, *tttt2*, and *tttt3* conformers (Figure 3.3).

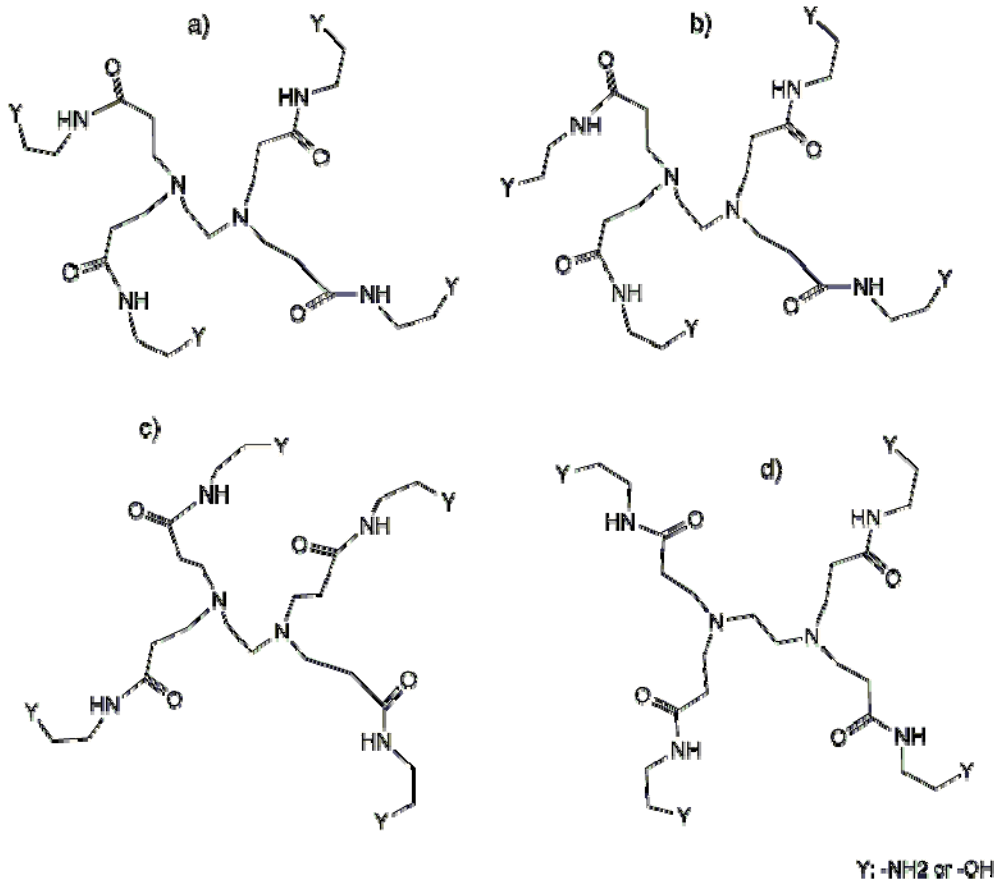

Figure 3.3. Schematic of G0 conformers. (a) *tttc (*b) *tttt1* (c) *tttt2* (d) *tttt3*. In this representation it is possible to observe that the structural conformations of *tttc* and *tttt1* are nearly the same except for the *cis* vs. *trans* position of one of their amide functional groups. The first three conformers have a NCCN core dihedral of approximately 60° whereas in *tttt3* the dihedral value is 180°. In *tttt2* an intramolecular ~NH---O~ hydrogen bond is noticeable

Intramolecular (interbranch) interactions depend on the conformer structures: in G0-NH_2, both *tttt1* and *tttc* form H-bonds between an H atom of one terminal primary amine and the amide O of an adjacent branch, whereas *tttt2*, which adopts a more extended and symmetric geometry than *tttt1*, only forms H-bond between an amide O and an amide H of adjacent branches (Figure 3.3). Another conformer, *tttt3* (Figure 3.3) has three of their branches approximately coplanar, and the fourth slightly out of plane, along with a core dihedral angle NCCN of about 180^o. In G0-OH, *tttt2* has H-bonding similar to that of its analogous G0-NH_2, whereas *tttt1* and *tttc* form H-bonds between an H from an OH terminal group and an amide O of adjacent branches. The relative energies shown in Table 3.1 suggest that in vacuum both dendrimers prefer to adopt the all-*trans* conformation.

Table 3.1: ZPE-corrected electronic energies of PAMAM-G0 conformers at HF/6-31G(d) and B3LYP/6-31G(d)//HF/6-31G(d) levels of theory. Corresponding schematic geometries are shown in Figure 3.3

		HF/6-31G(d)		B3LYP/6-31G(d)//HF/6-31G(d)	
PAMAM	conformer	Energy (a.u.)	Rel. Energy[a]	Energy (a.u.)	Rel. Energy[a]
G0-NH_2	tttc	-1704.26357	6.31	-1714.92559	3.47
	tttt1	-1704.26948	2.60	-1714.93112	0.00
	tttt2	-1704.26684	4.25	-1714.92386	4.56
	tttt3	-1704.27362	0.00	-1704.27362	5.21
G0-OH	tttc	-1783.60323	18.76	-1794.43207	3.52
	tttt1	-1783.63313	0.00	-1794.43768	0.00
	tttt2	-1783.60349	18.59	-1794.42168	10.04
	tttt3	-1783.62879	2.72	-1794.42123	10.32

[a]Relative energies in kcal/mol, referred to the lowest energy conformer for each set of conformers within the same method

A substantial energy difference was found (Table 3.1) between *tttc* and *tttt* conformers. Table 3.1 indicates that for G0-NH_2, the lowest energy conformer at HF/6-31G(d) is *tttt3*, with a small difference of 2.6 kcal/mol (higher energy) for *tttt1*, however this difference reverts when electron correlation is introduced; thus B3LYP/6-

31G(d)//HF/6-31G(d) yields *tttt1* as the most stable conformer. The stability order between *tttt2* and *tttc* also reverts when electron correlation is included, which may be better described at the B3LYP/6-31G(d)//HF/6-31G(d) level. A different trend is found for G0-OH, where the calculated lowest energy conformer is *tttt1* regardless of the method used. At HF/6-31G(d) level, the *tttt2* and *tttc* are much less stable than *tttt1* and *tttt3*.

The relatively higher stability of *tttt1* compared with the corresponding *tttc* conformer is in agreement with the known preference for the amide *trans* over amide *cis* in protein backbones. Moreover, the difference in energy, calculated including correlation effect through DFT, between the G0 conformers *tttt1* and *tttc* is in the order of magnitude found for the *trans-cis* isomerization in gas phase of the peptide-bond containing analog N-methylacetamide.[115] It should be noticed that here we compare only *tttt1* and *tttc* conformers because of their apparent similarities that can be observed in Figure 3.3. The *tttt2* conformers are 4.56 and 10.4 kcal/mol less stable compared to *ttt1* for G0-NH_2 and G0-OH respectively. This difference may be explained based on the existence of at least two H-bond interactions in *tttc* and *tttt1,* whereas only one is present in the *tttt2* conformers.

When electron correlation is taken into account, it is observed that the *tttt2* conformer has an stabilizing intramolecular hydrogen bond and *tttt3* has none, the energy difference between them is relatively small (0.65 kcal/mol for G0-NH_2 and 0.28 kcal/mol for G0-OH), with *tttt2* the most stable, suggesting that not only hydrogen bond interactions but also the magnitude of the core dihedral angle may contribute to the conformers stability.

Given the somehow radial symmetry observed from our calculations, we organized and classified the G0-NH_2 and G0-OH atoms in types; the adopted nomenclature is listed in Table 3.2.

Table 3.2: Nomenclature used to describe atom types in PAMAM-G0-NH_2 and G0-OH

element	atom type	Description
Carbon	CC	C atom in core
Nitrogen	NC	N atom in core
Carbon	CN3	C atom in branch bound to NC
Carbon	CCO	C atom bound to CO
Carbon	CO	C atom in the carbonyl group
Nitrogen	N2	amide nitrogen
Carbon	CN2	C atom bound to amide nitrogen
Carbon	CY	Carbon atom bound to terminal group atom
Atom Y[a]	Y	Terminal group atom
Oxygen	O	Oxygen in carbonyl group
Hydrogen	HCC	H atom bound to CC
Hydrogen	HCN3	H atom bound to CN3
Hydrogen	HCCO	H atom bound to CCO
Hydrogen	HN2	H atom bound to N2
Hydrogen	HCN2	H atom bound to CN2
Hydrogen	HCY	H atom bound to CY
Hydrogen	HY	H atom bound to Y

[a]Atom Y is designated to represent the terminal group atoms: "N1" primary amine terminal nitrogen in G0-NH_2 and "OT" hydroxyl terminal oxygen in G0-OH

3.3.2 Low generation dendrimers: atomic charge distribution

The Mulliken charge distribution of PAMAM-G0 dendrimers in their *tttt1*, *tttt2* and *tttc* configurations was calculated at the B3LYP/6-31G(d)//HF/3-21G level of theory.

Comparing the atomic charges among conformers, we observe that in most cases, *tttt2* (the extended and more symmetric structure) shows the largest differences with the other two conformers.

Table 3.3 illustrates differences in Mulliken population charges due to the different terminal groups of PAMAM-G0. It is noticeable that the atomic charge varies significantly in the neighborhood of the terminal group whether –NH_2 or –OH. For example, the existence of negative charges on the primary amine N atoms higher than those in the O atoms belonging to hydroxyl terminal groups in G0–OH (atom type Y), and also higher than the charges on the tertiary amine N atoms inside the dendrimer

(atom type NC), could explain the ease of the protonation found in primary amines with respect to that in tertiary amines.[20,108,109,116,117]

Table 3.3: Mulliken atomic charges (B3LYP/6-31G(d)//HF/3-21G) averaged over all atoms of a given type (nomenclature in Table 3.2) for G0-NH_2 and G0-OH

atom	G0-NH_2			G0-OH		
type	tttc	tttt1	tttt2	tttc	tttt1	tttt2
CC	-0.17	-0.18	-0.15	-0.16	-0.16	-0.15
NC	-0.41	-0.40	-0.37	-0.40	-0.40	-0.37
CN3	-0.16	-0.16	-0.15	-0.17	-0.16	-0.14
CCO	-0.37	-0.37	-0.38	-0.37	-0.37	-0.38
CO	0.59	0.59	0.60	0.61	0.61	0.60
N2	-0.59	-0.59	-0.61	-0.60	-0.60	-0.60
CN2	-0.14	-0.14	-0.10	-0.13	-0.13	-0.14
CY	-0.13	-0.14	-0.16	-0.06	-0.06	-0.05
Y	-0.74	-0.75	-0.76	-0.65	-0.65	-0.63
O	-0.53	-0.53	-0.54	-0.54	-0.55	-0.53
HCC	0.16	0.16	0.13	0.15	0.15	0.14
HCN3	0.15	0.15	0.16	0.16	0.16	0.16
HCCO	0.17	0.17	0.15	0.17	0.16	0.16
HN2	0.34	0.34	0.35	0.36	0.36	0.35
HCN2	0.15	0.15	0.16	0.16	0.16	0.17
HCY	0.15	0.15	0.14	0.15	0.15	0.15
HY	0.31	0.31	0.31	0.42	0.42	0.40

* Atom Y is designated to represent the terminal group atoms: “N1” primary amine terminal nitrogen in G0-NH_2 and “OT” hydroxyl terminal oxygen in G0-OH

3.3.3 Dendrimer outer pocket: a host

In this section we provide qualitative insights on the configuration of outer pockets and focus on understanding how the different species –especially water and proton- present inside a dendrimer outer pocket can alter its configuration and consequently that of the complete dendrimer.

3.3.3.1 Justification for the convenience of modeling guest-host interactions with molecular fragments

There are a number of configurations a dendrimer might adopt as a function of generation as a consequence of the presence of cations/anions/water. This is illustrated with a simple calculation. Some assumptions are needed though: first, the configuration of all amide groups in the branches should remain *trans* as suggested by section 3.3.1.; second, there should be no backfolding of branches, so the dendrimer extends ideally forming outer pockets limited by two branches and reasonably planar (so this approach could not be extended to large generation dendrimers, especially to those spherical in shape).

For the particular arrangement of a dendrimer outer pocket (See Figure 3.2) and knowing that amide O atoms bear negative charges (See Table 3.3.), it can be postulated that in the presence of a cation (a positively charged ion), the amide O atoms orient inward toward the pocket whereas in the presence of an anion (a negatively charged ion), the amide H (atom type HN2) atoms orient inward toward the pocket. The latter is equivalent to say that the amide O orient outward from the pocket because the preferred configuration for the amide group in a branch was found to be *trans* rather than *cis* (section 3.3.1). Thus, we postulate that dendrimer outer pocket configurations can be determined on the basis of the orientation of the amide O atoms of their branches.

In Figure 3.4, the horizontal central line represents the core of the dendrimer with the core tertiary amine N atoms located at the end of the line. The magnitude of the dihedral formed by the tertiary amines N3 and the both methylene carbon atoms CN3 in EDA-core (core dihedral N3-CN3-CN3-N3) was assumed to be 180°. If a line – representing the innermost half of a branch- stemming out of either extreme of that line is drawn, then the amide O atom can be found either to its right (1) or to its left (2). With four branches, the possible number of combinations is $2^4 = 16$ but if the molecule is considered to have a symmetry plane that coincides with the plane of the figure, then a configuration 1111 seen from above is identical to a 2222 seen from below such plane. Therefore only eight different configurations could be possible for the core (Figure 3.4).

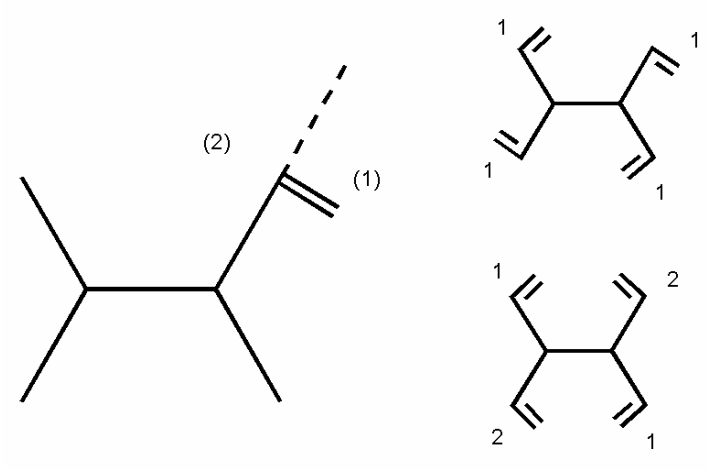

Figure 3.4. Orientation of amide O atoms in the dendrimer core. Left: Amide O can be found in either of two positions respect to its containing branch: "right" (1) when it lays at the right side of the dashed line –projected from the carbonyl C- and "left" (2) when the amide O lies at the left side of the same line. Right side: Two (out of eight) examples of core configuration

Next, we consider the orientation of the amide O atoms in the outer pockets. There could be at least three distinct ideal cases: when both amide O atoms orient outward from the pocket (A: outward-outward), when both amide O atoms orient inward toward the pocket (B: inward-inward) and when one amide O orients outward and the other inward (C: outward-inward). In Figure 3.5, the lines represent the branch extending from the branching point toward the surface terminal group.

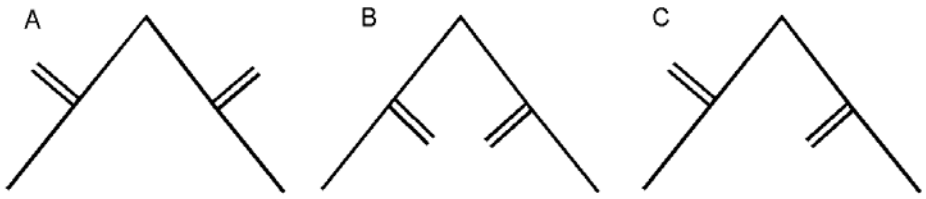

Figure 3.5. Orientation of amide O atoms in dendrimer outer pockets. (A) In both branches amide O atoms orient outwardly (outward-outward). (B) In both branches amide O atoms orient inwardly (inward-inward). (C) One amide O orients outwardly while the other orients inwardly (outward-inward)

As G1-OH can be built from G0-OH plus four outer pockets, how many different configurations are then possible? If we assume that each pocket can adopt either configuration (A, B or C in Figure 3.5) independently of the configurations of the other pockets, so that –for instance- the configuration AAAB is different from AABA, then consequently there are 3^4 possible configurations for the arrangement of four pockets having a fixed configuration for the dendrimer core. Thus, for G1-OH a total of 8 x 3^4 = 648 configurations can be generated. In Figure 3.6 we show as an example the core in '1111' arrangement (Figure 3.4) and pockets in AAAA arrangement (Figure 3.5).

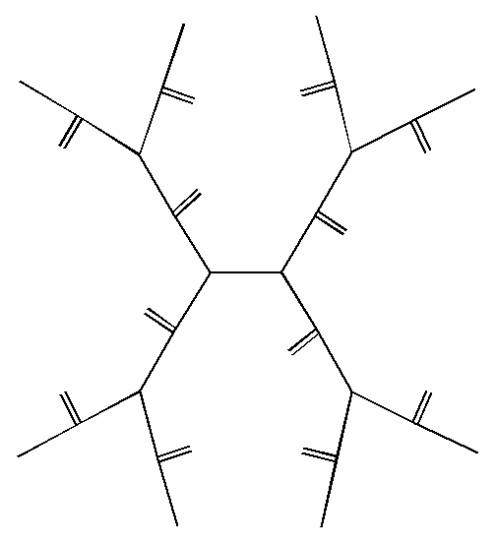

Figure 3.6. G1-OH configuration illustrating a core-'1111'-pockets-AAAA configuration

If the assumption that the new layer of branches will adopt a configuration independent of those that the inner branches/pockets adopt could be kept for G2, G3 and G4, then the Table 3.4 shows how many different configurations will be expected.

Table 3.4: Number of distinct configurations expected by considering different orientations of amide O in outer pockets as a function of dendrimer generation

generation	# configs
0	8
1	648
2	4251528
3	1.83×10^{14}
4	3.39×10^{29}

These numbers might be even higher if the amide O groups are allowed to adopt a *cis* configuration, or lower if the configuration of a given pocket is influenced by the configuration of other pockets; nonetheless overestimated, they remind us of a fact already noticed in the literature[118]: sampling in molecular dynamics or molecular mechanics becomes increasingly complex once one attempts to model accurately the multiple binding of ions/anions/water to a complete dendrimer. Therefore we believe our use of molecular fragments to represent outer pockets is justified.

3.3.3.2 Water encapsulation within *unprotonated* dendrimer outer pocket

In this section we turn to find *the number of waters that can be encapsulated within an unprotonated outer pocket.* Two stable configurations for the outer pocket without water (Figure 3.7) and three configurations for each of the cases where the outer pocket hosts one, two, three, and four water molecules were found.

Thermodynamic quantities for the following reactions (for n = 0-3) were calculated.

Addition of water to an outer pocket structure:

$$DF41\text{-}(H_2O)_n + H_2O \rightarrow DF41\text{-}(H_2O)_{n+1} \qquad (3.1)$$

Displacement of a water molecule from a dimer (a water molecule is added to the preexistent water-in-pocket structure):

$$DF41\text{-}(H_2O)_n + (H_2O)_2 \rightarrow DF41\text{-}(H_2O)_{n+1} + H_2O \qquad (3.2)$$

where the left hand side hydrated structure is chosen to be the lowest ZPE-corrected-energy configuration at a given value of *n*.

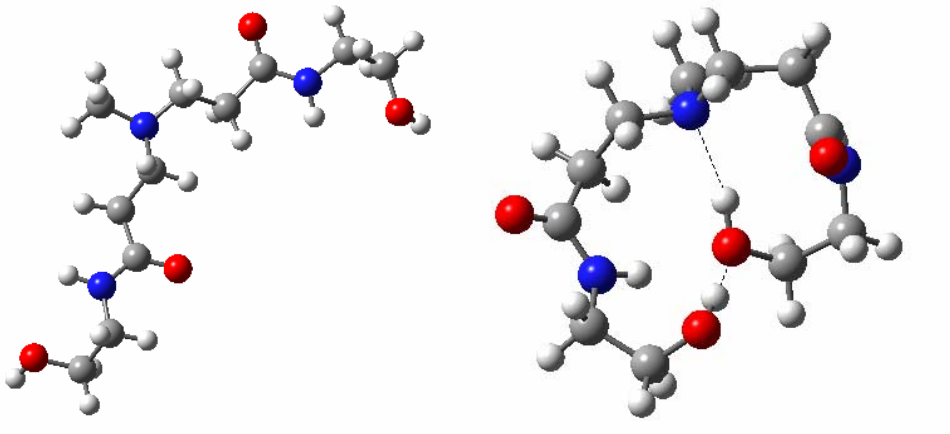

Figure 3.7 Reference fragments DF41. Left: Ref A; Right: Ref CoB with two hydrogen bonds: OH---N3 (2.05 Å), OH---OH (2.02 Å). Ref CoB is chosen as the reference fragment for thermodynamic calculations because it is slightly more stable than Ref A (E_0 (Ref CoB)- E_0(Ref CoA) = -0.68 kcal/mol)

Selected structures included in Tables 3.5 and 3.6 were chosen on the basis of the following criteria: for n = 0, the three yielding negative ΔG (eqn 3.2); for n =1, all four configurations found; for n = 2, the only one with negative ΔG (eqn 3.2) and for n = 3, the one with the lowest positive ΔG (eqn 3.2).

Table 3.5 shows a stepwise addition of water to an outer pocket that does not hold water initially. It is observed that the addition of the first water is thermodynamically feasible resulting in either 1C (ΔG = -1.1 kcal/mol) or 1E (ΔG = 0.04 kcal/mol). The addition of a second water is calculated with reference to configuration 1E and it is found feasible for either 2C (ΔG = -0.82 kcal/mol) or 2A (ΔG = -0.64 kcal/mol). The addition of a third water is calculated using 2C as reference and found not feasible (ΔG > 0). Therefore, two things can be inferred: that *the maximum number of water allowed by an unprotonated pocket is two* and that these waters are most likely hosted as they appear in configuration 2C.

Table 3.5: Electronic energies with ZPE correction (ΔE_0), enthalpies and free energies of reaction (kcal/mol) for formation of selected DF41-$(H_2O)_{n+1}$ configurations by addition of water to an outer pocket structure

n	product config	ΔE_0	ΔH	ΔG
0	1C	-7.8	-8.0	-1.1
0	1D	-8.2	-9.1	1.0
0	1E	-8.9	-9.3	0.04
1	2A	-8.1	-8.9	-0.64
1	2B	-7.3	-8.2	2.1
1	2C	-9.0	-9.7	-0.82
1	2E	-6.9	-7.6	2.1
2	3A	-8.4	-9.6	1.6
3	4C	-5.3	-6.0	4.2

Table 3.6: Electronic energies with ZPE correction (ΔE_0), enthalpies and free energies of reaction (kcal/mol) for formation of selected DF41-$(H_2O)_{n+1}$ configurations by displacement of a water molecule from a dimer

n	product config	ΔE_0	ΔH	ΔG
0	1C	-3.8	-3.4	-3.1
0	1D	-4.3	-4.5	-0.96
0	1E	-4.9	-4.7	-2.0
1	2A	-4.2	-4.4	-2.6
1	2B	-3.3	-3.6	0.14
1	2C	-5.0	-5.1	-2.8
1	2E	-3.0	-3.0	0.07
2	3A	-4.5	-5.0	-0.38
3	4C	-1.4	-1.4	2.2

The optimized structures in this and the next sections suggest a classification based on three ideal configurations (outward-outward, outward-inward and inward-inward, See Figure 3.5). In order to get insight on the configuration of the pocket upon hosting water we gather a few relevant parameters from the optimized structures data: 1) Distance between amide O atoms that provides an indication of how close or open the pocket is; 2) Distance between hydroxyl O atoms that reveals whether or not the pocket is being closed by a hydrogen bond between the –OH terminal groups. 3) The magnitude of the angle γ, this is, the angle formed by the amide O1 (branch 1)-tertiary amine N3-amide O2 (branch 2), and 4) angle α formed by carbonyl CO1(branch 1)- tertiary amine N3-carbonyl CO2 (branch 2) to get insights on the degree of openness of the pocket. Thus, these geometrical parameters -shown in Table 3.7- illustrate how the pocket geometrical configuration accommodates to host the water molecules.

Table 3.7: Summary of significant bond distances (in angstroms) and angles (in degrees) for selected DF41-$(H_2O)_n$ configurations

	bond distances (Å)		bond angles (degrees)	
config	O-O	OT-OT	α(CO-N3-CO)	γ(O-N3-O)
RefA	7.40	12.80	120.5	120.3
RefCoB	6.80	2.98	123.2	111.3
1C	7.19	8.44	142.1	131.0
1D	5.40	4.49	122.6	95.1
1E	6.13	2.83	90.10	90.40
2A	7.16	8.45	139.8	126.7
2B	5.70	4.94	125.5	100.5
2C	7.36	8.80	144.0	133.2
2E	6.13	2.78	90.6	90.5
3A	7.12	7.27	133.3	122.0
4C	7.61	6.63	132.0	120.2

The DFT calculated amide O-amide O (O-O) distance ranges between 5.40-7.61 Å, and the hydroxyl oxygen to hydroxyl oxygen distance (OT-OT) from 2.98 Å (closed configurations) to 12.80 Å (open configurations). The angle α ranges between 120.5-144.0° and the γ angle between 95.1-133.2°.

Configuration 2C (Figure 3.8) has both the maximum α and the maximum γ values, OT-OT distance of 8.80Å and O-O distance of 7.36 Å. Thus, it is mostly an outward-inward configuration. This is the trend that is observed from Table 3.7 for all but 1D, 2B and 4C.

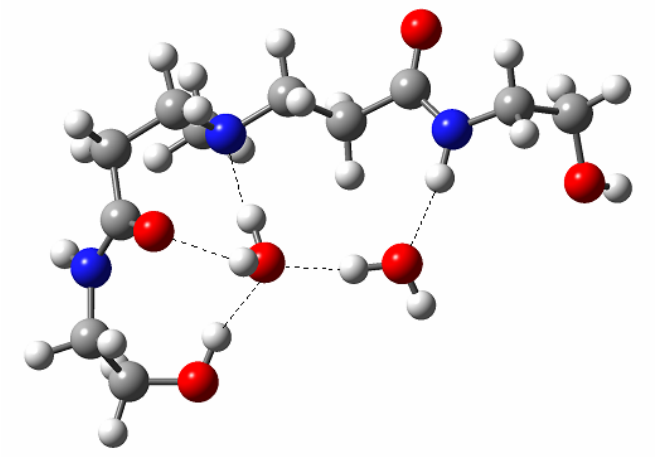

Figure 3.8. Configuration 2C for DF41-$(H_2O)_2$. H-bonds: H_2O---H_2O: 1.81 Å; OH_2---N: 1.86 Å; OH---OH_2: 1.89 Å; NH---OH_2: 1.93 Å and OH_2---O: 2.06 Å

3.3.3.3 Water encapsulation within *protonated* dendrimer outer pocket

Two stable configurations for the *protonated* outer pocket (DF41-H) without water were found. In both, the proton binds to the amide O atom of the adjacent branch (Figure 3.9).

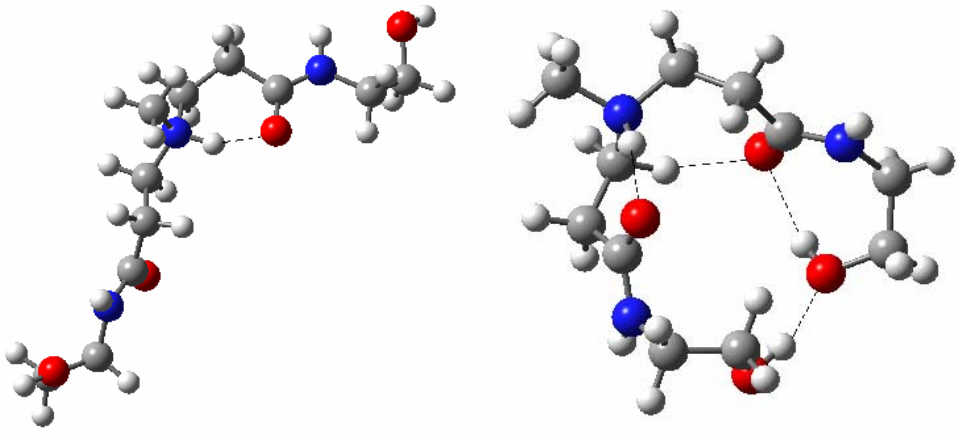

Figure 3.9: Protonated reference fragments DF41-H. Left: RefA; Right: RefCoB. The hydrogen bond length NH^+---O is 1.70 Å and 1.68 Å in RefA and RefCoB respectively. For RefCoB notice that there are also three additional hydrogen bonds OH---OH (1.88 Å), OH---O=C (2.12 Å) and HCH---O=C (2.10 Å). RefCoB is chosen as the reference fragment because it is slightly more stable than Ref A (E_0(ReCoB – E_0(RefA) = -1.2 kcal/mol)

Thermodynamic quantities for the following reactions for n = 0-2 were calculated as follows:

Addition of water to a *protonated* outer pocket structure:

$$[DF41\text{-}H\text{-}(H_2O)_n]^+ + H_2O \rightarrow [DF41\text{-}H\text{-}(H_2O)_{n+1}]^+ \quad (3.3)$$

Displacement of water from a dimer by a *protonated* outer pocket:

$$[DF41\text{-}H\text{-}(H_2O)_n]^+ + (H_2O)_2 \rightarrow [DF41\text{-}H\text{-}(H_2O)_{n+1}]^+ + H_2O \quad (3.4)$$

Addition of H_3O^+ to a *unprotonated* outer pocket structure:

$$DF41\text{-}(H_2O)_n + H_3O^+ \rightarrow [DF41\text{-}((H_3O)\text{-}(H_2O)_n)]^+ \quad (3.5)$$

Displacement of H_3O^+ from a monohydrated hydronium by a *unprotonated* outer pocket:

$$DF41\text{-}(H_2O)_n + H_2O\text{-}H_3O^+ \rightarrow [DF41\text{-}((H_3O)\text{-}(H_2O)_n)]^+ + H_2O \quad (3.6)$$

where the left hand side hydrated structure is chosen to be the lowest ZPE-corrected-energy configuration at a given value of *n*.

Table 3.8: **Average electronic energies with ZPE correction (E_0), enthalpies and free energies of reaction (kcal/mol) at 298.15 K for formation of [DF41-H-$(H_2O)_{n+1}$]$^+$ configurations according to eqn 3.3 and eqn 3.4**

	ΔE_0		ΔH		ΔG	
	eqn	eqn	eqn	eqn	eqn	eqn
n	3.3	3.4	3.3	3.4	3.3	3.4
1	-8.5	-4.5	-8.9	-4.3	-0.42	-2.4
2	-10.0	-6.0	-10.3	-5.8	-1.9	-3.9
3	-9.2	-5.3	-9.9	-5.3	-1.2	-3.2
av	-9.2	-5.3	-9.7	-5.1	-1.2	-3.2

In order to evaluate the results in Tables 3.9 and 3.10 –corresponding to eqn 3.5 and eqn 3.6 respectively- we chose configurations of DF41-$(H_2O)_{n+1}$, for n = 0-2 based on their lowest energy of reaction (ΔE_0) according to eqn 3.1. The selected configurations were 1E, 2C, 3A along with the reference fragment DF41 (RefCoB).

Table 3.9: **Electronic energies with ZPE correction (E_0), enthalpies and free energies of reaction (kcal/mol) for formation of selected [DF41-$((H_3O)$-$(H_2O)_n)$]$^+$ configurations according to eqn 3.5**

n	product config	ΔE_0	ΔH	ΔG
0	1B*	-96.0	-96.7	-85.3
0	1D	-90.9	-91.7	-80.6
0	1A	-90.8	-90.3	-84.5
1	2C*	-99.0	-100.4	-87.5
1	2E	-91.9	-92.5	-82.2
2	3C	-93.0	-93.5	-83.9
3	4A	-91.6	-91.7	-82.5

Table 3.10: Electronic energies with ZPE correction (E_0), enthalpies and free energies of reaction (kcal/mol) for formation of selected $[DF41\text{-}((H_3O)\text{-}(H_2O)_n)]^+$ configurations according to eqn 3.6

n	product config	ΔE_0	ΔH	ΔG
0	1B*	-60.4	-59.9	-57.4
0	1D	-55.4	-54.8	-52.7
0	1A	-55.3	-53.4	-56.5
1	2C*	-63.4	-63.6	-59.6
1	2E	-56.4	-55.7	-54.3
2	3C	-57.4	-56.6	-56.0
3	4A	-56.0	-54.8	-54.6

Based on the magnitude of their values, reaction energies described by eqn 3.5 and eqn 3.6 seem to describe a more likely scenario than those (see Table 3.8) by eqn 3.3 and 3.4. From the Tables 3.9 and 3.10 it is evident that the most likely reactions are those where 2C* & 1B* are generated where the proton interacts more closely to the amide oxygen, followed by 1A & 3C where the pocket arms are wide open. Finally, configurations 1D and 2E are the less stable, when the pocket is closed (Figure 3.10).

Can higher degrees of solvation still be reached? According to Tables 3.9 and 3.10 arriving at 3C is less likely that arriving at 2C* through a pathway described by eqn 3.5 and eqn 3.6. However once 2C* is obtained, a pathway described by the processes in eqn 3.3 and eqn 3.4 can follow and configuration 3C can be obtained. Thus, although the energies calculated for eqn 3.3 and eqn 3.4 are smaller compared to those found for eqn 3.5 and eqn 3.6 they can still make the hydration of the protonated complex possible. The effect on the geometry will be a transition from a structure –almost closed if looking at Figure 3.10- with internal amide O-proton hydrogen bond (2C*) to an open structure (3C). If this is the case, then this could reflect experimental trends that have found that the dendrimer expands upon protonation.[119]

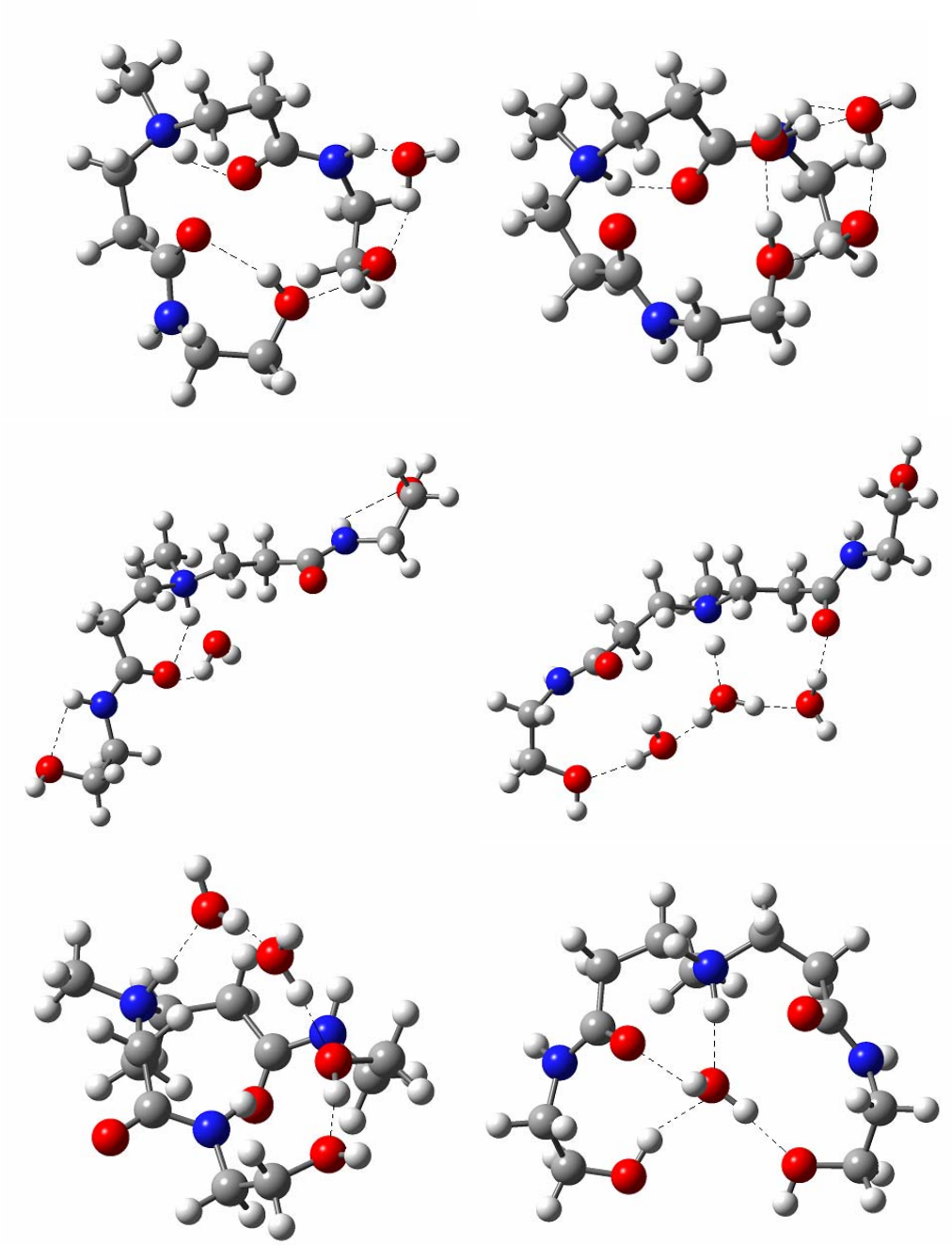

Figure 3.10. $[DF41\text{-}H\text{-}(H_2O)_n]^+$ configurations. Upper left: configuration 1B*; Upper right: configuration 2C*. Notice clearly the H-bond between the proton located at the tertiary amine N site and the amide O atom, configurations where the pocket arms are wide open. Middle left: configuration 1A; Middle right: configuration 3C; Configurations where the pocket appears closed and the amide O- proton H-bond is absent. Lower left: configuration 2E; Lower right: configuration 1D

From Table 3.11 it is observed that the range for the O-O distance is 4.14-6.56 Å, and from 2.73 to 13.90 Å for the OT-OT distance. The magnitude of the angle α ranges from 85.7° to 139.4° and that of the angle γ from 78.8 to 106.5°. Compared to the *unprotonated* pocket, the O-O distance values are shorter ; the angle α ranges also around lower values although in a broader range because it covers a series of configurations: "open" with large 130-139.4°, "closed" with 85.7-116.3° and internal amide O-H bond 86-91° ; and the γ angle ranges around lower values but its range of variation is similar.

Table 3.11: **Summary of significant bond distances and angles for [DF41-H-$(H_2O)_n$]$^+$ configurations**

		Bond distances (Å)		Bond angles (degrees)	
n	Config	O-O	OT-OT	α(CO-N3-CO)	γ(O-N3-O)
0	RefA	5.38	13.70	128.2	102.8
0	RefCoB	4.23	2.83	85.8	87.3
1	1B*	4.14	2.78	86.0	85.5
1	1D	4.18	4.04	116.3	78.8
1	1A	5.45	13.90	130.0	102.7
2	2C*	4.77	2.73	91.0	101.5
2	2A	5.73	10.10	121.2	102.8
2	2E	5.41	2.76	85.7	81.8
3	3C	6.56	13.20	139.4	106.5
3	3A	5.63	7.98	113.5	96.1
4	4A	6.42	11.72	139.3	104.7

At least two distinct configurations can be found: one where the amide O remains bound to the proton so that the water molecules bind outside that interaction. Configuration 2C* has the lowest OT-OT distance (they bind), its α angle is 91.0° and γ

is 101.5° (Table 3.11) deriving into a pattern that closely resembles a ‘outward-inward’ ideal configuration. On the other hand, the open wide configuration 3C has the maximum O-O distance, the maximum α and the maximum γ among the configurations found deriving into a pattern that closely resembles an ‘inward-inward’ ideal configuration (Figure 3.10).

3.4. Summary

The most stable configurations of PAMAM G0-NH_2 and G0-OH dendrimers are those where all secondary amide groups in the branches adopt *trans* conformation. On the other hand, differences in charge distribution between G0-NH_2 and G0-OH point out to the possibility of selective behavior toward specific substrates and/or ligands upon interactions of these terminal groups with the given substrates/ligands.

Our analysis of the charge distribution of small dendrimers revealed that the charge beared by amide O atoms in dendrimers branches is negative. This fact serves to classify outer pockets based on the relative orientation of the two amide O atoms found in an outer pocket. Three ideal cases can occur: both amide O atoms orient inward toward the pocket (inward-inward), both amide O orient outward from the pocket (outward-outward) and one amide O orients inward and the other outward (outward-inward). The classification enables also the calculation of an estimate of the number of configurations possible for low generation dendrimers that in turn reveals how challenging simulations of ions with large dendrimers can be and call for the use of simpler molecular fragments to reproduce outer pockets.

Outer pocket models constitute an initial approximation to the understanding of the effect of solvent and pH to PAMAM-G0-OH dendrimers. Thus, it was found that two water molecules can saturate an outer pocket when the pocket is *unprotonated*. This water loading capacity could not be accurately determined for a *protonated* pocket because under these conditions the dendrimer can adopt a more open configuration.

Geometrical analysis of the structure of an outer pocket hosting water showed that the outward-inward character is the dominant pattern in *unprotonated* outer pockets.

However, several patterns arise when protonation occurs: inward-inward, outward-inward and even outward-outward patterns. A transition from a configuration that resembles closely an ideal ‘outward-inward’ to another that is more of an ‘inward-inward’ -yet open to accept more water inside the pocket- is expected to take place in protonated pockets. As pockets are part of dendrimers, this shift in conformation upon protonation of tertiary amine should impact the configuration of larger dendrimers to the extent that such protonation occurs in those systems. Therefore, these results predict a swelling upon protonation as observed experimentally.[119]

CHAPTER IV
COMPLEXATION OF CU(II) IONS WITH THE LOWEST GENERATION PAMAM-OH DENDRIMER*

4.1 Introduction

As ion complexation precedes the formation of embedded metallic nanoclusters, a clear understanding of ion complexation and of the influence of the factors that affect the complexation process – such as pH, counterion, ligand exchange, and charge transfer- are needed. Due to their own peculiarities each ionic complexation requires individual study; this fact hampers the understanding of currently known systems and the search for new precursor-dendrimer systems for metal nanoparticle synthesis.

Interest in the understanding of complexation of one of the simplest ion-dendrimer systems namely Cu(II)-PAMAM is revealed by a number of experimental works directed towards its characterization[20,21,96,97,120] For instance, the extent of binding of Cu(II) to dendrimers was calculated by mass balance of Cu(II) content in aqueous solutions using atomic absorption spectroscopy (AAS)[20] and found to be a pH-dependent process. However, despite many attempts to elucidate the identity of the atoms constituting the first coordination shell of Cu(II) when it coordinates to PAMAM dendrimers in aqueous solutions, the issue is still in debate. Currently proposed coordination sites include all types of nitrogen[21,97,120,121] in $–NH_2$ terminated dendrimers and carboxylate groups in –COO terminated dendrimers.[122] It has been shown that $–NH_2$ terminal groups can be accounted as the main complexation sites for Cu(II)[120] in aqueous solutions of $–NH_2$ dendrimers whereas a less important role has been suggested for interior tertiary amines[21,120] and for amide N.[121] Presence of water -mainly in axial sites- has been inferred in a few studies[21,120] from comparisons to similar Cu(II) complexes, although such comparisons hardly support ruling out coordination to amide oxygen.[21,121]

---

* Reproduced in part with permission from Tarazona-Vasquez and Balbuena, *J. Phys. Chem. B* **2005**, *109*, 12480. Copyright 2005 American Chemical Society.

Most of the previous experimental work has focused on large generation $–NH_2$ terminated dendrimers, so the information about ion complexation in –OH terminated PAMAM dendrimers is scarce, especially in low generation dendrimers where we are not aware of any related study.

4.2 Methods

A 0.01 M solution of G0-OH which corresponds to 0.01 M and 0.02 M concentrations of Cu(II) for simulated ion-dendrimer loading ratios of 1:1 and 2:1 respectively determined the edge of the simulation cube: 54.962 Å –longer than the estimated diameter of G0-OH that is 15 Å. [54]

Partial charges for G0-OH atoms were assigned to atoms from its Mulliken charge distribution calculated at the B3LYP/6-31G(d)//HF/6-31G(d) level of theory (section 3.3.2). The Cu(II) cation was modeled as a point charge of +2. Chloride anions were added to ensure electroneutrality in the MD simulation system and modeled as a point charge of +1.

The energy and length parameters for the Lennard-Jones (LJ) potential for atoms other than Cu(II), water O and H were taken from the DREIDING force field.[87]

All cross- interaction parameters were determined by the Lorentz-Berthelot mixing rules. Polarization effects were effectively included in the SPC/E water model[89] but not accounted for the dendrimer nor for the Cu(II) models. Additional MD settings are presented in section 4.2.2.

In order to provide an adequate initial configuration to the system, some of the MD simulations were preceded by in vacuum molecular mechanics (MM) minimizations of the dendrimer/ion complex. In the chosen MM procedure, the atomic charges were calculated with a charge equilibration algorithm[85] using parameters of the universal force field UFF[86] as implemented in Gaussian03.[74] Since neither DREIDING nor UFF force fields have short-range Lennard-Jones parameters for Cu(II), they were approximated with those of Cu(I) in UFF; this is not a major approximation because the configurations obtained from MM were only used to initialize the full-solvent MD simulations where

appropriate parameters were used for each of the atoms including Cu(II) as discussed later. The MM convergence criteria (in atomic units) -default in Gaussian 03[74]- used was 0.00045 for the maximum force, 0.0003 for the RMS force, 0.0018 for the maximum displacement, and 0.0012 for the RMS displacement.

To complement our MD simulations, DFT calculations were done with Gaussian 03.[74] We used a 38-atom fragment consisting of two dendrimer branches growing from one tertiary amine N atoms because a complete description of the interactions between ion, dendrimer, and water was not possible to be addressed with QM calculations due to the system size.

4.2.1 Models for MD and DFT Simulations

Five different MD initial configurations were set up: three of them containing a single Cu(II) ion and two others containing two cations. Each of these initial configurations included the G0-OH dendrimer -in its lowest energy conformer unless otherwise specified-, one or two hexahydrated Cu(II) complexes and the corresponding amount of hydrated Cl^- complexes.

In all cases the G0-OH molecule was placed in the center of the simulation box. The initial locations of dendrimer and hexahydrated ion were selected either randomly, or via a molecular mechanics (MM) minimization. The initial configurations are qualitatively shown in Figure 4.1.

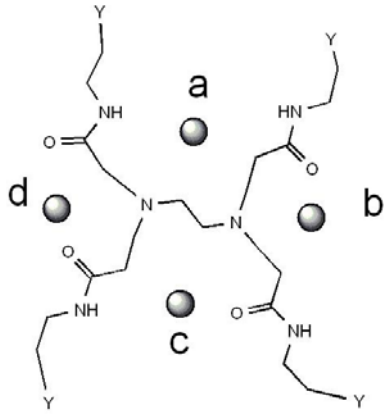

Figure 4.1. Choices of initial configurations other than random for the MD simulations of G0OH-Cu(II) complexes. Single ion configurations result from placing the ion either in position b (equivalent to d) or in position a (equivalent to c) and the two-ion configurations were obtained placing the ions in positions b and d. We did not attempt a configuration with ions in positions a and c as we deemed such configuration unstable (the first ion in either position a or c may coordinate to the core N and therefore the second ion (to be placed in either c or a) might not be able to coordinate to those same atom sites) Note: This figure is meant only to illustrate the criteria used to select initial configurations to be optimized with MM methods. Y: functional or surface group (–OH)

4.2.1.1 Monoionic Cu(II)-G0 complexes

Configuration A1: In these simulations, one hexahydrated Cu(II) is added *randomly* to the simulation box and MD simulations carried out for about 1 ns. Then, after *random* addition of two hydrated Cl^- anions in the voids surrounding the box-centered G0 molecule, additional MD simulations were run for another nanosecond.

Water is added in two steps. Firstly, about 1000 water SPC/E molecules are added to the system and additional 200 ps are run. The second step involves filling the simulation box with water molecules until approximately liquid water density –it is implicitly assumed that our simulated solution is diluted enough to have a density like pure liquid water- and simulations continue during 600 ps. This last simulation is referred below as a *full-solvent* simulation.

Configuration A2: In these simulations, one Cu(II) ion and its closest three water molecules are removed from the MM converged configuration calculated for Configuration B2 (*vide infra*) to become the initial configuration. As a result, Cu(II) is

initially *coordinated to two amide O, one core N and three water O, where no folding branches are present yet.* After 1 ns of MD two hydrated Cl^- are *randomly* added and one additional nanosecond is run. Finally water is added in two steps as in Configuration A1.

Configuration A3: In these simulations, one Cu(II) is placed *close to two amide O facing towards the two tertiary amine N (atom type NC) of the EDA-core*. Three water molecules are then added in initial locations estimated with the help of a visualization program and a MM minimization (*vide supra*) is performed. The procedure continues with one nanosecond of MD on the converged MM configuration and one additional nanosecond after *random* addition of two hydrated chloride anions. Finally, the addition of water molecules is performed as explained for Configuration A1.

4.2.1.2 Dicationic Cu(II) – G0 complexes

Configuration B1: Starting with the setup outlined for Configuration A1 before the addition of the water molecules, one additional hexahydrated Cu(II) is added *randomly* and the addition is followed by one ns of MD. Then two more hydrated Cl^- are added *randomly* to charge balancing the system and one additional ns of MD is run. Addition of water is done as described for Configuration A1.

Configuration B2: The initial configuration for these simulations consisted of two Cu(II) ions each one *coordinated to one tertiary amine N (atom type NC) in the EDA-core, two amide O and three water molecules* with the G0-OH central dihedral NCCN at about 180° as in its all-*trans* conformer *tttt3* (See Chapter III). MM optimization –as described above- is performed until convergence and followed by MD during an additional nanosecond. After completion, four hydrated Cl^- anions are added *randomly* and MD simulations are run for another nanosecond. Water is added to the system and MD simulations are carried out as explained in the previous cases.

In order to gain insights about the role of tertiary amine N in branching points, DFT optimizations are performed by placing a Cu(II) ion *near to two amide O atoms and the branching N.* One water molecule completes the equatorial tetracoordination and

two others are placed in the axial positions. Two alternative configurations met these initial arrangements differing only in the relative proximity of the hydroxyl terminal groups to Cu(II) and they are referred herein as *open* and *close* configurations. Then, one more configuration is generated and DFT optimized, where Cu(II) coordinates to one amide O, one hydroxyl O, and four water O (two in equatorial and two in axial positions) -reminiscent of one of the configurations found in our present MD simulations. Finally we attempted optimization of another configuration where Cu(II) coordinates to one amide O, three water O in the equatorial plane (O_{eq}), and two water O atoms in the axial sites (O_{ax}), in presence of another water located in the second shell of the ion but still inside the dendrimer fragment. Optimization of this configuration resulted in a local minimum with one negative value in the Hessian matrix; however since the magnitude of the corresponding frequency was so small (5 cm^{-1}) its presence should not be a sign of instability.

4.2.2 Protocol for MD simulations

As indicated in section 4.2.1, the total simulation time frame depends on each specific configuration, ranging from one to a few nanoseconds. Full-solvent simulations consisted of 400 ps of equilibration followed for collection of trajectories every 200 steps during the last 200 ps of production time. We emphasize that the simulation length of 600 ps used in our full-solvent simulations is justified both by rough estimates of relaxation times of PAMAM dendrimers smaller than fifth generation that are expected to be less than 100 ps -estimate inferred from Monte Carlo simulations[123,124] - and also by convergence achieved in the time evolution of the total energy in our MD simulations.

We use cubic periodic boundary conditions and account for the long-range electrostatic interactions with Ewald summation.[88] Although relatively small cutoffs in the order of 12 Å[125] are commonly used, we chose a larger cutoff of 22 Å to achieve a better description of electrostatic interactions.[126] Our longer cutoff is set according to the conventional multiple time-step algorithm[127] in which explicit calculation of forces is

implemented in an inner shell of a given radius –of 16 Å - and forces are updated for the outer shell -of 22 Å - every three MD timesteps. The timestep used was 0.001 ps.

The Nose-Hoover[92] thermostat –with 1.0 ps relaxation time- is used to keep the system temperature around 300K under the NVT ensemble formalism. These computational techniques are used as implemented in DL_POLY_2 molecular dynamics package.[93]

4.2.3 Estimation of Lennard-Jones parameters for Cu(II)

The modeling of the hydration of Cu(II) using AIMD techniques[128] has been questioned[129,130] because of the particular choice of DFT functional and the small system size. An alternative method -although also very demanding[129]- is QM/MM MD a molecular dynamics technique that treats a small region of the system with QM and the surroundings with MM using appropriate force fields.[129] However, classical MD methods are still the most popular due to their low computational cost, although they require a careful force field selection and parameterization.

Since our interest is to get a reasonable picture at a modest computational cost, we chose a simple set of force fields, namely a two-body Coulombic plus Lennard-Jones potential to describe the Cu(II)-water interactions and placed special efforts in the force field parameterization.

Cu(II) is modeled as a point charge of +2 -a reasonable assumption in light of recent research that has detected no other Cu species but Cu(II) when forming complexes to dendrimers.[64] To determine the LJ parameters for the Cu(II)-water interaction, the non-bonded distance and energy parameters corresponding to Cu(I) in tetrahedral coordination as reported in the UFF[86] potential were taken as initial values for the length and energy LJ parameters respectively. Then, maintaining the energy parameter unchanged, the length parameter was modified until obtaining a six-fold coordination (1^{st} shell running coordination number of six) and the first peak position in the Cu-OW radial distribution (Figure 4.2) matching both reported average values of 2.12 Å[131,132] and our own DFT calculations where the average $(4\ O_{eq} + 2\ O_{ax})/6$ amounts

to 2.12 Å - although our DFT calculated geometry is not strictly a distorted octahedron: the equatorial plane forms an angle different than 90° with the axial axis. To this purpose (optimization of the LJ length parameter) MD simulations for a system of one ion and 523 water molecules, with cutoff of 8.5 Å were performed. The initial configuration was given by a box-centered cation.

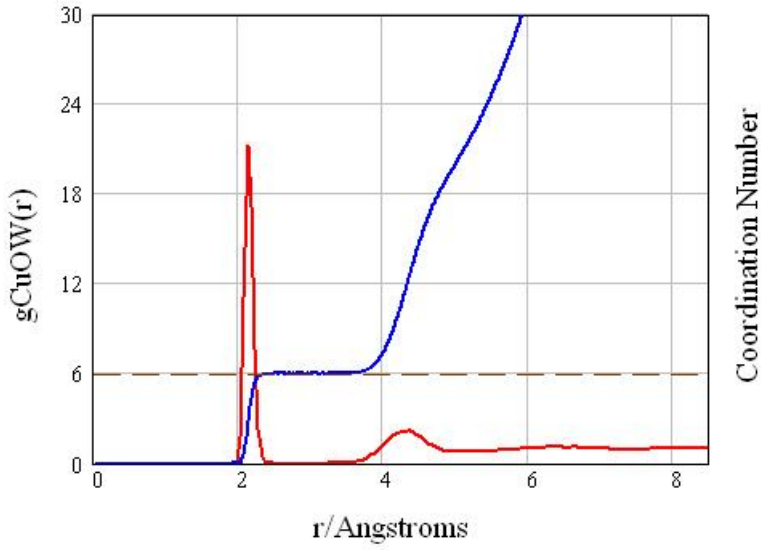

Figure 4.2. Radial distribution function (red line) and running coordination number (blue line) for the interactions Cu(II)-water (Cu(II)-OW)

The parameterization of two-body potential function to describe the Cu(II)-water interactions has been discussed by several authors. Rode and Schwenk[129] evaluated two approaches: classical pair + 3-body potential correction and a QM/MM approach. Our results are in agreement with theirs in the position of the $g_{Cu\text{-}OW}(r)$ first peak maximum (2.12 Å) and first shell coordination number of 6.0. However we obtain a higher peak height, about 20, compared with their values of 15 and 10 for the classical pair potential + three-body correction and for the QM/MM approach respectively. Two main differences may account for such discrepancy: the water model used by these authors is the BJH-CF2[133] whose geometry corresponds to gas-phase water, whereas the SPC/E

model we used is for liquid water that has longer O-H bond length and angle, representing the molecular properties of water in the liquid state. The second difference is their use of a three-body correction to the two-body potential. In their simulations and ours, the hydrated complex obtained with the classical potentials corresponds to a hexahydrate in octahedral configuration. But in their QM/MM model, these authors obtain an alternative octahedral distorted (4+2) configuration, showing equatorial and axial water molecules around the Cu(II) ion. Experimental residence times of water in the first shell of the ion have been reported to be 230 ps at 298 K as determined by NMR techniques[134] although it was argued that the technique might not to be accurate in the picosecond timescale.[129] It is speculated that due to the very short life time of a Jahn-Teller distortion the experiments cannot distinguish between alternative configurations, so the measurement corresponds to an average of all geometries. As our potential does not intend to reproduce Jahn-Teller effects we do not attempt to calculate any residence time of water in the Cu(II) first coordination sphere.

Finally, as the O-O LJ parameters are known for the SPC/E water model, the Lorentz-Berthelot rules were applied yielding a Cu(II)-Cu(II) length parameter of 2.9283 Å. The Cu(II)-Cu(II) energy parameter taken from UFF[86] is 0.050 kcal/mol.

4.3 Results and discussion

In this section we analyze radial distribution functions (*rdf*s) and the time evolution of distances between the ion and the various sites, obtained from MD simulations for the complete systems, as well as DFT calculated bond distances and energies for a 38-atom dendrimer fragment in contact with the hydrated ion.

From experimental work done in Cu(II)-dendrimer complexes is not clear whether Cu(II) coordinates to six or five atoms. Some studies state[64,135] that either trigonal bipyramidal or base pyramidal geometries are more likely to be found in such complexes. On the other hand, Diallo et al.[21] proposed two-site models that implicitly assume hexacoordination and other experimental work suggests a (4+2) coordination for Cu(II) when present in dilute aqueous solutions of similar complexes.[136,137] This debate

is reminiscent of the one held for Cu(II) in aqueous solutions where supportive evidence for penta-[128] and hexacoordination[129] has been presented. In line with the currently accepted six-fold coordination for Cu(II) in water[130,138] we assume that Cu(II) will retain its hexacoordination when forming complexes with molecules such as peptides[136] and dendrimers[21]. Table 4.1 displays the identity of the nearest six atoms to Cu(II) as well as their time averaged distances to Cu(II) obtained from the MD simulations initiated as described in section 4.2.1.

Closeness to both the amide oxygen (atom type O) and hydroxyl oxygen (atom type OT) is evident in all cases except in configuration A2 (two amide O are the closest atoms), and in one of the two Cu(II) in configuration B1. Moreover, when coordination to O and OT exists, the distance Cu(II)-hydroxyl O is slightly shorter than the distance to the closest amide O except in B2 where the opposite trend is observed.

Table 4.1: Time averaged bond distances (in Å) between Cu(II) and its six closest neighboring atoms. OT: hydroxyl O; O: amide O; OW: water O; NC: tertiary N in the EDA-core. Superscripts *a* and *b* designate two different Cu(II) ions in the dicationic complexes. Superscript c designates the average of the two closest average Cu(II)-NC bond distances (See figure 4.3)

	Configuration						
n-closest	A1	A2	A3	B1		B2	
atom	Cu(II)	Cu(II)	Cu(II)	Cu(II)[a]	Cu(II)[b]	Cu(II)[a]	Cu(II)[b]
1st	1.95 (OT)	1.92 (O)	1.92 (OT)	1.94 (OT)	1.95 (O)	1.91 (O)	1.93 (OT)
2nd	1.97 (O)	1.92 (O)	1.94 (O)	1.97 (O)	2.15 (OW)	1.95 (OT)	1.93 (O)
3rd	2.15 (OW)	1.94 (O)	2.17 (OW)	2.15 (OW)	2.15 (OW)	1.95 (O)	1.95 (O)
4th	2.16 (OW)	2.16 (OW)	2.17 (OW)	2.15 (OW)	2.15 (OW)	2.17 (OW)	2.16 (OW)
5th	2.16 (OW)	2.18 (OW)	2.17 (OW)	2.15 (OW)	2.16 (OW)	2.18 (OW)	2.17 (OW)
6th	2.17 (OW)	2.65[c] (NC)	2.17 (OW)	2.17 (OW)	2.16 (OW)	2.18 (OW)	2.18 (OW)

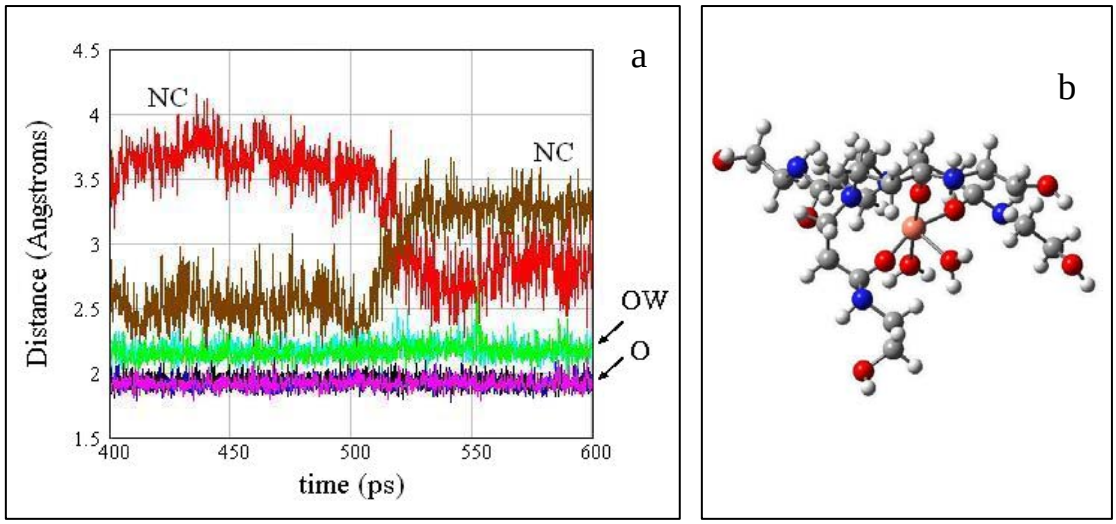

Figure 4.3. Time evolution of Cu(II)-closest atoms for configuration A2. (a) Time evolution for Cu(II) coordinated to three amide O (O), two water O (OW) and one core tertiary amine N (NC) (b) Snapshot after 600 ps MD. Note: the plot suggests that coordination to core N switches identity approximately every 100 ps

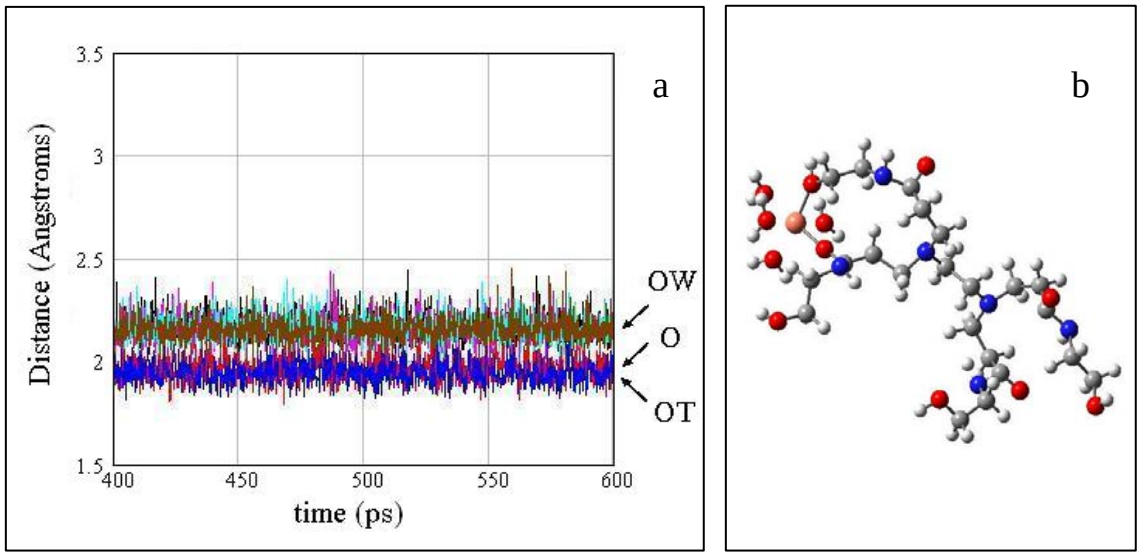

Figure 4.4. Time evolution of Cu(II)-closest atoms for configuration A1. (a) Distances between Cu(II) and one amide O (O, red line), one hydroxyl O (OT, blue line) and four water O (OW) b) Final configuration after 600 ps MD

The presence of two to five water molecules in the first coordination shell is evident. It is also noticeable -in all the cases- that even the farthest Cu(II)-non-OW distance –which ranges 1.94 Å to 1.97 Å- is closer than the closest Cu(II)-OW distance which ranges 2.15 Å to 2.17 Å. These results indicate that proximity to the amide O and hydroxyl O are preferred by the Cu(II) ion.

4.3.1 Cu(II) coordination to tertiary amines in core site and branching points

For configuration A2 the closest distances Cu(II)-NC average 2.78 Å and 2.52 Å (their average in turn is 2.65 Å (See Table 4.1). Further, the time evolution (Figure 4.3) of the distances Cu(II)-dendrimer atoms in this system suggests a loose coordination to these two tertiary amine N sites which contrasts with the steady behavior of the bond distances Cu(II)-OW, Cu(II)-OT and Cu(II)-O observed in the rest of configurations like A1 shown as an example in Figure 4.4. In the rest of configurations the Cu(II)-NC highest *rdf* peak (not shown) is found between 3.98 to 7.23 Å suggesting that the NC atoms are much less involved in binding to Cu (II), as expected for low generation dendrimers.[139]

On the other hand, DFT calculations with the 38-atom dendrimer fragment provide insights on how tertiary amine N binds to Cu(II) especially when water is coordinated to the ion. Our DFT calculated bond distances for Cu(II)-N3 (See Table 4.2) are 2.03 Å (for the naked ion) and 2.05 Å (for the ion hydrated with three water molecules) seem to agree more closely with experimental results for Cu-N distances that range 2.01-2.02 Å in like-complexes[137] than the single Cu(II)-NC bond distance obtained by MD for configuration A2. Thus, the agreement of the Cu-N distances with experimental data suggests that the DFT model may be a fair representation of the Cu-N3 interaction in dendrimer outer pockets, whereas our MD model reasonably describes the solvent and dendrimer effects found in G0.

Table 4.2: Bond distances Cu(II)-closest neighboring atoms from DFT calculations. Superscripts a-e are used to designate different atoms of the same type (two different O and five different OW). N3: tertiary amine, O: amide oxygen; OW: water oxygen, N2: amide nitrogen

complex	N3	O^a	O^b	OT	OW^a	OW^b	OW^c	OW^d	OW^e	N2
D38AF -Cu(II)	2.03	1.85	1.85							
D38AF -Cu(II)-6H_2O	5.26	1.99			2.05	1.98	2.00	2.32	2.60	4.05
D38AF -Cu(II)-4H_2O	5.86	1.99		2.03	2.00	2.03	2.21	3.38		3.55
D38AF -Cu(II)-3H_2O closed	2.05	1.99	1.99		2.06	2.28	2.49			4.01
D38AF -Cu(II)-3H_2O open	2.05	1.98	1.98		2.06	2.40	2.44			

Experimental evidence of Cu(II) binding to N atoms has been suggested by several authors. Unfortunately, the majority of these studies have been done on $–NH_2$ terminated dendrimers. For instance, release of Cu(II) to bulk solution upon protonation is often interpreted as proof that Cu(II) was binding to tertiary amine N prior to protonation.[21] However, in these dendrimers, primary amines (N1) are more basic than tertiary amines (N3). Therefore, it can not be concluded that Cu(II) was exclusively coordinated to tertiary amine sites. Neither can it be inferred that prior to protonation Cu(II) was bound *solely* to N1, because $–NH_2$ functional groups could bind preferentially protons rather than Cu(II) ions. On the other hand, the simultaneous binding of Cu(II) to both $–NH_2$ surface groups and tertiary amines was suggested by an EPR study[120] has been challenged by a recent study that proposed involvement of other atom sites like amide N.[121] This involvement was suggested on the basis that it is less likely to have Cu(II) simultaneously coordinated to N3 and N1 given the relative long distance between N1 and N3.

4.3.2 Cu(II) coordination to amide group

Coordination to either O or N amide atoms has not been inferred from experimental work,[21] although some evidence has been suggested by interpretation of FT EXAFS measurements[121]. However, assignment of coordination to either O or N is difficult[21] because of the acknowledged uncertainties inherent to the FT EXAFS fitting technique such as similarity in backscattering functions for O and N atoms which are close in

atomic weight, size, and electronic configuration.[64] Also, the reported measurement accuracy of ± 0.02 Å [21] may not reflect the errors incurred in the FT EXAFS fitting relying on the assumption of bond length invariance within the dendrimer structure[121] (i.e. C-C, C-N, C=O and other bond lengths retain their typical values found in smaller molecules[140] thus neglecting the effect of environmental variables such as the presence of Cu(II), solvent, branch folding, among others that may affect those bond lengths). For instance, our DFT study shows a lengthening of the C=O bond when Cu(II) binds to amide O in the presence of water. The calculated C=O bond lengths in a 38-atom-fragment interacting with Cu(II) and also with $Cu(II)(H_2O)_3$ are 1.28 Å for the naked ion, and 1.27 Å for the solvated ion, a difference of 0.05 Å from the accepted C=O bond length of 1.23 Å.[140] Thus, we suggest that DFT calculations could help in future refinements of EXAFS studies as reported recently.[141] Another factor that may affect the EXAFS results is the state of the sample used in the analysis, since changes in bond distance Cu(II)-water O when switching EXAFS measurements in fluorescence mode from powder to slurry[142] have been reported. In the following sections we discuss our results for Cu-amide interactions and relate them to experimental results.

4.3.2.1 Cu(II)-amide N bond distance

The time evolution of the Cu(II)-N2 bond distances (not shown) for configuration A2 shows a steady behavior with values that range from 3.83 Å to 3.91 Å confirming that Cu(II) is not as close to the amide N as it is to other atom sites. Also our DFT bond distances (Table 4.2) reveal that this proximity is at least in the range 3.55 Å to 4.05 Å, which is almost twice the distance of Cu(II) to coordinating atoms. Therefore we can not attribute a participation of the amide N in Cu(II) coordination as suggested by the EXAFS work of Tran et al.[121]

4.3.2.2 Cu(II)-amide O bond distance

The time evolution of Cu(II)-amide O distances indicate that they range from 1.91 Å to 1.97 Å (Table 4.1). On the other hand, the DFT calculations show that for the 38-atom

fragment the Cu(II)-O bond distance is 1.85 Å (Table 4.2) in absence of water, but upon addition of three water molecules this equatorial bond distance enlarges up to 1.98-1.99 Å (*vide infra*) -in the rest of configurations we found a Cu-O bond distance of 1.99 Å also- in closer agreement with experimental results for the Cu-N distances (that may be Cu-O distances considering the EXAFS interpretation problem discussed above) reported in works by Tran et al[121] and Diallo et al.[21]

Tran et al. also reported ^{13}C NMR and ^{1}H NMR results and attributed broadening of the C=O signal to coordination of nearby Cu(II) ion to the amide N; however the same phenomenon could also be attributed to Cu(II) coordination to the amide O. Thus, their interpretation of experimental data is not conclusive. Tran et al. [121] disregarded coordination to amide O stating that four or five N atoms were located at 1.98 Å and one N or O at 2.84 Å in the first Cu(II) coordination sphere.

Comparison of FT EXAFS fitted Cu(II)-equatorial atoms with literature values of Cu(II)-O bond distances for like-complexes is commonly used to rule out coordination to amide O. Diallo et al[21] followed this criteria and although they acknowledged that validation of their models is a pending issue they compared their EXAFS FT fittings (with assumed Cu-N distances of 2.00 Å ± 0.02 Å) to Cu(II)-O bond distances of 1.93 Å - 1.96 Å referring to published literature,[136,137,142] although the data described in those articles hardly ever support their assertions. In another set of experiments, Diallo et al.[21] conducted a pH-regulated Cu(II) uptake experiment in amido-terminated dendrimers and as no uptake of Cu(II) was observed at pH 5.0 they concluded that amido groups are unable to bind Cu(II). However, it is known that amido groups – that bear negative partial charge in the amide oxygen- can attract free protons to their neighborhood to form strong hydrogen bond interactions.[143] Therefore if protons are found sorbed in the dendrimer exterior, electrostatic repulsion between them and the potentially approaching Cu(II) ions can provide an alternative interpretation to the inability to find Cu(II) sorbed to the dendrimer, instead of being a signal of the absence of Cu-amido group interactions.

We conclude that the exposed arguments inferred from experimental information regarding lack of coordination to the amide O site are not convincing; instead fair agreement between experimental Cu-equatorial bond distances and our MD calculated Cu-O bond distances suggests coordination to amide O.

4.3.3 Cu(II) coordination to end group hydroxyl O

Table 4.1 shows that the shortest bond distance obtained by averaging its time evolution for individual atoms ranges 1.92 Å to 1.95 Å whereas the DFT bond distance found for the 38 atom-fragment-Cu(II)-$(H_2O)_4$ (Figure 4.5 part d) coordinated to four water O, 1 amide O and 1 hydroxyl O is 2.04 Å. Therefore there is a discrepancy between our DFT and MD values amounting at least up to 0.09 Å. One reason for such discrepancy might be attributed to inaccuracies in the LJ parameters used for hydroxyl O, taken from the DREIDING force field,[87] which may not faithfully describe a hydroxyl O.

4.3.4 Cu(II) coordination to water

Average values of the Cu-water oxygen (Cu(II)-OW) distances were reported in Table 4.1, and their time evolution in Figures 4.3 and 4.4 with values that range 2.15 Å to 2.18 Å. From the DFT calculations it is observed that the Cu(II)-water O bond distances differ depending on where water binds and on the configuration details. For instance, the equatorial water in the 38-atom-fragment-Cu(II)-$(H_2O)_3$ complex sits 2.06 Å away from Cu(II) both in the open and closed configuration whereas in the 38-atom-fragment-Cu(II)-$(H_2O)_4$ the two water molecules locate at 2.00 Å and 2.03 Å and at 2.01 Å –as an average- in the 38-atom-fragment-Cu(II)-$(H_2O)_6$. On the other hand, the axial waters in the 38-atom-fragment-Cu(II)-$(H_2O)_3$ are –in average- found at 2.39 Å and 2.42 Å for the closed and open configurations respectively, 2.46 Å for the 38-atom-fragment-Cu(II)-$(H_2O)_6$ whereas two axial waters in the 38-atom-fragment-Cu(II)-$(H_2O)_4$ complex are found at 2.21 Å and 3.38 Å. The latter value differs significantly from what it seems to be a typical bond distance for axial waters.

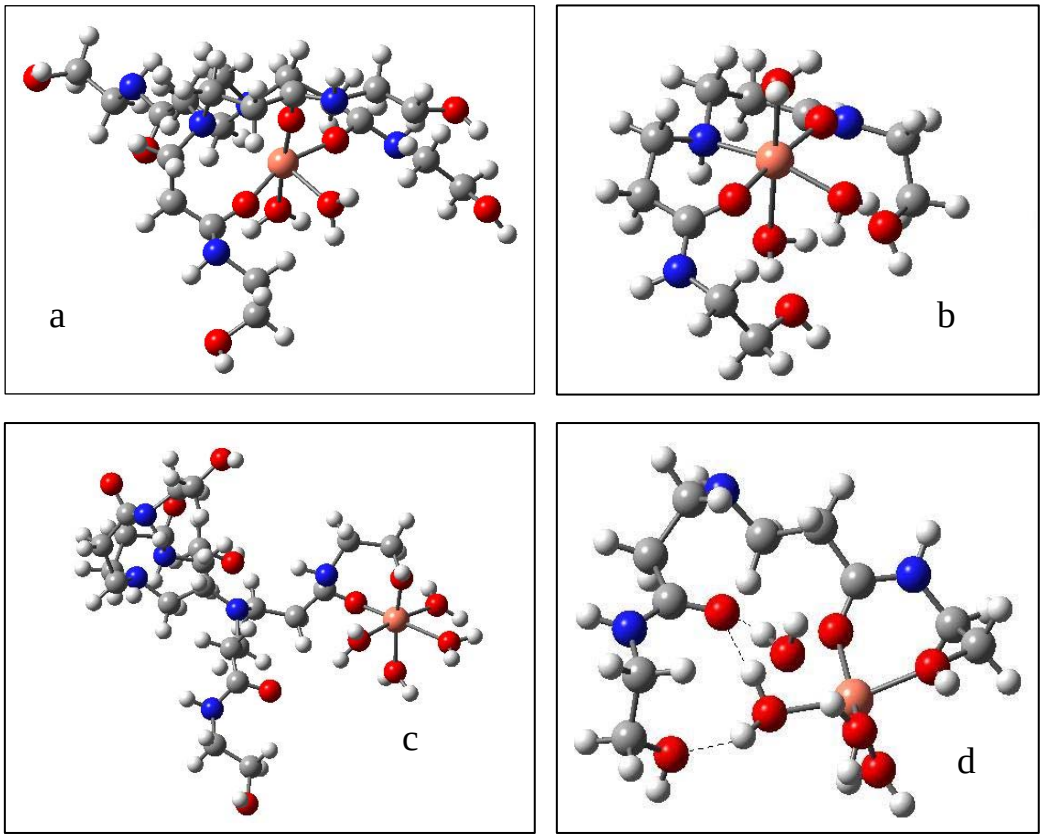

Figure 4.5. MD and DFT structures for monoionic Cu(II)-G0OH complexes. (a) Full-solvent MD final configuration A2 : Cu(II) is coordinated with two amide O, one tertiary N in EDA-core and one water O in equatorial position. Branch folding places one amide O in axial position (the other is occupied by one water O). For clarity, water molecules other than those in the first coordination sphere of the ion are not shown. (b) 38-atom-fragment-Cu(II)-$(H_2O)_3$ closed DFT (optimized structure) : Cu(II) coordinates in a similar fashion to (a) except that the branch folding effect is obviously not reproduced; another water O substitutes the amide O of the dendrimer branch. Here the equatorial water and one of the axial waters form hydrogen bonds R'-CH2-(OH)---HOH---(OH)-CH2-R' to both hydroxyl O atoms with lengths 2.12 Å and 1.99 Å respectively. These H-bonds may explain its enhanced stability compared to the "open" configuration. (c) Full-solvent MD final configuration A3 : Cu(II) is coordinated to one amide O, one hydroxyl O and four water O. (d) 38-atom-fragment-Cu(II)-$(H_2O)_4$ (optimized structure) : Coordination to one amide O, one hydroxyl O and two water O in equatorial plane and one water in axial position. One of the equatorial waters forms H-bond –dashed lines - as R'- C=O---HOH---(OH)-CH2-R at 1.81 Å (with carbonyl O) and 1.81 Å (with hydroxyl O). The fifth water is in quasi-axial position (bond distance larger than typical Cu-O axial bond distance) and forms H-bonds with one amide O at 1.78 Å and with the equatorial water at 1.60 Å

Coordination to axial sites with either one[121] or two[21,64] ligands suggested to be O-carriers has been proposed based on FT EXAFS spectra of Cu(II)-dendrimer solutions. Although the identity of those ligands has not been unambiguously determined[64], Diallo

et al. suggest those ligands are water based on their estimated Cu-O bond distances of 2.32 Å and 2.39 Å found for PAMAM G1 and G5.[21] D'Angelo et al. reported two axial Cu-O distances of 2.40 ± 0.06 Å in bi(glycinato)-Cu(II) complexes.[136] These distances are larger in 0.11 Å than those observed in EXAFS of Cu(II) aqueous solutions.[132,138] Evidence for equatorial coordinated water was found in the monoglycinato copper complex.[136]

Since our DFT calculations cannot reproduce the octahedral distorted structures, we can not report a unique Cu-O bond distance. Instead our results indicate that the Cu-O equatorial distance ranges from 2.00 Å to 2.06 Å and the axial distance ranges from 2.21 to 2.40 Å. Clearly the complexity introduced by the Jahn-Teller effect makes difficult not only accurate experimental determinations but also DFT calculations of complexes.

From the analysis of the MD trajectories predominance of water oxygen (atom type OW) is found in the first coordination shell. This should not be surprising as it is known that the G0 dendrimers are regarded as open dendrimers[144] so water can easily reach the dendrimer sites as mentioned by Ottaviani et al.[139] In summary, coordination of Cu(II) with O atoms is interesting because it is reminiscent of a tendency for Cu(II) to recover coordination to O atoms as in a hexahydrated Cu(II) complex. However we do not dismiss coordination to N atoms, but we suggest that the type of atom sites involved in binding of Cu(II) would depend on the solvent used and dendrimer size, surface group and shape, among other factors.

4.3.5 Full solvent effect

In this section we provide details about DFT optimized configurations of the 38-atom fragment complexed with hydrated Cu(II) and make some comparisons with configurations found in the MD simulations. Table 4.2 displays the main distances of Cu(II) to its closest neighboring atoms some of which have already been discussed in the preceding sections.

A comparison between a fully solvated system (Figure 4.5 part a, MD results) and one where only three water molecules are present (Figure 4.5 part b, DFT results) indicates that in spite of the presence of bulk water in the surrounding environment, “closed” configurations where the dendrimer branches contribute to a “cage” effect, can continue being energetically favorable as compared to “open” structures. In fact, a difference of ~ 6 kcal/mol is found by our gas-phase DFT calculations in favor of the closed over the open structure.[145] The binding of Cu(II) to the dendrimer fragment takes place by attachment to two amide O and the branching N atom (Figure 4.6 part a and Table 4.2), and such structure is maintained when Cu(II) is hydrated by three water molecules as in the open and closed configurations (Table 4.2). However, when Cu(II) is hydrated by four or six water molecules (Figures 4.5. part d and 4.6. part b), the coordinations to N and to one of the amide O are lost and substituted by coordination to water oxygen atoms.

In contrast to Figure 4.5.a, the single-ion attachment shown by Figure 4.5.c illustrates a more open configuration where the ion attaches to the terminal OH group and to one amide O, retaining four of the six water molecules present in the bulk water hexahydrate.

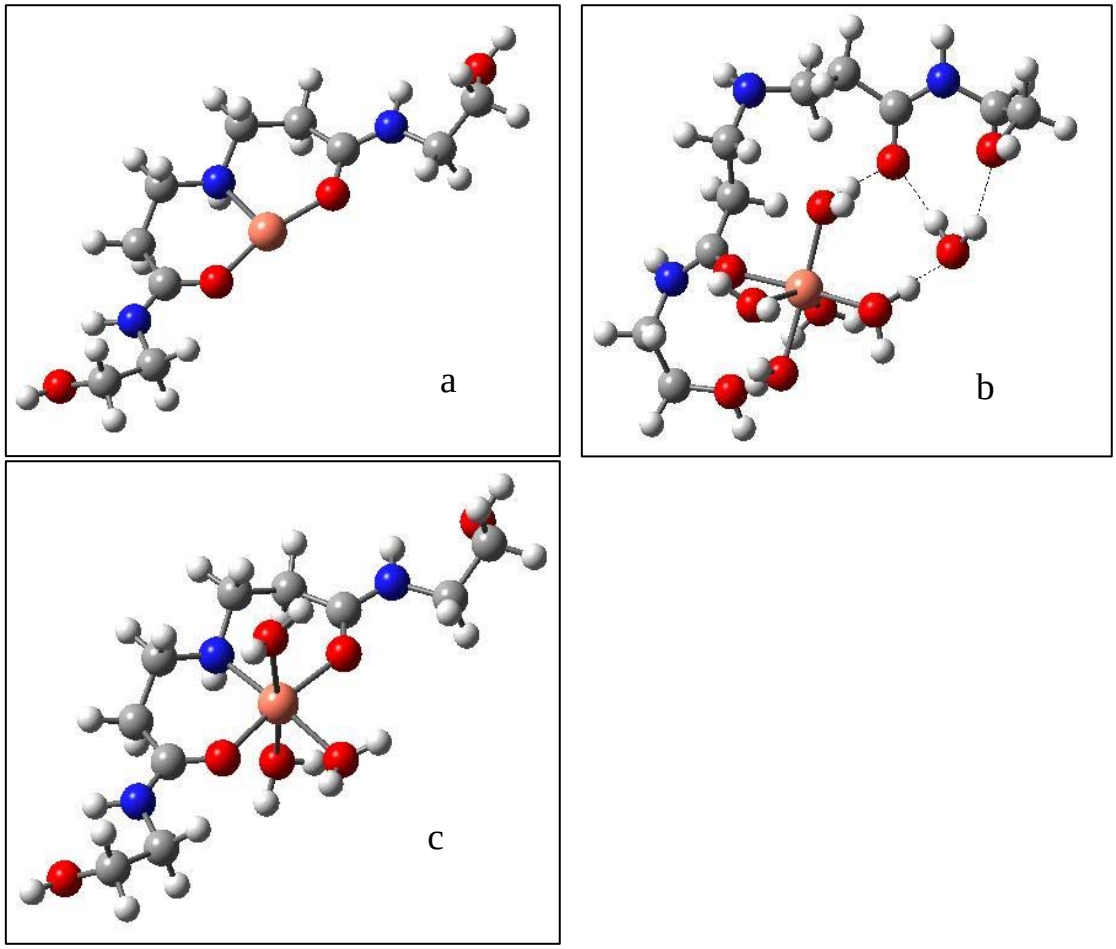

Figure 4.6. DFT optimized configurations of outer pocket-Cu(II) complexes. (a) 38-atom-fragment-Cu(II): Cooperative effect of two amide O to the branching N is evident. (b) 38-atom-fragment -Cu(II)-$(H_2O)_6$: Coordination to one amide O and five water O (3 equatorial and 2 axial). Water interacts with dendrimer atoms forming H-bonds: b1. R-CH2-(OH)---H, length: 1.83 Å. b2. The sixth water molecule sits in the second coordination shell and forms two hydrogen bonds –dashed lines- R'-C=O---HOH---(OH)-CH2-R in the adjacent branch at 1.81 Å (amide O) and 1.94 Å (hydroxyl O). (c) 38-atom-fragment -Cu(II)-$3H_2O$ open configuration: Coordination to one branching N, two amide O and one water O in equatorial plane and two water O in axial positions

Figure 4.7 displays snapshots of typical MD configurations. The MD snapshots shown in Figure 4.5.c and also those in Figures 4.4.b, 4.3.b, and 4.5.a correspond to stable configurations obtained after 600 ps of full-solvent simulations- they are representative of their respective equilibrated systems initiated from Configurations A1,

A2 and A3 *(vide supra)*. Figures 4.7.a and 4.7.b illustrate configurations of the two-ion attachment to G0-OH; in both cases a strong participation of the dendrimer branches is observed.

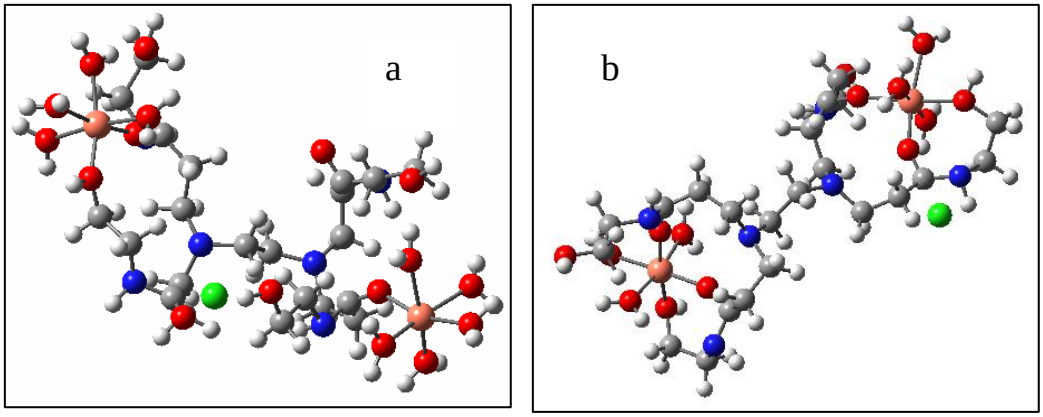

Figure 4.7. Snapshots of the fully solvated MD simulations of dicationic G0-OH-Cu(II) complexes. For clarity, water molecules beyond the ionic first coordination shell are not shown. (a) Coordination of one Cu(II) to an amide O , an hydroxyl O and four water O and another Cu(II) to one amide O and five water O in the opposite part of the dendrimer that remains open. Two branches and their environment can at least hold one Cu(II). (b) Coordination of both Cu(II) to two amide O, one hydroxyl O and three water O atoms. Again the flat configuration enables the attachment of two branches to each ion. The green atoms are Cl^- counterions

4.3.6 Interactions of Cu(II) with other Cu(II) ions and counterions

4.3.6.1 Cu(II)-Cu(II) bond distance

The Cu(II)-Cu(II) *rdf*s (data not shown) show a broad peak centered at about 12.5 Å with width of about 5 Å (measured at the bottom of the peak) for the Configuration B1 whereas for Configuration B2 a slightly narrower but sharper peak with height twice the aforementioned is observed at 10.88 Å. Time averaged distance Cu(II)-Cu(II) over all the configurations yield 12.6 Å and 11.3 Å for B1 and B2 configurations respectively. Thus, the results are not in agreement with the findings of Diallo et al.[21]: Cu(II)-Cu(II) coordination number of 1.9 and separation distances of 3.0 Å for G1-NH_2. The

calculated behavior may be partially explained by electrostatic repulsion but also by solvent screening thus suggesting that the solvent plays an important role in stabilizing up to two Cu(II) ions in low generation dendrimers.

Nevertheless we should exercise caution with this assertion as this study reveals that a monoionic charged complex could be stable as suggested by results from configuration A2 where an increased chelate effect (three branches coordinating a single ion) is clearly observed. Consequently a final word on this issue cannot be given yet.

4.3.6.2 Cu(II)-Cl^- and Cl^--Cl^- bond distances

The highest peak locations (data not shown) in the Cu(II)-Cl *rdf*s for configurations A1, A2, A3, B1 and B2 are 16.93 Å, 9.38 Å, 13.28 Å, 6.68 Å and 6.53 Å respectively. It is remarkable that only in one of them (B2) the peak is sharp and nearly four-fold larger than in the others. The Cu(II)-Cl distances in the single ion configurations (A1 to A3) indicate that the counterion is not significantly attracted by the Cu(II) ion suggesting that a solvent screening effect takes place. Therefore it can be concluded that the counterions are far enough from the Cu(II) ions to be regarded as ion pairs.

Finally, the Cl-Cl *rdf*s (data not shown) highest peak positions in the various simulations are 18.78 Å, 10.73 Å, > 22 Å, 5.38 Å and 9.48 Å showing that as an average counterions remain separated from each other in the bulk solution.

4.3.7. Atom site solvation by water: OT-HW, O-HW, N2-HW and NC-HW bond distances

In this section we report the first –not necessarily the highest - peak location for the interactions of the H atom in water (HW) with the following atom sites: hydroxyl O (OT), amide O (O), amide N (N2), and tertiary amine N in the EDA-core (NC). These atoms are selected among other atom types because they bear the highest negative partial charges according to DFT charge distribution calculations discussed in Chapter III.

Table 4.3: First peak locations (Å) and respective peak heights (dimensionless) for OT-HW, O-HW, N2-HW and NC-HW *rdf*s. OT: hydroxyl O; O: amide O; N2: amide N; NC: tertiary amine in EDA-core

	OT-HW		O-HW		N2-HW		NC-HW	
configuration	position	height	position	height	position	height	position	height
A1	1.68	1.02	1.73	1.05	1.93	0.27	1.93	0.06
A2	1.68	1.38	1.73	0.37	1.88	0.12	1.83	0.14
A3	1.68	1.08	1.73	1.11	1.93	0.27	1.98	0.007
B1	1.63	1.07	1.73	0.66	1.88	0.24	1.98	0.017
B2	1.68	0.70	3.13	0.53	1.88	0.09	1.93	0.219

Table 4.3 shows that with the exception of the hydroxyl oxygen (OT), the dendrimer atoms do not have a significant amount of water molecules in their closest vicinity. This is inferred by the height of the first peak, which is in most cases much lower than one, i.e., the atomic density found at the first peak location is much lower than the bulk atomic density. The H-bond length OT-HW seems to be unusually short so it may be indicative of inadequacies in the force field description of the OH group –as suggested in section 4.3.3.

4.4 Summary

The current MD simulations of PAMAM-G0-OH dendrimers incorporating the full solvent effect reveal that both “closed” configurations where the dendrimer branches contribute to a “cage” effect, and “open” structures may be found. “Closed” configurations are however slightly more energetically favorable than the “open” ones. Moreover, “closed” configurations are also found in dicationic Cu(II)-G0 complexes with strong participation of the dendrimer branches in the complexation. Coordination to amide oxygen and water oxygen seems to be dominant whereas coordination to the tertiary amine nitrogen in EDA-core is expected to be less frequently found and weaker.

On the other hand, DFT calculations in dendrimer outer pockets showed that Cu(II) is able to bind to tertiary amines and to amide O and also to water molecules. This could occur in similar environments for large dendrimers granted that backfolding of branches does not occur.

CHAPTER V
TETRACHLOROPLATINATE ANION AND ITS MONO- AND DIAQUATED SPECIES: STRUCTURE AND ENERGETICS*

5.1 Introduction

Tetrachlorometallate alkaline salts such as tetrachloroplatinate (K_2PtCl_4) and tetrachloropalladate (K_2PdCl_4) have been extensively used as precursors in the liquid phase synthesis of Pt, Pd, and bimetallic PtPd nanoparticles.[106,146-150] However, the focus of our study is only on tetrachloroplatinate and its mono- and diaquated species.

Aquation (or hydrolysis) of $PtCl_4^{2-}$ occurs with exchange of chloride ligands by water (solvent) molecules. Because the first aquation step is proportional to the initial concentration of $PtCl_4^{2-}$ [151], the larger the concentration of precursor salt, the faster aquation takes place until thermodynamical equilibrium is reached. pH determines which species are present.[151,152]

The distribution of $PtCl_4^{2-}$ anion and its mono- and di-aquated species at equilibrium conditions is calculated as a function of the initial concentration of precursor salt with the equilibrium constants (at 25 °C and μ = 0.5) assigned for the first and second aquation[1] and used to compute the percentage of abundance of these species shown in Figure 5.1 (See mathematical derivation in Appendix A).

Initial concentrations for K_2PtCl_4 as high as 0.04-0.09 M[62] and as low as 10 μM[63] have been used in dendrimer templated synthesis of nanoparticles although typical values are in the range of 0.001 to 0.003 M.[61,147] Depending on the type of solution used (fresh or aged) $PtCl_4^{2-}$ and its mono- and diaquated species can be found present in solution. For instance a completely equilibrated solution of 0.09 M –concentration used in NMR experiments with G2OH[62]– should contain 68 % of $PtCl_4^{2-}$, 31 % of $PtCl_3(H_2O)^-$ and 1 % of $PtCl_2(H_2O)_2$.

---

* Reproduced in part with permission from Tarazona-Vasquez and Balbuena, *J. Phys. Chem. A* **2007**, *111*, 932. Copyright 2007 American Chemical Society.

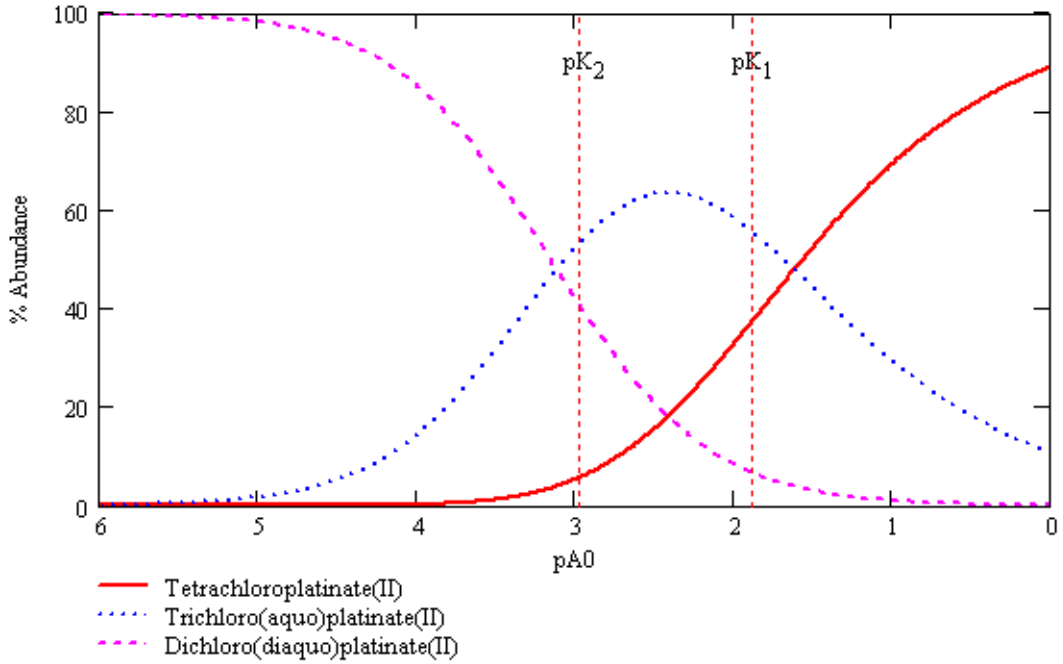

Figure 5.1. Percent of abundance at equilibrium (aged) conditions of tetrachloroplatinate ($PtCl_4^{2-}$) and its mono- and diaquated species as a function of initial concentration of precursor salt K_2PtCl_4 (pA0). At high initial concentration the tetrachloroplatinate anion is predominant whereas the diaquated is the predominant species at low concentration in its *cis* and *trans* isomeric forms. At medium concentration (about 0.01-0.001M) the predominant species is the monoaquated one. A percentage of abundance for each species is defined as [species A]x100/[total]; constants K_1 and K_2 are given by Cotton and Wilkinson[1]; 'pA0' in the abscissa axis is defined as $pA_0^{2-} = -\log([K_2PtCl_4]_0)$

Even if fresh $PtCl_4^{2-}$ solutions were used, its aquation in the bulk solution could take place before it reaches the dendrimer to which it ought to complex. Therefore, it is important to study how feasible the reaction of all these Pt(II) complexes with water is because it can provide a reference to determine how much more (or less) feasible the hydration of the same Pt(II) complexes is when they react with water already in dendrimer outer pockets.

5.2 Methods

DFT was used to obtain minimum energy geometries with no symmetry constraints. The optimization of the geometries was followed by second derivative matrix calculations that provided estimates for the zero point energy (ZPE) and temperature corrections to the enthalpy and Gibbs free energy at 298 K. The calculations were carried out with Gaussian03 suite of programs [74]

The suitability of combining the 6-31+g(d) basis set for light atoms (C, H, O, N and Cl) and Hay and Wadt [84] relativistic pseudopotentials (LANL2DZ) for transition metal atoms was put to test. Calculations for Ni hydrates were made with two basis sets: 6-31g(d) and 6-31+g(d). The gas phase binding energy calculated as $\Delta E_{9,10}$ = $E([Ni(H_2O)_{10}]^{2+})$-$E([Ni(H_2O)_9]^{2+})$-$E(H_2O)$ was -11.10 kcal/mol for B3LYP/6-31g(d)/LANL2DZ. However such value was calculated to be -7.8 kcal/mol for B3LYP/6-31+g(d)/LANL2DZ, in excellent agreement with the reported experimental value[153] of -7.9 kcal/mol. Therefore, it would be adequated to combine basis sets (6-31+g(d) and LANLDZ) for use with B3LYP -and especially for cationic species- to reproduce experimental values of binding energies. In fact, a similar combination has been previously used in a study involving a Pt(II) salt binding an organic molecule.[154]

For sake of consistency, the basis set combination is used for all modeled species regardless they are anions, cations or neutral species. However, in this chapter and the subsequent ones we do not claim we have found the true absolute thermodynamic quantities for a given reaction but rather, relative energies (binding energy, enthalpy and free energy) were evaluated in order to provide accurate insights on the feasibility of the reactions that take place upon interaction of the species with water molecules.

5.3 Results

In order to better describe the configurations shown in the next sections, it will be assumed that there are six binding sites for the hydration of square planar anion $PtCl_4^{2-}$ and its mono- and diaquated species: four sites in the plane of the molecule to be

referred as *equatorial* while and two more above and below the central atom to be referred as *axial*.

5.3.1 $PtCl_4^{2-}$

None of the calculated structures for $PtCl_4^{2-}$ and $PtCl_4^{2-}$-H_2O have stable states with spin multiplicities higher than one. Therefore the same was assumed for its mono- and diaquated species. The following reaction describes the reaction of hydrated $PtCl_4^{2-}$ species (n = number of waters hydrating the reactant) with a water dimer and it is used to model its hydration:

$$(PtCl_4^{2-})(H_2O)_n + (H_2O)_2 \rightarrow (PtCl_4^{2-})(H_2O)_{n+1} + H_2O \qquad (5.1)$$

Several configurations for the hydrated product of this reaction were found (See Appendix C, Table C-1) but only the lowest energy configurations (l.e.c) are shown in Figure 5.2 and Table 5.1.

Table 5.1: Energetics of hydration of $PtCl_4^{2-}$ (kcal/mol) according to eqn 5.1 with n=0-3

n	product config	ΔE_0	ΔH	ΔG
0	1A	-12.2	-12.0	-10.0
1	2A	-11.1	-10.9	-8.8
2	3A	-9.7	-9.8	-6.4
3	4A	-8.6	-7.6	-9.0

The optimized square planar geometry of $PtCl_4^{2-}$ has a Pt-Cl distance of 2.42 Å, distance larger than experimental bond distances (2.31 Å) in K_2PtCl_4 crystals[155] In the l.e.c for $PtCl_4^{2-}$-H_2O, the water molecule sits in an equatorial site; in the l.e.c. for $PtCl_4^{2-}$-$(H_2O)_2$, the two water molecules occupy diametrically opposed equatorial sites; in the l.e.c. for $PtCl_4^{2-}$-$(H_2O)_3$ the water molecules occupy three equatorial sites and in the l.e.c. for $PtCl_4^{2-}$-$(H_2O)_4$ four water molecules saturate the equatorial sites.

In none of these cases, isolated individual waters were found in axial positions. This is in agreement with Ayala et al.[156] who on the basis of the similarity between the XANES spectra of solid state and aqueous solutions of $PtCl_4^{2-}$ concluded that no water molecules were able to bind stably in the axial region. In any case, no oxygen atom was found directly coordinated with the Pt atom.

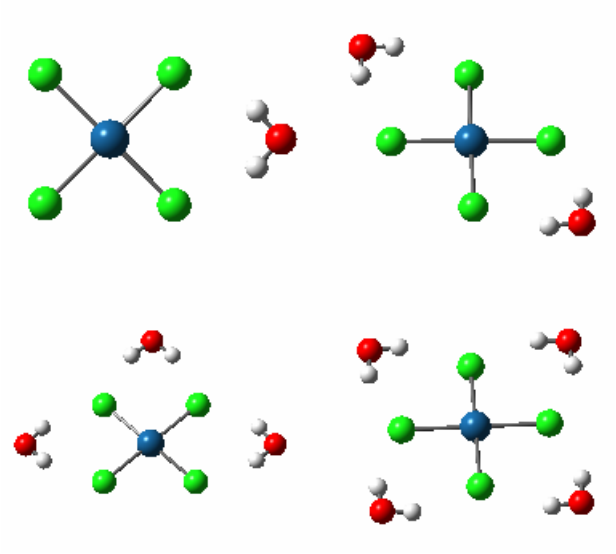

Figure 5.2. Lowest energy configurations for $PtCl_4^{2-}$---$(H_2O)_n$ binding one to four water molecules. Upper left: Conf. 1A, $PtCl_4^{2-}$ –(H_2O); Upper right: Conf. 2A, $PtCl_4^{2-}$ –$(H_2O)_2$. Lower left: Conf. 3A, $PtCl_4^{2-}$ –$(H_2O)^3$; Lower right: Conf. 4A, $PtCl_4^{2-}$ –$(H_2O)_4$

5.3.2 $PtCl_3(H_2O)^-$

The following reaction describes the reaction of hydrated $PtCl_3(H_2O)^-$ (n = number of waters hydrating the reactant) with a water dimer and it is used to model its hydration:

$$(PtCl_3(H_2O)^-)(H_2O)_n + (H_2O)_2 \rightarrow (PtCl_3(H_2O)^-)(H_2O)_{n+1} + H_2O \qquad (5.2)$$

Several configurations for the hydrated product of this reaction were found (See Appendix C, Table C-2) but only the lowest energy configurations (l.e.c) are shown in Figure 5.3. Two distinct types of *equatorial* sites are apparent: a site Cl-Cl located

between two Cl^- ligands –like the four equatorial sites observed for $PtCl_4^{2-}$ -and a site Cl-O located between a Cl^- and water oxygen (Figure 5.3).

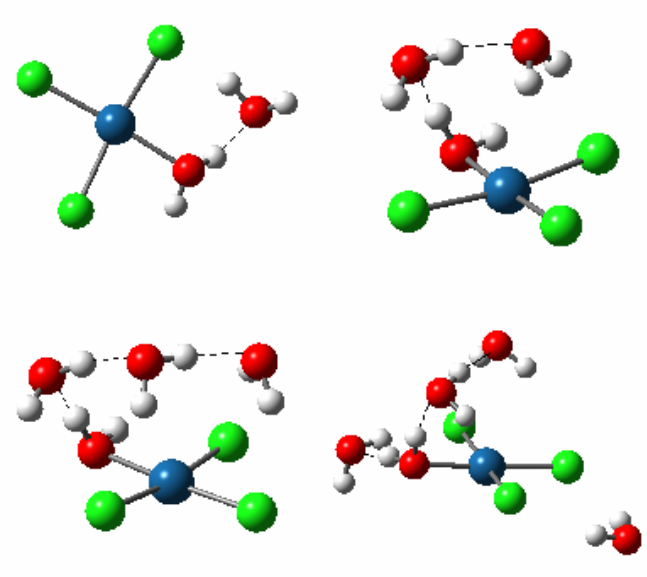

Figure 5.3. Lowest energy configurations for $PtCl_3(H_2O)^-$---$(H_2O)_n$ binding one to four water molecules. Upper left: $PtCl_3(H_2O)^-$---(H_2O) with a H-bond Pt-HOH---OH_2 at 1.76 Å; Upper right: $PtCl_3(H_2O)^-$ –$(H_2O)_2$ with H-bonds Pt-HOH---OH_2 at 1.72 Å and H_2O---OH_2 at 1.90 Å;. Lower left: $PtCl_3(H_2O)^-$ –$(H_2O)_3$ with H-bonds Pt-HOH---OH_2 at 1.66 Å and two H_2O---OH_2 at 1.77 Å and 1.86 Å respectively over the molecular square plane; Lower right: $PtCl_3(H_2O)^-$ –$(H_2O)_4$ with H-bonds Pt-HOH---OH_2 at 1.78 Å and two H_2O---OH_2 at 1.74 Å and 1.89 Å respectively over the molecular square plane

For $PtCl_3H_2O^-$---H_2O, two different configurations for a water molecule occupying each distinct equatorial site were found; however the l.e.c. is that where water occupies the Cl-O site (Figure 5.3). In the l.e.c. for $PtCl_3H_2O^-$---$(H_2O)_2$, a water dimer is oriented across the molecular plane from a Cl-O site toward the diametrically opposed Cl-Cl site; in the l.e.c. for $PtCl_3H_2O^-$---$(H_2O)_3$, a water trimer is on top of the molecular plane center and resembles the l.e.c for $PtCl_3H_2O^-$---$(H_2O)_2$; in the l.e.c. for $PtCl_3H_2O^-$---$(H_2O)_4$ a water dimer is on top of the molecular plane, one water binds to the water ligand and another is in a Cl-Cl equatorial site. In the latter case, ΔG of reaction (Table 5.2) is 0.2

kcal/mol, which considering the error margin involved in DFT calculations it could still be considered thermodynamically feasible (ΔE_0 = -0.6 kcal/mol), although this seems not as clear as in the case of $PtCl_4^{2-}$ discussed above.

In all the preceding hydrated configurations having dimers and trimers on top of the molecular plane, the closest Pt-O distances were found to be 3.31 Å and 3.56 Å respectively values comparable to the previously calculated Pt-O (3.3 Å).[156] However, in none of these cases water molecules stay over the axial sites.

Table 5.2: Energetics of hydration of $PtCl_3(H_2O)^-$ (kcal/mol) according to eqn 5.2 with n=0-3

n	product config	ΔE_0	ΔH	ΔG
0	1A	-5.1	-4.7	-3.3
0	1B	-7.9	-8.3	-4.2
1	2C	-8.0	-8.1	-4.9
2	3A	-7.8	-8.1	-4.4
3	4C	-0.6	0.2	0.2

5.3.3 *cis*-$PtCl_2(H_2O)_2$

The following reaction describes the reaction of hydrated *cis*-$PtCl_2(H_2O)_2$ (n = number of waters hydrating the reactant) with a water dimer and it is used to model its hydration:

$$(cis\text{-}PtCl_2(H_2O)_2)(H_2O)_n + (H_2O)_2 \rightarrow (cis\text{-}PtCl_2(H_2O)_2)(H_2O)_{n+1} + H_2O \qquad (5.3)$$

Several configurations for the hydrated product of this reaction were found (See Appendix C, Table C-3) but only the lowest energy configurations (l.e.c) are shown in Figure 5.4 and Table 5.3. Three distinct sites in *equatorial* position are apparent: one Cl-Cl site and two Cl-O sites as described above, and an additional O-O located between the two water oxygen atoms belonging to water molecules located in *cis* positions to each other.

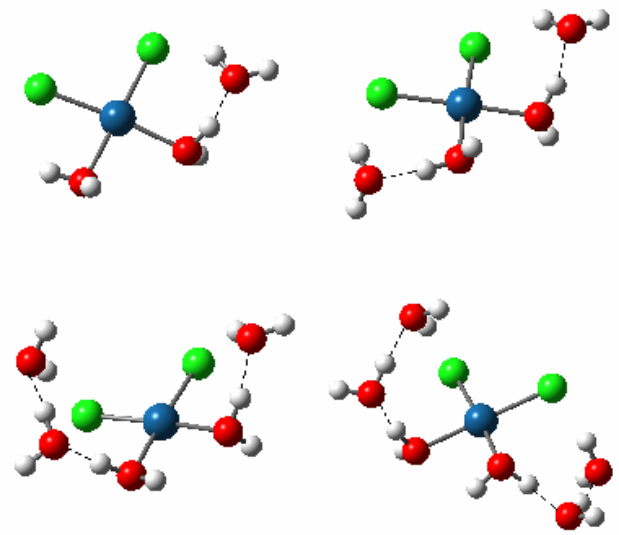

Figure 5.4. Lowest energy configurations for *cis* -$PtCl_2(H_2O)_2$---$(H_2O)_n$ binding one to four water molecules. Upper left: *cis* -$PtCl_2(H_2O)_2$ –(H_2O). There is an H-bond Pt-OH_2---OH_2 with length 1.67 Å ; Upper right: *trans*-$PtCl_2(H_2O)_2$ –$(H_2O)_2$. Two H-bonds Pt-OH_2---OH_2 at 1.66 and 1.64 Å; Lower left: *trans*-$PtCl_2(H_2O)_2$ –$(H_2O)_3$. Two H-bonds Pt-OH_2---OH_2 stemming from adjacent water ligands at 1.61 Å and 1.66 Å and one inter-solvent H-bond HOH---O at 1.72 Å ; Lower right: *trans*-$PtCl_2(H_2O)_2$ –$(H_2O)_4$; Two H-bonds Pt-OH_2---OH_2 stemming from adjacent water ligands at 1.60 Å and 1.61 Å and two H-bond networks above and below the complex (HOH---O) at 1.71 Å and 1.72 Å

The l.e.c. of *cis*-$PtCl_2(H_2O)_2$---H_2O is that where water occupies the Cl-O site; in the next stable configuration water occupies the O-O site, and in the least stable water occupies the Cl-Cl site. This trend is similar to that observed for $PtCl_3(H_2O)^-$---H_2O. In the l.e.c. for *cis*-$PtCl_2(H_2O)_2$--$(H_2O)_2$ each water occupies a Cl-O site; in the l.e.c. for *cis*-$PtCl_2(H_2O)_2$--$(H_2O)_3$ a water molecule occupies a Cl-O site and a water dimer occupies the other Cl-O site, and in the l.e.c. for *cis*-$PtCl_2(H_2O)_2$--$(H_2O)_4$, water dimers occupy both Cl-O sites as their centers of mass locate above and below the molecular plane. No configurations where water binds to axial sites were observed.

Table 5.3: Energetics of hydration of *cis*-$PtCl_2(H_2O)_2$ (kcal/mol) according to eqn 5.3 with n=0-3

n	product config	ΔE_0	ΔH	ΔG
0	1A	1.5	2.3	2.0
0	1B	-6.8	-7.1	-4.3
0	1C	-4.0	-3.9	-1.9
1	2B	-7.3	-7.3	-4.9
2	3A	-4.4	-4.6	-0.9
3	4A	-7.6	-8.0	-3.2

5.3.4 *trans*-$PtCl_2(H_2O)_2$

The following reaction describes the reaction of hydrated *trans*-$PtCl_2(H_2O)_2$ (n = number of waters hydrating the reactant) with a water dimer and it is used to model its hydration:

$$(trans\text{-}PtCl_2(H_2O)_2)(H_2O)_n + (H_2O)_2 \rightarrow (trans\text{-}PtCl_2(H_2O)_2)(H_2O)_{n+1} + H_2O \quad (5.4)$$

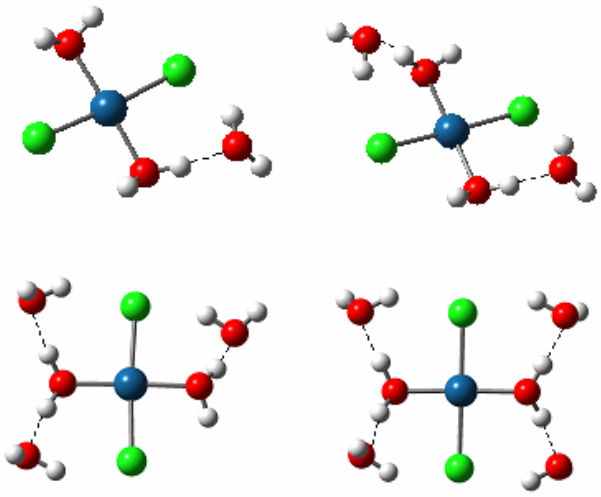

Figure 5.5. Lowest energy configurations for *trans*-$PtCl_2(H_2O)_2$---$(H_2O)_n$ binding one to four water molecules. Upper left: *trans*-$PtCl_2(H_2O)_2$ –(H_2O). There is a hydrogen bond Pt-OH_2---OH_2 1.63 Å; Upper right: *trans*-$PtCl_2(H_2O)_2$ –$(H_2O)_2$. Two hydrogen bonds Pt-OH_2---OH_2 both at 1.64 Å; Lower left: *trans*-$PtCl_2(H_2O)_2$ –$(H_2O)_3$. Three H-bonds Pt-OH_2---OH_2 with lengths 1.65 Å, 1.70 Å and 1.71 Å; Lower right: *trans*-$PtCl_2(H_2O)_2$ –$(H_2O)_4$; Four H-bonds Pt-OH_2---OH_2 with lengths 1.70-1.72 Å

Several configurations for the hydrated product of this reaction were found (See Appendix C, Table C-4) but only the lowest energy configurations (l.e.c) are shown in Figure 5.5 and Table 5.4. For this molecule, all four *equatorial* sites are Cl-O sites.

In l.e.c. for *trans*-$PtCl_2(H_2O)_2$---H_2O, the water molecule sits on the equatorial site; in the l.e.c. for *trans*-$PtCl_2(H_2O)_2$--$(H_2O)_2$, the two water molecules occupy two diametrically opposed equatorial sites; in the l.e.c. for *trans*-$PtCl_2(H_2O)_2$--$(H_2O)_3$ the three water molecules occupy three equatorial sites; and in the l.e.c. for the *trans*-$PtCl_2(H_2O)_2$---$(H_2O)_4$, all equatorial sites are occupied by water molecules. No water molecules in axial positions were observed.

Table 5.4: Energetics of hydration of *trans*-$PtCl_2(H_2O)_2$ (kcal/mol) according to eqn 5.4 with n=0-3

n	product config	ΔE_0	ΔH	ΔG
0	1A	-9.7	-9.9	-6.6
1	2B	-8.9	-9.1	-5.6
2	3Z	-4.7	-4.5	-2.8
3	4Z	-4.9	-4.7	-2.5

Comparison between structures of *cis*- and *trans*-$PtCl_2(H_2O)_2$ with similar degrees of hydration might provide insights about the predominant species in aqueous solution. From Table 5.5 it is observed that the *trans* isomer is more stable than the *cis* configuration. When there are no hydration waters this difference is minimal, it becomes a maximum at $n_{hyd} = 3$.

Table 5.5: Differences in ΔE0, ΔH, and ΔG (kcal/mol) between the lowest energy configurations of *cis* and *trans*-$PtCl_2(H_2O)_2$—$(H_2O)_n$ (E_{cis}-E_{trans}) with n_{hyd} the number of waters of hydration

n_{hyd}	$\Delta\Delta E_0$	$\Delta\Delta H$	$\Delta\Delta G$
0	0.25	0.29	0.80
1	3.1	3.0	3.0
2	4.6	4.9	3.7
3	4.9	4.8	5.6
4	1.7	1.6	2.2

The experimental value for the equilibrium constant [*cis*]/[*trans*] is 1.2.[157] From the relationship between thermodynamics and equilibrium constant is deduced that ΔG for the isomerization *trans* ➔ *cis* is -0.1 kcal/mol. Therefore it is expected a slight predominance of the *cis* isomer over *trans* in aqueous solutions. However it has also been stated[158] that in gas phase the *trans* isomer is marginally more stable than the isomer *cis*. This in agreement with the trend observed in our calculations. Nonetheless, we are still unable to match the experimental result in aqueous solution. One reason might be that the maximum amount of explicit water used (n_{hyd} = 4) is still insufficient to describe a full-solvent effect. Despite the availability of a number of sampling techniques for free energy calculations-among which multicanonical and umbrella sampling are representative [159]- such *cis-trans* energy difference would be extremely difficult to prove by any of the current implementations of MD simulations due to inherent limited time scale[160], slow convergence[159] and large number of simulations required,[161] and because the reproducibility error[162], sampling accuracy,[163] and statistical uncertainty[161] are larger than the energy difference that has been reported experimentally.[157] Therefore we leave the question open from the theoretical point of view.

5.4 Summary

No water of hydration in the axial sites –above and below the Pt atom- was found for the most stable configurations of the tetrachloroplatinate anion and its mono- and diaquated products at all degrees of hydration studied.

In the mono- and diaquated products of aquation of tetrachloroplatinate anion, water molecules bind strongly to two adjacent water ligand and chloride ligand (Cl-O sites) and weakly to two adjacent chloride ligands (Cl-Cl sites).

All four equatorial sites for *trans*-$PtCl_2(H_2O)_2$ are the same (Cl-O sites). Perhaps this is the reason why –at least at the degrees of hydration studied here- the *trans* isomer has been found more stable than the *cis* isomer.

A slight preference for the isomer *cis*-$PtCl_2(H_2O)_2$ in aqueous solution can be inferred from experiments.[157] The fact that our results show a slight preference for *trans*-$PtCl_2(H_2O)_2$ point out that the number of water molecules used in our calculations is still insufficient to reproduce a full-solvent effect. Thus, as it is likely that both species coexist in aqueous solution –at low precursor salt concentration- both species will be taken in account when considering the speciation of $PtCl_4^{2-}$ in the next chapters.

CHAPTER VI

NON COVALENT BINDING OF TETRACHLOROPLATINATE ANION AND MONO- AND DIAQUATED SPECIES TO PAMAM-OH DENDRIMER OUTER POCKETS*

6.1 Introduction

Dendrimer-templated synthesis is a promising novel technique[32,117] that purports the manufacture of stable metal nanoparticles with uniform size distribution.[164] The resulting nanoparticles produced with this technique are being investigated as potential catalysts not only as encapsulated nanoparticles[106,117] but also by depositing the nanocomposite on a support and removing the template.[55]

Templated synthesis techniques involve a dendrimer as template (T), metal precursor (C-P; C: counterion and P: precursor) and water as solvent (S). Usually, two solutions are prepared, one where the PAMAM dendrimer is dissolved (interactions T-S are established), and another where a metal precursor is dissolved (interactions P-S and C-S are established). Upon mixing of these solutions, the possibility of having P-T and C-T interactions opens up. Therefore, metal precursor (P) and counterion (C) start competing for displacing the solvent (S) out of the pockets (See Figure 6.1). For a successful complexation, the P-T interactions need to be not only stronger than P-S and T-S but also stronger than C-T.

In fact, it is reasonable to assume that the precursor molecule (C-P) will first reach and interact with the dendrimer outer regions. It is also reasonable to assume that the larger the dendrimer, the more symmetric it is, and therefore the more likely for the outer regions to look similar to their adjacent ones. If the dendrimer is large and symmetric, then the dendrimer-precursor interactions are most likely to be local, at least in their initial stages. Thus, since the localized nature of the interactions renders unnecessary the

---

* Reproduced in part with permission from Tarazona-Vasquez and Balbuena, J. Phys. Chem. A 2007, 111, 945. Copyright 2007 American Chemical Society.

modeling of a complete dendrimer, we model those outer regions and calculate the strength of their interactions with metal precursors and solvent and counterions.

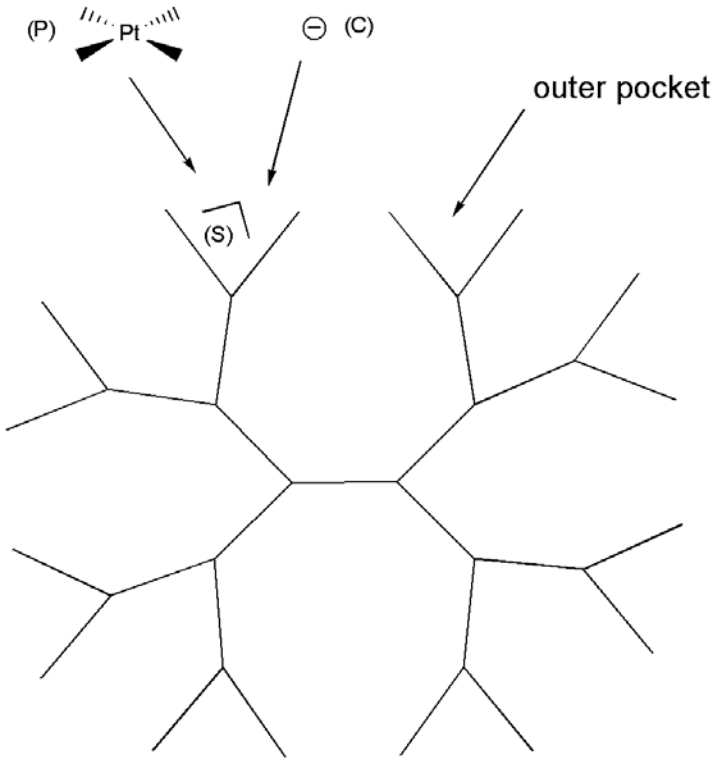

Figure 6.1: Competition between precursor (P) and counterion (C) to displace the solvent (S) that lies inside a dendrimer (T) outer pocket

In this Chapter, we do not only characterize the non covalent binding (NCB) of $PtCl_4^{2-}$ to dendrimer sites, but also the NCB of its mono- and di-aquated species such as $PtCl_3(H_2O)^-$ that has been detected by NMR measurements.[62] In addition to that, the effect of pH[22] is indirectly taken in account by considering unprotonated and protonated dendrimer pockets. The effect of other competing species in solution [165] –like counterions K^+ and Cl^-- is also taken in account.

6.2 Methods

Fragments DF41 and DF41-H were used to model the protonated and unprotonated outer pocket respectively (See Section 3.2. for details). Pocket encapsulation of six guest species was considered: $PtCl_4^{2-}$, $PtCl_3(H_2O)^-$ and $PtCl_2(H_2O)_2$ in *cis* and *trans* forms, and the counterions K^+ and Cl^-.

For the metal complex, non covalent binding[96] (NCB) involves no exchange of first shell ligands (either Cl^- or H_2O) during the initial course of their interaction with the dendrimer pocket. Energies of reaction (ΔE_0, ΔH and ΔG) of displacement reactions that model this exchange have been calculated. Also, by comparing these reaction energies with those of processes where the host is absent (like studied in Chapter V) we have defined the terms "binding affinity" and "relative binding affinity". Thus, the term "binding affinity" refers to the likelihood of a particular displacement reaction (in kcal/mol) whereas "relative binding affinity" refers to a ratio of two displacement reactions (dimensionless number). However, similarly to what was stated in Chapter V, we do not claim that absolute values of thermodynamic quantities for a given NCB reaction have been found. We are rather satisfied with a qualitative description of the feasibility of guest exchange reactions when such guest is other than water.

There are at least two facts that underscore the inadequacy of the choice of adding a continuum medium. First, the outer pocket is not an independent entity but is rather surrounded by other branches and pockets; and second, the outer pocket is able to accept water through the space permitted by the relative distance between its –OH groups. Putting both facts together, it is reasonable to assume that outer pockets locate in the middle of an environment of heterogeneous rather than homogeneous dielectric constant, thus discouraging the use of a continuum to treat the solvent effect. However, in selected cases the solvent effect was addressed by calculation of the reaction energies considering a water dimer encapsulated within dendrimer outer pockets.

DFT was used to obtain minimum energy geometries. The optimization was followed by second derivative matrix calculations that provided the zero point energy

(ZPE) and the thermal and free energy corrections to the electronic energy. The calculations were done with Gaussian 03 suite of programs.[74]

Additional insights on NCB might be obtained by MD simulations. However they are expected to be computationally very expensive in terms of CPU time due to the extensive sampling required (See Chapter III) and is therefore not addressed here.

6.3 Results

6.3.1 Binding affinity for water

In this section, we report the binding affinity of several molecular species *B* with charge *m* toward a free water dimer.

Table 6.1: Electronic energies with ZPE correction (E_0), enthalpies and free energies of reaction (kcal/mol) for the formation of monohydrated species B. Subscripts a and b indicate two different configurations of the protonated fragment DF41-H^+ (see text)

species B	ΔE_0	ΔH	ΔG
K^+	-14.4	-13.6	-14.4
$\{K\text{-}(H_2O)\}^+$	-11.4	-10.7	-11.4
$\{K\text{-}(H_2O)_2\}^+$	-9.5	-8.8	-9.7
Cl^-	-9.7	-9.9	-10.8
OH^-	-24.6	-25.1	-24.3
$PtCl_4^{2-}$	-12.2	-12.0	-10.0
$PtCl_3(H_2O)^-$	-7.9	-8.3	-4.2
cis-$PtCl_2(H_2O)_2$	-6.8	-7.1	-4.3
trans-$PtCl_2(H_2O)_2$	-9.7	-9.9	-6.6
DF41	-4.9	-4.7	-2.0
DF41-H^+_a	-2.9	-3.1	0.4
DF41-H^+_b	-8.0	-8.2	-4.3

The binding affinity is calculated with the following reactions:

Formation of monohydrated species B:

$$B^m + (H_2O)_2 \rightarrow [B(H_2O)]^m + H_2O \qquad (6.1)$$

and hydration of monohydrated species B:

$$[B(H_2O)]^m + H_2O \rightarrow [B(H_2O)_2]^m \qquad (6.2)$$

Table 6.2: Electronic energies with ZPE correction (E_0), enthalpies and free energies of reaction (kcal/mol) for the hydration of monohydrated species B. Subscripts a and b indicate two different configurations of the protonated fragment DF41-H^+ (see text)

species B	ΔE_0	ΔH	ΔG
K^+	-15.4	-15.3	-9.4
$\{K\text{-}(H_2O)\}^+$	-13.4	-13.3	-7.7
$\{K\text{-}(H_2O)_2\}^+$	-11.3	-11.2	-4.8
Cl^-	-12.4	-13.2	-4.4
OH^-	-20.9	-21.5	-14.0
$PtCl_4^{2-}$	-15.0	-15.5	-6.8
$PtCl_3(H_2O)^-$	-9.7	-10.4	-0.94
cis-$PtCl_2(H_2O)_2$	-11.2	-11.9	-2.9
trans-$PtCl_2(H_2O)_2$	-12.8	-13.7	-3.6
DF41	-9.0	-9.7	-0.82
DF41-H^+_a	-9.9	-10.1	-1.6
DF41-H^+_b	-11.9	-12.9	-2.2

The protonated reactants listed in the last two rows of Table 6.1 and 6.2 deserve further explanation. For each ΔE_0, ΔH or ΔG, the values in Table 6.1 are calculated with respect to the lowest energy configuration of a tertiary amine N-*protonated* fragment DF41-H^+ (fragment RefCoB in Figure 3.9, Chapter III). Two distinct configurations are obtained: DF41-H_3O^+ where a water molecule binds to the proton (DF41-H^+_a), and DF41-H^+---H_2O where water binds to the hydroxyl terminal groups (DF41-H^+_b). The last

one is the most stable configuration (ΔG: -4.3 kcal/mol) according to eqn 6.1. Taking these two structures as reference, water molecules are added according to eqn 6.2, yielding DF41-H_3O^+-H_2O (Configuration 2E in Figure 3.10, Chapter III), where the additional water binds inside the pocket and DF41-H^+---$(H_2O)_2$ (Configuration 2C* in Figure 3.10, Chapter III), where a water dimer forms and binds to the hydroxyl terminal groups in a water-tetramer like form.

6.3.2 Binding affinity for hydronium

A water molecule rather than a hydronium ion is most likely to be released when a given species encounters a monohydrated hydronium: eqn 6.3 describes the formation of a protonated monohydrated species *B* with charge *m* with water as subproduct. The thermodynamic values are reported in Table 6.3:

Formation of protonated monohydrated species B

$$B^m + (H_2O)(H_3O)^+ \rightarrow B^m(H_3O)^+ + H_2O \qquad (6.3)$$

Table 6.3: **Electronic energies with ZPE correction (E_0), enthalpies and free energies of reaction (kcal/mol) for the formation of protonated monohydrated species B**

species B	ΔE_0	ΔH	ΔG
Cl^-	-132.8	-131.9	-135.3
OH^-	-192.6	-191.7	-194.3
$PtCl_4^{2-}$	-181.7	-181.5	-179.3
$PtCl_3(H_2O)^-$	-86.8	-85.9	-84.8
cis-$PtCl_2(H_2O)_2$	-1.6	-0.9	-0.4
trans-$PtCl_2(H_2O)_2$	-5.1	-4.3	-3.4
DF41	-60.4	-59.9	-57.4

6.3.3 Binding affinity for water in a tertiary amine N-*protonated* outer pocket

In sections 6.3.1 and 6.3.2 we presented energetics of reaction of species *B* with a free water dimer and 'protonated water dimer'. In this section we discuss the energetics for a reaction where species *B* is exchanged with a water molecule from the water dimer hosted by a dendrimer pocket (as found in Chapter III).

From the group of guest species analyzed in the previous sections, only K^+ was excluded from this study due to its positive charge. By calculating the "relative binding affinity" of a given species for water dimer in presence of the host pocket and comparing it to those calculated in Sections 6.3.1 and 6.3.2 (in the absence of the pocket), we can determine whether or not a particular species will be able to reach the pocket and stay bound there. As this section copes with interactions of DF41-H with other species, we chose the configuration 2C* (See Figure 3.10, Chapter III) as the reference (reactant side) for the calculation of reaction energies according to eqn 6.4.

Formation of monohydrated species B inside tertiary amine N-*protonated* pocket

$$[\{DF41\text{-}H\}(H_2O)_2]^+ + B^m \rightarrow [\{DF41\text{-}H\}B(H_2O)]^{m+1} + H_2O \qquad (6.4)$$

Eqn 6.4 is a process analog to eqn 6.3 reported in Section 6.3.2. However, only results for eqn 6.4 are reported in Table 6.4. The lowest energy configuration structures for the product $[\{DF41\text{-}H\}B(H_2O)]^{m+}$ are shown in Figure 6.2.

Table 6.4: **Electronic energies with ZPE correction (E_0), enthalpies and free energies of reaction (kcal/mol) for the formation of monohydrated species B tertiary amine N protonated pocket**

species B	ΔE_0	ΔH	ΔG
Cl^-	-86.7	-85.5	-89.6
[a]OH^-	-132.1	-131.2	-134.6
$PtCl_4^{2-}$	-146.2	-144.5	-143.5
$PtCl_3(H_2O)^-$	-54.4	-52.9	-52.1
cis-$PtCl_2(H_2O)_2$	-1.3	-0.3	2.6
trans-$PtCl_2(H_2O)_2$	2.2	2.7	7.2

[a]This structure is indeed$\{DF41\text{-}H_2O\text{-}(H_2O)\}$ (OH^- binds to H^+ to yield H_2O) instead of $\{DF41\text{-}H\}OH\text{-}(H_2O)$

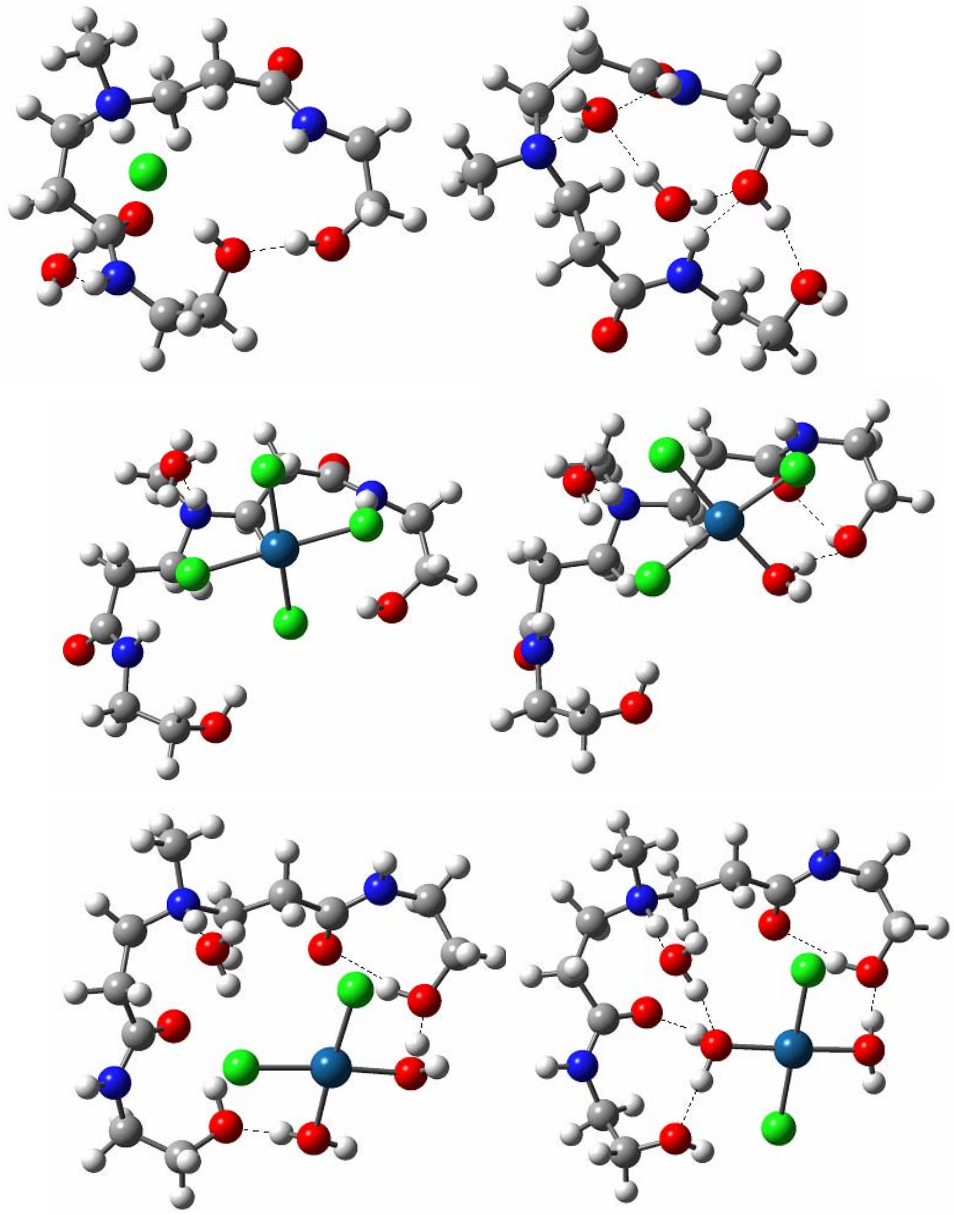

Figure 6.2. Lowest energy configurations for $\{(DF41\text{-}H)B(H_2O)\}^{m+1}$ with m the charge of species B (guest) interacting with a PAMAM outer pocket (host). Upper left: $\{DF41\text{-}H/Cl\text{-}(H_2O)\}^-$ with ~OH---OH: 1.88 Å, NH---OH_2: 1.96 Å ; Upper right: DF41-H_2O-(H_2O). The initial configuration for this structure had proton and water separated by a water molecule. The optimized structure shows that the proton migrated to the neighboring water; on the other hand this water molecule donates a proton to the hydroxyl anion producing another water molecule. Hydrogen bonds, N---HOH: 1.84 Å, H_2O---HN: 2.21 Å, H_2O---HOH: 1.92 Å, H_2O---OH: 1.95 Å, NH---OH: 2.03 Å and OH---OH: 1.83 Å; Middle left: $\{DF41\text{-}H/PtCl_4\text{-}(H_2O)\}^-$ with NH^+---HOH: 1.76 Å; Middle right: $\{DF41\text{-}H/PtCl_3\text{-}(H_2O)\}$ with NH^+---HOH: 1.72 Å, Pt(II)-OH_2---OH: 1.72 Å, OH---O: 2.09 Å ; Lower left: $\{DF41\text{-}H/cis\text{-}PtCl_2\text{-}(H_2O)\text{-}(H_2O)\}^+$ with NH^+---HOH: 1.73 Å, OH---O: 1.82 Å and two Pt(II)-OH_2---OH: 1.61 Å and 1.59 Å; Lower right: $\{DF41\text{-}H/trans\text{-}PtCl_2\text{-}(H_2O)\text{-}(H_2O)\}^+$ with NH^+---HOH: 1.78 Å, OH---O: 1.86 Å,two Pt(II)-OH_2---OH: 1.65 Å and 1.61 Å, Pt(II)- H_2O---H_2O: 1.84A° and Pt(II)-OH_2---O: 1.70 Å

6.3.4 Binding affinity for water in an *unprotonated* outer pocket

In this section, reaction energies are calculated assuming that the structure [DF41-$(H_2O)_2$] (configuration 2C in Chapter III) represents an encapsulated water dimer reacting with species *B* (with charge *m*) in the following displacement reactions. The results for eqn 6.5 are given in Table 6.5. Binding affinity calculations were done not only for K^+ but also for the anions and uncharged species.

Formation of monohydrated species B inside *unprotonated* pocket:

$$[DF41\text{-}(H_2O)_2] + B^m \rightarrow [DF41\text{-}B(H_2O)]^m + (H_2O) \qquad (6.5)$$

Table 6.5: Electronic energies with ZPE correction (E_0), enthalpies, and free energies (kcal/mol) for the formation of monohydrated species B inside unprotonated pocket

species B	ΔE_0	ΔH	ΔG
K^+	-49.3	-47.9	-49.0
$\{K\text{-}(H_2O)\}^+$	-41.0	-40.0	-39.5
$\{K\text{-}(H_2O)_2\}^+$	-35.4	-35.1	-30.5
Cl^-	-31.5	-30.7	-33.6
OH^-	-62.3	-63.0	-60.4
$PtCl_4^{2-}$	-36.8	-35.9	-32.9
$PtCl_3(H_2O)^-$	-12.0	-11.2	-8.0
cis-$PtCl_2(H_2O)_2$	-10.3	-10.2	-5.0
trans-$PtCl_2(H_2O)_2$	-11.9	-12.1	-5.4

6.3.5 Hydration of counterions in *unprotonated* outer pockets

In Chapter III, we have shown that water can be hosted by both *unprotonated* and *protonated* pockets and the present results suggest that other species can also be hosted with at least one water molecule (Section 6.3.4).

Succesive hydration of DF41-B^m

$$DF41\text{-}B^{m}(H_2O)_n + (H_2O)_2 \rightarrow [DF41\text{-}B^{m}\text{-}(H_2O)_{n+1}] + H_2O \qquad (6.6)$$

Unlike eqn 6.5 where a pocket hosting water exchanges one of them for an incoming guest, eqn 6.6 begins with the assumption that DF41-B^m is formed (n = 0) and then additional water molecules $(H_2O)_n$ bind in a hydration-like manner. Thus, we study hydration of Cl^- and K^+, which are simpler to be tested compared with Pt(II) metal complexes due to their smaller size and complexity. Because –as it will be seen in section 6.4.2- the relative binding affinity (for water inside the pocket) of OH^- is lower than those of K^+ and Cl^-, OH^- is excluded from the discussion here. Also as the concentration of OH^- is low at neutral or lower pH its probability to interact with water should decrease accordingly. This is not the case with the other counterions. For instance, K^+ concentration is two-fold the initial concentration of the precursor salt (K_2PtCl_4).

Table 6.6 presents the reaction energies according to eqn 6.6 corresponding to the lowest energy configurations –in a few cases only one was found- at a given degree of hydration.

Table 6.6: Electronic energies with ZPE correction (E_0), enthalpies, and free energies (kcal/mol) for the successive hydration of counterions in unprotonated pockets

product	config	ΔE_0	ΔH	ΔG
DF41-$\{K(H_2O)\}^+$	1A	-18.2	-18.8	-11.3
DF41-$\{K(H_2O)_2\}^+$	2A	-6.1	-5.7	-5.0
DF41-$\{K(H_2O)_3\}^+$	3A	-5.7	-5.9	-2.4
DF41-$\{K(H_2O)_4\}^+$	4A	-3.2	-3.4	1.7
DF41-$\{Cl(H_2O)\}^-$	1A	-4.9	-5.2	-0.21
DF41-$\{Cl(H_2O)_2\}^-$	2A	-4.4	-4.5	-1.5

The ΔE_0 and ΔG for the reaction DF41 + K^+ ➔ DF41-K^+ are -45.0 and -40.5 kcal/mol respectively whereas for the reaction DF41 + Cl^- ➔ DF41-Cl^- are -40.5 and -36.2 kcal/mol. Although the additional binding of water is not as feasible as these reactions, it is still significant particularly for the first water of hydration: if DF41-$\{K(H_2O)\}^+$ is formed, ΔE_0 and ΔG are -18.8 and -11.3 kcal/mol respectively (Table 6.6). However when DF41-$\{Cl(H_2O)\}^-$ is formed by a similar reaction, the values for ΔE_0 and ΔG are much lower: -4.9 and -0.21 kcal/mol respectively.

In DF41-$\{K(H_2O)\}^+$, K^+ binds to two amide O, one hydroxyl O and a water O, all of them in relatively equatorial positions, with bond lengths ranging 2.61 to 2.97 Å, the longer distance being for K^+-O water, whereas the K^+-tertiary amine distance is longer (3.90 Å). On the other hand, in DF41-$\{Cl(H_2O)\}^-$ (Figure 6.2), Cl^- binds to two hydroxyl H, one water H, two amide H and perhaps to two methylene Hs. Bond distances range from 2.30 (hydroxyl H) to 3.01 Å (methylene H). Therefore a coordination number of 5-7 can be inferred. This is in agreement with experimental results.[166] For both of these structures, the additional water molecule completes the first shell coordination of the ion.

Beyond the first water molecule, K^+ and Cl^- accept waters but not in their first coordination shell. Thus, the additional water in DF41-$\{Cl(H_2O)\}^-$ joins two hydroxyl oxygen atoms and faces toward the outside of the pocket. Additional water in K^+ can still be added axially, with bond distances ranging 2.62-3.08 Å, the longer being the distance first-added O water-K^+. Binding of a third water is still favorable and the bond distances range from 2.62 Å to 2.77 Å (the longer for amide O-K^+). The first and second-added water stay outside the first coordination shell (Figure 6.3). The K^+-N3 bond distance elongates to 4.02 Å. Therefore no binding to N3 is inferred.

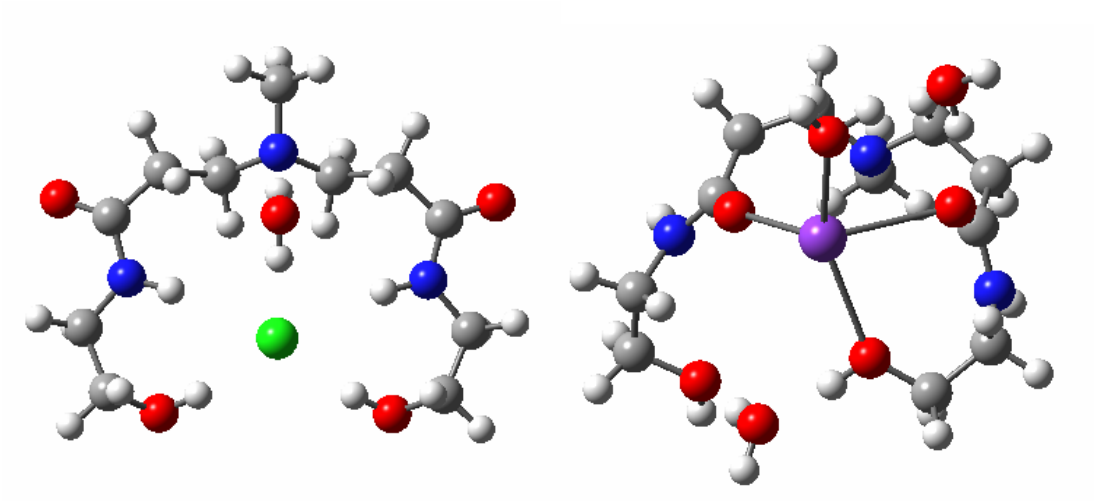

Figure 6.3. Low energy configurations of hydrated counterions in outer pockets. Left: $[DF41\text{-}Cl^{-}(H_2O)]^{-}$; Right: $[DF41\text{-}K\text{-}(H_2O)_3]^{+}$

Further addition of water is thermodynamically unfavorable: bond distances range 2.69-2.98 Å (the longer distance corresponds to the interaction with two waters) and one water molecule locates in the second coordination shell. Our results point out that K^{+} is at least tetra-coordinated when interacts with the pocket in agreement with experiments done in proteins.[167]

6.4 Discussion

Results from sections 6.3.1 and 6.3.4 are compared in section 6.4.1 in order to investigate the effect of protonation on the binding of guests inside an outer pocket. Results from sections 6.3.2 and 6.3.3 are discussed in section 6.4.2 with the goal of analyzing the effect of hydration on the binding of species (other than water) to a water dimer as well as how this binding affinity is affected in the presence of an outer pocket. Finally, in section 6.4.3 we attempt to rationalize the results of section 6.3.5 so that we can gain insight into conformational changes in the outer pocket configuration needed for the hosting of particular guests.

6.4.1 Effect of tertiary amine N-*protonated* outer pocket on the binding of guest species

Reaction energies for formation of *protonated* monohydrated species or binding affinity for monohydrated hydronium for all species studied but potassium ion, are shown in Table 6.3 (*vide supra*). It is evident that electrostatic attraction between an anion such as $PtCl_4^{2-}$ and H_3O^+ will be strong; yet it was found to be lower than that of OH^- despite of the $PtCl_4^{2-}$ charge being double that of OH^-. On the other hand, H_3O^+ interactions with uncharged species like $PtCl_2(H_2O)_2$ are weaker and a trade-off between the attraction exerted by negatively charged ligands such as Cl^- and the repulsion between Pt^{2+} and the H_3O^+ hydrogen atoms is evident. As a result, a difference between *cis*- and *trans*-$PtCl_2(H_2O)_2$ binding affinity can be observed due to their different geometry. Considering only the uncharged complexes in absence of host, the binding affinity for monohydrated hydronium follows the order: *unprotonated* pocket >> *trans*-$PtCl_2(H_2O)_2$ > *cis*-$PtCl_2(H_2O)_2$, whereas among the species charged with -1 it follows the order: OH^- > Cl^- > $PtCl_3(H_2O)^-$.

Regarding interactions with a *protonated* pocket (host), the binding affinity (Table 6.4) reverts for uncharged species: *cis*-$PtCl_2(H_2O)_2$ >*trans*-$PtCl_2(H_2O)_2$ with respect to the affinities for the free monohydrated hydronium, whereas the same order of binding is found for species charged with -1: OH^- > Cl^- > $PtCl_3(H_2O)^-$. It should be noticed also that the binding affinity of $PtCl_4^{2-}$ is larger than that of OH^-.

Next we assume that the relative probability of finding a particular species in either of two scenarios: inside or outside of the pocket, is proportional to their energy ratio: ΔE(*Protonated* Pocket)/ΔE(Outside of Pocket) where the energies correspond to the reaction energies in Tables 6.4 and 6.3 respectively. The energy ratios are summarized in Table 6.7. C*is*- and *trans*-$PtCl_2(H_2O)_2$ have a very small binding affinity for monohydrated hydronium (Table 6.3, *vide supra*) and a low or even positive ΔG (Table 4, *vide supra*). Therefore their energy ratio was not included in Table 6.7. This suggests that tertiary amine N-*protonated* pockets are not able to attract neutral species, such as *cis* and *trans* $PtCl_2(H_2O)_2$.

Table 6.7: Ratio ΔE(protonated pocket)/ΔE(outside of pocket), based on data from Tables 6.4 and 6.3. Each column corresponds to an energy ratio involving ΔE_0, ΔH, and ΔG respectively

	energy ratios		
species B	ΔE_0	ΔH	ΔG
Cl^-	0.7	0.6	0.7
OH^-	0.7	0.7	0.7
$PtCl_4^{2-}$	0.8	0.8	0.8
$PtCl_3(H_2O)^-$	0.6	0.6	0.6

The energy ratios shown in Table 6.7 suggest that $PtCl_4^{2-}$ (ratio 0.8) is slightly more likely to interact with a protonated pocket than Cl^-, OH^- and $PtCl_3(H_2O)^-$ (ratios 0.6-0.7). Nonetheless because all these ratios are lower than 1.0, it is expected that these species prefer to interact mainly with H_3O^+ in the surrounding medium outside of the pocket. This finding suggests why protonation does not help complexation at moderate [61] precursor concentration. For comparison, it is interesting to note that the values of the reaction free energies of Cl^- and OH^- in *protonated* pockets are of the same order of magnitude of their hydration energies in their fully solvated states. This suggests that the *protonated* pocket exerts a comparable interaction to that of a polar solvent; however, such interaction is weaker than that with a free monohydrated hydronium ion as may exist in the solution medium surrounding the dendrimer.

6.4.2 Effect of *unprotonated* outer pocket on the binding of guest species

Free energies of reaction corresponding to the formation of monohydrated species or binding affinity for water dimer (Table 6.1, *vide supra*) are larger than those of the hydration of these monohydrated species (Table 6.2), except for DF41 and DF41-H^+_a. Tables 6.1 and 6.2 also show that the high binding affinity of K^+ for water decreases as the number of solvation molecules increases. This trend is similar in almost all the other species (Figure 6.4 and Table C-1 in Appendix C) but is more dramatic for OH^-.

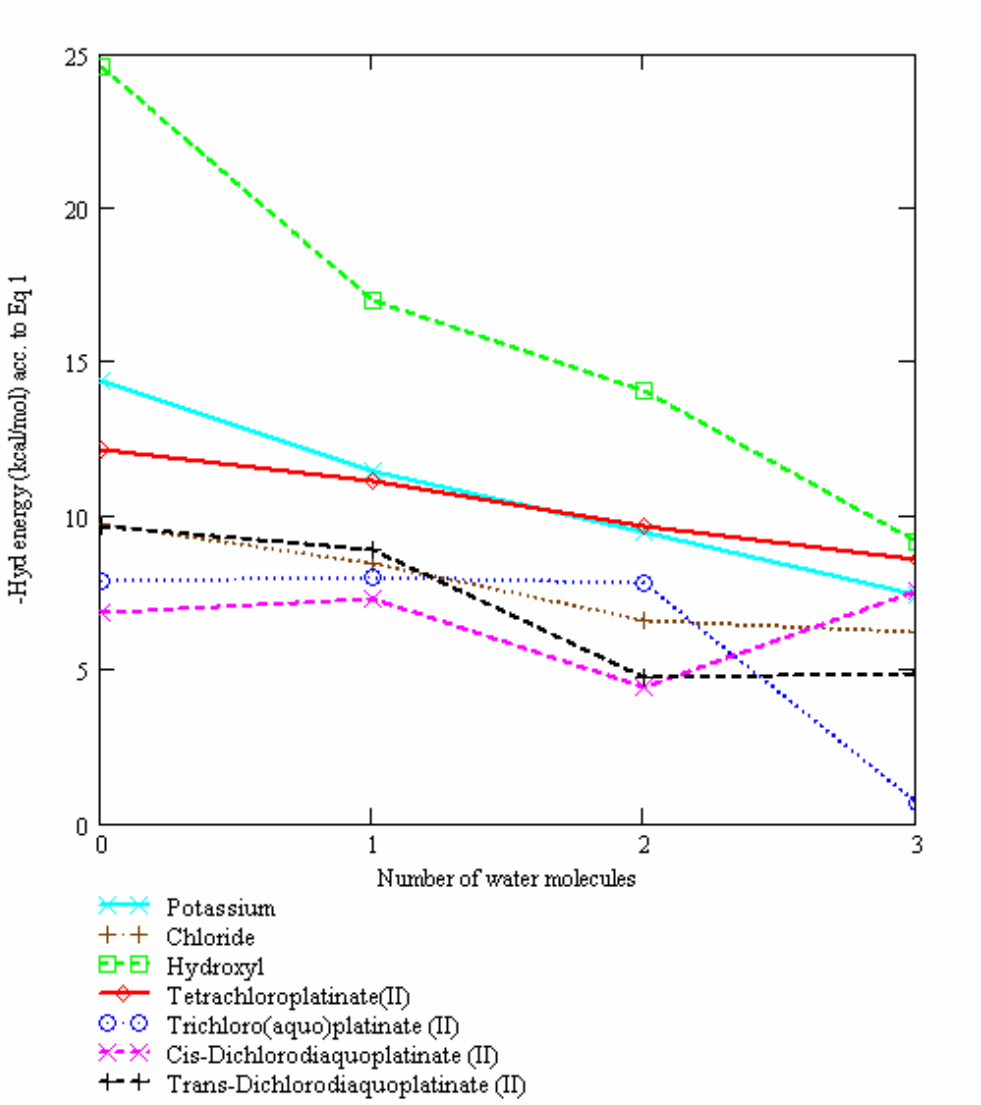

Figure 6.4: Hydration energy (ΔE_0 according to the equation: $B(H_2O)_n + (H_2O)_2 \Longrightarrow B(H_2O)_{n+1} + H_2O$) vs. number of water molecules in the reactant. The negative of the value of the energy is plotted in the y-axis so that a decreasing ability toward hydration is observed in almost all ions and particularly in OH^-

On the other hand, Table 6.5 illustrates how the host affects the binding affinity of hydrated potassium species for a *pocketed water dimer*, which binds strongly within pockets; yet the more solvation molecules surrounding the ion, the less feasible the

retention of water already present in the pocket (exchange) or the binding of additional water without pocket involvement (hydration).

Considering only the free uncharged complexes according to eqn 6.1, the binding affinity for water dimer (Table 6.1) follows the order *trans*-$PtCl_2(H_2O)_2$ >*cis*-$PtCl_2(H_2O)_2$ > unprotonated pocket, whereas among the species charged with -1, the water binding affinities of OH^- and Cl^- are higher than that of $PtCl_3(H_2O)^-$. In spite of its higher charge, $PtCl_4^{2-}$ binding affinity for water is comparable to that of Cl^-.

When interactions with an *unprotonated* pocket (host) are considered, the binding affinity (Table 6.5) in uncharged complexes for a pocketed water dimer follows the order: *trans*- $PtCl_2(H_2O)_2$ > *cis*-$PtCl_2(H_2O)_2$ whereas among species charged with -1 the order is OH^- > Cl^- > $PtCl_3(H_2O)^-$. The binding affinity of $PtCl_4^{2-}$ for pocketed water is lower than that of OH^- although similar to that of Cl^-. Thus, whether the host is present or not the affinity strength follows a similar ordering.

As in section 6.4.1, the relative probability of finding a particular species inside or outside of the pocket, is assumed to be proportional to their energy ratio (E(*Unprotonated* Pocket)/E(Non-Pocket)). This energy ratio or relative binding affinity for water dimer, defined as the ratio between the reaction energies calculated with eqn 6.5 (Formation of monohydrated species *B* inside *unprotonated* pocket) and eqn 6.1 (Formation of monohydrated species *B* outside *unprotonated* pocket), is shown in Table 6.8. It could also be regarded as a partition coefficient among two scenarios (pocket vs. outside of pocket) and can consequently provide qualitative insights into the ability of the pocket to host particular guests.

Table 6.8: Ratio ΔE(unprotonated pocket)/ΔE(outside of pocket) based on data from Tables 6.5 and 6.1. Each column corresponds to an energy ratio involving ΔE_0, ΔH, and ΔG respectively

	energy ratios		
species B	ΔE_0	ΔH	ΔG
K^+	3.4	3.5	3.4
$K\text{-}(H_2O)^+$	3.6	3.7	3.5
$K\text{-}(H_2O)_2^+$	3.7	4.0	3.1
Cl^-	3.2	3.1	3.1
OH^-	2.5	2.5	2.5
$PtCl_4^{2-}$	3.0	2.9	3.3
$PtCl_3(H_2O)^-$	1.5	1.4	1.9
cis-$PtCl_2(H_2O)_2$	1.5	1.4	1.1
trans-$PtCl_2(H_2O)_2$	1.2	1.2	0.8

The energy ratios shown in Table 6.8 suggest that host-guest interactions in the unprotonated pocket are much stronger than those between water and the guest (in absence of the host). All ratios are higher than 1.0 except the ΔG ratio for *trans*-$PtCl_2(H_2O)_2$. Also, Table 6.8 clearly suggests that $PtCl_4^{2-}$ is a suitable competitor of K^+ and Cl^- for the pocket sites.

Next we define new relative binding affinities as the ratios of energies (ΔE_0, ΔH, ΔG) for hydration of species *B* inside an *unprotonated* pocket (according to eqn 6.5) over the sum of the energies given by eqn 6.1 (Formation of monohydrated species *B* without *unprotonated* pocket) and eqn 6.2 (Hydration of monohydrated species *B* without *unprotonated* pocket). The rationale for this division is that the negative free energies calculated with eqn 6.2 indicate that such reaction of species *B* with a water dimer (eqn 6.1) will continue according to eqn 6.2.

The calculated ratios shown in Table 6.9 are lower than those in Table 6.8. These new ratios indicate also that not only *trans*-$PtCl_2(H_2O)_2$ but also its *cis* isomer are less

likely to be encapsulated within an *unprotonated* pocket –both ratios for these species are lower than 1.0. The relative binding affinity (energy ratio) of OH^- is lower than those of K^+, Cl^- and $PtCl_4^{2-}$, although similar to that of $PtCl_3(H_2O)^-$. Aside from this, Table 6.9 expresses the trend described by Table 6.8.

Table 6.9: Ratio ΔE(unprotonated pocket)/ΔE(outside of pocket) based on data from Tables 6.1, 6.2 and 6.5. Each column corresponds to an energy ratio involving ΔE_0, ΔH, and ΔG respectively

	energy ratios		
species B	ΔE_0	ΔH	ΔG
K^+	1.7	1.7	2.1
$K\text{-}(H_2O)^+$	1.7	1.7	2.1
$K\text{-}(H_2O)_2^+$	1.7	1.8	2.1
Cl^-	1.4	1.3	2.2
OH^-	1.4	1.4	1.6
$PtCl_4^{2-}$	1.4	1.3	2.0
$PtCl_3(H_2O)^-$	1.4	0.6	1.5
cis-$PtCl_2(H_2O)_2$	0.6	0.5	0.7
trans-$PtCl_2(H_2O)_2$	0.5	0.5	0.5

This analysis suggests that any charged species will prefer binding inside rather than outside an *unprotonated* outer pocket. To illustrate and test this conclusion, several configurations of DF41-$PtCl_4^{2-}$ were optimized and two of them were selected: the lowest energy configuration (l.e.c.) for a tetrachloroplatinate (II) hosted inside a pocket (Figure 6.5, upper right) and another with the ion located outside but attached to the pocket (Figure 6.5, upper left). A reaction energy defined as $\Delta E_0 = E_0(DF41\text{---}PtCl_4^{2-}) - \{E_0(DF41)+E_0(PtCl_4^{2-})\}$ yielded -45.0 kcal/mol and -35.0 kcal/mol for the 'inside pocket l.e.c.' and the 'outside but attached to the pocket' l.e.c, respectively. The ratio of these

energies is larger than 1.0, suggesting similar conclusions as those from Tables 8 and 9: it is more likely for charged species to bind inside rather than outside unprotonated pockets. Therefore, it is reasonable to assume that after initial interaction of $PtCl_4^{2-}$ with the outer pockets exposed to bulk water, the precursor anion will bind inside the pocket.

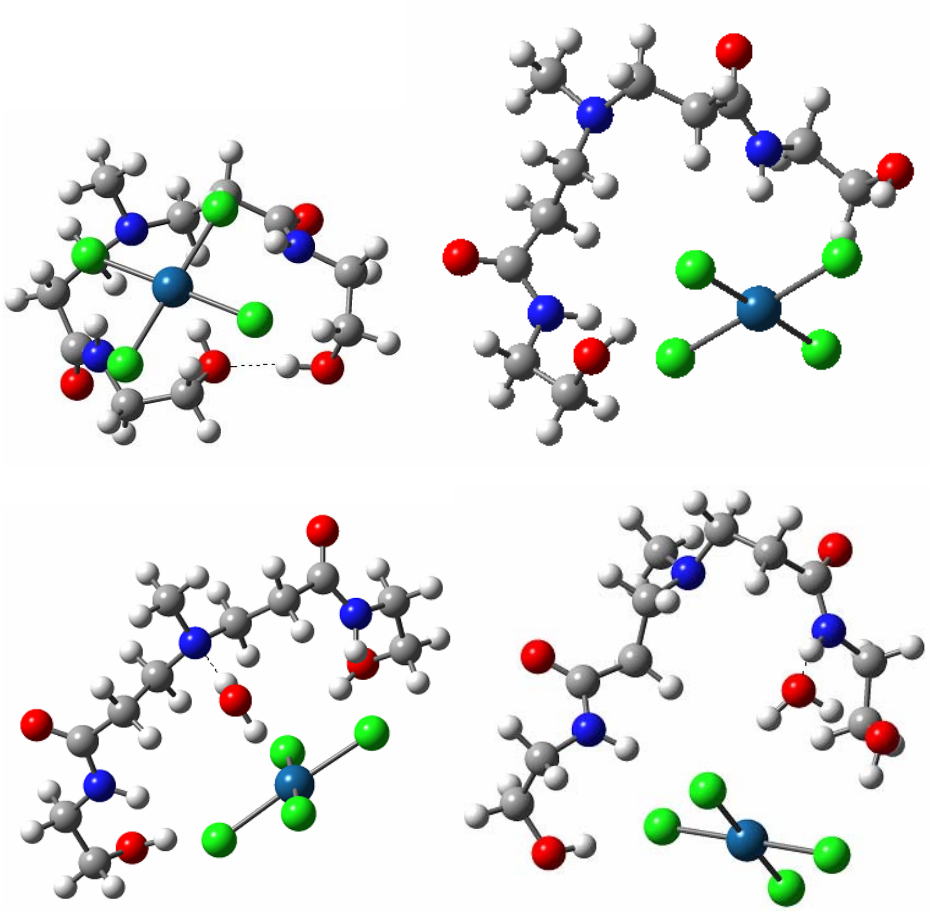

Figure 6.5. Configurations of DF41-$PtCl_4^{2-}$ and DF41-H_2O-$PtCl_4^{2-}$. Upper Left: '$PtCl_4^{2-}$ outside but attached to the pocket' configuration. Pocket remains closed with terminal hydroxyl groups binding with a hydrogen bond ~OH---OH of 1.83 Å Upper Right: '$PtCl_4^{2-}$ inside the pocket'. This is the l.e.c.; Lower Left: DF41-H_2O-$PtCl_4^{2-}$: with a hydrogen bond ~N3---HOH: 2.05 Å; Lower Right: DF41-H_2O-$PtCl_4^{2-}$: with ~N2---HOH: 1.91 A°. The energy difference between the two structures in the bottom row is 0.2 kcal/mol (ΔG). Orientation of their amide O atoms in both branches is found to point outwardly in relation to the pocket (See Chapter III)

6.4.3 Conformational change in outer pockets upon interaction with guests

A series of angles help to characterize the outer pocket in relation to the orientation of their amide O atoms: angle γ , formed by amide O1(branch 1)-tertiary amine N3-amide O2(branch 2); angle α, formed by carbonyl CO1(branch 1)-N3-carbonyl CO2(branch 2).

Table 6.10: Bond distances (Å) and angles (degrees) for configurations of pocket-counterion-water configurations. Note: The four first rows correspond to [DF41-K-$(H_2O)_n$]$^+$ (with n = 0-3) configurations and the last two to [DF41-Cl-$(H_2O)_n$]- with n = 0-1

		Bond Distances		Angles	
		Å		α	γ
n	Config	O-O	OT-OT	CO-N3-CO	O-N3-O
0	0B	4.65	11.72	125.9	87.6
1	1A	4.44	4.66	118.3	81.8
2	2A	4.61	4.66	119.8	84.3
3	3A	4.55	4.77	115.7	82.6
0	0A	9.18	5.11	128.9	150.7
1	1A	9.35	4.99	136.5	151.4

From Table 6.10, it is observed that when K^+ enters the pocket with water, the O-O distance ranges 4.44- 4.65 Å and that the OT-OT distance ranges 4.66-11.72 Å. The α angle ranges 115.7-125.9°; the γ angle ranges 81.8-87.6°.

This range of variation of several geometric parameters for configurations of K^+ and water binding in *unprotonated* pocket was then compared with the values for binding of water alone (See Chapter III) observing first that the amide O-O bond distances are shorter and that their range of variation is narrower; also their OT-OT bond distance is longer –suggesting the absence of hydrogen bond between hydroxyl terminal groups-, and the values of the angle α (Table 6.10) as well as those of the angle γ (Table 6.10) are significantly lower and with narrower range of variation. All these observations

point out to the fact that cations like K^+ induce the orientation of both amide O atoms in the pocket into inward-inward positions.

A similar comparison made for the binding of Cl^- to the pocket respect to the values for water-*unprotonated* pocket structures (See Chapter III) indicates that the O-O bond distance is larger, the minimum OT-OT is larger and therefore no H-bond between hydroxyl terminal groups exists, values of angle α are within the range measured for water-*unprotonated* pocket structures while the value of γ angles is significantly larger. The longer O-O bond distances and values for the angle γ point out to the fact that anions like Cl^- induce orientation of both amide O atoms into outward-outward positions.

These results hint to a markedly different configurational rearrangement of the outer pockets –and consequently of the larger dendrimer- when either positively or negative charged ions are hosted. This is less obvious for asymmetric guest structures –whether on charge distribution or geometry- than for symmetric ones.

Therefore reorientation of branches in the dendrimer (pocket regions) has to occur when a given species is hosted inside a pocket. For instance, although Cl^- is a suitable competitor for $PtCl_4^{2-}$ species and both bear negative charges, none of them accommodates in an inward-outward configuration -the preferred configuration of unprotonated outer pocket hosting a water dimer (See Chapter III). Therefore configurational rearrangement in the dendrimer should take place to allow those species in.

6.5 Summary

Tertiary amine-N protonated pockets are not likely to host neutral species like *cis*- and *trans*-$PtCl_2(H_2O)_2$, but only anions. Yet the fact that no species among the anions studied has a larger binding affinity for encapsulated water than for a monohydrated hydronium might explain why complexation of Pt(II) with PAMAM dendrimer has not been observed –at the best of our knowledge- in protonated dendrimers.[61]

Binding affinity of the species studied for water dimer decreases upon hydration. Effect of solvent inside pockets has not been possible to study for Pt(II) complexes but only for K^+ showing same trend. However binding affinity increases when reacting with a water dimer encapsulated within an unprotonated pocket and although all species can bind to it not all do it with the same strength. For instance, host-guest interactions are weak when the guest is either *cis*- and *trans*-$PtCl_2(H_2O)_2$ but strong when such guests are either K^+, Cl^- or $PtCl_4^{2-}$. The relative binding affinity order is: $K^+ \sim PtCl_4^{2-} \sim Cl^- > OH^- > PtCl_3H_2O^- >$ *cis*-$PtCl_2(H_2O)_2 >$ *trans*-$PtCl_2(H_2O)_2$. Therefore, charged species are more likely to bind inside rather than outside unprotonated pockets.

It is expected that the dominant species in freshly prepared solutions of K_2PtCl_4 be $PtCl_4^{2-}$. Therefore the aquation of $PtCl_4^{2-}$ into its mono and di-aquated species before it reaches the dendrimer pockets would not be desirable because the aquated complexes bind weakly to outer pockets. Given that $PtCl_4^{2-}$ has to compete with K^+ already, then it would not adequate to use aged and diluted solutions of K_2PtCl_4 to obtain nanoparticles because these solutions contain Pt(II) aquated species predominantly. The same rationale ought to apply to other Pt(II) metal precursors yielding similar species.

Finally, the most notable local configurational change that takes place upon hosting of guest species by a pocket is the orientation of its amide O that depends on the nature of the guest (See Chapter III). These local configuration changes are likely to affect the configuration of the larger dendrimer the pockets belong to.

In summary, important insights on the complexation ability of dendrimer outer pockets in both a protonated and unprotonated scenario toward molecular guests have been obtained through thermodynamic and geometric analysis. A complementary study on the next step of the complexation, the ligand exchange reaction (LER) will be discussed in the next chapters.

CHAPTER VII
SOLVENTLESS LIGAND EXCHANGE REACTION OF TETRACHLOROPLATINATE ANION IN PAMAM-OH DENDRIMER OUTER POCKETS

7.1 Introduction

In the previous Chapter non covalent binding of Pt(II) species was studied. In this Chapter we study the subsequent process, namely the exchange of one of the ligands (either chloride or water) of the Pt(II) species for another ligand. This stage of the complexation is named ligand exchange reaction (LER).

Most of the experimental work to date has been mainly devoted to elucidate some aspects of the LER. For instance, XPS experiments determined a Pt/Cl ratio of 1:3 after mixing K_2PtCl_4 with PAMAM dendrimer, suggesting then that LER to a N site had occurred.[61] Later NMR experiments not only suggested a monodentate binding of Pt(II) to nitrogen atom sites in the dendrimer but also bi- and tridentate binding.[62] And, recent EXAFS experiments suggested the presence not only of nitrogen atoms but also oxygen atoms in the first coordination shell of the Pt(II) ion.[55] Nevertheless, the identity of the Pt(II) species that reacts with the dendrimer atom binding sites, the size of the activation barriers for the ligand exchange reaction and the stability of the resulting Pt(II)-N complexes[62] as well as the exact locations for the attachment of Pt(II) species to the dendrimers have not been established yet.[55]

7.2 Methods and models

In order to understand how the branches of the dendrimer affect the binding of metal precursor species it is necessary to use simple molecules such as trimethylamine, n-methyl-acetamide and methanol (Figure 7.1) as single site models. This would allow to model binding sites (N3, N2 and OT) at its simplest in a branchless environment. Also, in addition to the DF41 fragment previously used (Chapter III), we modeled a dendrimer branch with a 27-atom fragment (DF27). See Figure 7.1 for details.

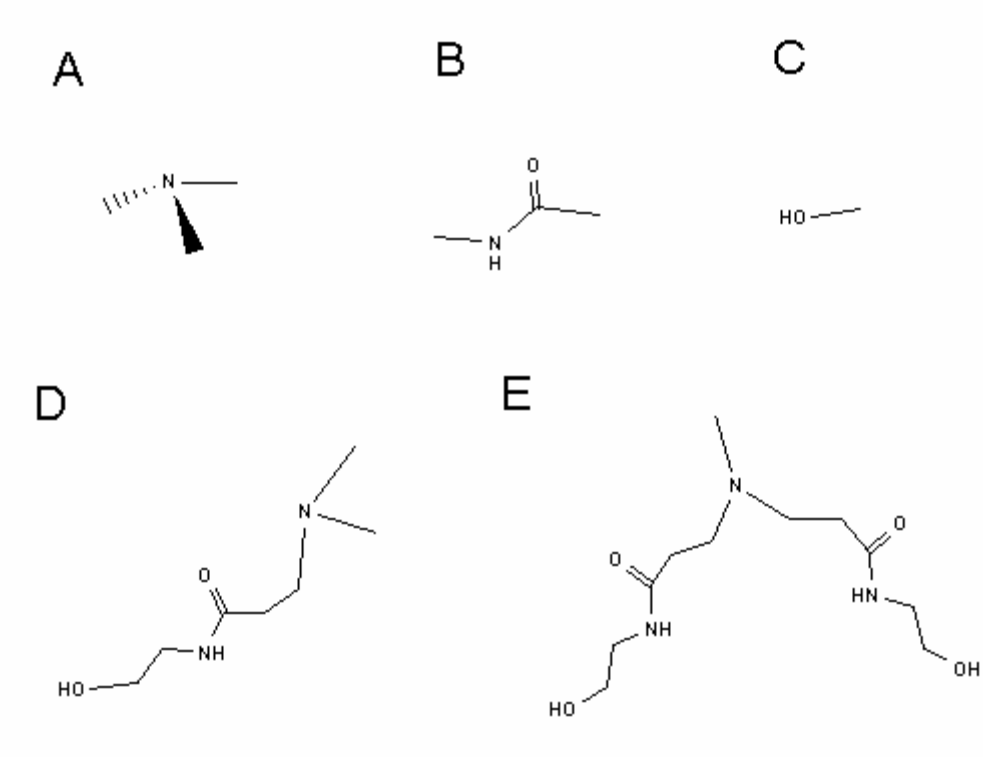

Figure 7.1. Single molecule and outer pocket fragments. (A) Tri-methylamine, (B) n-methyl acetamide (NMA), (C) Methanol, (D) DF27: Single branch, (E) DF41: Outer pocket. DF stands for Dendrimer Fragment and the two-digit number indicates the number of atoms that composes the fragment (See section 3.2.)

DFT was used to optimize minimum energy as well as transition state (TS) structures with no symmetry constraints. TS structures were located by either running the Berny optimization[75] to a saddle point –traditional TS search- or using the Synchronous Transit-Guided Quasi Newton (STQN) TS optimization method[76] or both. The optimization of the geometries was followed by second derivative matrix calculations that provided estimates for the ZPE and temperature corrections to the entalphy and Gibbs free energy at 298K. The activation energy (Ea) is defined as the difference in entalphy of the relevant states. No claim that the absolute values of the binding energies have been found is held (as stated in Chapter V and VI). The calculations were done with Gaussian 03[74] suite of programs.

7.3 Results

7.3.1 Search for the most favorable binding site for complexation of tetrachloroplatinate anion ($PtCl_4^{2-}$)

Binding of Pt(II) to both tertiary amine N (N3) and secondary amide N (N2) in PAMAM dendrimers[62] and to secondary amide O[168] (O) and to hydroxyl O[169] (OH) in other compounds has been suggested by experimental work. Therefore several structures (for selected geometric parameters, see Table D-1, Appendix D) of the form Fragment-$PtCl_3^-$ where a Cl^- ligand has been replaced by a dendrimer atom site (N3, N2, O and OH) were calculated.

Solventless complexation of $PtCl_4^{2-}$ leading to the LER product structures (D in Fig. 7.2) follows three steps: a NCB reaction (process A→B), LER (process B→D) and the third step can be the release of Cl^- (process D→ E) which can be either endo- or exotermic. The overall complexation process represented by eqn 7.1 is A→E (Fig. 7.2)

Fragment + $PtCl_4^{2-}$ ===> Fragment-[$PtCl_3^-$] + Cl^- (7.1)

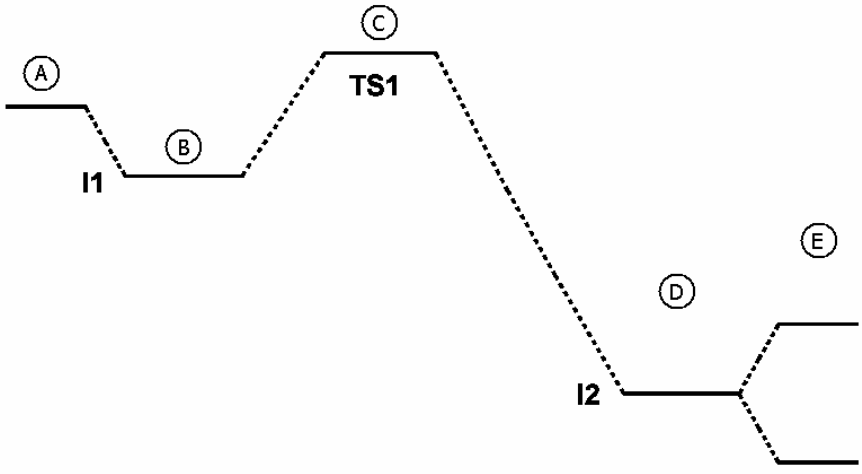

Figure 7.2. Reaction profile for the overall complexation of $PtCl_4^{2-}$ with molecular fragments according to eqn 7.1. A) Fragment + $PtCl_4^{2-}$ are separated; B) Fragment and $PtCl_4^{2-}$ interact through NCB resulting in Fragment---$PtCl_4^{2-}$ (structure I1) ; C) Transition state structure for Fragment---$PtCl_4^{2-}$ (structure TS1); D) Fragment---$PtCl_3^-$---Cl^- (structure I2); E) Fragment---$PtCl_3^-$ + Cl^- are separated either endotermically or exotermically

Although Figure 7.2 depicts a TS structure between I1 and I2, no TS search was performed neither solvent effect was considered in this section, Figure 7.2 is presented here to illustrate the general procedure followed in other sections. This thermodynamic analysis approach ought to be understood as a test to find out the most favorable site for the complexation of $PtCl_4^{2-}$ and is meant to be qualitative rather than quantitative. ΔG values for the overall complexation of $PtCl_4^{2-}$ described by eqn 7.1 are presented in Table 7.1.

Table 7.1. ΔG of reaction (kcal/mol) for the overall complexation of $PtCl_4^{2-}$ with molecular fragments according to eqn 7.1. Dendrimer atom sites: tertiary amine N (N3), secondary amide N (N2), amide O (O), hydroxyl O (OH)

Model	Site	Fragment	ΔG
Single Site molecule	N3	$N(CH_3)_3$	-51.1
	N2	CH_3-CO-NH-CH_3	-48.4
	OH	CH_3OH	-48.0
	O	CH_3-CO-NH-CH_3	-40.7
Single branch	N3	DF27	-56.3
	N2	DF27	-48.8
	OH	DF27	-49.0
	O	DF27	-39.4
Outer pocket	N3	DF41	-60.0
	N2	DF41	-53.9
	OH	DF41	-54.8
	O	DF41	-48.9

The calculations of the overall complexation energy for $PtCl_4^{2-}$ binding to N3, N2, OH and O sites points out firstly that monodentate binding of $PtCl_4^{2-}$ to the dendrimer is feasible; second, that it is more likely to have Pt(II) binding to a tertiary amine N (N3). These calculations also suggest that branches can enhance the binding of $PtCl_4^{2-}$ to all sites and to tertiary amine N (N3) in particular.

7.3.2 Search for the most likely precursor when tertiary amine nitrogen (N3) is the binding site

We extend the thermodynamical analysis of Section 7.3.1 to mono- and di-aquated complexes of $PtCl_4^{2-}$. Calculated TS structures and activation energies are analyzed to assess the kinetic effect. The N3 site is modeled with a single site ($N(CH_3)_3$) in section 7.3.2.1 and with a DF41 fragment in section 7.3.2.2 enabling us to evaluate the effect of branches on the activation energies.

7.3.2.1 LER of Pt(II) complexes with $N(CH_3)_3$

The LER step of the complexation of Pt(II) complexes to $N(CH_3)_3$ is given by the following equation:

$[N(CH_3)_3\text{-}PtC'_xD'_y]$ (I1) ➔ TS ➔ $[N(CH_3)_3\text{-}PtC'_{x-1}D'_y\text{---}C']$ (I2) (7.2)

Where $PtC'_xD'_y$ represents $PtCl_4^{2-}$ and its mono- and di-aquated complexes and C' is the leaving ligand.

Table 7.2: ΔG of reaction and activation energies (E_a), in kcal/mol, for the LER between Pt(II) complexes and the tertiary amine N site (N3) of $N(CH_3)_3$ according to eqn 7.2

Species	E_a	ΔG_{LER}
$PtCl_4^{2-}$ [a]	20.5	-55.3
$PtCl_3(H_2O)^-$	16.6	-5.9
cis-$PtCl_2(H_2O)_2$	21.6	-8.0
trans-$PtCl_2(H_2O)_2$	25.6	-6.4

[a] $E(N(CH_3)_3\text{---}PtCl_3^-) + E(Cl^-) - E(N(CH_3)_3\text{---}PtCl_4^{2-})$

The free energy change ΔG_{LER} (ΔG_{I2-I1}) involved with the release of Cl^- is calculated to be -55.3 kcal/mol (Table 7.2) because a LER structure (I2) for $PtCl_4^{2-}$ could not be found (for selected geometric parameters see Table D-2, Appendix D). For the other three complexes their calculated free energies of reaction are not significantly different. Therefore regarding only these three species, it can be said that complexation is most likely to be kinetically rather than thermodynamically controlled. The lowest activation energy (E_a) found for $PtCl_3(H_2O)^-$ suggests that the reaction (eqn 7.2) will be easier to perform with $PtCl_3(H_2O)^-$.

7.3.2.2 LER of Pt(II) complexes with DF41

The larger number of atoms in DF41 results in a number of isomeric configurations for both reactants (for a collection of snapshots of DF41-$PtC'_xD'_y$ structures see Tables D-3 to D-6, and for selected bond distances see Table D-7, Appendix D) and products of eqn 7.3 and eqn 7.4 and thus makes the tracing of reaction profiles more challenging. It also makes necessary to make a distinction between ΔG_{LER} (ΔG_{I2-I1}) –defined as the difference of free energy between the stationary points (reactant (I1) and product (I2)) placed at either side of the TS structure involved in the LER of Pt(II) species to N3 site- and $\Delta G_{LER(overall)}$ –defined as the difference in free energy in passing from l.e.c.rs (lowest energy configurations in reactants side) to l.e.c.ps (lowest energy configurations in products) (See Figure 7.3).

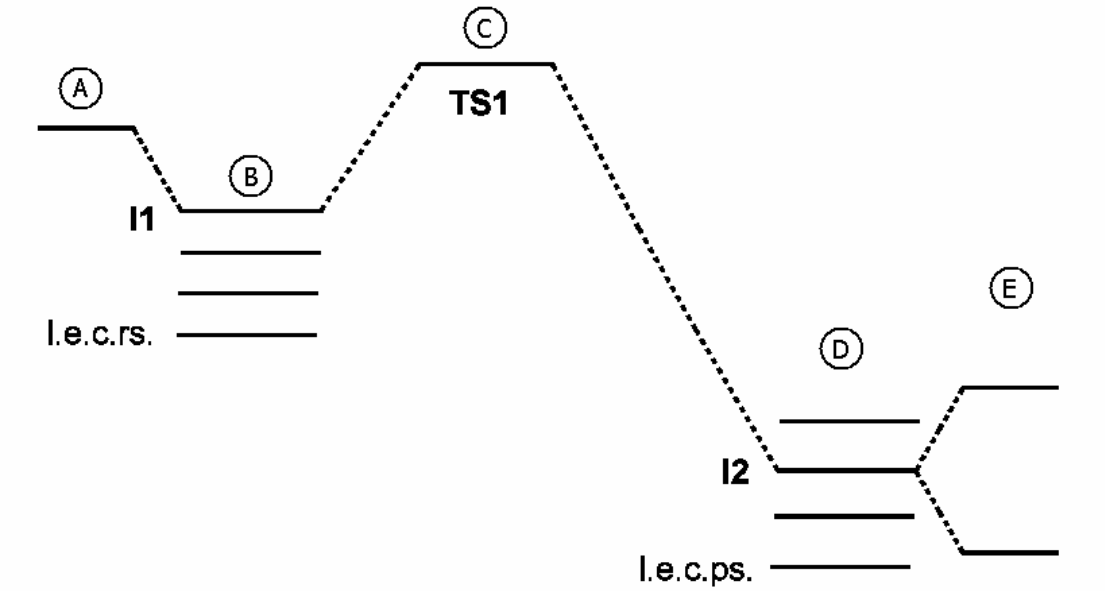

Figure 7.3. Reaction profile for the overall complexation of $PtC'_xD'_y$ with molecular fragments according to eqn 7.3 and eqn 7.4. A) DF41-H_2O + $PtC'_xD'_y$ are separated; B) DF41-H_2O and $PtC'_xD'_y$ interact in various ways resulting in an array of DF41---$PtC'_xD'_y$ configurations. The configuration of lowest energy is termed l.e.c.rs whereas the configuration that leads to the transition state structure (TS1) is termed I1. These two structures may or may not be the same; C) TS structure for DF41---$PtC'_xD'_y$ (structure TS1); D) DF40-N3---$PtC'_{x-1}D'_y$ ----C'. The configuration of lowest energy is termed l.e.c.ps whereas the configuration following from the transition state structure (TS1) is termed I2. These two structures may or may not be the same; E) DF40-N3---$PtC'_{x-1}D'_y$ + C' are separated. Note: this is a simplified and generic representation of a reaction profile when DF41 is involved. See Figures 7.5, 7.8 and 7.11 for specific reaction profiles

The relevant equations for this process are:

NCB: [DF41-H_2O] + $PtC'_xD'_y$ ➔ [DF41-$PtC'_xD'_y$] + H_2O (7.3)

LER: [DF41-$PtC'_xD'_y$] + H_2O ➔ [DF41-$PtC'_{x-1}D'_y$] + [C'-H_2O] (7.4)

where $PtC'_xD'_y$ represents the Pt(II) complexes and C' the leaving ligand.

What follows is a description of the LER part of the complexation between DF41 and each of the four Pt(II) complexes studied here. Although numerous reaction profiles could be traced, we have attempted to describe at least one starting from the lowest energy configuration of DF41---$PtC'_xD'_y$ (l.e.c.rs) all the way down to the lowest energy configuration in the LER products side (l.e.c.ps). Yet the calculation of the full reaction profile (all the intermediates and TS structures) has not been possible for some Pt(II)

complexes due to its complexity. Nonetheless the TS between I1 and I2 was calculated for all cases (for selected geometric parameters, see Table D-8, Appendix D).

7.3.2.2.1 When Pt(II) complex is $PtCl_4^{2-}$

A TS structure (See Figure 7.4) was calculated with Berny optimization of a trigonal-bipyramidal-like TS structure.[170] I1 and I2 (See Figure 7.4) structures were obtained by optimization of initial configurations set up by subtracting or adding a fraction of the imaginary frequency displacement vector from the TS atomic coordinates, respectively. Therefore Ea and $\Delta G_{I2\text{-}I1}$ were calculated to be 27.5 and -4.7 kcal/mol, respectively.

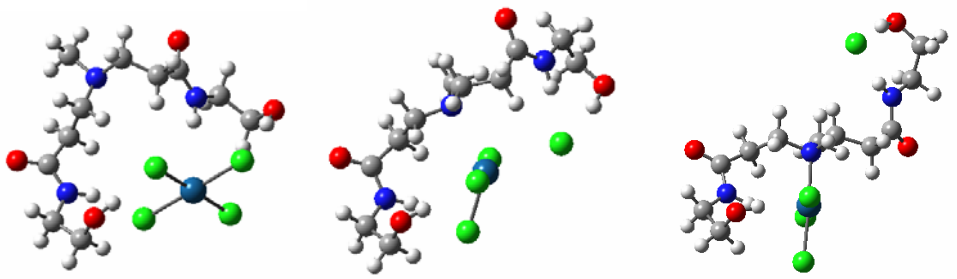

Figure 7.4. Solventless binding of $PtCl_4^{2-}$ to tertiary amine (N3) in unprotonated pocket. Left: I1; Middle: TS; Right: I2: The leaving ligand, Cl^-, interacts with the secondary amide hydrogen (N2-H---Cl: 2.29 Å) and with the hydroxyl hydrogen (~O-H---Cl: 2.14 Å) of the open branch

7.3.2.2.2 When Pt(II) complex is $PtCl_3(H_2O)^-$

$PtCl_3(H_2O)^-$ reacts through a number of steps described by the following equations starting with the NCB product DF41---$PtCl_3(H_2O)^-$ (I1B) that is obtained –according to eqn 7.3- with a ΔG_{NCB} = -7.7 kcal/mol. (for reaction energies according to eqn 7.3 and selected geometric parameters of several DF41---$PtC'_xD'_y$ conformers, see Tables D-4 to D-7 respectively, Appendix D).

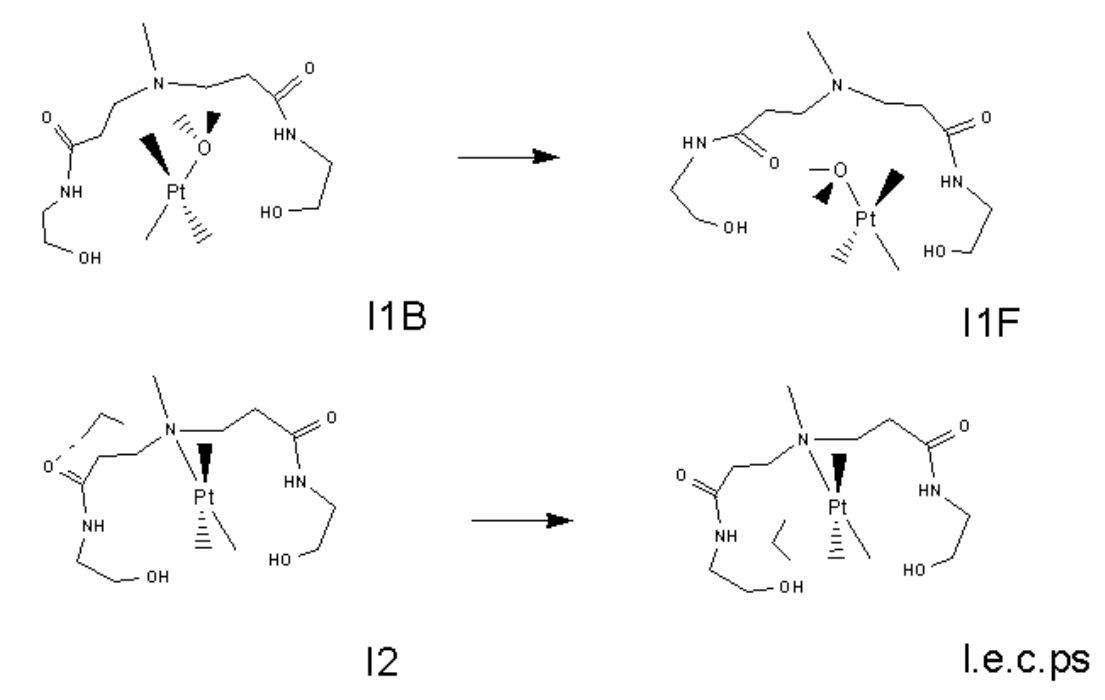

Figure 7.5. Stable points along the solventless LER: DF41---$PtCl_3(H_2O)^-$ ===> DF40-N3---$PtCl_3^-$---(H_2O)

Step 1: Accommodation of $PtCl_3(H_2O)^-$ inside the pocket

The reactant (I1B) and product (I1F) are represented in Figure 7.5.

DF41---$PtCl_3(H_2O)^-$ (I1B) ===> DF41---$PtCl_3(H_2O)^-$ (I1F)

Ea and $\Delta G_{I1F-I1B}$ are 12.1 and 3.8 kcal/mol, respectively. During this step a ~N3---H_2O-Pt hydrogen bond (length = 1.67 Å) is broken and another ~C=O---H_2O-Pt hydrogen bond (length = 1.73 Å) is formed and the orientation of the amide O atoms in the pocket change from outward-outward (I1B) to outward-inward (I1F).

Step 2: LER: Pt(II) binds to N3

The reactant (I1F) and product (I2) are represented in Figure 7.5.

DF41---$PtCl_3(H_2O)^-$ (I1F) ===> DF40-N3---$PtCl_3^-$---(H_2O) (I2)

Ea and ΔG_{I2-I1F} are 20.5 and -3.3 kcal/mol, respectively. Once this step is complete, the leaving ligand (H_2O) forms a ~C=O---HOH hydrogen-bond of length 1.91 Å. The orientation of the amide O atoms in the pocket changes back to outward-outward.

Step 3: Re-accommodation of water inside pocket (leading to l.e.c.ps)

The reactant (I2) and product (l.e.c.ps) are represented in Figure 7.5.

DF40-N3---$PtCl_3^-$---(H_2O) (I2) ===> DF40-N3---$PtCl_3^-$---(H_2O) (l.e.c.ps)

ΔG for this step is -4.0 kcal/mol. No TS structure was calculated in between stationary points. Taking the three first steps above together yield a $\Delta G_{LER(overall)}$ = -3.5 kcal/mol. The next step, ligand release, is not thermodynamically favorable (ΔG = 2.5 kcal/mol) although $LER_{overall}$ + ligand release is still favorable (ΔG = -1.0 kcal/mol).

Table 7.3 summarizes all the stationary points found along the reaction energy profile whereas Figures 7.6 and 7.7 illustrate the reaction energy profile and the evolution of the main distances of this process respectively.

Table 7.3: Difference in electronic energy with ZPE correction (ΔE_0), enthalpy (ΔH) and free energy (ΔG) (kcal/mol) relative to energetics of DF41-H_2O + $PtCl_3(H_2O)^-$ (E(DF41-H_2O) + E($PtCl_3(H_2O)^-$)= 0.0 kcal/mol) for stationary points along the reaction profile of the solventless complexation: DF41-H_2O + $PtCl_3(H_2O)^-$ => DF40-N3-$PtCl_3^-$ + $(H_2O)_2$

Stationary point	ΔE_0	ΔH	ΔG
I1B (l.e.c.rs)	-11.7	-10.9	-7.7
TSA	0.1	1.3	1.8
I1F	-6.9	-5.9	-3.8
TS1	13.9	14.7	19.1
I2	-11.8	-11.0	-7.2
l.e.c.ps	-15.6	-14.5	-11.2
I3 (separated products)	-9.7	-8.8	-8.7

Figure 7.6. Reaction profile for solventless reaction: DF41-H_2O + $PtCl_3(H_2O)^-$=> DF40-N-$PtCl_3^-$ + $(H_2O)_2$

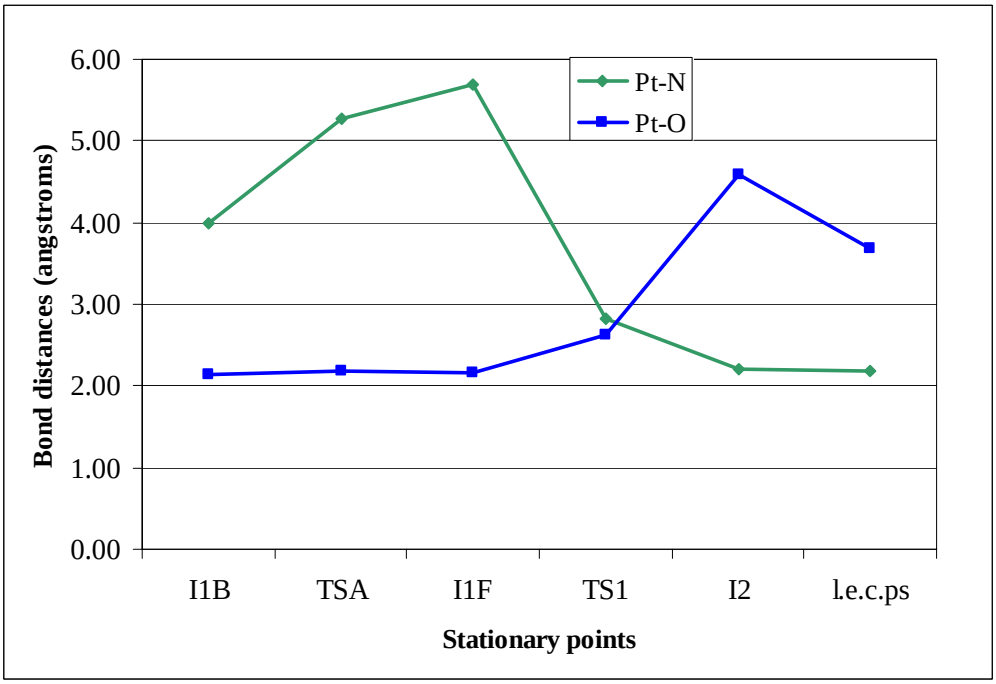

Figure 7.7. Evolution of bond distances Pt-N(entering ligand) and Pt-O (leaving ligand) along the course of the solventless LER: DF41---$PtCl_3(H_2O)^-$ ===> DF40-N3---$PtCl_3^-$---(H_2O)

7.3.2.2.3 When Pt(II) complex is *cis*-$PtCl_2(H_2O)_2$

Solventless LER of *cis*-$PtCl_2(H_2O)_2$ takes place according to the following steps starting with the NCB product DF41- *cis*-$PtCl_2(H_2O)_2$ (I1) that is obtained –according to eqn 7.3- with a ΔG_{NCB} = -5.2 kcal/mol.

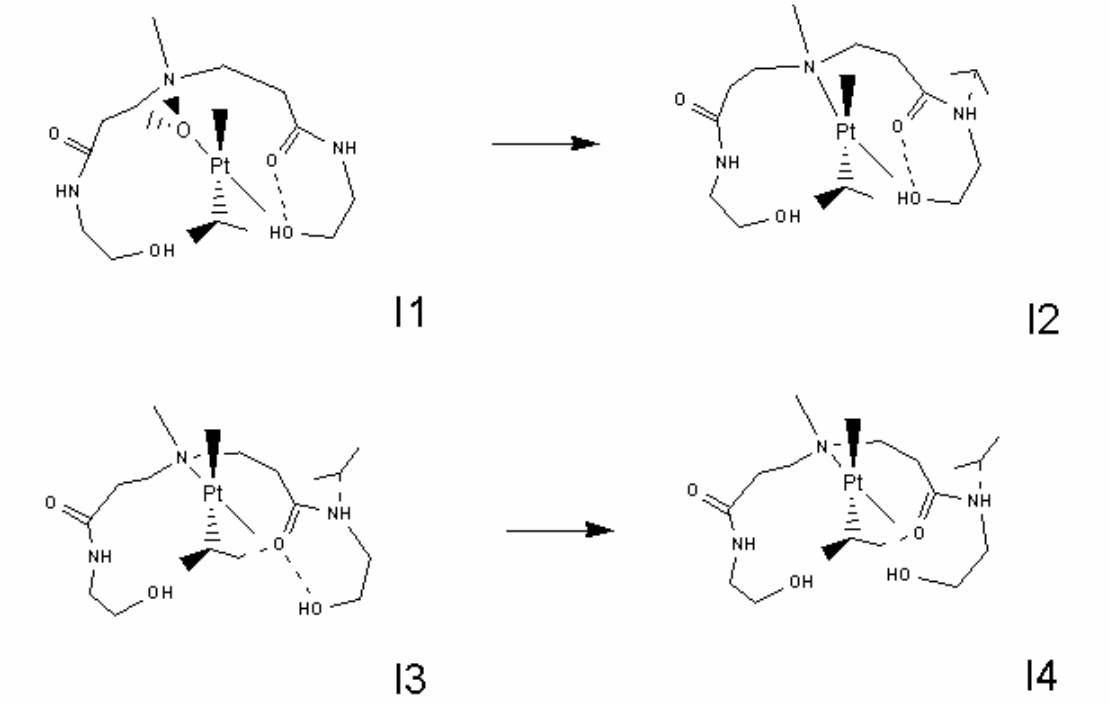

Figure 7.8. Stable points along the solventless LER: DF41---*cis*-$PtCl_2(H_2O)_2$ ===> DF40-N3-*cis*-$PtCl_2(H_2O)$---(H_2O)

Step 1: LER: Pt(II) binds to N3

The reactant (I1) and product (I2) are represented in Figure 7.8.

DF41---*cis*-$PtCl_2(H_2O)_2$ (I1) ===> DF40-N3---*cis*-$PtCl_2(H_2O)$---(H_2O) (I2)

Ea and $\Delta G_{I2\text{-}I1}$ are 21.1 and -9.9 kcal/mol, respectively. Three hydrogen bonds keep *cis*-$PtCl_2(H_2O)_2$ bound to the dendrimer pocket. But once the reaction is complete, the

~N3---HOH hydrogen bond of length 1.61 Å is broken. The leaving ligand H_2O forms another (~NH----OH_2) hydrogen bond of length 1.89 Å.

The next two steps involve accommodation of the *cis*-$PtCl_2(H_2O)$ moiety inside the pocket.

Step 2: Breaking of ~Pt-OH_2---(OH)~ hydrogen bond

The reactant (I2) and product (I3) are represented in Figure 7.8. One of the two original hydrogen bonds (~Pt-OH_2---(OH)~ of bond length = 1.67 Å) in configuration I1 is broken but a weaker hydrogen bond (~Pt-OH_2---O=C~ of bond length 1.83 Å) is formed. This may explain why ΔG_{I3-I2} is 3.6 kcal/mol. Ea is 5.1 kcal/mol.

Step 3: Breaking of ~OH---O=C~ hydrogen bond

The reactant (I3) and product (I4) are represented in Figure 7.8. Upon reaction, the hydrogen bond ~OH---O=C~ (bond length = 1.88 Å) is broken. Then, the hydroxyl terminal group (OH) binds to the *cis*-$PtCl_2(H_2O)$ moiety (~OH---Cl bond distance = 2.31 Å). Ea and ΔG_{I4-I3} are 1.3 and -0.47 kcal/mol, respectively.

Without considering the last two steps in the profile reaction, ΔG_{LER} = -9.9 kcal/mol. The next step, ligand release (ΔG_{I5-I4} summed up with ΔG_{I3-I2} and ΔG_{I4-I3}) is not thermodynamically favorable (ΔG = 5.7 kcal/mol). However $LER_{overall}$ + ligand release is still favorable (ΔG = -4.2 kcal/mol). Table 7.4 summarizes all the stationary points found along the reaction energy profile whereas Figures 7.9 and 7.10 illustrate the reaction energy profile and the evolution of the main distances of this process.

Table 7.4: **Difference in electronic energy with ZPE correction (ΔE_0), enthalpy (ΔH) and free energy (ΔG) (kcal/mol) relative to energetics of DF41-H_2O + *cis*-$PtCl_2(H_2O)_2$ (E(DF41-H_2O) + E(*cis*-$PtCl_2(H_2O)_2$) = 0.0 kcal/mol) for stationary points along the reaction profile of the solventless complexation: DF41-H_2O + *cis*-$PtCl_2(H_2O)_2$ => DF40-N3- *cis*-$PtCl_2(H_2O)$ + $(H_2O)_2$**

Stationary point	ΔE_0	ΔH	ΔG
I1	-10.1	-10.1	-5.2
TS1	10.8	11.0	15.4
I2	-20.9	-20.8	-15.1
TS2	-15.6	-15.7	-9.2
I3	-16.7	-16.4	-11.5
TS3	-15.2	-15.1	-9.1
I4	-17.7	-17.3	-12.0
I5 (separated products)	-12.1	-11.8	-9.4

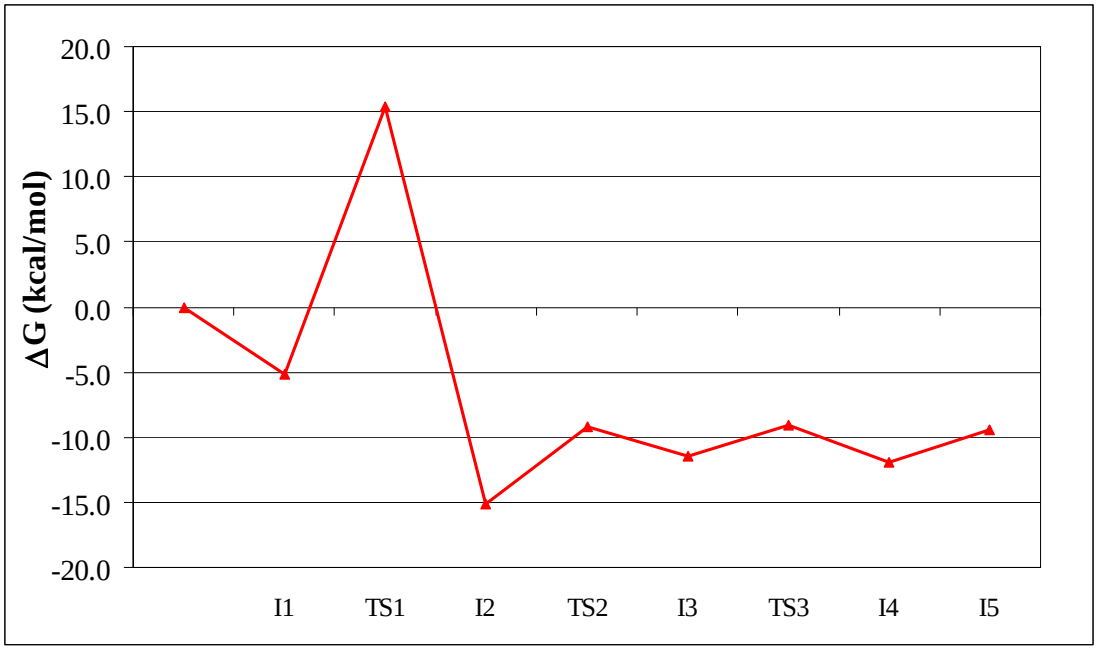

Figure 7.9. Reaction profile for the solventless reaction: DF41-H_2O + *cis*-$PtCl_2(H_2O)_2$ ==> DF40-N3- *cis*-$PtCl_2(H_2O)$ + $(H_2O)_2$

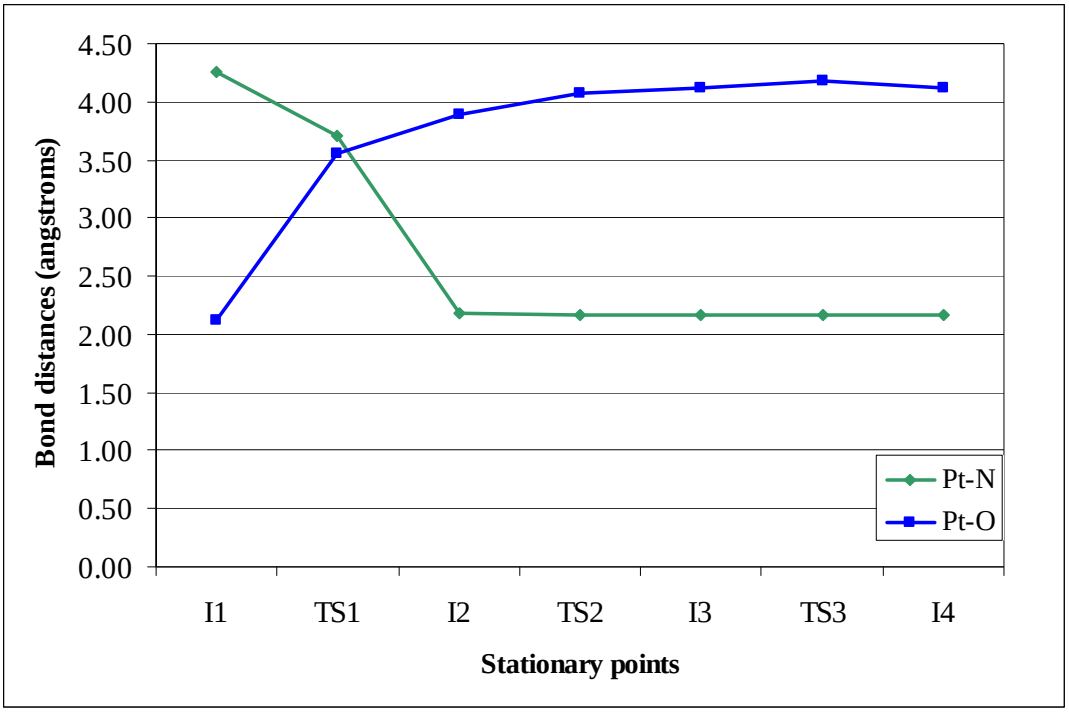

Figure 7.10. Evolution of bond distances Pt-N(entering ligand) and Pt-O (leaving ligand) along the course of the solventless LER: DF41---*cis*-$PtCl_2(H_2O)_2$ ===> DF40-N3-*cis*-$PtCl_2(H_2O)$---(H_2O)

7.3.2.2.4 When Pt(II) complex is *trans*-$PtCl_2(H_2O)_2$

Solventless LER of *trans*-$PtCl_2(H_2O)_2$ takes place according to the following steps starting with the NCB product DF41-*trans*-$PtCl_2(H_2O)_2$ (I1) that is obtained with a ΔG_{NCB} = -7.7 kcal/mol.

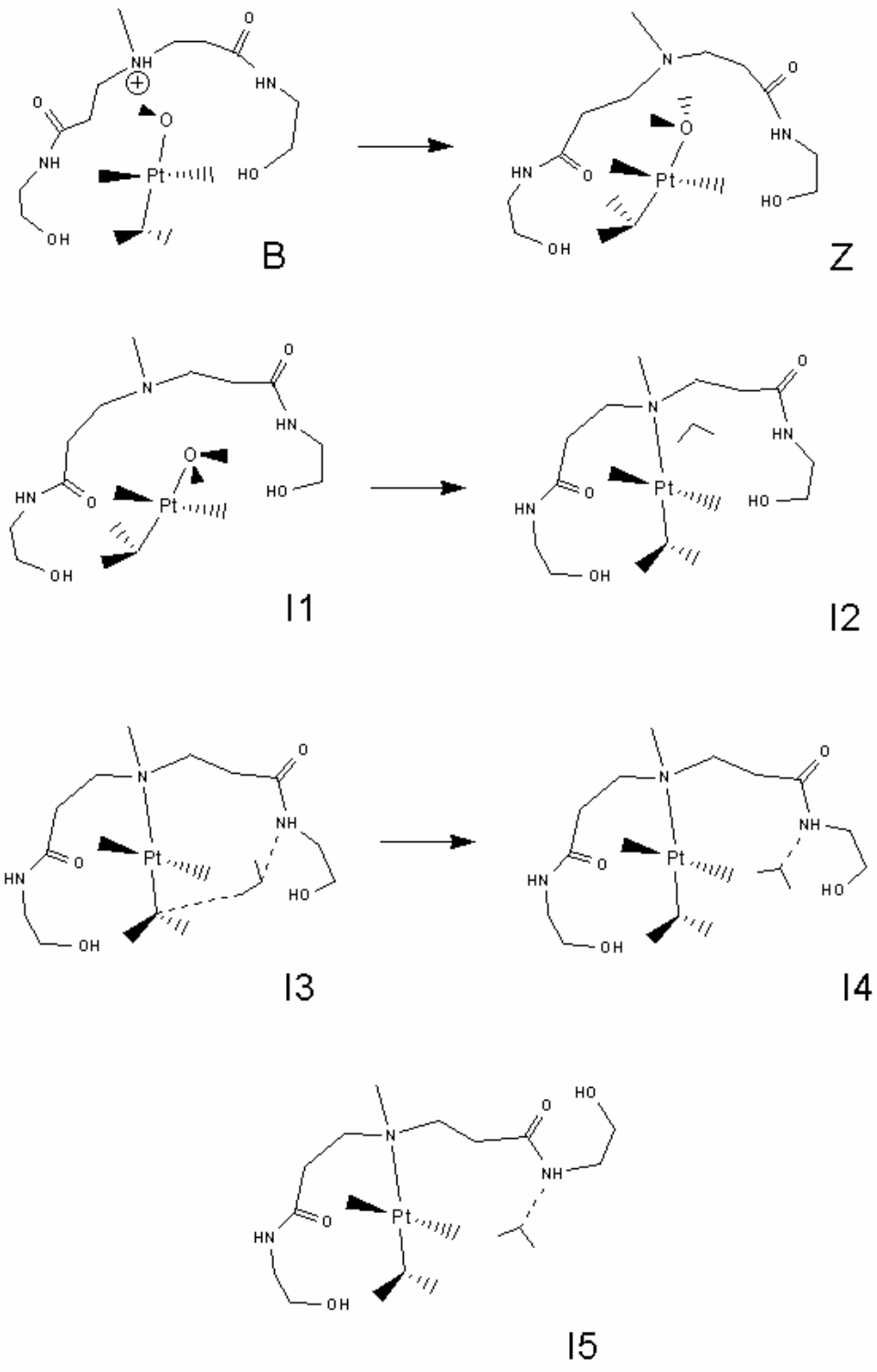

Figure 7.11. Stable points along the solventless LER: DF41---*trans*-$PtCl_2(H_2O)_2$ ===> DF40-N3-*trans*-$PtCl_2(H_2O)$---(H_2O)

Step 1: Accommodation of *trans*-$PtCl_2(H_2O)_2$ inside pocket

The reactant (B) and product (Z) are represented in Figure 7.11. Ea and ΔG_{Z-B} are 2.5 and 4.6 kcal/mol, respectively. During this step a branch rotates to better accommodate *trans*-$PtCl_2(H_2O)_2$. This is achieved by forming a Pt-OH_2---O=C~ hydrogen bond (bond length = 1.75 A°) in addition to the existent Pt-OH_2---(OH)~ (bond length = 2.13 A°). It should be noticed also that in the product the tertiary amine site (N3) is no longer protonated.

Step 2: Breaking of N3---H_2O-Pt hydrogen-bond

The reactant (Z) and product (I1) are represented in Figure 7.11. Ea and ΔG_{I1-Z} are 9.0 and 4.1 kcal/mol, respectively. During this step, the water bound to N3 rotates, thus breaking the N3---H_2O-Pt hydrogen-bond (bond length = 1.56 Å).

Step 3: LER. Pt(II) binds to N3

The reactant (I1) and product (I2) are represented in Figure 7.11.

DF41---*trans*-$PtCl_2(H_2O)_2$ ===> DF40-N3-*trans*-$PtCl_2(H_2O)$---(H_2O)

Ea and ΔG_{I2-I1} are 18.3 kcal/mol and -7.7 kcal/mol. The Pt-OH_2---O=C~ hydrogen bond formed in step 1 is broken.

Step 4: Accommodation of water inside the pocket

The reactant (I2) and product (I3) are represented in Figure 7.11. No TS structure was sought. ΔG_{I3-I2} is -0.54 kcal/mol. A ~NH---OH_2 hydrogen bond is formed (bond length = 2.03 Å).

Step 5: Accommodation of water inside the pocket

The reactant (I3) and product (I4) are represented in Figure 7.11. No TS structure was sought. ΔG_{I3-I2} is -1.7 kcal/mol. The ~NH---OH_2 hydrogen bond formed in step 4 shortens a bit (bond length = 1.96 Å).

Step 6: Accommodation of water inside the pocket

The reactant (I4) and product (I5) are represented in Figure 7.11. No TS structure was sought. ΔG_{I3-I2} is -1.8 kcal/mol. The ~NH---OH_2 hydrogen bond formed in step 4 shortens a bit further (bond length = 1.92 Å). One of the dendrimer pocket branches rotate forming an internal ~C=O---OH~ bond of 1.86 Å.

Considering all the steps (from l.e.c.rs to l.e.c.ps), $\Delta G_{LER(overall)}$ = -3.0 kcal/mol. The next step, ligand release, is not thermodynamically favorable (ΔG = 1.5 kcal/mol). However $LER_{overall}$ + ligand release is still favorable (ΔG = -1.5 kcal/mol). Table 7.5 summarizes all the stationary points found along the reaction energy profile whereas Figures 7.12 and 7.13 illustrate the reaction energy profile and the evolution of the main distances of this process.

Table 7.5: **Difference in electronic energy with ZPE correction (ΔE_0), enthalpy (ΔH) and free energy (ΔG) (kcal/mol) relative to energetics of DF41-H_2O + *trans*-$PtCl_2(H_2O)_2$ (E(DF41-H_2O) + E(*trans*-$PtCl_2(H_2O)_2$) = 0.0 kcal/mol) for stationary points along the reaction profile of the solventless complexation: DF41-H_2O + *trans*-$PtCl_2(H_2O)_2$ => DF40-N3- *trans*-$PtCl_2(H_2O)$ + $(H_2O)_2$**

Stationary point	ΔE_0	ΔH	ΔG
B	-11.8	-11.1	-7.7
TSA	-9.3	-8.6	-6.1
Z	-6.4	-5.7	-3.1
TSB	2.5	3.3	5.3
I1	-1.1	0.0	1.0
TS	17.7	18.3	23.3
I2	-9.8	-8.4	-6.7
I3	-11.6	-10.5	-7.2
I4	-13.0	-12.1	-8.9
I5	-15.5	-14.8	-10.7
I6 (separated products)	-13.4	-13.5	-9.2

Figure 7.12. Reaction profile for the solventless reaction: DF41-H_2O + *trans*-$PtCl_2(H_2O)_2$ ==> DF40-N3- *trans*-$PtCl_2(H_2O)$ + $(H_2O)_2$

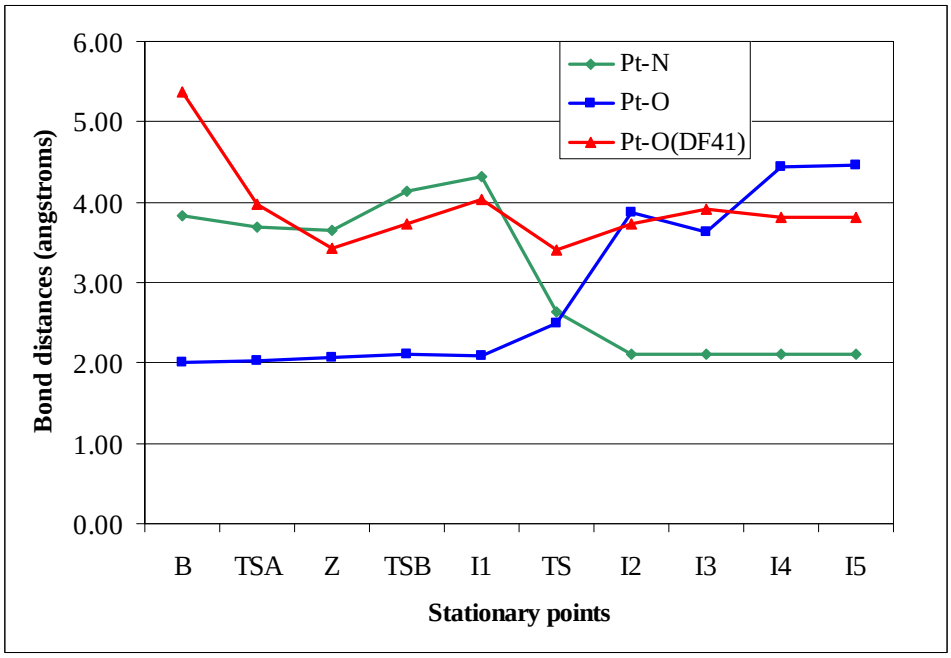

Figure 7.13. Evolution of bond distances Pt-N(entering ligand) and Pt-O (leaving ligand) along the course of the solventless LER: DF41---*trans*-$PtCl_2(H_2O)_2$ ===> DF40-N3-*trans*-$PtCl_2(H_2O)$---(H_2O). Evolution of Pt-O(DF41) is also followed. Note: Pt-O(DF41) is the distance between Pt atom and an amide O. See text for details

Table 7.6: ΔG of reaction (kcal/mol) for the individual processes of the complexation between Pt(II) compounds and the tertiary amine site (N3) of DF41 according to DF41---PtC'$_x$D'$_y$ ==> DF40-N-PtC'$_{x-1}$D'$_y$---C'$_x$

	Species ($PtC'_xD'_y$)			
Process	$PtCl_4^{2-}$	$PtCl_3(H_2O)^-$	*cis*-$PtCl_2(H_2O)_2$	*trans*-$PtCl_2(H_2O)_2$
NCB[a]	-33.2	-7.7	-5.2	-7.7
l.e.c.rs to I1	0.0	3.8	0.0	8.7
I1 to I2 (LER)	-4.7	-3.3	-9.9	-7.7
I2 to l.e.c.ps	0.0	-4.0	0.0	-4.0
l.e.c.rs to l.e.c.ps ($LER_{overall}$)	-4.7	-3.5	-9.9	-3.0
Ligand release (lr)	-31.0	2.5	5.7	1.5
$LER_{overall}$ + lr	-35.7	-1.0	-4.2	-1.5
Total (NCB + $LER_{overall}$ + lr)	-68.9	-11.2[b]	-15.1[b]	-10.7[b]

[a]NCB yields DF41-X, product of the following reaction: DF41-H2O + X ➔ DF41-X + H2O
[b]These values do not include the ligand release (lr) energy

The NCB order of binding ($PtCl_4^{2-}$ > $PtCl_3(H_2O)^-$~ *trans*-$PtCl_2(H_2O)_2$ > *cis*-$PtCl_2(H_2O)_2$ follows somewhat the trend in electrostatic charge of the Pt(II) complexes. Cl^- is released upon LER of $PtCl_4^{2-}$ whereas when its mono- and diaquated complexes undergo LER, H_2O is released. The ΔG_{LER} (ΔG_{I2-I1}) order of binding (*cis*-$PtCl_2(H_2O)_2$ > *trans*-$PtCl_2(H_2O)_2$ > $PtCl_4^{2-}$ > $PtCl_3(H_2O)^-$) seems to suggest that di-aquated Pt(II) species (uncharged molecules) are more ready to exchange their ligand (water) for N3, although there is no favorable tendency to let it go away the pocket (as ligand release energies are positive). The $\Delta G_{LER(overall)}$ order of binding coincides with ΔG_{LER} only when I1 is the l.e.c.rs. This is not the case for $PtCl_3(H_2O)^-$ nor for *trans*-$PtCl_2(H_2O)_2$. Therefore it should be easier in principle for *cis*-$PtCl_2(H_2O)_2$ and $PtCl_4^{2-}$ to undergo LER. However other factors should be considered too. For instance, Table 7.7 shows that the activation energies increase due to the presence of branches when either $PtCl_4^{2-}$ or $PtCl_3(H_2O)^-$ react directly with the N3 site. This seems to cast doubts on whether

$PtCl_4^{2-}$ really binds directly to N3 or not, especially because the barrier for its aquation to $PtCl_3(H_2O)^-$ (23.7 kcal/mol) is lower than the barrier for direct LER (27.5 kcal/mol).

Table 7.7: Energy barriers (Ea) toward the LER of $PtC'_xD'_y$ complexes in absence and presence of dendrimer branches compared with barriers toward aquation of $PtC'_xD'_y$

Species	No branches $N(CH_3)_3$	Branches (DF41)	Aquation
$PtCl_4^{2-}$	20.5	27.5	23.7[a]
$PtCl_3(H_2O)^-$	16.6	20.5	16.6/29.9
cis-$PtCl_2(H_2O)_2$	21.6	21.1	
trans-$PtCl_2(H_2O)_2$	25.6	18.3	

[a] Experimental value: 21.0 kcal/mol[151]

Table 7.7 also shows that the activation energy remains high toward binding to N3 in the presence of branches for *cis*-$PtCl_2(H_2O)_2$ (from 21.6 kcal to 21.1 kcal/mol). This fact together with its weak NCB energy (-5.2 kcal/mol, Table 7.6) suggest that this Pt(II) complex may not be able to directly bind to N3.

Table 7.7 also shows a reduction of about 7.3 kcal/mol in the activation energy when *trans*-$PtCl_2(H_2O)_2$ binds to N3 in outer pocket environments with respect to $N(CH_3)_3$. However there are other factors to weigh here. First, its NCB free energy is weak (-7.7 kcal/mol, Table 7.6); second, *trans*-$PtCl_2(H_2O)_2$ is not as readily available as other Pt(II) complexes would be because it can only appear once the large activation energy (29.9 kcal/mol) for the second aquation of $PtCl_4^{2-}$ toward *trans*-$PtCl_2(H_2O)_2$ is overcome; third, its I1 structure can only be reached once the two kinetic barriers (section 7.3.2.2.4) of thermodynamically unfeasible elementary reactions are overcome.

From Table 7.7 it is observed also that when Pt(II) complexes bind to the N3 site of an outer pocket (DF41) Ea follows the trend -from greater to least: $PtCl_4^{2-}$ > *cis*-$PtCl_2(H_2O)_2$ > $PtCl_3(H_2O)^-$ > *trans*-$PtCl_2(H_2O)_2$. From this trend, we realize that $PtCl_3(H_2O)^-$ has the second *lowest* E_a. On the other hand, we noticed that $PtCl_3(H_2O)^-$

can be obtained from the first aquation of $PtCl_4^{2-}$, a process with lower E_a than direct LER of $PtCl_4^{2-}$ to N3 in DF41 as annotated before. In fact, geometry analysis shows that the Pt-N3 distance in I1 is 3.93 Å for $PtCl_3(H_2O)^-$ (5.60 Å when facing $PtCl_4^{2-}$) when binding to $N(CH_3)_3$ (Values taken from Table D-2, Appendix D) However there is no significant difference in the Pt-N3 distance between $PtCl_4^{2-}$ (5.72 Å) and $PtCl_3(H_2O)^-$ (5.70 Å) when binding to DF41 occurs (Values taken from Table D-8, Appendix D). Other factors are: a barrier of 12.1 kcal/mol that needs to be overcome in order to arrive at the I1 structure and the fact that the barrier to aquate $PtCl_3(H_2O)^-$ to *cis*-$PtCl_2(H_2O)_2$ is lower (16.6 kcal/mol) than needed to overcome the barrier to bind of Pt(II) to N3 (20.5 kcal/mol) making depletion of $PtCl_3(H_2O)^-$ to form *cis*-$PtCl_2(H_2O)_2$ more likely.

Finally, we have to account for the presence of counterions that can occupy the dendrimer pockets and compete with the Pt(II) complexes as seen in Chapter VI. It is observed that the highest NCB free energy of a counterion binding a DF41 pocket (ΔG = -62.3 kcal/mol. See Table D-9, Appendix D) is lower than the NCB+LER free energy to bind $PtCl_4^{2-}$ to N3 site (ΔG = -68.9 kcal/mol. See Table D-9, Appendix D). This is true only for $PtCl_4^{2-}$ and not for the mono- and diaquated complexes. Therefore, thermodynamics suggests that the free energy made available by direct LER of mono- and diaquated complexes of $PtCl_4^{2-}$ preceded by NCB binding is not enough to overcome the competition of other ions (e.g. counterions) for the outer pockets (DF41).

7.4 Summary

When $PtCl_4^{2-}$ exchanges a Cl^- and attempts to bind to dendrimer sites, it is more likely to bind to a tertiary amine N (N3). This is in agreement with experimental results.[62]

By comparing the results of the complexation of Pt(II) species to N3 in both a single site molecule and an unprotonated outer pocket, it was found that the branches of outer pockets improve slightly the thermodynamic stability of Pt(II)-N3 moieties while increasing at the same time the kinetic barrier toward LER for some Pt(II) complexes like $PtCl_4^{2-}$ and $PtCl_3(H_2O)^-$.

An important finding was to realize that the combined NCB+LER free energy to bind a $PtCl_4^{2-}$ to an outer pocket N3 site was greater than the NCB free energy to bind any other competitor ion.

The energy barrier for the LER of $PtCl_4^{2-}$ to N3 site was found to be the highest among all Pt(II) complexes studied and higher than the barrier for aquation of $PtCl_4^{2-}$. However, the second lowest activation energy corresponds to $PtCl_3(H_2O)^-$. This suggests that an alternative pathway of less resistance conducting and aided by the solvent rather than direct LER of $PtCl_4^{2-}$ could actually be occurring. Therefore, the impact of the solvent (water) on the LER reaction is studied in the next Chapter.

CHAPTER VIII
SOLVENT MEDIATED LIGAND EXCHANGE REACTION OF TETRACHLOROPLATINATE ANION IN PAMAM-OH DENDRIMER POCKETS

8.1 Introduction

The study of solventless LER was a helpful initial approximation to the real case where solvent should be accounted for. This Chapter is mainly devoted to the effect of solvent on the LER of tetrachloroplatinate anion and its mono- and diaquated species. Binding to secondary amide site (N2) that was suggested in NMR studies[62] and Chapter VII is also studied, whereas binding of $PtCl_4^{2-}$ to hydroxyl O site (OH) was not analyzed because it was not detected in experimental work.

8.2 Methods

DFT was used to obtain minimum energy as well as TS structures with no symmetry constraints. TS structures were located by running either a Berny optimization[75] to a saddle point –traditional TS search- or the Synchronous Transit-Guided Quasi Newton (STQN) method[76] or both. The optimization of the geometries was followed by second derivative matrix calculations that provided estimates for the zero point energy (ZPE) and temperature corrections to the enthalpy and the Gibbs free energy at 298K. The activation energy (Ea) is calculated as the difference in enthalpy of the relevant states. No claim is held that the absolute values of the binding energies have been found –as stated in Chapters V, VI and VII. The calculations were done with Gaussian 03 suite of programs.[74]

8.3 Results and discussion

As it was found that outer pockets can host two water molecules (Chapter III), the addition of one water molecule to address the solvent effect is a convenient and adequate approximation. However to determine whether or not it is feasible to have a water

molecule and a Pt(II) complex in the same pocket we calculated thermodynamics of water release from a structure that contains them both initially (reactant) according to eqn 8.1. Results are given in Table 8.1.

$$DF41\text{-}H_2O\text{-}PtC'_xD'_y + H_2O \rightarrow DF41\text{-}PtC'_xD'_y + (H_2O)_2 \qquad (8.1)$$

Table 8.1: Electronic energy with ZPE correction (ΔE_0), enthalpy (ΔH) and free energy (ΔG) of reaction (kcal/mol) for release of water according to eqn 8.1

Pt(II) complex	ΔE_0	ΔH	ΔG
$PtCl_4^{2-}$	5.1	4.9	2.8
$PtCl_3(H_2O)^-$	5.4	5.4	3.1
cis-$PtCl_2(H_2O)_2$	6.4	6.7	2.1
trans-$PtCl_2(H_2O)_2$	4.6	4.8	1.1

As all reactions are found unfavorable toward release of water we conclude that co-hosting water with Pt(II) complexes is feasible and therefore the addition of one water to study the impact of water on the LER of Pt(II) complexes is justified.

In Chapter VII, we found that the most favorable dendrimer outer pocket atom site for solventless complexation of $PtCl_4^{2-}$ was the tertiary amine nitrogen (N3). To test whether this is still true when a water molecule is co-hosted with $PtCl_4^{2-}$, we calculated the ΔG of reaction (eqn 8.2) for the overall complexation of $PtCl_4^{2-}$ in the presence of one water molecule to tertiary amine N (N3), secondary amide N (N2), hydroxyl O (OH) and amide O (O).

$$DF41\text{-}H_2O\text{-}PtCl_4^{2-} + H_2O \rightarrow DF40\text{-}(Site)\text{-}PtCl_3^-\text{-}H_2O + Cl^-(H_2O) \qquad (8.2)$$

The calculated free energies of reaction were -35.7, -31.2, -29.0 and -24.6 kcal/mol for sites N3, OH, N2 and O respectively. The order of binding was not altered: N3 is still the most favorable dendrimer outer pocket atom site for the complexation of $PtCl_4^{2-}$ even when water is present.

8.3.1 LER of $PtCl_4^{2-}$ with DF41: solvent-mediated pathway

The effect of the water molecule on the complexation of Pt(II) complexes to tertiary amine nitrogen (N3) binding site is tested.

8.3.1.1 When the Pt(II) complex is $PtCl_4^{2-}$ and Pt(II) binds to N3

The energetics of stable points along the reaction profile was calculated with reference to the energetics of the product of the following NCB reaction:

$$DF41\text{-}(H_2O)_2 + PtCl_4^{2-} \rightarrow DF41\text{-}H_2O\text{-}PtCl_4^{2-} + H_2O \qquad (8.3)$$

As the product of reaction 8.3 could appear in several $DF41\text{-}H_2O\text{-}PtCl_4^{2-}$ configurations. The configuration of lowest energy (l.e.c.rs) was chosen (see Figure 6.5, lower right). However, structure I1 (see Figure 6.5, lower left) was chosen as the configuration that leads to the LER of $PtCl_4^{2-}$ first, because there a water molecule bridges a tertiary amine N (N3) and $PtCl_4^{2-}$ and second, because the energy needed to pass from l.e.c.rs. to I1 was found to be low (ΔG = 0.25 kcal/mol). From there, solvent mediated reaction of $PtCl_4^{2-}$ with N3 could proceed through a number of steps described by the following equations:

Step 1: Aquation of $PtCl_4^{2-}$ to $PtCl_3(H_2O)^-$ inside a pocket

$$DF41\text{-}H_2O\text{-}PtCl_4^{2-}\ (I1) \rightarrow DF41\text{-}PtCl_3(H_2O)^-\text{---}Cl^-\ (I2) \qquad (8.4)$$

The reactant (I1) and the product (I2) are represented in Figure 8.1. The Ea and $\Delta G_{I2\text{-}I1}$ for this step are 23.6 kcal/mol and -1.8 kcal/mol.

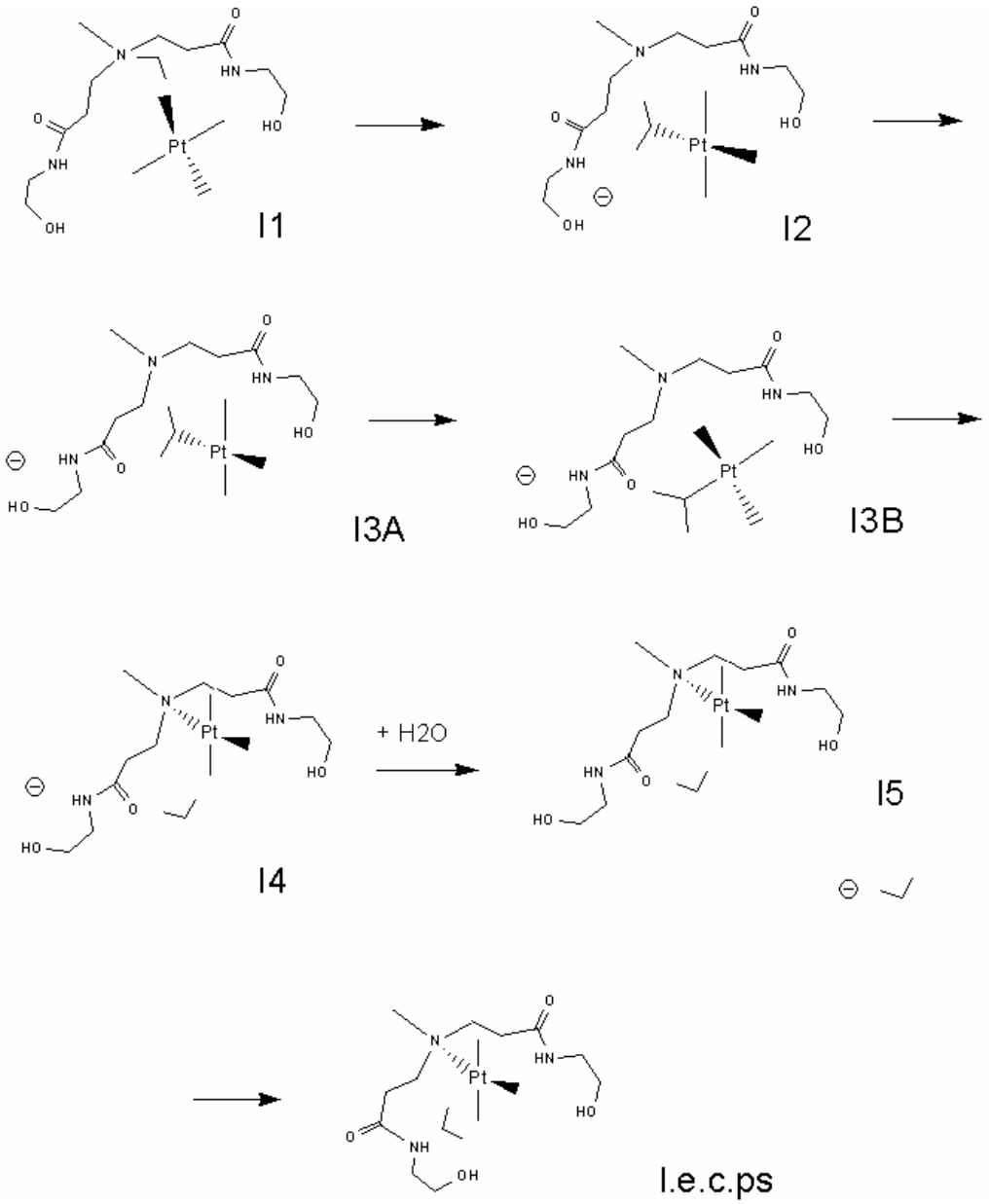

Figure 8.1. Stable points along the solvent mediated LER: [DF41-H_2O---$PtCl_4^{2-}$] ==> [DF40-N3-$PtCl_3^-$---$Cl(H_2O)^-$]. (a) I1 is the NCB product DF41-H_2O---$PtCl_4^{2-}$ (b) I2 is the aquated product DF41-$PtCl_3(H_2O)^-$--Cl^- (c) I3A is the aquated product DF41-$PtCl_3(H_2O)^-$---Cl^- after branch rotation (d) I3B is the aquated product DF41-$PtCl_3(H_2O)^-$--Cl^- upon reaccommodation of I3A inside the pocket (e) I4 is the LER product DF40-N-$PtCl_3^-$--$(H_2O)^-$---Cl^- (f) I5 is the LER structure DF40-N-$PtCl_3^-$---(H_2O) resulting upon release of Cl^- as $Cl(H_2O)^-$ (g) l.e.c.ps is the lowest energy configuration for DF40-N-$PtCl_3^-$---(H_2O) in the product side, resulting upon closure of the open branch

Step 2: Breaking of Cl---HOH interaction

The reactant (I2) and the product (I2B) are represented in Figure 8.2. ΔG_{I2B-I2} for this step is -1.0 kcal/mol.

Step 3: Rotation of a branch

The reactant (I2B) and the product (I3A) are represented in Figure 8.2. $\Delta G_{I3A-I2B}$ for this step is -3.5 kcal/mol. This step resembles a similar branch rotation observed in the solventless LER of $PtCl_4^{2-}$ to the tertiary amine site (N3) (Chapter VII).

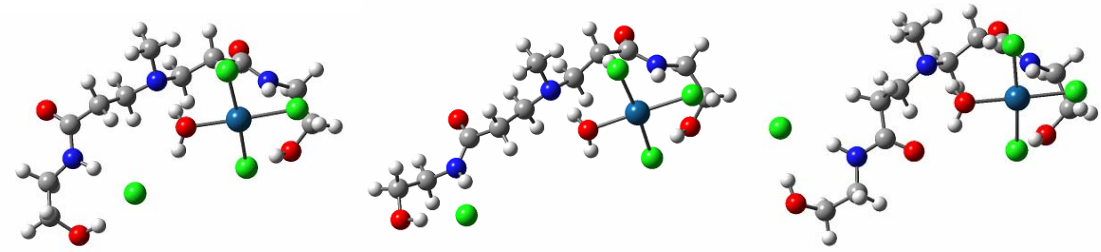

Figure 8.2. Rotation of a branch (step 3) in the solvent mediated reaction of $PtCl_4^{2-}$ with an outer pocket. Left: I2: δ1 and δ2 are -172.7° and 95.8° respectively; Middle: I2B: δ1 and δ2 are 165.7° and 142.2° respectively; Right: I3A; δ1 and δ2 are -114.2° and 127.0° respectively. Note: δ1 and δ2 are dihedral angles (in degrees) in the left branch, N3-C-C-C(carbonyl) and C-C-C(carbonyl)-N2

Step 4: Re-accommodation of $PtCl_3(H_2O)^-$ inside the pocket

The reactant (I3A) and the product (I3B) are represented in Figure 8.1. The Ea and $\Delta G_{I3B-I3A}$ for this step are 3.1 kcal/mol and -1.0 kcal/mol.

DF41-$PtCl_4^{2-}$---H_2O (I3A) ➔ DF41-$PtCl_3(H_2O)^-$--Cl^- (I3B) (8.5)

A ~N3---H_2O-Pt hydrogen bond (bond length = 1.81 Å) is broken in reactant structure I3A yielding a product with a ~C=O---H_2O-Pt hydrogen bond (bond length = 1.68 Å). This configurational change can be paralleled to a similar one observed in the solventless LER of $PtCl_3(H_2O)^-$ to N3 site (See Chapter VII for details). Comparing them, we observe that in the present case, the reaction is more feasible (ΔG varies from +3.8 to -1.0 kcal/mol) and the activation energy decreases (from 12.1 to 3.1 kcal/mol).

This can be due to both a weaker hydrogen-bond in the reactant (~N3---H_2O-Pt hydrogen bond length varies from 1.67 Å to 1.81 Å) and a stronger hydrogen bond in the product (~C=O---H_2O-Pt hydrogen bond varies from 1.73 Å to 1.68 Å).

Step 5: LER: Pt(II) binds to N3

The reactant (I3B) and the product (I4) are represented in Figure 8.1.

DF41-$PtCl_3(H_2O)^-$---Cl^- (I3B) ➔ DF40-N-$PtCl_3^-$---(H_2O)---Cl^- (I4) (8.6)

The Ea and $\Delta G_{I4\text{-}I3B}$ for this step are 21.6 kcal/mol and +0.47 kcal/mol ($\Delta E_{0(I4\text{-}I3B)}$ = -1.0 kcal/mol). Another reaction by which DF41-$PtCl_3(H_2O)^-$---Cl^- releases the accompanying Cl^- could occur simultaneously. (See section 8.3.1.2).

Step 6: Ligand release (removal of chloride)

A mechanistic sequence between the reactant (I4) and the product (I5) (both represented in Figure 8.1) was not traced. However, the reaction:

DF40-N-$PtCl_3^-$---(H_2O)---Cl^- (I4) + H_2O

➔ DF40-N-$PtCl_3$---(H_2O) (I5) + $Cl(H_2O)^-$ (8.7)

was found to be thermodynamically favorable ($\Delta G_{I5\text{-}I4}$ = -24.8 kcal/mol)

Step 7: Closure of the open branch

A mechanistic sequence between the reactant (I5) and the product (l.e.c.ps.) (both represented in Figure 8.1) was not traced. However, the reaction:

DF40-N-$PtCl_3^-$--(H_2O) (I5)

➔ DF40-N-$PtCl_3^-$---(H_2O) (l.e.c.ps) (8.8)

was found to be thermodynamically favorable ($\Delta G_{l.e.c.ps.\text{-}I5}$ = -3.8 kcal/mol). And. admission of an additional water molecule in the pocket as described by the following reaction

DF40-N3-$PtCl_3^-$---(H_2O) (l.e.c.ps) + $(H_2O)_2$

➔ DF40-N3-$PtCl_3^-$---$(H_2O)_2$ + H_2O (8.9)

was also found thermodynamically favorable (ΔG = -3.2 kcal/mol). Table 8.2 summarizes all the stationary points found along the reaction energy profile whereas Figures 8.3 and 8.4 illustrate the reaction energy profile and the evolution of the main bond distances of this process.

Table 8.2: Difference in electronic energy with ZPE correction (ΔE_0), enthalpy (ΔH) and free energy (ΔG) of reaction (kcal/mol) relative to those of DF41-H_2O--$PtCl_4^{2-}$ (E(l.e.c.rs)) = 0.0 kcal/mol) for stationary points along the reaction profile of the solvent mediated LER: [DF41-H_2O--$PtCl_4^{2-}$] + H_2O ===> [DF40-N3-$PtCl_3(H_2O)$]$^-$ + $Cl(H_2O)^-$. Reaction profile shown in Figure 8.3

Stationary point	ΔE_0	ΔH	ΔG
l.e.c.rs	0.0	0.0	0.0
I1	0.62	1.08	-0.25
TS1	24.6	24.7	23.5
I2	-1.3	-1.5	-2.1
I2B	-3.1	-3.6	-3.1
I3A	-6.1	-6.4	-6.6
TS3A	-3.0	-3.3	-3.6
I3B	-5.9	-5.8	-7.5
TS3B	16.0	15.8	16.3
I4	-6.9	-6.9	-7.1
I5	-28.5	-28.8	-31.9
l.e.c.ps	-34.3	-34.8	-35.7

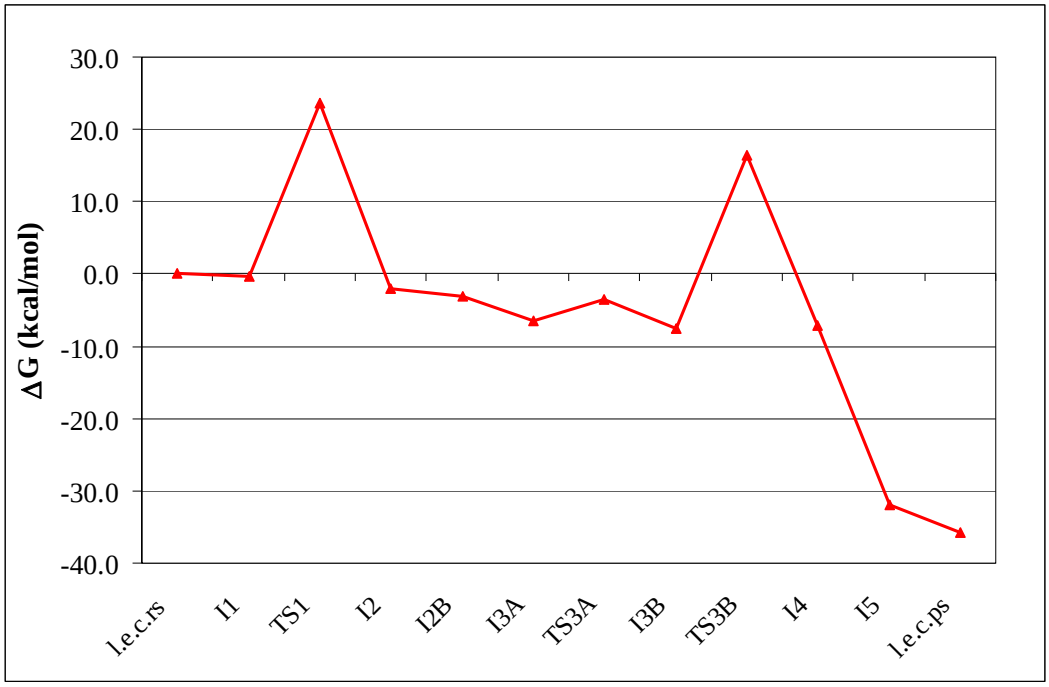

Figure 8.3. Reaction profile for the solvent mediated reaction [DF41-H_2O--$PtCl_4^{2-}$] + H_2O ===> [DF40-N3-$PtCl_3(H_2O)$]$^-$ + $Cl(H_2O)^-$

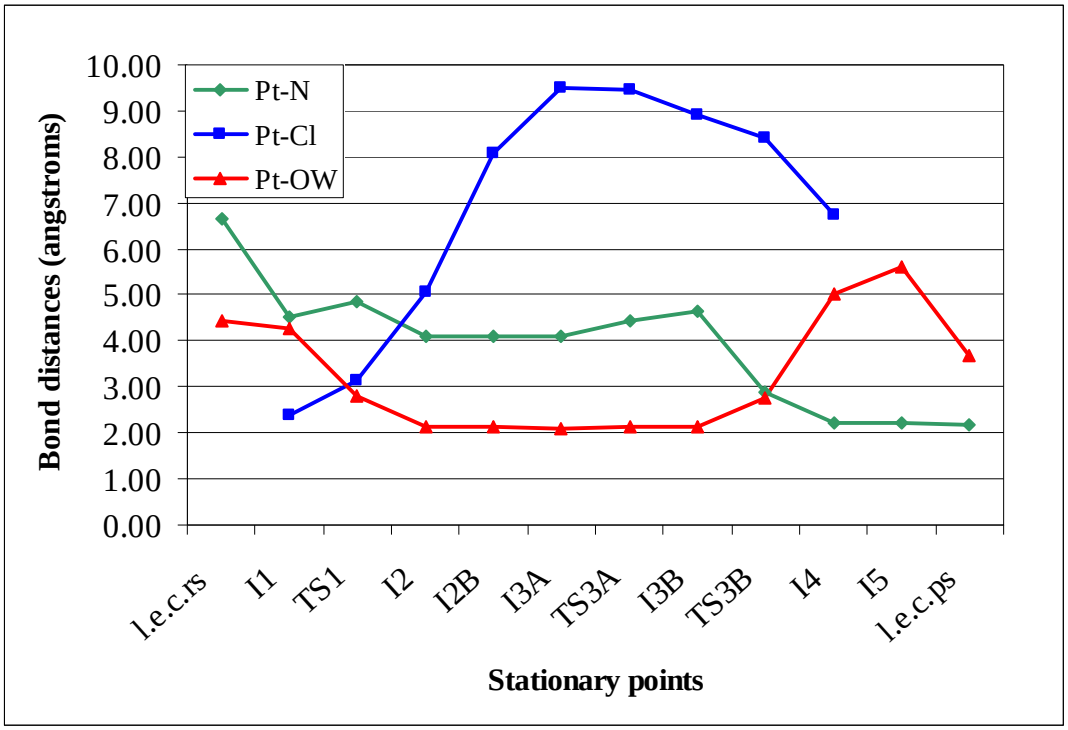

Figure 8.4. Evolution of bond distances: Pt-N(entering ligand), Pt-Cl (leaving ligand) and Pt-OW (water of solvation) along the course of the solvent mediated reaction [DF41-H_2O--$PtCl_4^{2-}$] + H_2O ===> [DF40-N3-$PtCl_3(H_2O)$]$^-$ + $Cl(H_2O)^-$

8.3.1.2 When the Pt(II) complex is $PtCl_3(H_2O)^-$ and Pt(II) binds to N3

In section 8.3.1.1 (Step 5) we mentioned that another reaction could take place simultaneously with the LER of $PtCl_3(H_2O)^-$ to the N3 site. That reaction is described by eqn 8.10:

DF41-$PtCl_3(H_2O)^-$---Cl^- (I3B) + H_2O

➔ DF41-$PtCl_3(H_2O)^-$ (J) + $Cl^-(H_2O)$ (8.10)

I3B (in eqn 8.10) is the configuration that results after aquation of $PtCl_4^{2-}$ to yield $PtCl_3(H_2O)^-$ and a Cl^- ion that remains in the pocket. Eqn 8.10 postulates the release of that Cl^- ion outside the pocket, leaving only $PtCl_3(H_2O)^-$ inside the pocket. No

mechanism has been traced for this particular reaction. Nevertheless, we found the reaction to be thermodynamically favorable (ΔG = -19.4 kcal/mol).

The product of eqn 8.10 (labeled J) could also be another DF41-$PtCl_3(H_2O)^-$ intermediate in the solventless LER of $PtCl_3(H_2O)^-$ described by eqn 8.11:

DF41-$PtCl_3(H_2O)^-$ ➔ [DF40-N3-$PtCl_3^-$---(H_2O)]$^-$ (8.11)

To illustrate this point, we put together the reaction profile of the solventless LER of $PtCl_3(H_2O)^-$ to N3 (Figure 7.6, Chapter VII) and the reaction profile of the solvent-mediated reaction of $PtCl_4^{2-}$ with N3 (Figure 8.3) up to the point before the LER of $PtCl_4^{2-}$ to N3 site takes place. Both profiles are connected by J (see eqn 8.10) and sketched in Figure 8.5.

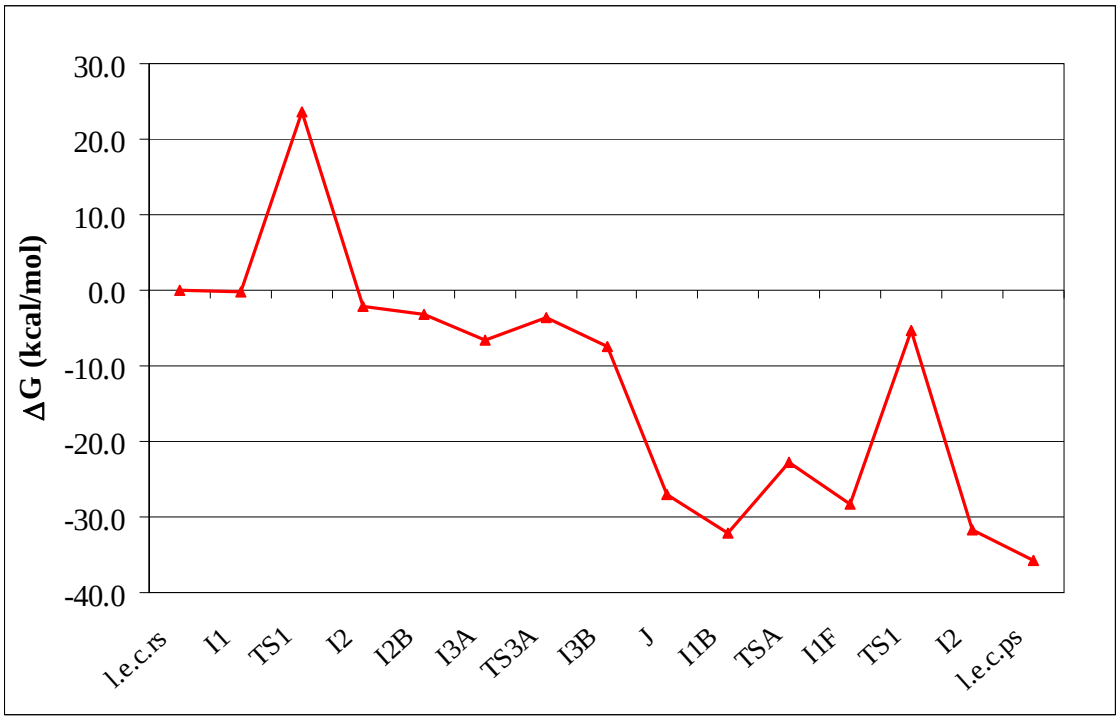

Figure 8.5. Reaction profile for the solvent mediated reaction [DF41-H_2O--$PtCl_4^{2-}$] + H_2O ==> [DF40-N3-$PtCl_3^-$---(H_2O)] + $Cl(H_2O)^-$. It was obtained by connecting the solventless LER of $PtCl_3(H_2O)^-$ to N3 (spanning from I1B to l.e.c.ps in the right side of the plot) to the reaction profile for solvent-mediated LER of $PtCl_4^{2-}$ with N3 up to the point where the aquated species (DF41-$PtCl_3(H_2O)^-$---Cl^-, I3B) is generated (spanning from l.e.c.rs to I3B in the left side of the plot)

The product of eqn 8.10 labeled J can also react with a water dimer according to the displacement reaction (ΔG = -4.6 kcal/mol) described by eqn 8.12:

$DF41\text{-}PtCl_3(H_2O)^-$ (J) + $(H_2O)_2$

$\rightarrow$ $DF41\text{-}PtCl_3(H_2O)^-\text{---}(H_2O)$ (C7B) + H_2O (8.12)

In the product configuration C7B, $PtCl_3(H_2O)^-$ can then react with the accompanying water to yield either *cis*-$PtCl_2(H_2O)_2$ (section 8.3.1.2.1.) or *trans*-$PtCl_2(H_2O)_2$ (section 8.3.1.2.2.) followed by the LER of the diaquated Pt(II) complexes to N3.

8.3.1.2.1 When Pt(II) binds to N3 through a pathway where *cis*-$PtCl_2(H_2O)_2$ is formed as intermediate

Binding Pt(II) to N3 through a pathway that includes *cis*-$PtCl_2(H_2O)_2$ can occur according to the following sequence of steps, where I1B –one among several isomeric conformers of $DF41\text{-}PtCl_3(H_2O)^-\text{---}H_2O$ is assumed to be obtained from rearrangement of water in conformer C7B (ΔG = -0.15 kcal/mol). The water ligand in the Pt(II) complex in I1B (Figure 8.6) forms a hydrogen bond with one amide O (bond length = 1.73 Å). The accompanying water forms a hydrogen bond ~N2-H---OH_2 (bond length = 1.92 Å) and ~OH----OH_2 of the other branch (bond length = 1.85 Å).

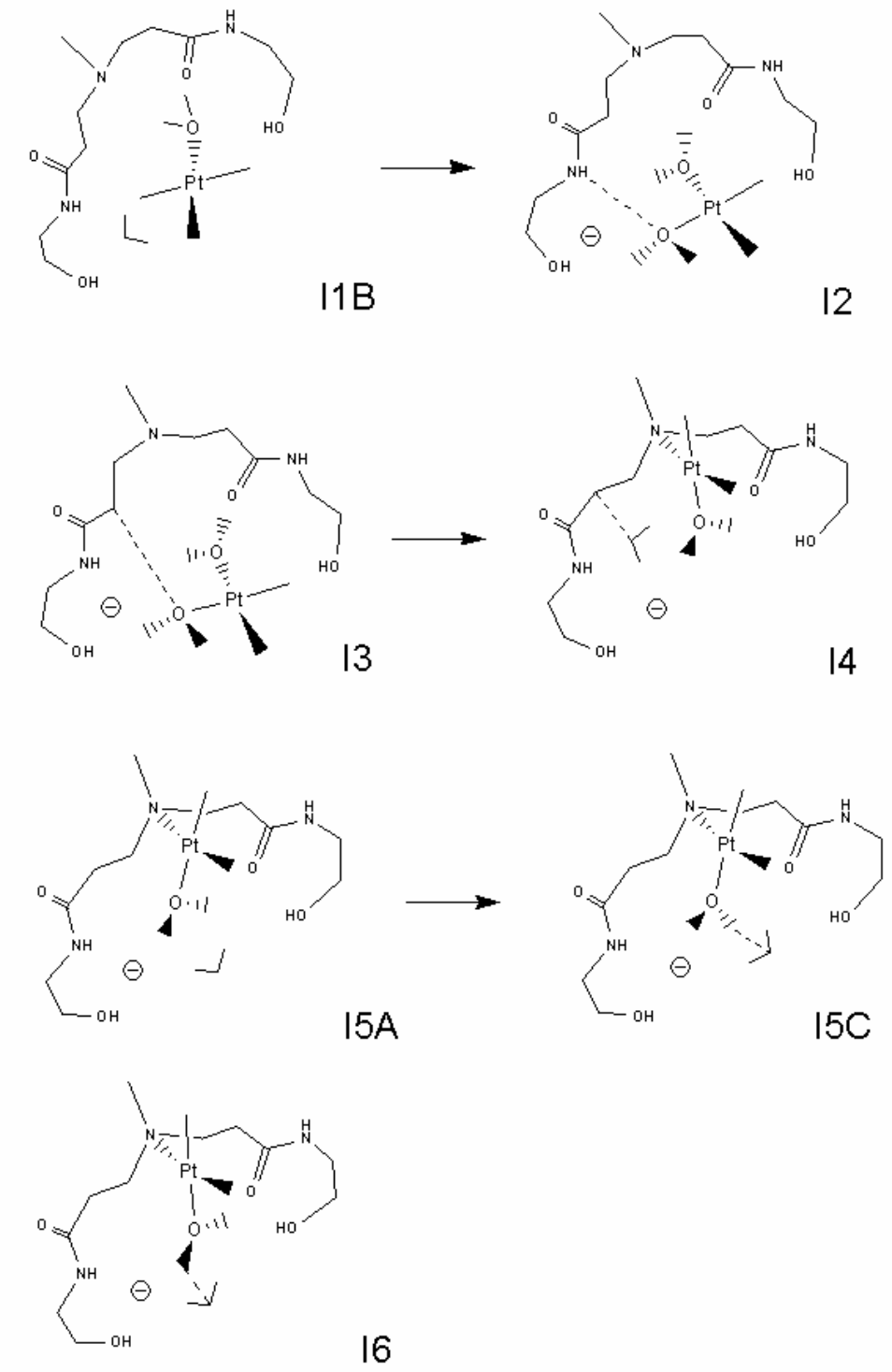

Figure 8.6. Stable points along the solvent mediated LER: [DF41-$PtCl_3(H_2O)^-$---(H_2O)] ==> [DF40-N3-*cis*-$PtCl_2(H_2O)$---$Cl(H_2O)^-$]

Step 1: Aquation of $PtCl_3(H_2O)^-$ to *cis*-$PtCl_2(H_2O)_2$ inside the pocket

The reactant (I1B) and product (I2) are represented in Figure 8.6.

DF41-$PtCl_3(H_2O)^-$---H_2O (I1B)

➔ DF41-*cis*-$PtCl_2(H_2O)_2$----Cl^- (I2) (8.13)

Ea and $\Delta G_{I2\text{-}I1B}$ are 23.9 kcal/mol and +5.3 kcal/mol respectively. A ~N2-H---OH_2-Pt hydrogen bond (bond length = 2.12 Å) is formed.

Step 2: Re-accommodation of *cis*-$PtCl_2(H_2O)_2$ inside pocket

The reactant (I2) and product (I3) are represented in Figure 8.6.

DF41-*cis*-$PtCl_2(H_2O)_2$----Cl^- (I2)

➔ DF41-*cis*-$PtCl_2(H_2O)_2$----Cl^- (I3) (8.14)

Ea(ΔE_0) and $\Delta G_{I3\text{-}I2}$ are 0.09 kcal/mol (so practically a barrierless reaction) and -2.2 kcal/mol respectively. The ~N2-H---OH_2-Pt hydrogen bond formed in previous step is broken and a weaker ~CH_2---OH_2-Pt forms (bond length = 2.77 Å).

Step 3: LER. Pt(II) binds to N3

The reactant (I3) and product (I4) are represented in Figure 8.6.

DF41-*cis*-$PtCl_2(H_2O)_2$---Cl^- (I3)

➔ DF40-N3- *cis*-$PtCl_2(H_2O)$---(H_2O)---Cl^- (I4) (8.15)

Ea and $\Delta G_{I4\text{-}I3}$ are 18.9 kcal/mol and -3.4 kcal/mol respectively. The released water still forms a ~CH_2---OH_2 hydrogen bond (bond length = 2.81 Å).

The following reaction entails release of the Cl^- ligand:

DF41-*cis*-$PtCl_2(H_2O)_2$---Cl^- (I3) + H_2O

➔ DF41-*cis*-$PtCl_2(H_2O)_2$ + $Cl(H_2O)^-$ (8.16)

but it is not likely to occur (ΔG= +26.3 kcal/mol).

Step 4: Re-accommodation of water inside pocket

The reactant (I4) and product (I5A) are represented in Figure 8.6.

DF40-N3- *cis*-$PtCl_2(H_2O)$---(H_2O)---Cl^- (I4)

➔ DF40-N3- *cis*-$PtCl_2(H_2O)$---(H_2O)---Cl^- (I5A) (8.17)

No TS structure could be found. $\Delta G_{I5A\text{-}I4}$ is -1.4 kcal/mol and the ~CH_2---OH_2 hydrogen bond is broken.

Step 5: Binding of free water to the water of *cis*-$PtCl_2(H_2O)$ moiety

The reactant (I5A) and product (I5C) are represented in Figure 8.6.

DF40-N3-*cis*-$PtCl_2(H_2O)$--(H_2O)---Cl^- (I5A)

➔ DF40-N3- *cis*-$PtCl_2(H_2O)$---(H_2O)---Cl^- (I5C) (8.18)

A Pt-OH_2---OH_2 hydrogen bond is formed (bond length = 1.79 Å). No TS structure could be found. $\Delta G_{I5C-I5A}$ is -0.77 kcal/mol.

Step 6: Binding of coordination water to amide ~C=O in dendrimer

The reactant (I5C) and product (I6) are represented in Figure 8.6.

DF40-N3- *cis*-$PtCl_2(H_2O)$---(H_2O)---Cl^- (I5C)

➔ DF40-N3- *cis*-$PtCl_2(H_2O)$---(H_2O)---Cl^- (I6) (8.19)

Ea and ΔG_{I4-I3} are 4.6 kcal/mol and -0.12 kcal/mol respectively. The Pt-OH_2---OH_2 bond length shortens to 1.54 Å and another bond length is formed (Pt-OH_2---O=C~ , 1.95 Å)

The next step, Cl^- ligand release, is described by the following reaction:

DF40-N3- *cis*-$PtCl_2(H_2O)$---(H_2O)---Cl^- (I5C) + H_2O

➔ DF40-N3- *cis*-$PtCl_2(H_2O)$---(H_2O) + $Cl(H_2O)^-$ (8.20)

and found thermodynamically unfavorable (ΔG = 24.8 kcal/mol). Table 8.3 summarizes all the stationary points found along the reaction energy profile whereas Figures 8.7 and 8.8 illustrate the reaction energy profile and the evolution of the main bond distances of this process.

Table 8.3: Difference in electronic energy with ZPE correction (ΔE_0), enthalpy (ΔH) and free energy (ΔG) of reaction (kcal/mol) relative to those of DF41-H_2O--$PtCl_4^{2-}$ (E(l.e.c.rs.) = 0.0 kcal/mol) for stationary points along the reaction profile of the solvent mediated LER: [DF41-$PtCl_3(H_2O)^-$---(H_2O)] ==> [DF40-N3-*cis*-$PtCl_2(H_2O)$---$Cl(H_2O)^-$]. Reaction profile shown in Figure 8.7

Stationary point	ΔE_0	ΔH	ΔG
J	-23.2	-23.4	-27.0
C7B	-32.1	-32.4	-31.6
I1B	-32.7	-33.7	-31.7
TS1	-8.6	-9.8	-7.3
I2	-27.2	-28.3	-26.4
TS2	-27.1	-28.7	-25.2
I3	-28.9	-30.0	-28.7
TS3	-9.6	-11.1	-6.7
I4	-34.1	-35.3	-32.1
I5A	-34.3	-35.3	-33.4
I5C	-36.7	-38.1	-34.2
TS5	-31.9	-33.5	-28.7
I6	-37.6	-39.4	-34.3

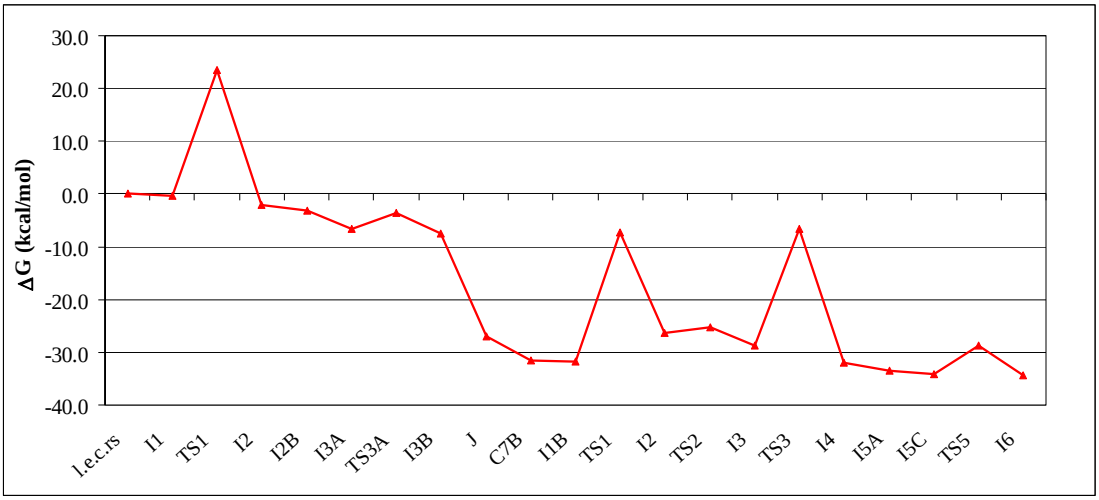

Figure 8.7. Reaction profile for the solvent mediated reaction [DF41-H_2O--$PtCl_4^{2-}$] + $(H_2O)_2$ ==> [DF40-N3-*cis*-$PtCl_2(H_2O)$---$Cl(H_2O)^-$] + $Cl(H_2O)^-$. It was obtained by attaching the solvent mediated LER of $PtCl_3(H_2O)^-$ aquated to *cis*-$PtCl_2(H_2O)_2$ and binding to N3 (spanning from I1B to I6 in the right side of the plot) to the reaction profile for solvent mediated LER of $PtCl_4^{2-}$ with N3 up to the point where the aquated species (DF41-$PtCl_3(H_2O)^-$---Cl^-, I3B) is generated (spanning from l.e.c.rs to I3B in the left side of the plot)

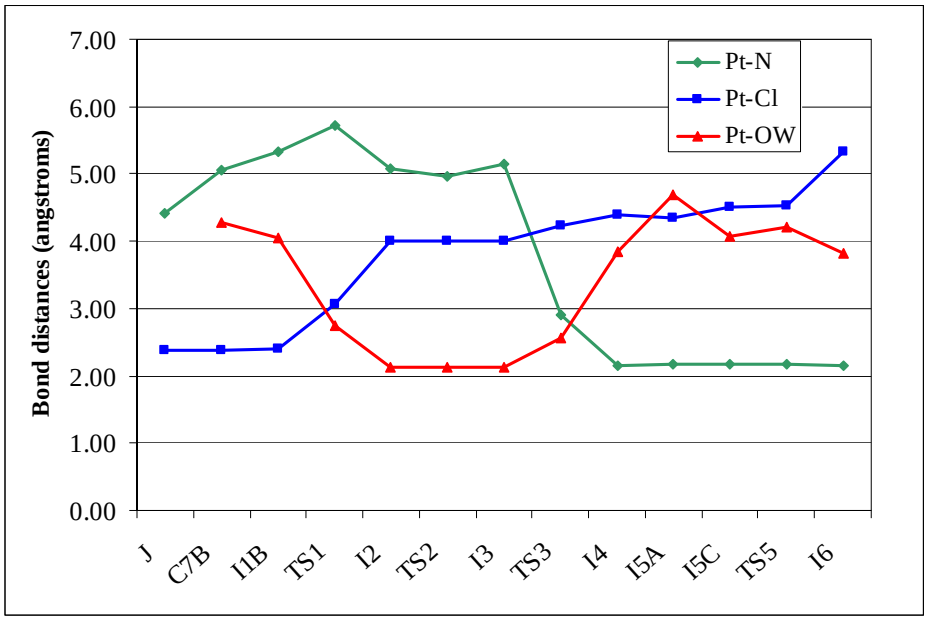

Figure 8.8. Evolution of bond distances: Pt-N(entering ligand), Pt-Cl (leaving ligand) and Pt-OW (water of solvation) along the course of the solvent mediated LER: [DF41-$PtCl_3(H_2O)^-$---(H_2O)] ==> [DF40-N3-*cis*-$PtCl_2(H_2O)$---$Cl(H_2O)^-$]

8.3.1.2.2 When Pt(II) binds to N3 through a pathway where *trans*-$PtCl_2(H_2O)_2$ is formed as an intermediate

Binding of Pt(II) to N3 through a pathway that involves *trans*-$PtCl_2(H_2O)_2$ can take place according to the following sequence of steps (See Figure 8.9) where we assume I1 –one among several isomeric conformers of DF41-$PtCl_3(H_2O)^-$---H_2O – to be obtained from rearrangement of water in conformer C7B (ΔG = -2.5 kcal/mol). The water ligand in the Pt(II) complex I1 forms two hydrogen bonds, one with ~N3---H_2O (bond length = 1.98 Å) and another with ~N2-H---OH_2 (bond length = 1.94 Å)

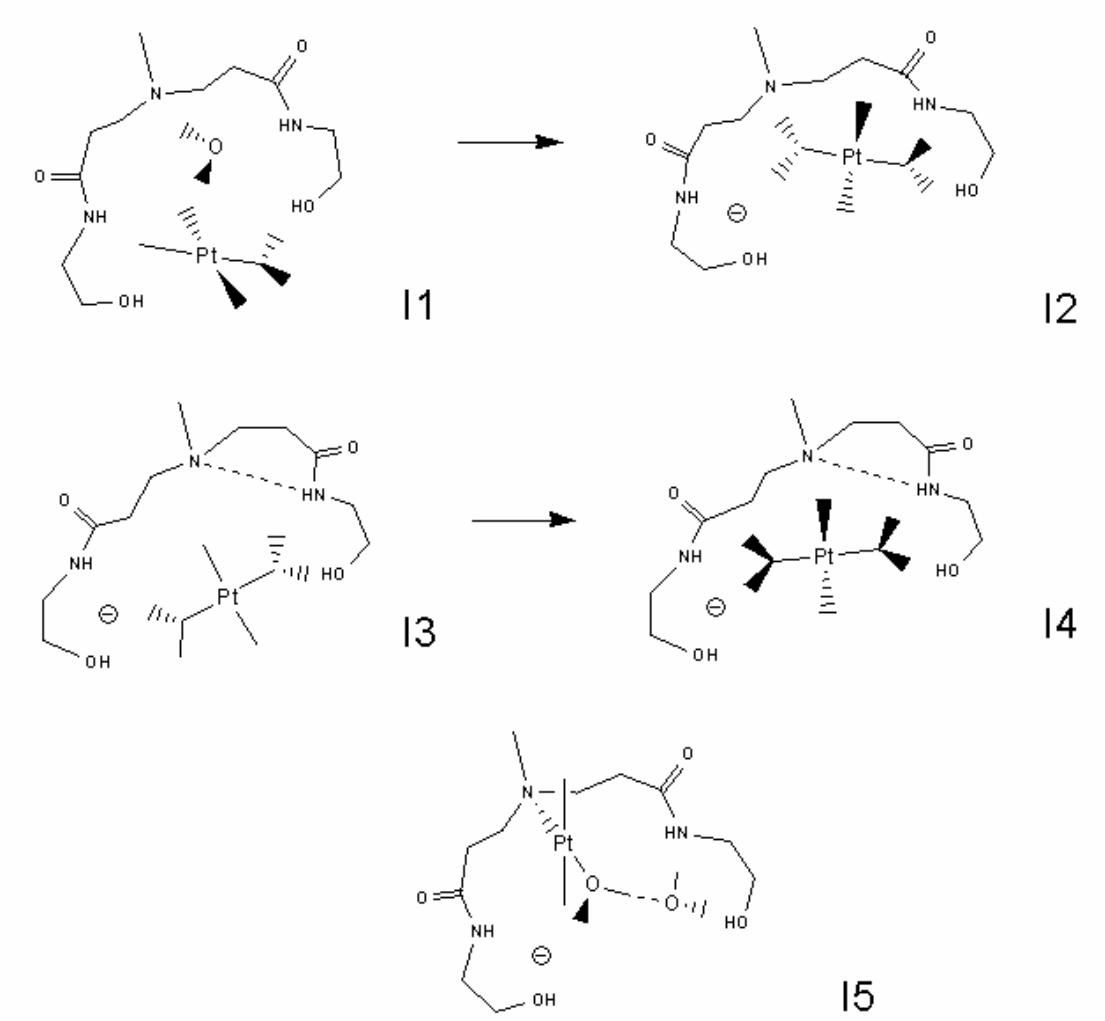

Figure 8.9. Stable points along the solvent mediated LER: [DF41-$PtCl_3(H_2O)^-$---(H_2O)] ==> [DF40-N3-*trans*-$PtCl_2(H_2O)$---$Cl(H_2O)^-$]

Step 1: Aquation of $PtCl_3(H_2O)^-$ to *trans*-$PtCl_2(H_2O)_2$ inside the pocket

The reactant (I1) and the product (I2) are represented in Figure 8.9.

DF41- $PtCl_3(H_2O)^-$---H_2O (I1) ➔ DF41-*trans*-$PtCl_2(H_2O)_2$---Cl^- (I2) (8.21)

Ea and ΔG_{I2-I1} are 29.5 kcal/mol and + 6.3 kcal/mol respectively. A ~N3---H_2O-Pt hydrogen bond (bond length = 1.77 Å) is formed.

Step 2: Reaccomodation of *trans*-$PtCl_2(H_2O)_2$ inside pocket

The reactant (I2) and the product (I3) are represented in Figure 8.9.

DF41-*trans*-$PtCl_2(H_2O)_2$---Cl^- (I2)

➔ DF41-*trans*-$PtCl_2(H_2O)_2$---Cl^- (I3) (8.22)

No TS structure could be found. ΔG_{I3-I2} is -0.35 kcal/mol. The ~N3---H_2O-Pt is broken while a ~N3---H-N2~ hydrogen bond (bond length = 2.08 Å) is formed. The following reaction entails release of the Cl^- ligand:

DF41-*trans*-$PtCl_2(H_2O)_2$---Cl^- (I2) + H_2O

➔ DF41-*trans*-$PtCl_2(H_2O)_2$ + $Cl(H_2O)^-$ (8.23)

but it is not likely to occur (ΔG= +21.5 kcal/mol).

Step 3: Re-accommodation of *trans*-$PtCl_2(H_2O)_2$ inside pocket

The reactant (I3) and the product (I4) are represented in Figure 8.9.

DF41-*trans*-$PtCl_2(H_2O)_2$---Cl^- (I3)

➔ DF41-*trans*-$PtCl_2(H_2O)_2$---Cl^- (I4) (8.24)

No TS structure could be found. ΔG_{I4-I3} is +1.5 kcal/mol. No major change in the binding except that I4 is closer to N3 than I3 is (See Figure 8.11).

Step 4: LER. Pt(II) binds to N3

The reactant (I4) and the product (I5) are represented in Figure 8.9.

DF41-*trans*-$PtCl_2(H_2O)_2$---Cl^- (I4)

➔ DF40-N3-*trans*-$PtCl_2(H_2O)$---(H_2O)---Cl^- (I5) (8.25)

ΔG_{I5-I4} is -1.6 kcal/mol. No TS structure could be found. Therefore a strict comparison between the reaction profile of *trans*-$Cl_2(H_2O)$ (Figure 8.10) and *cis*-$PtCl_2(H_2O)$ (Figure 8.7) cannot be made.

The next step, Cl^- ligand release is described by the following reaction:

DF40-N3- *trans*-$PtCl_2(H_2O)$---(H_2O)---Cl^- (I5) + H_2O

➔ DF40-N3- *trans*-$PtCl_2(H_2O)$---(H_2O) + $Cl(H_2O)^-$ (8.26)

The reaction is thermodynamically not favorable (ΔG= +19.5 kcal/mol).

Table 8.4 summarizes all the stationary points found along the reaction energy profile whereas Figures 8.10 and 8.11 illustrate the reaction energy profile and the evolution of the main bond distances of this process.

Table 8.4: Difference in electronic energy with ZPE correction (ΔE_0), enthalpy (ΔH) and free energy (ΔG) of reaction (kcal/mol) relative to those of DF41-H_2O--$PtCl_4^{2-}$ (E(l.e.c.rs) = 0.0 kcal/mol) for stationary points along the reaction profile of the solvent mediated LER: [DF41-$PtCl_3(H_2O)^-$---(H_2O)] ==> [DF40-N3-*trans*-$PtCl_2(H_2O)$---$Cl(H_2O)^-$]. Reaction profile shown in Figure 8.10

Stationary Point	ΔE_0	ΔH	ΔG
J	-23.2	-23.4	-27.0
C7B	-32.1	-32.4	-31.6
I1	-35.3	-36.3	-34.1
TS1	-5.3	-6.8	-2.7
I2	-30.0	-31.6	-27.8
I3	-29.5	-31.0	-28.1
I4	-27.4	-28.6	-26.6
I5	-31.5	-33.1	-28.2

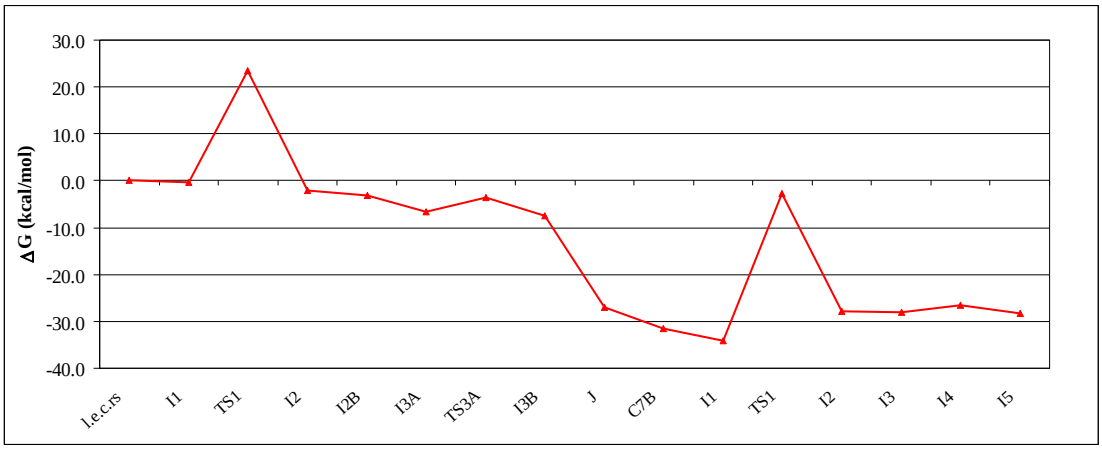

Figure 8.10. Reaction profile for the solvent mediated reaction [DF41-H_2O--$PtCl_4^{2-}$] + $(H_2O)_2$ ==> [DF40-N3-*trans*-$PtCl_2(H_2O)$---$Cl(H_2O)^-$] + $Cl(H_2O)^-$. It was obtained by attaching the solvent mediated LER of $PtCl_3(H_2O)^-$ aquated to *trans*-$PtCl_2(H_2O)_2$ and binding to N3 (spanning from I1 to I5 in the right side of the plot) to the reaction profile for solvent mediated LER of $PtCl_4^{2-}$ with N3 up to the point where the aquated species (DF41-$PtCl_3(H_2O)^-$---Cl^-, I3B) is generated (spanning from l.e.c.rs to I3B in the left side of the plot). Note: The reason why this profile and the one corresponding to *cis*-$PtCl_2(H_2O)_2$ (See Figure 8.7) do not look similar in shape is because the TS structure between I4 and I5 could not be found

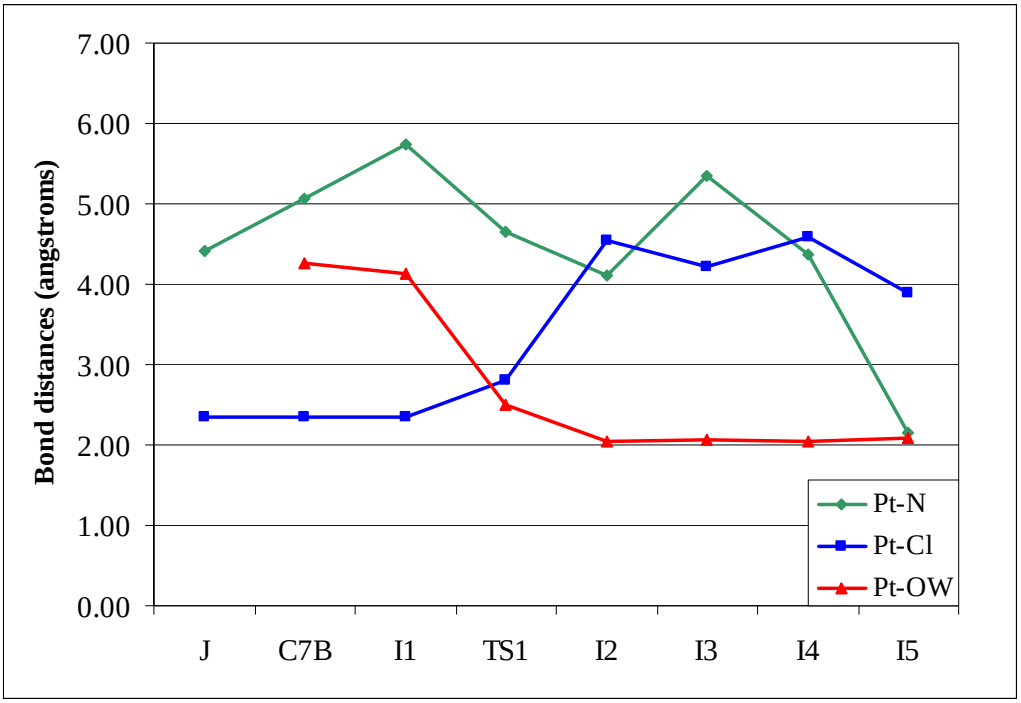

Figure 8.11. Evolution of bond distances: Pt-N(entering ligand), Pt-Cl (leaving ligand) and Pt-OW (water of solvation) along the course of the solvent mediated LER: [DF41-$PtCl_3(H_2O)^-$---(H_2O)] ==> [DF40-N3-*trans*-$PtCl_2(H_2O)$---$Cl(H_2O)^-$]

8.3.1.3 When the Pt(II) complex is $PtCl_3(H_2O)^-$ and Pt(II) binds to secondary amide nitrogen (N2)

In this section, we tested whether monodentate binding to secondary amide N (N2) is also possible as suggested by earlier NMR experiments.[62] N-methyl acetamide (NMA) was previously used by us as a single site model of N2 sites and O (Chapter VII, Figure 7.1) but here (section 8.3.1.3.1.) is used only as a single site model of N2. The DF41 fragment is also used (section 8.3.1.3.2.).

8.3.1.3.1 LER of Pt(II) complexes with n-methyl acetamide

The thermodynamics of binding of Pt(II) species to n-methyl acetamide (NMA) secondary amide N site (N2) is calculated according to the following equation:

NMA---$PtC'_xD'_y$ (I1) ➔ TS ➔ NMA---$PtC'_{x-1}D'_y$---C' (I2) (8.27)

where $PtC'_xD'_y$ represents $PtCl_4^{2-}$ and its mono- and diaquated complexes and C' is the leaving ligand. Results are shown in Table 8.5.

Table 8.5: ΔG of reaction (ΔG_{I2-I1}), activation enthalpies (Ea) (both in kcal/mol) and TS amide group dihedral angle (in degrees) for the LER between Pt(II) complexes species and the secondary amide site N (N2) of n-methyl acetamide (NMA) according to eqn 8.28

Pt(II) complex	Ea[a]	ΔG_{I2-I1}	TS amide group dihedral[b]
$PtCl_4^{2-}$ [a]		-30.3[d]	
$PtCl_3(H_2O)^-$	15.4	3.5	139.4
cis-$PtCl_2(H_2O)_2$	24.5	11.6	17.9
trans-$PtCl_2(H_2O)_2$	27.9	5.5	132.1

[a]No TS structure was found for $PtCl_4^{2-}$
[b]Value of dihedral angle (H-N2-C=O) in amide group of NMA in the TS structure
[c]ΔG_{I2-I1} = E(NMA---$PtCl_3^-$) + E(Cl^-) – E(NMA---$PtCl_4^{2-}$)
[d]The free energy associated with the release of Cl^- is included in the ΔG value of -30.3 kcal/mol

The energy barrier toward the LER (Ea = 15.4 kcal/mol) for $PtCl_3(H_2O)^-$ is smaller compared to those of either *cis*- (Ea = 24.5 kcal/mol) or *trans*-$PtCl_2(H_2O)_2$ (Ea = 27.9 kcal/mol). However, the positive values for ΔG of reaction suggest that the binding of the mono- and diaquated complexes of $PtCl_4^{2-}$ is unlikely to be observed.

In the TS structures for $PtCl_3(H_2O)^-$ and *trans*-$PtCl_2(H_2O)_2$, the NMA amide group orientation tend to the *trans* position (as found in Chapter III) whereas a tendency toward the *cis* position is found in the TS structure for *cis*-$PtCl_2(H_2O)_2$ as reflected by the value of the TS amide group dihedral (Table 8.5).

8.3.1.3.2 LER of $PtCl_3(H_2O)^-$ with DF41

Table 8.5 suggested that the lowest activation energy (Ea) is found when $PtCl_3(H_2O)^-$ binds to the N2 site (amide group oriented *trans*). But a TS structure search with the same amide group orientation (*trans*) for DF40-N2-$PtCl_3^-$---H_2O---H_2O failed. Instead,

such TS structure was found when the orientation of the amide group was switched from *trans* to *cis*. This is a remarkable finding, first because such orientation of amide groups in dendrimer branches is not the most preferred configuration in low generation dendrimers (Chapter III) nor in related compounds,[171] and second, because it suggests that binding to N2 occurs only when the amide group in the dendrimer branches is oriented in *cis* rather than in *trans* position.

Binding Pt(II) to N2 through the following sequence of steps, where I1-one among several isomeric conformers of DF41-$PtCl_3(H_2O)^-$---H_2O is assumed to be obtained from rearrangement of water in conformer C7B (ΔG= -1.1 kcal/mol). In I1, $PtCl_3(H_2O)^-$ binds to the amide O through a hydrogen bond of its water ligand H (bond length = 1.67 Å) whereas the pocket adopts a very peculiar configuration by joining its two branches by means of a ~N3---H-N2~ hydrogen bond (bond length = 2.05 Å). This pocket configuration is kept along the LER course.

Step 1: LER. Pt(II) binds to N2

The reactant (I1) and product (I2) are represented in Figure 8.12.

DF41-$PtCl_3(H_2O)^-$---(H_2O) (I1) ➔ DF40-N2-$PtCl_3^-$---(H_2O)---(H_2O) (I2) (8.28)

Ea and ΔG_{I2-I1} are 21.9 kcal/mol and +5.8 kcal/mol respectively. Upon reaction, the released water bridges the dendrimer branch amide O with a Cl^- ligand of the $PtCl_3^-$ moiety.

Step 2: Re-accommodation of $PtCl_3(H_2O)^-$ inside pocket

The reactant (I2) and product (I3) are represented in Figure 8.12.

DF40-N2-$PtCl_3^-$---(H_2O)---(H_2O) (I2)

➔ DF40-N2-$PtCl_3^-$---(H_2O)---(H_2O) (I3) (8.29)

No TS structure was sought. ΔG_{I3-I2} is +4.6 kcal/mol. The released water keeps the Cl^- ligand and amide O bridged but forms an additional hydrogen bond (OH_2---NH~, bond length = 1.96 Å)

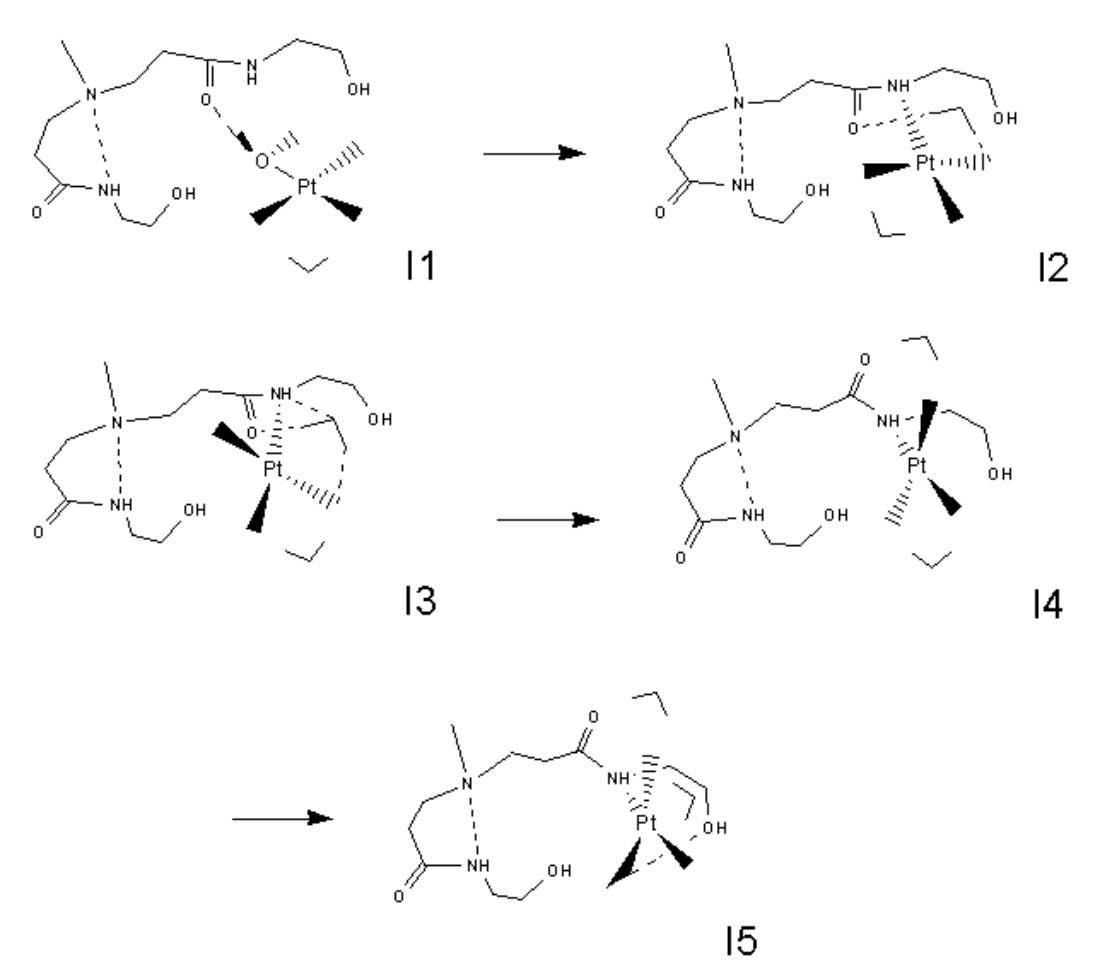

Figure 8.12. Stable points along the solvent mediated LER: [DF41-$PtCl_3(H_2O)^-$---(H_2O)] ==> [DF40-N2-$PtCl_3^-$---$(H_2O)_2$]

Step 3: Re-accommodation of $PtCl_3(H_2O)^-$ inside pocket

The reactant (I3) and product (I4) are represented in Figure 8.12.

DF40-N2-$PtCl_3^-$---(H_2O)---(H_2O) (I3)

➔ DF40-N2-$PtCl_3^-$---(H_2O)---(H_2O) (I4) (8.30)

No TS structure was sought. ΔG_{I4-I3} is -5.6 kcal/mol. The Cl---HOH---O~ bridge still remains but the amide O group configuration starts changing from *cis* to *trans*. (See Figure 8.12) A rotation is ensued.

Step 4: Re-accommodation of $PtCl_3(H_2O)^-$ inside pocket

The reactant (I4) and product (I5) are represented in Figure 8.12.

DF40-N2-$PtCl_3^-$---(H_2O)---(H_2O) (I4)

➔ DF40-N2-$PtCl_3^-$---(H_2O)---(H_2O) (I5) (8.31)

No TS structure was sought. ΔG_{I5-I4} is -2.6 kcal/mol. No significant change between I4 and I5 except that the tip of one of the branches binding $PtCl_3^-$ to the N2 site rotates to hold $PtCl_3^-$ tighter.

Table 8.6 summarizes all the stationary points found along the reaction energy profile whereas Figures 8.13 and 8.14 illustrate the reaction energy profile and the evolution of the main bond distances of this process.

Table 8.6: Difference in electronic energy with ZPE correction (ΔE_0), enthalpy (ΔH) and free energy (ΔG) of reaction (kcal/mol) relative to those of DF41-H_2O---$PtCl_4^{2-}$ (E(l.e.c.rs) = 0.0 kcal/mol) for stationary points along the reaction profile of the solvent mediated LER: [DF41-$PtCl_3$(H_2O)$^-$---(H_2O)] ==> [DF40-N2-$PtCl_3^-$---(H_2O)$_2$]. Reaction profile shown in Figure 8.13

Stationary point	ΔE_0	ΔH	ΔG
J	-23.2	-23.4	-27.0
C7B	-32.1	-32.4	-31.6
I1	-32.2	-32.6	-32.7
TS1	-10.4	-10.7	-10.9
I2	-25.7	-25.5	-26.9
I3	-23.9	-24.5	-22.3
I4	-26.5	-26.2	-27.9
I5	-29.0	-28.7	-30.5

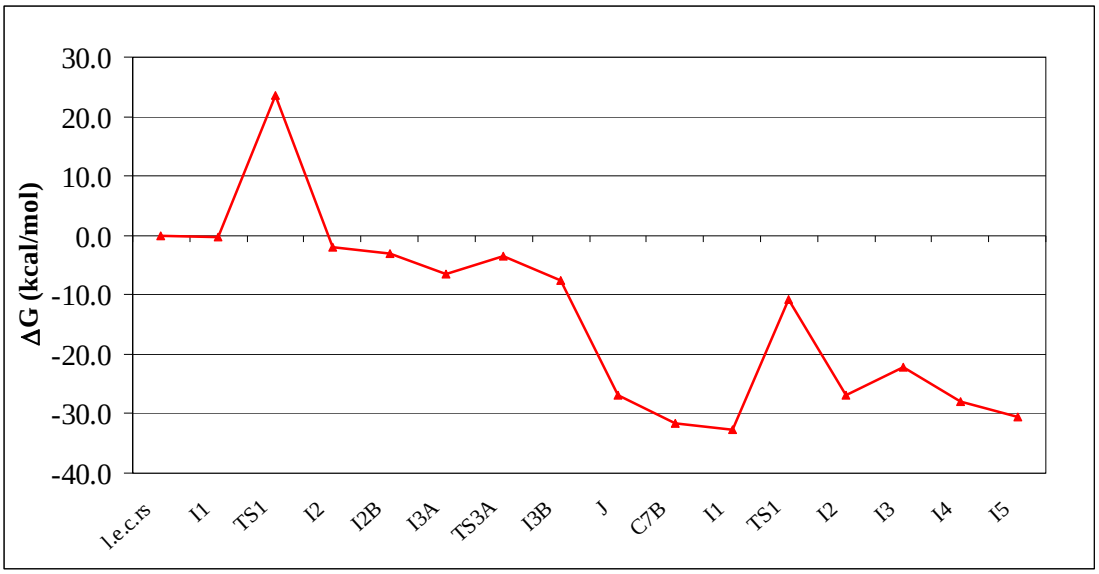

Figure 8.13. Reaction profile for the solvent mediated reaction [DF41-H_2O--$PtCl_4^{2-}$] + $(H_2O)_2$ ==> [DF40-N2-$PtCl_3^-$---$(H_2O)_2$] + $Cl(H_2O)^-$. It was obtained by connecting the LER of $PtCl_3(H_2O)^-$ as it binds to N2 (spanning from I1 to I5 in the right side of the plot) to the reaction profile for solvent mediated LER of $PtCl_4^{2-}$ with N3 up to the point where the aquated species (DF41-$PtCl_3(H_2O)^-$---Cl^-, I3B) is generated (spanning from l.e.c.rs to I3B in the left side of the plot)

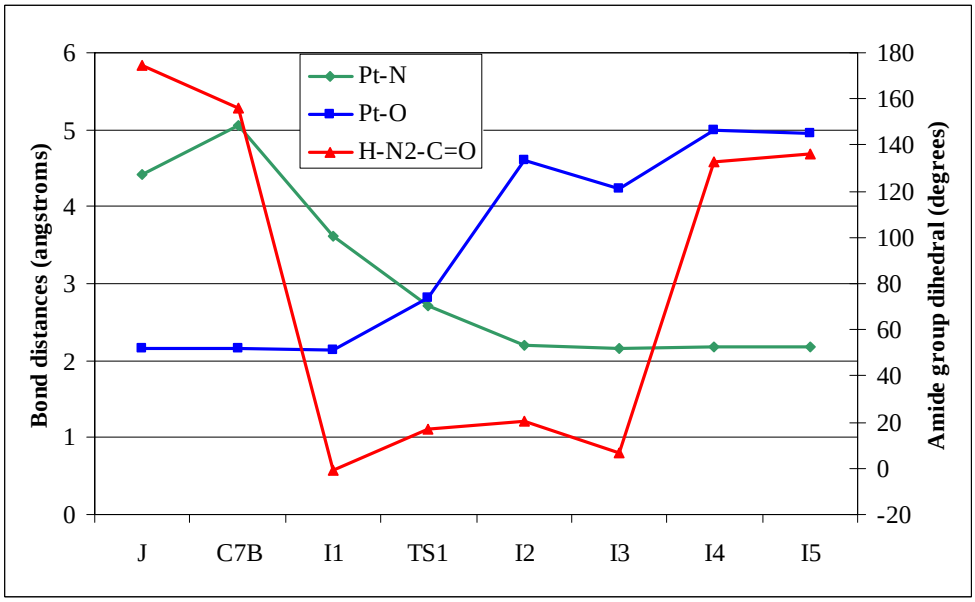

Figure 8.14. Evolution of bond distances: Pt-N(entering ligand), Pt-Cl (leaving ligand) and Pt-O (leaving ligand) and of amide group dihedral (H-N2-C=O) along the course of the solvent mediated LER: [DF41-$PtCl_3(H_2O)^-$---(H_2O)] ==> [DF40-N2-$PtCl_3^-$---$(H_2O)_2$]

Table 8.7 summarizes the free energies and activation energies of the elementary steps of aquation to obtain various aquation products.

Table 8.7: ΔG of reaction and activation enthalpies (Ea) (both in kcal/mol) for the aquation of $PtCl_4^{2-}$ to its mono- and diaquated forms in two environments: inside outer pocket (DF41) and outside outer pocket

Aquation product	Outside outer pocket		Inside outer pocket	
	ΔG	Ea	ΔG	Ea
$PtCl_3(H_2O)^-$	-50.2	23.7	-1.8	23.6
cis-$PtCl_2(H_2O)_2$	30.6	16.6	5.3	23.9
trans-$PtCl_2(H_2O)_2$	29.8	29.9	6.3	29.5

It is observed that it is feasible to obtain $PtCl_3(H_2O)^-$ inside outer pocket (ΔG = -1.8 kcal/mol) with an energy barrier (Ea = 23.6 kcal/mol) that is not significantly different than that for obtaining $PtCl_3(H_2O)^-$ outside the pocket (gas phase aquation, Ea = 23.7 kcal/mol); both values are comparable to the experimental value in solution (Ea = 21.0 kcal/mol).[151]

Now, as seen in section 8.3.1.1, once $PtCl_3(H_2O)^-$ has been obtained in the pocket, three more steps of rearranging water could follow before binding of Pt(II) to –for instance- tertiary amine site (N3) can take place. Next step can either conduce to binding to N3 yielding DF40-N3-$PtCl_3^-$---H_2O (ΔE_0 = -1.0 kcal/mol, Ea = 21.6 kcal/mol) or it could release Cl^- (ΔG = -19.4 kcal/mol). Upon release of Cl^-, a $PtCl_3(H_2O)^-$ pocket-encapsulated structure remains. This can either react with N3 through a solventless pathway and yield DF40-N3-$PtCl_3^-$---H_2O (Chapter VII) or admit an additional water (ΔG = -4.6 kcal/mol, section 8.3.1.2), reorganize water and yield either *cis*- or *trans*-$PtCl_2(H_2O)_2$.

From Table 8.7 it is observed that the ΔG of reaction for the elementary step of aquation to either *cis*- $PtCl_2(H_2O)_2$ (+5.3 kcal/mol) or *trans*-$PtCl_2(H_2O)_2$ (+6.3 kcal/mol)

respectively are positive. In fact, the barrier to obtain *cis*-$PtCl_2(H_2O)_2$ (23.9 kcal/mol) is even higher than that required to obtain it in the absence of pocket (gas phase aquation, Ea = 16.6 kcal/mol). Table 8.8 indicates that the elementary LER is less feasible in the solvent mediated LER (*cis*/*trans*: -3.4/-1.6 kcal/mol) than in the solventless LER (*cis*/*trans*: -9.9/-7.7 kcal/mol). Now, focusing on *cis*-$PtCl_2(H_2O)_2$, it is observed that the solvent-mediated barrier to the LER (18.9 kcal/mol) is lower than the solventless barrier (21.1 kcal/mol).

Table 8.8: ΔG_{LER}, $\Delta G_{LER(overall)}$ and activation enthalpies (Ea) (all three in kcal/mol) for both the solventless and the solvent-mediated LER of Pt(II) complexes species to tertiary amine site (N3) –unless otherwise indicated

	Solventless LER				Solvent mediated LER		
Pt(II) species (site)	ΔG_{LER}	$\Delta G_{LER(overall)}$	Ea[a]	Ea[b]	ΔG_{LER}	$\Delta G_{LER(overall)}$	Ea[b]
$PtCl_3(H_2O)^-$	-3.3	-3.5	16.6	20.5	+0.47[c]	-35.7	21.6
cis-$PtCl_2(H_2O)_2$	-9.9	-9.9	21.6	21.1	-3.4	-34.3	18.9
trans-$PtCl_2(H_2O)_2$	-7.7	-3.0	25.6	18.3	-1.6	-28.2	
$PtCl_3(H_2O)^-$ (N2)			15.4		+5.8	-30.5	21.9

[a]Single molecules: $N(CH_3)_3$ for N3; N-methylacetamide for N2
[b]Dendrimer outer pocket: DF41 fragment
[c]$\Delta E_{0(LER)}$ = -1.0 kcal/mol

The values for the overall solvent mediated LER –Table 8.8, $\Delta G_{LER(overall)}$- suggest that it is easier to obtain $PtCl_3(H_2O)^-$ and this happens with less number of steps than obtaining either *cis*-$PtCl_2(H_2O)_2$ or *trans*-$PtCl_2(H_2O)_2$. In Table 8.9, the overall complexation of $PtCl_4^{2-}$ to the dendrimer atom site N3 in the absence and presence of branches is compared. Comparison to the aquation of $PtCl_4^{2-}$ with a dimer is also provided.

Step A: Non-covalent binding (NCB: eqn 8.32 & eqn 8.33; hydration: eqn 8.34)

$DF41\text{-}(H_2O)_2 + PtCl_4^{2-} \rightarrow DF41\text{---}H_2O\text{---}PtCl_4^{2-} + H_2O$ (8.32)

$N(CH_3)_3$---$(H_2O)_2$ + $PtCl_4^{2-}$ ➔ $N(CH_3)_3$---H_2O---$PtCl_4^{2-}$ + H_2O (8.33)

$(H_2O)_2$ + $PtCl_4^{2-}$ ➔ $PtCl_4^{2-}$---H_2O + H_2O (8.34)

Step B: Covalent binding (Ligand exchange reaction: N3 for Cl^- (eqn 8.35 & eqn 8.36) and O for Cl^- (eqn 8.37))

DF41---H_2O--- $PtCl_4^{2-}$ + H_2O ➔ DF40-N-$PtCl_3^-$---(H_2O) + $Cl(H_2O)^-$ (8.35)

$N(CH_3)_3$---H_2O--- $PtCl_4^{2-}$ + H_2O ➔ $(CH_3)_3$-N---$PtCl_3^-$---H_2O + $Cl(H_2O)^-$ (8.36)

$PtCl_4^{2-}$---H_2O + H_2O ➔ $PtCl_3(H_2O)^-$ + $Cl(H_2O)^-$ (8.37)

Total: NCB + covalent binding

DF41-$(H_2O)_2$ + $PtCl_4^{2-}$ ➔ DF40-N-$PtCl_3^-$---(H_2O) + $Cl(H_2O)^-$ (8.38)

$N(CH_3)_3$---$(H_2O)_2$ + $PtCl_4^{2-}$ ➔ $(CH_3)_3$-N---$PtCl_3^-$---H_2O + $Cl(H_2O)^-$ (8.39)

$(H_2O)_2$ + $PtCl_4^{2-}$➔ $PtCl_3(H_2O)^-$ + $Cl(H_2O)^-$ (8.40)

Table 8.9: ΔG of reaction (kcal/mol) for the steps of overall solvent-mediated complexation of $PtCl_4^{2-}$ to site N3 (in dendrimer outer pocket and single molecule) and for aquation of $PtCl_4^{2-}$

Steps	Reaction		
	Aquation of $PtCl_4^{2-}$	Complexation of $PtCl_4^{2-}$ (Single molecule)	Complexation of $PtCl_4^{2-}$ (Outer pocket)
A. NCB	-10.0	-6.7	-33.1
B. Covalent binding	-50.2	-59.3	-35.7
Total	-60.2	-66.0	-68.8

Table 8.9 shows that the complexation of $PtCl_4^{2-}$ in outer pockets is thermodynamically more favorable than its aquation outside the pocket and in branchless environments. And the free energy values indicate that branches provide a marginal but important advantage in the complexation of $PtCl_4^{2-}$.

Therefore the use of PAMAM dendrimer pockets as templates is justified from a thermodynamic point of view -although other reasons, like protection of the subsequent nanoparticles against agglomeration may apply too.

It should be noticed that there is no significant difference between the barriers to bind $PtCl_3(H_2O)^-$ through a solvent mediated pathway (Table 8.8) to N3 (Ea = 21.6 kcal/mol) than to N2 (Ea = 21.9 kcal/mol) and second, that the binding to the dendrimer atom site may occur in very different ways. This confirms that the product will be largely determined by the thermodynamics -that is more favorable to N3.

Binding to secondary amide nitrogen (N2) is predicted to occur when the aquated product $PtCl_3(H_2O)^-$ binds to an amide group oriented in *cis* rather than in *trans* position -interestingly, the single molecule model (NMA) predicted binding to amide group oriented in *trans* position. The ΔG of reaction and the activation energies to bind Pt(II) to N2 increased when switching from a single molecule model (ΔG = +3.5 kcal/mol; Ea =15.4 kcal/mol) to an outer pocket (ΔG = +5.8 kcal/mol; Ea = 21.9 kcal/mol).

Also, we found that Pt(II) may have water oxygen atoms in its first coordination shell as suggested by recent EXAFS experiments.[55] However due to the complexity of the pathways -existence of numerous steps leading to such kind of structures- we suggest that these might not be the predominant structures resulting from the complexation of $PtCl_4^{2-}$ with PAMAM –OH terminated dendrimers.

Finally, it should be noticed that our present study is a first approximation to a very complex and demanding mechanistic study. We acknowledge that our primary focus has not been to determine precise reaction mechanisms but rather to broaden our understanding of the role of the solvent. Other open questions include the effect of additional water molecules which will certainly complicate tracing the mechanistic pathway.

8.4 Summary

Monodentate binding of Pt(II) to dendrimer atom sites is likely to be thermodynamically rather than kinetically driven.

Tertiary amine nitrogen (N3) is still the preferred dendrimer atom binding site for the LER of Pt(II) species in presence of solvent. However, the LER is mediated by the solvent: a water molecule aquates tetrachloroplatinate anion ($PtCl_4^{2-}$) inside the pocket prior to the reaction of Pt(II) with the N3 site to yield a Pt(II)-N3 monodentate complex. Such aquation step could be taken as the rate limiting step (rls).

Several pathways toward Pt(II)-N3 monodentate complex were evaluated. In two of them, the resulting moiety is $PtCl_3^-$ in agreement with previous experiments. [62] The low number of intermediates and the low number of transition states in the LER leading to $PtCl_3^-$ are a strong argument to consider these two pathways as the main pathways followed by Pt(II) while binding to N3.

In this study we have also found pathways that could lead to Pt(II)-N3 complexes, but with $PtCl_2(H_2O)$ rather than $PtCl_3^-$ as the resulting moiety. This finding could explain why water oxygen atoms in the first coordination shell of Pt(II) were suggested in recent EXAFS experiments.[55] However, the higher complexity of these pathways (more intermediates and transition states) compared to those leading to $PtCl_3^-$ moieties suggest that $PtCl_3^-$ moieties are likely to be the dominant type of Pt(II)-N3 monodentate complexes.

Binding of Pt(II) to a secondary amide site (N2) was also found feasible but only when the involved secondary amide group (~NH-(CO)~) was able to switch its configuration from *trans* to *cis*.

CHAPTER IX
NON COVALENT BINDING AND LIGAND EXCHANGE REACTION IN HIGH GENERATION PAMAM-OH DENDRIMERS

9.1 Introduction

Experimental characterization techniques[55,61,62] have been devoted mainly to elucidate types of binding and coordination environments in the LER. For instance, a ^{195}Pt NMR study on the LER of PAMAM-G2OH with Pt(II) suggested that two resonances at -2133 ppm and -2200 ppm correspond to bidentate binding of Pt(II) to two N3 sites and to one N3 and one N2 site respectively. Tridentate binding of Pt(II) to three tertiary amine N, three secondary amide N and to one tertiary amine N and two secondary amide N was also suggested.[62] However, the NMR experiments did not suggest molecular-level detail structures nor insights whether the resulting moieties were *trans*- or *cis*-$PtCl_2$.

Having addressed monodentate binding of tetrachloroplatinate anion and its mono- and diaquated Pt (II) species both in the absence of (Chapter VII) and in the presence of (Chapter VIII) explicit solvent, we devote this chapter to determine the feasibility of not only bidentate but also tridentate binding of Pt(II) to dendrimer atom sites. Finally we will attempt to assemble all the insights obtained in previous chapters to propose a structure for the binding of Pt(II) complexes to large dendrimers, particularly G4OH in view of its use in characterization experiments.[55,62]

9.2 Methods

Three types of dendrimer pockets have been modeled with fragments: first, an outer pocket (See Figure 3.1) was modeled with a 41-atom fragment (DF41, Figure 9.1, part A); second, a one-layer-inner pocket (See Figure 3.1) was modeled with a 50-atom fragment (DF50, Figure 9.1, part B); and finally, a one layer-inner pocket connected to two branches of adjacent outer pockets was modeled with a 76-atom fragment (DF76, Figure 9.1, part C).

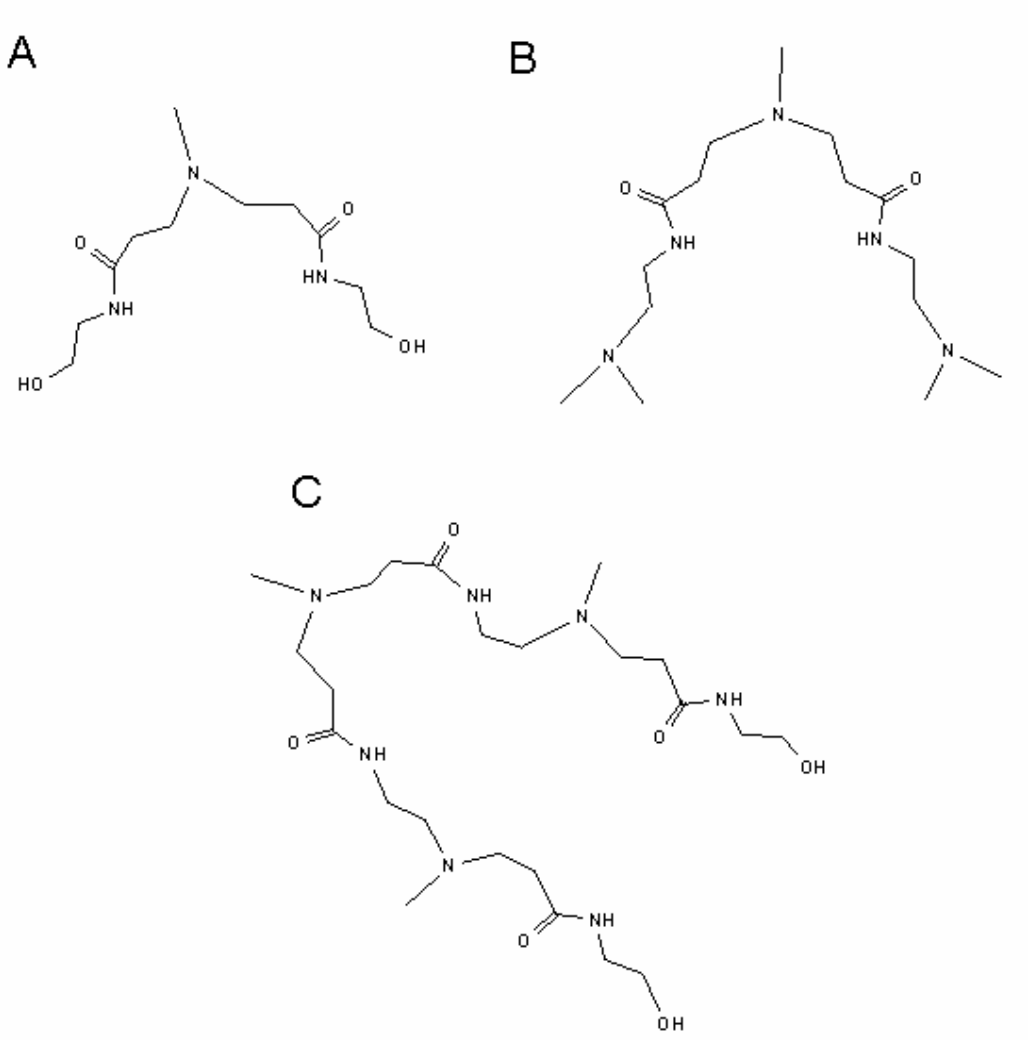

Figure 9.1: Model fragments of PAMAM dendrimer pockets. (A) DF41: Outer pocket; (B) DF50: One layer-inner pocket; (C) DF76: One layer-inner pocket and branches corresponding to two neighboring outer pockets. Note: DF stands for Dendrimer Fragment and the two-digit number indicates the number of atoms that composes the fragment

DFT was used to optimize minimum energy as well as TS geometries without symmetry constraints. The TS structure of section 8.3.1.1. was located with the Synchronous Transit-Guide Quasi-Newton (STQN) method[76]. The optimization of the geometries was followed by second derivative matrix calculations –except for DF76- that provided estimates for the zero point energy (ZPE) and temperature corrections to

the Gibbs free energy at 298K. The calculations were done with Gaussian 03 [74] suite of programs.

9.3 Results and discussion

9.3.1 Bidentate binding of Pt(II) in dendrimer outer pocket

9.3.1.1 Bidentate binding of Pt(II) to two N3 sites

Bidentate binding to two tertiary amine sites was studied with the outer pocket fragment (DF41) and $N(CH_3)_3$. The following reactions apply:

Step 1: NCB between a $N(CH_3)_3$ and DF40-N-$PtCl_3^-$---H_2O-Cl^- (product of eqn 8.6)

DF40-N-$PtCl_3^-$---H_2O-Cl^- + N'$(CH_3)_3$—H_2O

➔ DF40-N-$PtCl_3^-$(H_2O)---N'$(CH_3)_3$---Cl^- + H_2O (9.1)

Step 2A: Chloride exchange reaction giving the *cis*-product

DF40-N-$PtCl_3^-$(H_2O)---N'$(CH_3)_3$---Cl^-

➔ (DF40-N), $(CH_3)_3$N'-*cis*-$PtCl_2$-(H_2O)---Cl^----Cl^- (9.2)

Or

Step 2B: Chloride exchange reaction giving the *trans*-product

DF40-N-$PtCl_3^-$(H_2O)---N'$(CH_3)_3$---Cl^-

➔ (DF40-N), $(CH_3)_3$N'-*trans*-$PtCl_2$-(H_2O)---Cl^----Cl^- (9.3)

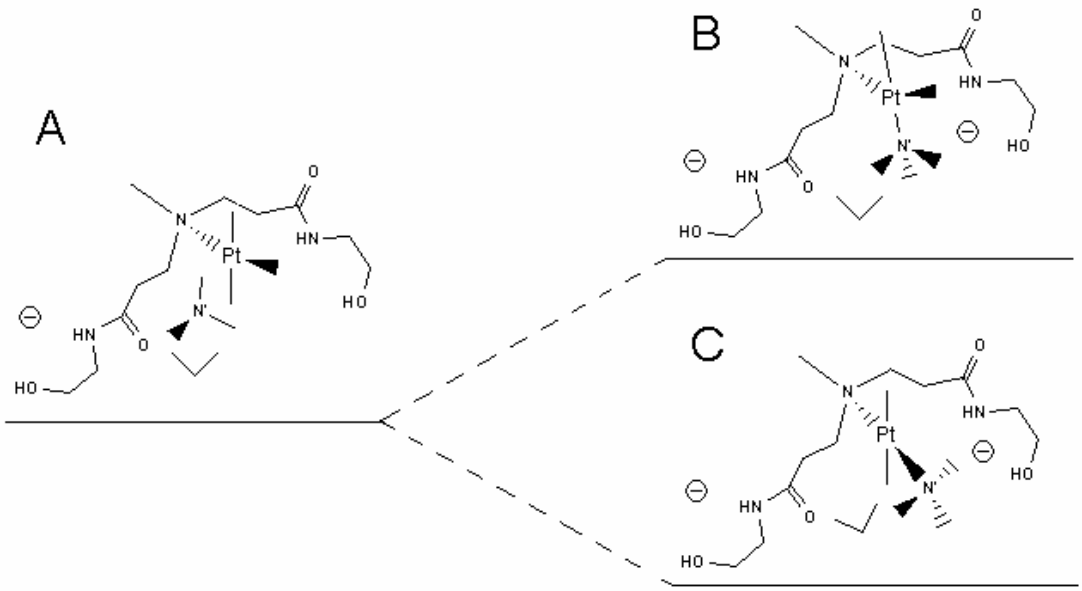

Figure 9.2. Bidentate binding of Pt(II) to two N3 sites. A) DF40-N-$PtCl_3^-(H_2O)$---N'$(CH_3)_3$ (product of eqn 9.1); B) (DF40-N), $(CH_3)_3$N'-*cis*-$PtCl_2$-(H_2O)---Cl^----Cl^-; C) (DF40-N), $(CH_3)_3$N'-*trans*-$PtCl_2$-(H_2O)---Cl^----Cl^-. A transition state was found only for the reaction A → C (eqn 9.3) but not for A → B (eqn 9.2). Notice that the leaving Cl^- ligand stays inside the pocket interacting with neighboring hydrogen atoms

ΔG of reaction for eqns 9.1, 9.2 and 9.3 was calculated to be 7.4, 8.5 and -7.8 kcal/mol respectively. A TS structure could not be found for the reaction yielding the isomer *cis*. But for the reaction that yields the *trans* isomer, the activation entalphy was calculated to be 15.3 kcal/mol. Although the activation energy for producing the *cis*-isomer is unknown, the size of this *cis-trans* stability difference (16.3 kcal in ΔG) suggests that the reaction is thermodynamically rather than kinetically driven. Thus, the isomer *trans* (the thermodynamically preferred product) rather than the *cis* is likely to be the main product. Upon reaction, the water that bridges an amide O and a Cl^- ligand in the $PtCl_3^-$ moiety (Figure 9.2, A) is slightly displaced respect to its initial position while the Cl^- that locates far from the reaction site remains as an spectator.

9.3.1.2 Bidentate binding of Pt(II) to N3 and N2 sites

Outer pockets have one N3 and two N2 sites. But as N3 and N2 are close neighbors -two methylene groups in between- only the formation of *cis* isomer was calculated (ΔG = 10.5 kcal/mol) according to the following reaction (where reactant structure is the product of eqn 8.18):

$$\text{DF40-N3-}cis\text{-}PtCl_2(H_2O)\text{---}H_2O\text{---}Cl^- \rightarrow \text{DF39-(N3,N2)-}cis\text{-}PtCl_2\text{----}(H_2O)_2\text{---}Cl^- \quad (9.4)$$

9.3.2 Bidentate binding of Pt(II) in one-layer-inner pocket

In order to assess how bidentate binding takes place in environments other than outer pockets, four configurations describing binding to two tertiary amine N (N3) and to one tertiary amine N (N2) and one secondary amide N (N2) in both *cis* & *trans* arrangements were calculated with the DF50 fragment (Figure 9.1, B).

The results indicate that the configuration of minimum energy is that where Pt(II) binds to two tertiary amine N atom sites (N3) in *trans* position. From Table 9.1 it can also be noticed that the *cis-trans* stability difference for this type of binding is large (ΔG = 20.2 kcal/mol). This value is slightly higher than that found for outer pockets (ΔG =16.3 kcal/mol) and further supports the aforementioned assertion (section 9.3.1.1), that bidentate binding to two N3 sites is thermodynamically rather than kinetically driven. The stability difference is still large even with respect to the next stable –also *trans*-configuration (ΔG = 14.3 kcal/mol, Table 9.1) where simultaneous binding to one tertiary amine N (N3) and to one secondary amide N (N2) takes place. Optimized structures are shown in Figure 9.3.

Table 9.1: Stability (kcal/mol) of DF48-(site,site)-$PtCl_2$ structures relative to the configuration of minimum energy. N3: tertiary amine N, N2: secondary amide N

Configuration	ΔG
DF48-(N3,N3)-*trans*-$PtCl_2$	0.0
DF48-(N3,N2)-*trans*-$PtCl_2$	14.3
DF48-(N3,N3)-*cis*-$PtCl_2$	20.2
DF48-(N3,N2)-*cis*-$PtCl_2$	24.7

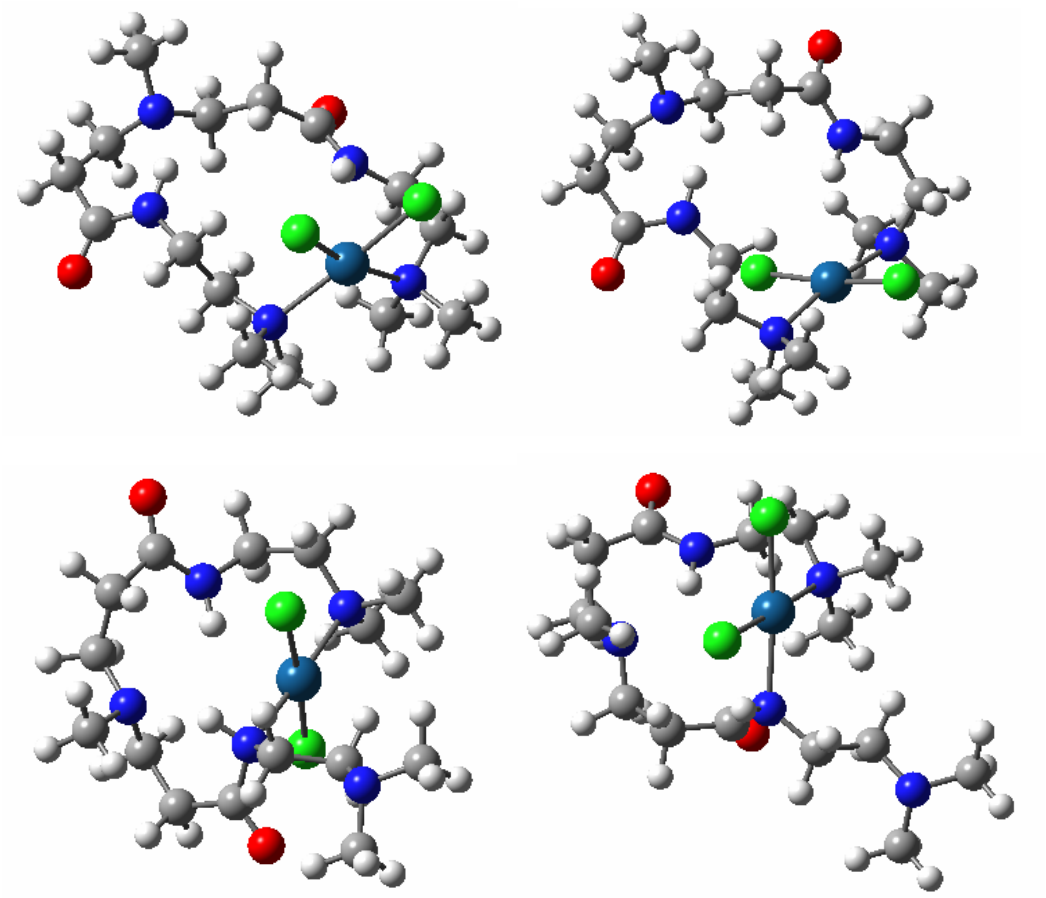

Figure 9.3. Bidentate binding of Pt(II) in one-layer-inner pocket. Upper left: DF48-(N3,N3)-*cis*-$PtCl_2$; Upper right: DF48-(N3,N3)-*trans*-$PtCl_2$; Lower left: DF48-(N3,N2)-*trans*-$PtCl_2$. Lower right: DF48-(N3,N2)-*cis*-$PtCl_2$

9.3.3 Bidentate binding of Pt(II) in one-layer-inner pocket connected to two branches of adjacent outer pockets

In previous sections, it was shown that bidentate binding of Pt(II) to two tertiary amine N (N3) sites is the preferred configuration. In this section we seek to find out how the $PtCl_2$ moiety is held inside the one-layer-inner pocket by exploring bidentate binding of Pt(II) in a larger fragment that includes two branches of adjacent outer pockets: DF76 (Figure 9.1, C). Four different configurations were found (Figure 9.4). It can be observed that perpendicular rather than in-plane accommodation of the Cl^- ligands -with respect to the plane containing the three tertiary amine N sites (N3)- is the configuration of minimum energy (Table 9.2).

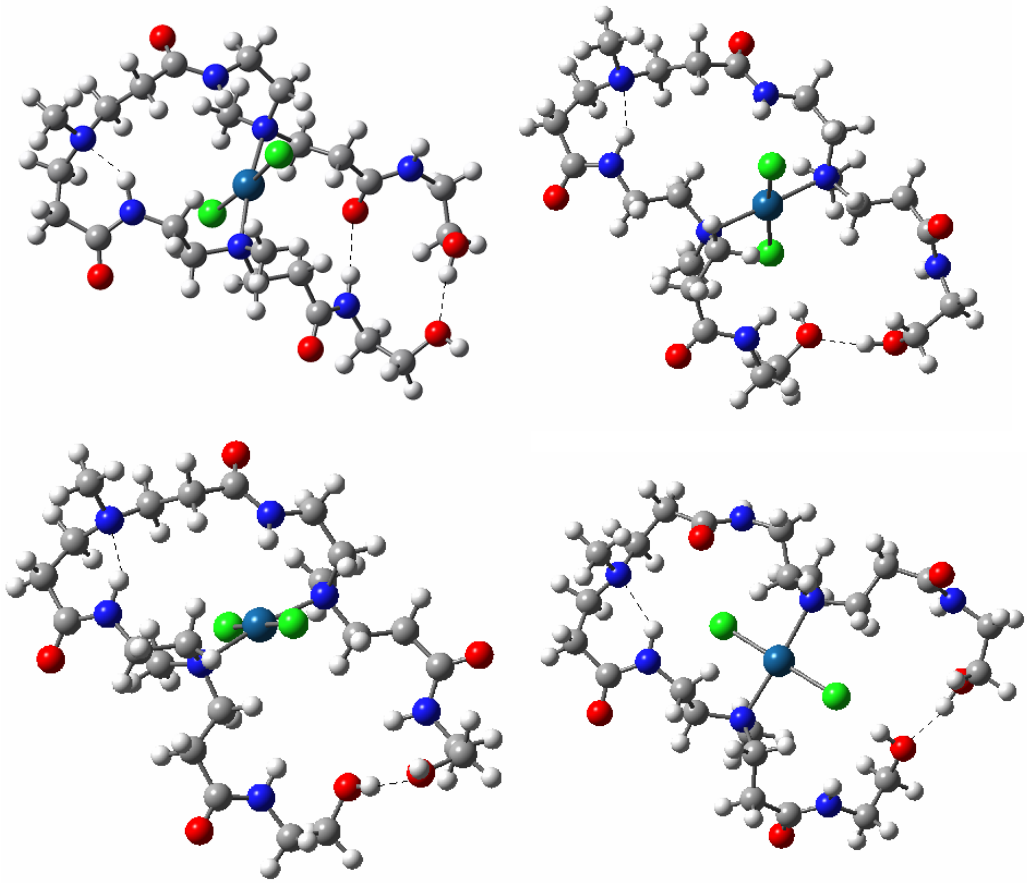

Figure 9.4. DF74-(N3,N3)-*trans*-$PtCl_2$ configurations. Upper left: Configuration E; Upper right: Configuration C; Lower left: Configuration B; Lower right: Configuration D

In all DF74-(N3,N3)-*trans*-$PtCl_2$ configurations there are hydrogen bonds ~N2-H---N3~ and ~O-H---(OH)~ and an extra H-bond ~N2-H---O=C~ is present for the most stable configuration. However, there is no strict correlation between the length of the ~N2-H---N3~ hydrogen bond and the relative stability of these four configurations (Table 9.2 and Figure 9.4): Config. C is more stable than Config. B (in 3.4 kcal/mol) even though Config. B's hydrogen bond is shorter (See Table 9.3). This observation highlights structural factors that can also contribute to the stability of the complex $PtCl_2$-dendrimer such as the magnitude of the dihedral angle N2-C-C-N3.

Table 9.2: Stability (kcal/mol) of DF74-(N3-N3)-*trans*-$PtCl_2$ structures relative to the configuration of minimum energy. N3: tertiary amine N

Configuration	ΔE_{el}
E	0.0
C	5.0
B	8.4
D	12.3

It is reasonable to assume that the most stable configuration for the dihedral angles N2-C-C-N3 (with N3 being one of the atom binding sites) is *anti* rather than *gauche*,[172] because the substituents in the tertiary amine N are a branch and a methyl group that can be regarded as bulky. Considering that, it is possible to explain why Config. C (δ(N2-C-C-N3), branch 1 = 173.3°) is more stable than Config. B (δ(N2-C-C-N3), branch 1 = 85.1°).

Table 9.3: H-bond length (angstroms) and dihedral angles δ(N2-C-C-N3) (degrees) in DF74-N3,N3-*trans*-$PtCl_2$ configurations

Config.	~N2-H---N3~ H-bond	~OH---(OH)~ H-bond	~N2-H---O=C~ H-bond	δ(N2-C-C-N3) Branch 1	δ(N2-C-C-N3) Branch 2
E	1.95	1.90	2.14	139.6	51.8
C	2.10	1.85		173.3	80.9
B	2.01	1.84		85.1	72.2
D	2.13	1.89		143.0	87.6

9.3.4. Tridentate binding of Pt(II) to nitrogen atom sites

Tridentate binding of Pt(II) to a dendrimer outer pocket is represented in the following equation (where reactant is the product of eqn 9.4):

DF39-(N3,N2)-*cis*-$PtCl_2$----$(H2O)_2$---Cl^-

➔ DF38-(N3,N2,N2)-PtCl---$(H2O)_2$---Cl^----Cl^- (9.5)

The mechanism followed by this reaction is not examined in this project. Nonetheless, the results indicate that it is not feasible from a thermodynamic point of view (ΔG = 10.0 kcal/mol).

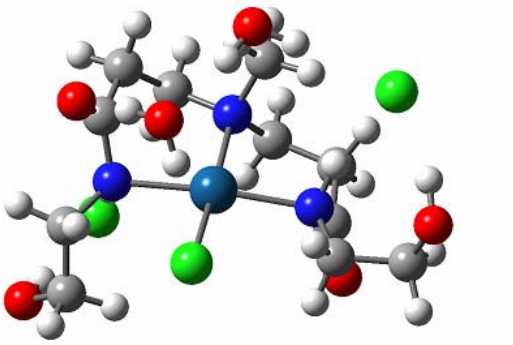

Figure 9.5: Configuration DF38-(N3,N2,N2)-PtCl---$(H_2O)_2$---Cl^----Cl^- . Note: product of eqn 9.5

The other two types of tridentate binding were not studied for two reasons: first, although binding to three and four nitrogen atoms -two ammonia and one/two guanine (N7) nitrogen atoms[173]- and binding to two ammonia and two primary amide nitrogen[174]

have been reported, we are not aware of any compound where either three tertiary *amine* N or secondary *amide* N atoms are involved in binding. Thus, binding of Pt(II) to three dendrimer nitrogen atom sites remains an open question.

9.3.5 Pt(II) complexation to large dendrimers

In Chapter VI we assumed that our fragment models intend to represent dendrimer outer regions or pockets. In this section, we extrapolate our findings to interpret how binding in large dendrimers -such as G4OH- takes place.

In the following subsections, the following assumptions hold: first, that Pt(II) binds to either one tertiary amine N (N3) (monodentate binding) or two tertiary amine N (N3) atoms (bidentate binding); second, that although it has been shown that it is possible to have water O in the first coordination shell of Pt(II) (Chapter VIII) we have not considered such a case; third, that the amide O atoms in the outer pockets orient either outward-outward, outward-inward or inward-inward (Chapter III); fourth, that all amide groups orient in *trans* position (Chapter III); fifth, that the amide O atoms in the core (subgeneration G0) orient clockwise; and sixth that the dendrimer-Pt(II) complex is electroneutral.

9.3.5.1 When only monodentate binding occurs

It can be argued that water molecules enter the pocket. In fact, our calculations have shown that outer pockets can accommodate at least two water molecules (Chapter III) and one water and one Pt(II) complex (Chapter VIII). Thus, Figure 9.6 may represent the initial stages of the interaction of Pt(II) and relevant counterions with the dendrimer and should be regarded as a first approximation to the real case.

Knowing that binding to N3 sites is feasible and having demonstrated that K^+ ions can be sorbed inside the dendrimer (Chapter VI), we hypothesize a scenario where K^+ ions help stabilize the dendrimer/complex structure inside a G1-OH dendrimer (Figure 9.6). Thus, the binding of four $PtCl_3^-$ and four K^+ ions (making the whole particle neutral) is represented in Figure 9.6. Although Figure 9.6 represents a G1OH dendrimer,

it may also describe monodentate binding in the outer pockets of a large dendrimer such as G4OH, at least in the early stages of Pt(II) complexation.

Figure 9.6 suggests that no dendrimer region is occupied by Cl^-. However we believe this is still justified because of the following reasons: 1) the free energy to bind Cl^- is lower than the free energy to bind $PtCl_4^{2-}$ (See Chapter VI); 2) even when $PtCl_3^-$ and Cl^- may coexist in the pocket at some point during the complexation process, Cl^- is eventually removed (See Chapter VII and VIII) and 3) the affinity of Cl^- for exterior water dimers is larger than that for the pocket-encapsulated water (Chapter VI). All these arguments make Figure 9.6 a reasonable approximation.

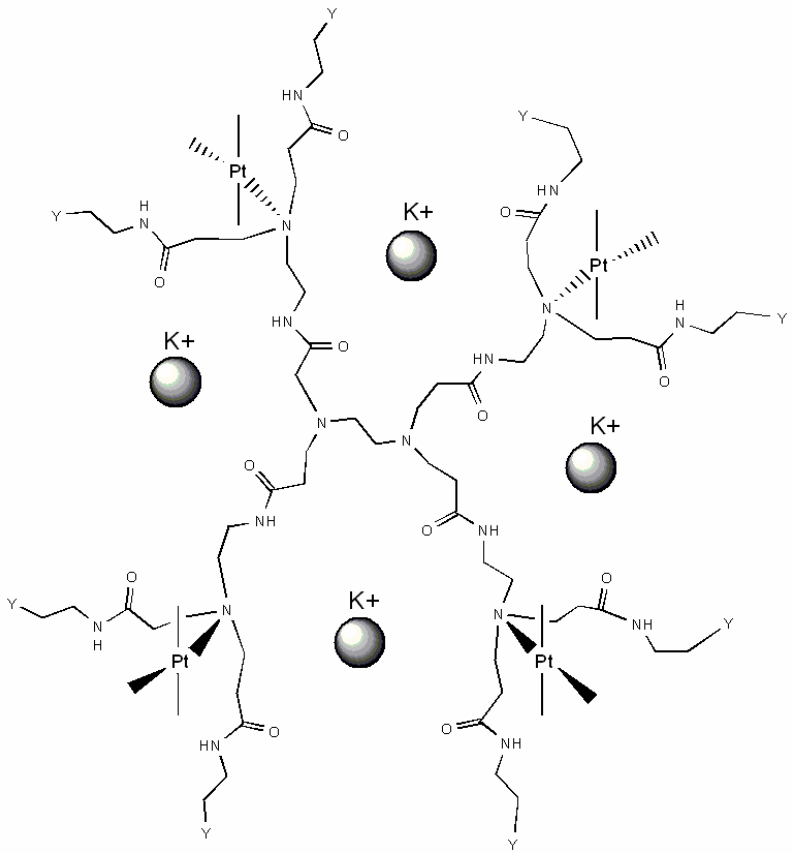

Figure 9.6. Monodentate binding of Pt(II) to G1OH: proposed configuration G1OH + 4 $PtCl_3^-$ + 4 K^+. As the orientation of the outer pocket will most likely remain outward-outward after release of the Cl^- ligand, this helps the admission of K^+ ions in adjacent and void pockets. For sake of clarity, the water molecules that could not only occupy the outer pockets but also solvate the binding species are omitted. Y: functional group, specifically –OH

9.3.5.2 When only bidentate binding occurs

At least two alternative orientations of the outer pockets could be proposed. In the first (Figure 9.7), one of the neighboring outer pockets orients amide O outward-inward (Chapter III) –hosting water- and the other orients them outward-outward –so that Cl^- ions be hosted (Chapter VI).

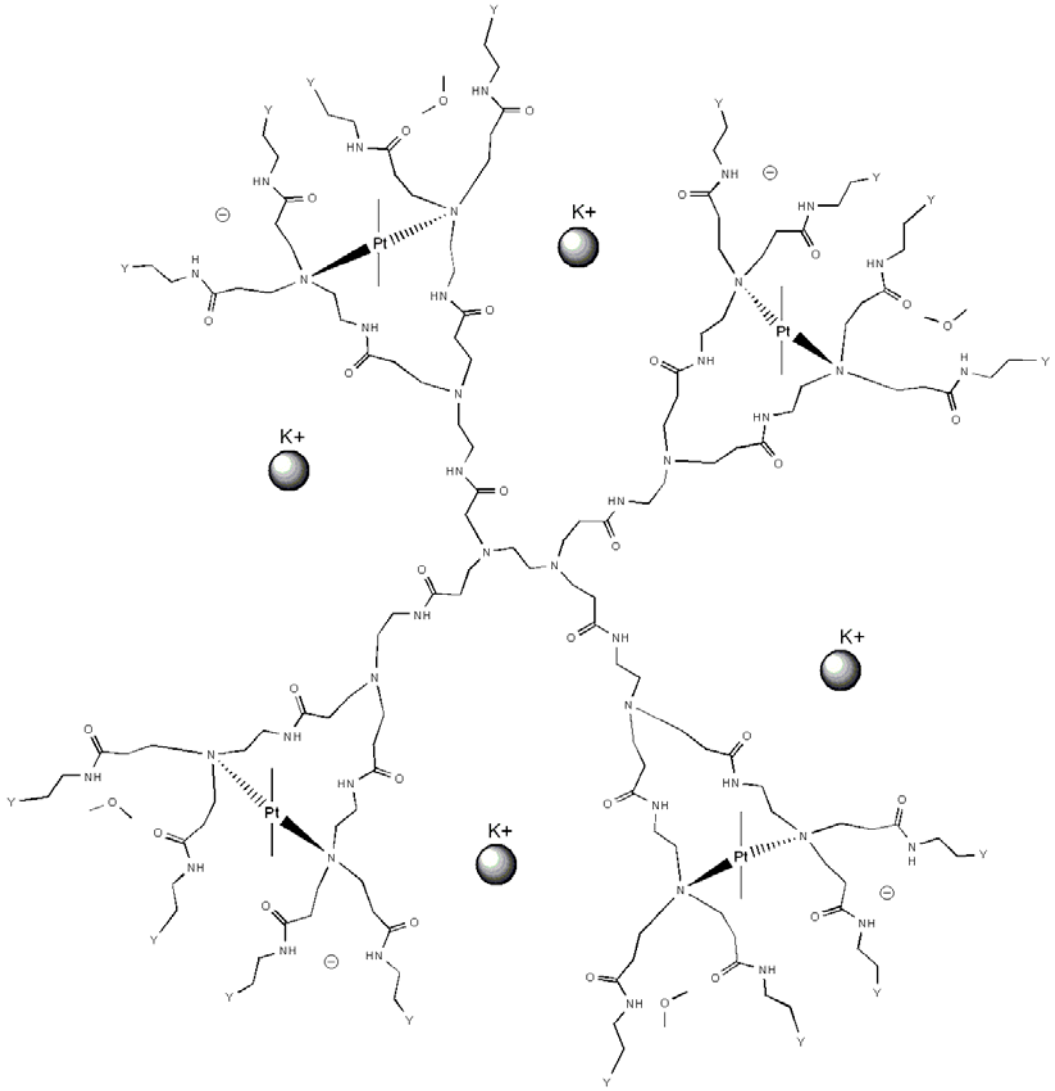

Figure 9.7. Bidentate binding of Pt(II) to G2OH: proposed configuration G2OH + 4 $PtCl_2$ + 4 K^+ + 4 Cl^- + 4 H_2O. Two outer pockets and a one-layer-inner pocket can be counted as one each G2 branch. Water molecules can occupy the voids too but have not been represented for sake of clarity. Y: functional group, specifically –OH

Then, as in the outside of each G2 branch the orientation is outward-outward, K^+ ions can bind to the exposed amide O (Chapter VI). In this manner, the charge neutrality of the complex is fulfilled. However, another possible configuration (not shown) may have the two neighboring outer pockets orienting their amide O atoms outward-inward and accepting only waters in their interior.

9.3.5.3 When both mono- and bidentate binding occur

Figure 9.6 and 9.7 represent scenarios where 'only monodentate' and 'only bidentate' binding respectively take place. However, mono- and bidentate binding may occur simultaneously as suggested by the second and third ^{195}Pt NMR peaks measured in the spectra for G4OH-Pt(II) dendrimer[62]-in this particular spectra, no NMR resonances corresponding to binding to N2 sites were found, thus making our assumption of Pt(II) interacting primarily with N3 sites more than adequate.

In order to build up a model including mono- and bidentate binding, we need first a reasonable estimate of the loading capacity of the dendrimer that has been estimated to be 40 Pt(II) complexes per dendrimer[61,103]; second, to take into account that G4OH has 56 N3 sites - without counting the two N3 sites in the core (G0) and the four N3 sites in subgeneration G1-; third, that $PtCl_3^-$ moieties bind to one N3 site; fourth, that $PtCl_2$ moieties bind to two N3 sites while hindering the binding of a $PtCl_3^-$ moiety to the next innermost N3 site. With all these considerations, we propose the binding of 32 $PtCl_3^-$ and 8 $PtCl_2$ to G4OH dendrimer according to Figure 9.8.

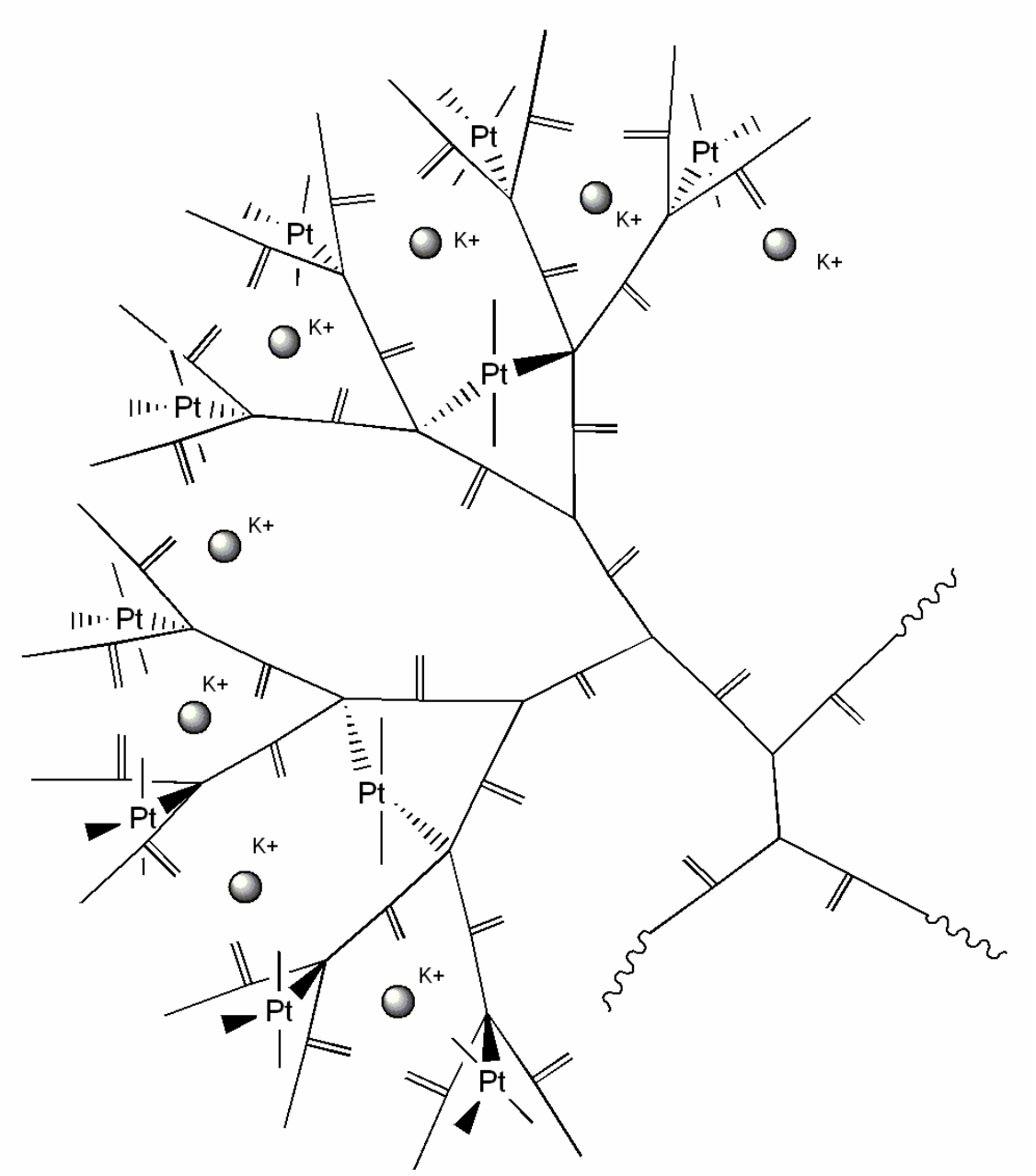

Figure 9.8. Binding of Pt(II) in a G4-OH dendrimer: proposed configuration of 8 $PtCl_3^-$ + 2 $PtCl_2$ + 8 K^+ for one branch in G4OH. The six innermost N3 sites have been assumed to be unavailable for binding. This configuration may account for the sorption of 40 Pt(II) complexes. Notice that only one out of four branches is drawn and that although the $PtCl_2$ moieties appear bound in a two-layers-inner pocket whose environment nonetheless resembles that of a one-layer-inner pocket

However, from the G4OH-Pt(II) complexation NMR data reported by Pellechia et al.[62] a ratio $PtCl_3^-/PtCl_2$ of 5/3 rather than a ratio 4/1 -as represented in Figure 9.8- is observed. We speculate that the ratio 5/3 can be a statistical average across several G4OH-Pt(II) composites with various $PtCl_3^-/PtCl_2$ ratios. Table 9.4 shows the ratios available in those G4OH-Pt(II) composites given that all N3 sites are occupied. To calculate these ratios, we realize that two of the outermost N3 sites -binding a $PtCl_3^-$ moiety each- could bind instead a $PtCl_2$ moiety provided such binding does not affect the binding of the neighboring innermost $PtCl_2$ moiety – as represented in Figure 9.8.

Table 9.4: Theoretical number of Pt(II) complexes sorbed in a G4OH dendrimer for a *full* N3 site occupation. This is based on successive replacements of two $PtCl_3^-$ moieties in the outermost N3 sites by one $PtCl_2$ moiety in a G4OH-Pt(II) complex as represented in Figure 9.8

N° of $PtCl_3^-$ moieties	N° of $PtCl_2$ moieties	Total of Pt(II) moieties	Ratio $PtCl_3^-/PtCl_2$
32	8	40	4/1
24	12	36	2/1
16	16	32	1/1
8	20	28	2/5
0	24	24	All $PtCl_2$

Notice that Table 9.4 assumes full N3 site occupation and that the experimental $PtCl_3^-/PtCl_2$ ratio 5/3 could be the statistical average of G4OH-Pt(II) composites with ratios 2/1 (66.6%) and 1/1 (33.3%). For this estimate composites with lower ratios (such as 2/5 and 'All $PtCl_2$') are not considered because it is more difficult for Pt(II) to bind to two sites (bidentate binding) than to one (monodentate binding). Then the average load of Pt(II) would be 34.6 Pt(II) per G4OH dendrimer. This value differs not only from the experimentally estimated Pt(II):G4OH: ratio of 40:1 but also from the estimated by the NMR and AFM experiments by Pellechia et al [62] who measured 32 Pt(II) rather than 40 Pt(II) as an average occupation. Their results seem to suggest then that not all N3 sites

are necessarily occupied by Pt(II) complexes. Therefore, it seems more likely that a *partial* rather than a *full* N3 site occupation occurs. If so, then 20 $PtCl_3^-$ and 12 *trans*-$PtCl_2$ moieties are bound to a G4OH dendrimer and can be regarded to be representative of the experimental statistical average. This structure (not shown) can be derived from Figure 9.8 by removing from it three $PtCl_3^-$ (two of them in adjacent pockets) and placing an extra $PtCl_2$ in one-layer-inner pocket.

9.4 Summary

Pt(II) binds not only to one dendrimer atom site but also to two tertiary amine sites (N3) (bidentate binding). However whether binding of Pt(II) to three dendrimer nitrogen atom sites (N3 or N2) (tridentate binding) takes place remains an open question.

In bidentate binding of Pt(II) to PAMAM dendrimers, the isomer *trans* rather than the *cis* is the preferred configuration and this binding process is likely to be thermodynamically driven due to the large difference in stability between the isomers *cis* and *trans*. It was also found that *trans*-$PtCl_2$ moieties are likely to orient perpendicular with respect to a plane described by two tertiary amine binding sites and the immediate innermost N3 site. Both, steric factors and hydrogen bond may explain the stability of a particular configuration.

Finally, we suggest that partial occupation rather than full occupation of tertiary amine sites (N3) takes place when Pt(II) binds to G4OH dendrimers. We speculate this to be the case also for larger –OH terminated dendrimers.

CHAPTER X
CONCLUSIONS AND RECOMMENDATIONS FOR FUTURE WORK

10.1 Conclusions

The major conclusions of this project are as follows:

- Our present work predicts that dendrimer outer pockets can encapsulate a water dimer and exchange it for counterions and Pt(II) complexes. However, the three ions more likely to become encapsulated are K^+, Cl^- and $PtCl_4^{2-}$. This finding strongly suggests that fresh rather than aged solutions of $PtCl_4^{2-}$ should be used in dendrimer templated synthesis of Pt nanoparticles when K_2PtCl_4 is used.
- It would be obvious to predict that non covalent binding (NCB) of cations like Cu(II) will not take place in protonated pockets. However, the fact that non covalent binding of anionic precursors such as $PtCl_4^{2-}$ would not take place in protonated pockets is a novel finding. Moreover, our results strongly suggest that complexation of $PtCl_4^{2-}$ takes place in unprotonated pockets.
- Upon encapsulation within a pocket, aquation of $PtCl_4^{2-}$ can take place. Thus, it can be said that the ligand exchange reaction is mediated by water and that the rate limiting step for this overall complexation is the aquation of $PtCl_4^{2-}$ within the pockets. The predominant pathway followed in the complexation of $PtCl_4^{2-}$ will likely lead to $PtCl_3^-$ moieties rather than moieties where water O is present in the first coordination sphere, e.g. $PtCl_2(H_2O)$.
- Unlike Cu(II) that binds preferentially to oxygen sites (like dendrimer amide O and water O) as well as to tertiary amine N, Pt(II) binds preferentially to tertiary amine N and in lesser degree to secondary amide N. Binding to secondary amide N takes place only when the configuration of the amide group in the branches of PAMAM dendrimers switches from *trans* (its preferred configuration) to *cis*.
- Although branches help to encapsulate $PtCl_4^{2-}$ effectively in the outer pocket during the NCB, their presence also causes an increase in the magnitude of the

energy barrier of the successive ligand exchange reaction. Nonetheless, the overall complexation of $PtCl_4^{2-}$ in outer pockets is still more likely than either aquation of $PtCl_4^{2-}$ or complexation of $PtCl_4^{2-}$ with trimethylamine.

10.2 Recommendations for future work

The main recommendations derived from this project for future work are listed as follows:

- The present analysis of the complexation of Pt(II) to dendritic polymers can be extended to study the complexation of other metal ion-dendrimer systems. Not only systems with Pt(II) complexes such as $PtCl_6^{2-}$ as precursors can be tested but particularly those with square planar complexes such as $PdCl_4^{2-}$, $AuCl_4^{-}$, etc.
- The proposal that partial rather than full occupation of N3 sites by Pt(II) raises the question of what species occupies the other N3 sites. This poses itself as an interesting challenge and opportunity for experiments and theory alike, and it should be relevant because the impact of those guests upon the complexation process is unknown.
- Considering that the partial occupation of N3 sites by $PtCl_3$ and *trans*-$PtCl_2$ moieties proposed in this work and that experimental predictions that Pt dimers form upon reduction of the Pt(II)-dendrimer complexes are both accurate, then the next step toward our understanding of dendrimer-templated synthesis will entail investigation of the reduction step. The effect of the solvent on the reducing agent, the type of complex formed between Pt(II) atoms, a viable pathway by which such complex is formed and the elimination of the Cl ligand are some of the questions such study ought to answer.
- Finally as our work could not decide whether tridentate binding of Pt(II) occurs or not, we suggest that experimental X-ray measurements of like-complexes be determined in order to elucidate this.

REFERENCES

(1) Cotton, F. A.; Wilkinson, G. *Advanced Inorganic Chemistry*, 4th ed.; Wiley: New York, 1980.

(2) Thompson, K. H.; Orvig, C. *Science* **2003**, *300*, 936.

(3) Donnelly, P. S.; Xiao, Z.; Wedd, A. G. *Curr. Opin. Chem. Biol.* **2007**, *11*, 128.

(4) Lippard, S. J. *Nat. Chem. Biol.* **2006**, *2*, 504.

(5) Pagel, K.; Vagt, T.; Koksch, B. *Org. Biomol. Chem.* **2005**, *3*, 3843.

(6) Krebs, J. F.; Borovik, A. S. *J. Am. Chem. Soc.* **1995**, *117*, 10593.

(7) Kruppa, M.; Konig, B. *Chem. Rev.* **2006**, *106*, 3520.

(8) Sharma, A. C.; Borovik, A. S. *J. Am. Chem. Soc.* **2000**, *122*, 8946.

(9) Krebs, J. F.; Borovik, A. S. *Chem. Commun.* **1998**, *5*, 553.

(10) Padden, K. M.; Krebs, J. F.; MacBeth, C. E.; Scarrow, R. C.; Borovik, A. S. *J. Am. Chem. Soc.* **2001**, *123*, 1072.

(11) Striegler, S. *J. Chromatogr. B* **2004**, *804*, 183.

(12) Becker, J. J.; Gagne, M. R. *Acc. Chem. Res.* **2004**, *37*, 798.

(13) Butler, A. *Science* **1998**, *281*, 207.

(14) Iranzo, O.; Kovalevsky, A. Y.; Morrow, J. R.; Richard, J. P. *J. Am. Chem. Soc.* **2003**, *125*, 1988.

(15) Ivanov, I.; Tainer, J. A.; McCammon, J. A. *Proc Natl Acad Sci U S A* **2007**, *104*, 1465.

(16) Tanaka, K.; Clever, G. H.; Takezawa, Y.; Yamada, Y.; Kaul, C.; Shionoya, M.; Carell, T. *Nature Nanotechnol.* **2006**, *1*, 190.

(17) Sels, B.; De Vos, D.; Buntinx, M.; Pierard, F.; Kirsch-De Mesmaeker, A.; Jacobs, P. *Nature* **1999**, *400*, 855.

(18) Etorki, A. M.; Hillman, A. R.; Ryder, K. S.; Glidle, A. *J. Electroanal. Chem.* **2007**, *599*, 275.

(19) Gohdes, J. W.; Duran, B. L.; Clark, N. C.; Robison, T. W.; Smith, B. F.; Sauer, N. N. *Separ. Sci. Technol.* **2001**, *36*, 2647.

(20) Diallo, M. S.; Balogh, L.; Shafagati, A.; Johnson, J. H., Jr.; Goddard, W. A., III; Tomalia, D. A. *Environ. Sci. Technol.* **1999**, *33*, 820.

(21) Diallo, M. S.; Christie, S.; Swaminathan, P.; Balogh, L.; Shi, X.; Um, W.; Papelis, C.; Goddard, W. A., III; Johnson Jr, J. H. *Langmuir* **2004**, *20*, 2640.

(22) Diallo, M. S.; Christie, S.; Swaminathan, P.; Johnson, J. H., Jr.; Goddard, W. A., III. *Env. Sci. & Tech.* **2005**, *39*, 1366.

(23) Xu, Y.; Zhao, D. *Environ. Sci. Technol.* **2005**, *39*, 2369.

(24) Xu, Y.; Zhao, D. *Ind. Eng. Chem. Res.* **2006**, *45*, 1758.

(25) Rether, A.; Schuster, M. *React. Funct. Polym.* **2003**, *57*, 13.

(26) Sand, W.; Gehrke, T. *Res. Microbiol.* **2006**, *157*, 49.

(27) Pang, X.; Zhitomirsky, I. *Langmuir* **2004**, *20*, 2921.

(28) McNally, E. A.; Zhitomirsky, I.; Wilkinson, D. S. *Mater. Chem. Phys.* **2005**, *91*, 391.

(29) Nagarajan, N.; Humadi, H.; Zhitomirsky, I. *Electrochim. Acta* **2006**, *51*, 3039.

(30) Zhitomirsky, I. *J. Appl. Electrochem.* **2004**, *34*, 235.

(31) Severin, K. *Curr. Opin. Chem. Biol.* **2000**, *4*, 710.

(32) Cushing, B. L.; Kolesnichenko, V. L.; O'Connor, C. J. *Chem. Rev.* **2004**, *104*, 3893.

(33) Perignon, N.; Marty, J.-D.; Mingotaud, A.-F.; Dumont, M.; Rico-Lattes, I.; Mingotaud, C. *Macromolecules* **2007**, *40*, 3034.

(34) NSTC. National Nanotechnology Initiative - Strategic Plan. **http://www.nano.gov/NNI_Strategic_Plan_2004.pdf** (accessed October 2007).

(35) Reiss, G.; Hutten, A. *Nat. Mater.* **2005**, *4*, 725.

(36) Farokhzad, O. C.; Cheng, J.; Teply, B. A.; Sherifi, I.; Jon, S.; Kantoff, P. W.; Richie, J. P.; Langer, R. *Proc Natl Acad Sci U S A* **2006**, *103*, 6315.

(37) Allen, T. M.; Cullis, P. R. *Science* **2004**, *303*, 1818.

(38) Sato, M.; Webster, T. J. *Expert Rev. Med. Devic.* **2004**, *1*, 105.

(39) Wagner, V.; Dullaart, A.; Bock, A.-K.; Zweck, A. *Nat. Biotechnol.* **2006**, *24*, 1211.

(40) Bell, A. T. *Science* **2003**, *299*, 1688.

(41) Astruc, D.; Lu, F.; Aranzaes, J. R. *Angew. Chem. Int. Ed.* **2005**, *44*, 7852.

(42) Cahen, D.; Hodes, G. *Adv. Mat.* **2002**, *14*, 789.

(43) Dillon, A. C.; Jones, K. M.; Bekkedahl, T. A.; Kiang, C. H.; Bethune, D. S.; Heben, M. J. *Nature* **1997**, *386*, 377.

(44) Dai, H.; Hafner, J. H.; Rinzler, A. G.; Colbert, D. T.; Smalley, R. E. *Nature* **1996**, *384*, 147.

(45) Goldhaber-Gordon, D.; Goldhaber-Gordon, I. *Nature* **2001**, *412*, 594.

(46) Zhang, M.; Fang, S.; Zakhidov, A. A.; Lee, S. B.; Aliev, A. E.; Williams, C. D.; Atkinson, K. R.; Baughman, R. H. *Science* **2005**, *309*, 1215.

(47) Sazonova, V.; Yaish, Y.; Ustunel, H.; Roundy, D.; Arias, T. A.; McEuen, P. L. *Nature* **2004**, *431*, 284.

(48) Barone, P. W.; Baik, S.; Heller, D. A.; Strano, M. S. *Nat. Mater.* **2005**, *4*, 86.

(49) Ahir, S. V.; Terentjev, E. M. *Nat. Mater.* **2005**, *4*, 491.

(50) Ahn, E. S.; Gleason, N. J.; Nakahira, A.; Ying, J. Y. *Nano Lett.* **2001**, *1*, 149.

(51) Ahn, E. S.; Gleason, N. J.; Ying, J. Y. *J. Am. Ceram. Soc.* **2005**, *88*, 3374.

(52) Bansal, A.; Yang, H.; Li, C.; Cho, K.; Benicewicz, B. C.; Kumar, S. K.; Schadler, L. S. *Nat. Mater.* **2005**, *4*, 693.

(53) Crosby, A. J.; Lee, J.-Y. *Polym. Rev.* **2007**, *47*, 217.

(54) Scott, R. W. J.; Wilson, O. M.; Crooks, R. M. *J. Phys. Chem. B* **2005**, *109*, 692.

(55) Alexeev, O. S.; Siani, A.; Lafaye, G.; Williams, C. T.; Ploehn, H. J.; Amiridis, M. D. *J. Phys. Chem. B* **2006**, *110*, 24903.

(56) Ye, H.; Crooks, R. M. *J. Am. Ceram. Soc.* **2005**, *127*, 4930.

(57) Ye, H.; Crooks, R. M. *J. Am. Ceram. Soc.* **2007**, *129*, 3627.

(58) Liu, D.; Gao, J.; Murphy, C. J.; Williams, C. T. *J. Phys. Chem. B* **2004**, *108*, 12911.

(59) Gu, Y.; Xie, H.; Gao, J.; Liu, D.; Williams, C. T.; Murphy, C. J.; Ploehn, H. J. *Langmuir* **2005**, *21*, 3122.

(60) van Heerbeek, R.; Kamer, P. C.; van Leeuwen, P. W.; Reek, J. N. *Chem. Rev.* **2002**, *102*, 3717.

(61) Zhao, M.; Crooks, R. M. *Adv. Mater.* **1999**, *11*, 217.

(62) Pellechia, P. J.; Gao, J.; Murphy, C. J. *Inorg. Chem.* **2004**, *43*, 1421.

(63) Mazzitelli, C. L.; Brodbelt, J. S. *J. Am. Soc. Mass Spectrom.* **2006**, *17*, 676.

(64) Floriano, P. N.; Noble, C. O., IV; Schoonmaker, J. M.; Poliakoff, E. D.; McCarley, R. L. *J. Am. Chem. Soc.* **2001**, *123*, 10545.

(65) Vrbka, L.; Vondrasek, J.; Jagoda-Cwiklik, B.; Vacha, R.; Jungwirth, P. *Proc Natl Acad Sci U S A* **2006**, *103*, 15440.

(66) Gumbart, J.; Wang, Y.; Aksimentiev, A.; Tajkhorshid, E.; Schulten, K. *Curr. Opin. Struc. Biol.* **2005**, *15*, 423.

(67) Adcock, S. A.; McCammon, J. A. *Chem. Rev.* **2006**, *106*, 1589.

(68) Sotomayor, M.; Schulten, K. *Science* **2007**, *316*, 1144.

(69) Senn, H. M.; Thiel, W. *Top. Curr. Chem.* **2007**, *268*, 173.

(70) Santiso, E. E.; Gubbins, K. E. *Mol. Simulat.* **2004**, *30*, 699.

(71) De Angelis, F.; Fantacci, S.; Sgamellotti, A. *Coordin. Chem. Rev.* **2006**, *250*, 1497.

(72) Car, R.; Parrinello, M. *Phys. Rev. Lett.* **1985**, *55*, 2471.

(73) Frisch, M. J.; Trucks, G. W.; Schlegel, H. B.; Scuseria, G. E.; Robb, M. A.; Cheeseman, J. R.; Zakrzewski, V. G.; Montgomery, J. A.; Stratmann, R. E.; Burant, J. C.; Dapprich, S.; Millam, J. M.; Daniels, A. D.; Kudin, K. N.; Strain, O. F. M. C.; Tomasi, J.; Barone, B.; Cossi, M.; Cammi, R.; Mennucci, B.; Pomelli, C.; Adamo, C.; Clifford, S.; Ochterski, J.; Petersson, G. A.; Ayala, P. Y.; Cui, Q.; Morokuma, K.; Malick, D. K.; Rabuck, A. D.; Raghavachari, K.; Foresman, J. B.; Ciolovski, J.; Ortiz, J. V.; Stefanov, V. V.; Liu, G.; Liashensko, A.; Piskorz, P.; Komaroni, I.; Gomperts, R.; Martin, R. L.; Fox, D. J.; Keith, T.; Al-Laham, M. A.; Peng, C. Y.; Nanayakkara, A.; Gonzalez, C.; Challacombe, M.; Gill, P. M. W.; Johnson, B.; Chen, W.; Wong, M. W.; Andres, J. L.; Head-Gordon, M.; Replogle, E. S.; Pople, J. A. *Gaussian 98*, Revision A.11; Gaussian Inc.: Pittsburgh PA, 1998.

(74) Frisch, M. J.; Trucks, G. W.; Schlegel, H. B.; Scuseria, G. E.; Robb, M. A.; Cheeseman, J. R.; Montgomery, J. A., Jr.; Vreven, T.; Kudin, K. N.; Burant, J. C.; Millam, J. M.; Iyengar, S. S.; Tomasi, J.; Barone, V.; Mennucci, B.; Cossi, M.; Scalmani, G.; Rega, N.; Petersson, G. A.; Nakatsuji, H.; Hada, M.; Ehara, M.; Toyota, K.; Fukuda, R.; Hasegawa, J.; Ishida, M.; Nakajima, T.; Honda, Y.; Kitao, O.; Nakai, H.; Klene, M.; Li, X.; Knox, J. E.; Hratchian, H. P.; Cross, J. B.; Bakken, V.; Adamo, C.; Jaramillo, J.; Gomperts, R.; Stratmann, R. E.; Yazyev, O.; Austin, A. J.; Cammi, R.; Pomelli, C.; Ochterski, J. W.; Ayala, P. Y.; Morokuma, K.; Voth, G. A.; Salvador, P.; Dannenberg, J. J.; Zakrzewski, V. G.; Dapprich, S.; Daniels, A. D.; Strain, M. C.; Farkas, O.; Malick, D. K.; Rabuck, A. D.; Raghavachari, K.; Foresman, J. B.; Ortiz, J. V.; Cui, Q.; Baboul, A. G.; Clifford, S.; Cioslowski, J.; Stefanov, B. B.; Liu, G.; Liashenko, A.; Piskorz, P.; Komaromi, I.; Martin, R. L.; Fox, D. J.; Keith, T.; Al-Laham, M. A.; Peng, C. Y.; Nanayakkara, A.; Challacombe, M.; Gill, P. M. W.; Johnson, B.; Chen, W.; Wong, M. W.; Gonzalez, C.; Pople., J. A. *Gaussian 03*, Revision C.02; Gaussian, Inc.: Wallingford CT, 2004.

(75) Schlegel, H. B. *J. Comp. Chem.* **1982**, *3*, 214.

(76) Peng, C.; Ayala, P. Y.; Schlegel, H. B.; Frisch, M. J. *J. Comp. Chem.* **1996**, *17*, 49.

(77) Foresman, J. B.; Frisch, A. *Exploring Chemistry with Electronic Structure Methods*, 2nd ed.; Gaussian, Inc.: Pittsburgh, PA, 1996.

(78) Levine, I. N. *Physical Chemistry*, 4th ed.; McGraw-Hill, 1994.

(79) Slater, J. C. *Phys. Rev.* **1951**, *81*, 385.

(80) Becke, A. D. *Phys. Rev. A* **1988**, *38*, 3098.

(81) Vosko, S. H.; Wilk, L.; Nusair, M. *Can. J. Phys.* **1980**, *58*, 1200.

(82) Lee, C.; Yang, W.; Parr, R. G. *Phys. Rev. B* **1988**, *37*, 785.

(83) Becke, A. D. *J. Chem. Phys.* **1993**, *98*, 5648.

(84) Hay, P. J.; Wadt, W. R. *J. Chem. Phys.* **1985**, *82*, 270.

(85) Rappe, A. K.; Goddard, W. A., III. *J. Phys. Chem.* **1991**, *95*, 3358.

(86) Rappe, A. K.; Casewit, C. J.; Colwell, K. S.; Goddard, W. A., III; Skiff, W. M. *J. Am. Chem. Soc.* **1992**, *114*, 10024.

(87) Mayo, S. L.; Olafson, B. D.; Goddard, W. A., III. *J. Phys. Chem.* **1990**, *94*, 8897.

(88) Smith, W.; Forester, T. R. *Comput. Phys. Commun.* **1994**, *79*, 52.

(89) Berendsen, H. J. C.; Grigera, J. R.; Straatsma, T. P. *J. Phys. Chem.* **1987**, *91*, 6269.

(90) Ryckaert, J. P.; Ciccotti, G.; Berendsen, H. J. C. *J. Comput. Phys.* **1977**, *23*, 327.

(91) Smith, W.; Forester, T. R. *Comput. Phys. Commun.* **1994**, *79*, 63.

(92) Hoover, W. *Phys. Rev. A* **1985**, *31*, 1695.

(93) Smith, W.; Forester, T. R. *DL_POLY*; Daresbury Laboratory: Daresbury, United Kingdom, 1996.

(94) Frechet, J. M. J. *J. Polym. Sci. Part A: Polym. Chem.* **2003**, *41*, 3713.

(95) Esumi, K. *Top. Curr. Chem.* **2003**, *227*, 31.

(96) Balogh, L.; Tomalia, D. A.; Hagnauer, G. L. *Chem. Innovation* **2000**, *30*, 19.

(97) Crooks, R. M.; Lemon III, B. I.; Sun, L.; Yeung, L. K.; Zhao, M. *Top. Curr. Chem.* **2001**, *212*, 81.

(98) Balogh, L.; Tomalia, D. *J. Am. Chem. Soc.* **1998**, *120*, 7355.

(99) Sooklal, K.; Hanus, L. H.; Ploehn, H. J.; Murphy, C. J. *Adv. Mater.* **1998**, *10*, 1083.

(100) Tomalia, D. A.; Naylor, A. M.; Goddard, W. A., III. *Angew. Chem. Int. Ed.* **1990**, *29*, 138.

(101) Zhao, M.; Sun, L.; Crooks, R. M. *J. Am. Chem. Soc.* **1998**, *120*, 4877.

(102) Zhao, M.; Crooks, R. M. *Chem. Mater.* **1999**, *11*, 3379.

(103) Zhao, M.; Crooks, R. M. *Angew. Chem. Int. Ed.* **1999**, *38*, 364.

(104) Esumi, K.; Susuki, A.; Yamahira, A.; Torigoe, K. *Langmuir* **2000**, *16*, 2604.

(105) Barron, J. A.; Bernhard, S.; Houston, P. L.; Abruna, H. D. *J. Phys. Chem. A* **2003**, *107*, 8130.

(106) Esumi, K.; Isono, R.; Yoshimura, T. *Langmuir* **2004**, *20*, 237.

(107) Balogh, L.; Valluzzi, R.; Laverdure, K. S.; Gido, S. P.; Hagnauer, G. L.; Tomalia, D. A. *J. Nanoparticle Res.* **1999**, *1*, 353.

(108) Cakara, D.; Kleimann, J.; Borkovec, M. *Macromolecules* **2003**, *36*, 4201.

(109) Niu, Y.; Sun, L.; Crooks, R. M. *Macromolecules* **2003**, *36*, 5725.

(110) Fu-Ren, F. F.; Mazzitelli, C. L.; Brodbelt, J. S.; Bard, A. J. *Anal. Chem.* **2005**, *77*, 4413.

(111) Mulliken, R. S. *J. Chem. Phys.* **1955**, *23*, 1833.

(112) Mulliken, R. S. *J. Chem. Phys.* **1955**, *23*, 1841.

(113) Mulliken, R. S. *J. Chem. Phys.* **1955**, *23*, 2338.

(114) Gitsov, I.; Frechet, J. M. J. *J. Am. Chem. Soc.* **1996**, *118*, 3785.

(115) Jorgensen, W. L.; Gao, J. *J. Am. Chem. Soc.* **1988**, *110*, 4212.

(116) Tomalia, D. A.; Baker, H.; Dewall, J.; Hall, M.; Kallos, G.; Martin, S.; Roeck, J.; Ryder, J.; Smith, P. *Polymer J.* **1985**, *17*, 117.

(117) Crooks, R. M.; Zhao, M.; Sun, L.; Chechik, V.; Yeung, L. K. *Acc. Chem. Res.* **2001**, *34*, 181.

(118) Maiti, P. K.; Cagin, T.; Wang, G.; Goddard, W. A. *Macromolecules* **2004**, *37*, 6236.

(119) Betley, T. A.; Banaszak Holl, M. M.; Orr, B. G.; Swanson, D. R.; Tomalia, D. A.; Baker Jr., J. R. *Langmuir* **2001**, *17*, 2768.

(120) Ottaviani, M. F.; Montalti, F.; Turro, N. J.; Tomalia, D. A. *J. Phys. Chem. B* **1997**, *101*, 158.

(121) Tran, M. L.; Gahan, L. R.; Gentle, I. R. *J. Phys. Chem. B* **2004**, *108*, 20130.

(122) Ottaviani, M. F.; Bossmann, S.; Turro, N. J.; Tomalia, D. A. *J. Am. Chem. Soc.* **1994**, *116*, 661.

(123) Mansfield, M. L.; Klushin, L. I. *Macromolecules* **1993**, *26*, 4262.

(124) Naidoo, K. J.; Hughes, S. J.; Moss, J. R. *Macromolecules* **1999**, *32*, 331.

(125) Krol, M. *J. Mol. Mod.* **2003**, *9*, 316.

(126) Lee, I.; Athey, B. D.; Wetzel, A. W.; Meixner, W.; Baker, J. R., Jr. *Macromolecules* **2002**, *35*, 4510.

(127) Streett, W. B.; Tildesley, D. J.; Saville, G. *Mol. Phys.* **1978**, *35*, 639.

(128) Pasquarello, A.; Petri, I.; Salmon, P. S.; Parisel, O.; Car, R.; Toth, E.; Powell, D. H.; Fischer, H. E.; Helm, L.; Merbach, A. E. *Science* **2001**, *291*, 856.

(129) Schwenk, C. F.; Rode, B. M. *Chem. Phys. Chem.* **2003**, *4*, 931.

(130) Erras-Hanauer, H.; Clark, T.; van Eldik, R. *Coord. Chem. Rev.* **2003**, *238-239*, 233.

(131) Marcus, Y. *Chem. Rev.* **1988**, *88*, 1475.

(132) Beagley, B.; Eriksson, A.; Lindgren, J.; Persson, I.; Pettersson, L. G. M.; Sandstrom, M.; Wahlgren, U.; White, E. W. *J. Phys. Condens. Matter* **1989**, *1*, 2395.

(133) Bopp, P.; Janscó, G.; Heinzinger, K. *Chem. Phys. Lett.* **1983**, *98*, 129.

(134) Helm, L.; Merbach, A. E. *Coord. Chem. Rev.* **1999**, *187*, 151.

(135) Bosman, A. W.; Schenning, A. P. H. J.; Janssen, R. A. J.; Meijer, E. W. *Chem. Ber./Recl.* **1997**, *130*, 725.

(136) D'Angelo, P.; Bottari, E.; Festa, M. R.; Nolting, H.-F.; Pavel, N. V. *J. Phys. Chem. B* **1998**, *102*, 3114.

(137) Choy, J.-H.; Kim, D.-K.; Park, J.-C.; Choi, S.-N.; Kim, Y.-J. *Inorg. Chem.* **1997**, *36*, 189.

(138) Persson, I.; Persson, P.; Sandstrom, M.; Ullstrom, A. S. *J. Chem. Soc. Dalton Trans.* **2002**, 1256.

(139) Ottaviani, M. F.; Valluzzi, R.; Balogh, L. *Macromolecules* **2002**, *35*, 5105.

(140) *Handbook of Chemistry and Physics*; 77th ed.; Lide, D. R., Ed.; CRC Press: Boca Raton, FL, 1997.

(141) Bromley, S. T.; Sankar, G.; Catlow, C. R. A.; Maschmeyer, T.; Johnson, B. F. G.; Thomas, J. M. *Chem. Phys. Lett.* **2001**, *340*, 524.

(142) Carrado, K. A.; Wasserman, S. R. *J. Am. Chem. Soc.* **1993**, *115*, 3394.

(143) Cox, C.; Wack, H.; Lectka, T. *Angew. Chem. Int. Ed.* **1999**, *38*, 798.

(144) Naylor, A. M.; Goddard, W. A., III; Kiefer, G. E.; Tomalia, D. A. *J. Am. Chem. Soc.* **1989**, *111*, 2339.

(145) Tarazona-Vasquez, F.; Balbuena, P. *J. Phys. Chem. B* **2005**, *109*, 12480.

(146) Scott, R. W. J.; Datye, A. K.; Crooks, R. M. *J. Am. Chem. Soc.* **2003**, *125*, 3708.

(147) Xie, H.; Gu, Y. L.; Ploehn, H. J. *Nanotechnology* **2005**, *16*, S492.

(148) Yang, L.; Luo, Y.; Jia, X.; Ji, Y.; You, L.; Zhou, Q. *J. Phys. Chem. B* **2004**, *2004*, 1176.

(149) Chung, Y.-M.; Rhee, H.-K. *Catal. Lett.* **2003**, *85*, 159.

(150) Lang, H.; May, R. A.; Iversen, B. L.; Chandler, B. D. *J. Am. Chem. Soc.* **2003**, *125*, 14832.

(151) Grantham, L. F.; Elleman, T. S.; Martin, D. S. J. *J. Am. Chem. Soc.* **1955**, *77*, 2965.

(152) Wu, L.; Schwederski, B. E.; Margerum, D. W. *Inorg. Chem.* **1990**, *29*, 3578.

(153) Blades, A. T.; Jayaweera, P.; Ikonomou, H. G.; Kebarle, P. *Int. J. Mass. Spectrom. and Ion Proc.* **1990**, *102*, 251.

(154) Raber, J.; Zhu, C.; Eriksson, L. A. *J. Phys. Chem. B* **2005**, *109*, 11006.

(155) Ohba, S.; Sato, S.; Saito, Y.; Ohshima, K.; Harada, J. *Acta Cryst.* **1983**, *B39*, 49.

(156) Ayala, R.; Sánchez Marcos, E.; Díaz-Moreno, S.; Solé., V. A.; Muñoz-Paez, A. *J. Phys. Chem. B* **2001**, *105*, 7588.

(157) Elding, L. I. *Acta Chem. Scand.* **1970**, *24*, 1527.

(158) Hush, N. S.; Schamberger, J.; Backsay, G. B. *Coord. Chem. Rev.* **2005**, *249*, 299.

(159) Bitetti-Putzer, R.; Dinner, A. R.; Yang, W.; Karplus, M. *J. Chem. Phys.* **2006**, *124*, 174901.

(160) Carloni, P.; Rothlisberger, U.; Parrinello, M. *Acc. Chem. Res.* **2002**, *35*, 455.

(161) Simonson, T.; Archontis, G.; Karplus, M. *Acc. Chem. Res.* **2002**, *35*, 430.

(162) Bartels, C.; Schaefer, M.; Karplus, M. *J. Chem. Phys.* **1999**, *111*, 8048.

(163) VandeVondele, J.; Rothlisberger, U. *J. Chem. Phys.* **2000**, *113*, 4863.

(164) Niu, Y.; Crooks, R. M. *C. R. Chimie* **2003**, *6*, 1049.

(165) Xu, Y.; Zhao, D. *Ind. Eng. Chem. Res.* **2006**, *45*, 7380.

(166) Ohtaki, H.; Radnai, T. *Chem. Rev.* **1993**, *93*, 1157.

(167) Harding, M. M. *Acta Cryst.* **2002**, *D58*, 872.

(168) Kaminskaia, N. V.; Kostic, N. M. *Inorg. Chem.* **2001**, *40*, 2368.

(169) Steinborn, D.; Junicke, H.; Bruhn, C. *Angew. Chem. Int. Ed. Engl.* **1997**, *36*, 2686.

(170) Deeth, R. J.; Elding, L. I. *Inorg. Chem.* **1996**, *35*, 5019.

(171) Scherer, G.; Kramer, M. L.; Schutkowski, M.; Reimer, U.; Fischer, G. *J. Am. Chem. Soc.* **1998**, *120*, 5568.

(172) Kazerouni, M. R.; Hedberg, L.; Hedberg, K. *J. Am. Chem. Soc.* **1994**, *116*, 5279.

(173) Bancroft, D. P.; Lepre, C. A.; Lippard, S. J. *J. Am. Chem. Soc.* **1990**, *112*, 6860.

(174) Liu, F.; Chen, W. *Eur. J. Inorg. Chem.* **2006**, *2006*, 1168.

APPENDIX A

Equilibrium Distribution of Tetrachloroplatinate (II) anion and its mono- and di-aquated species

By assuming a complete dissociation of the tetrachloroplatinate salt in the anion and cation and enough time for equilibrium concentrations to be reached, three distinct scenarios that depend on the concentration of the salt dissolved could be observed:

1) A barely hydrated tetrachloroplatinate (II) anion at high salt concentration
2) A trichloroaquopalatinate (II) anion at medium concentrations
3) A dichlorodiaquoplatinate (II) anion at low concentrations as the dominant specie

Two equations describe the hydrolysis of tetrachloroplatinate, reactions in equilibrium with constants given by Cotton and Wilkinson.[1]

First hydrolysis of tetrachloroplatinate anion

$PtCl_4^{2-} + H_2O \leftrightarrows [PtCl_3(H_2O)]^- + Cl^-$ K_1

Second hydrolysis

$[PtCl_3(H_2O)]^- + H_2O \leftrightarrows [PtCl_2(H_2O)_2] + Cl^-$ K_2

which for our purposes will be abbreviated as

$A^{2-} \rightarrow A^- + Cl^-$

$A^- \rightarrow A + Cl^-$

The following variables are used in the mathematical solution of the equilibrium.

A_0: initial salt concentration

$pK_1 = -\log(K_1)$

$pK_2 = -\log(K_2)$

$pA_0 = -\log(A_0)$

$pCl = -\log(Cl)$

Equilibrium considerations

$$\frac{A^{-} * Cl^{-}}{A^{2-}} = 10^{-pK_1} \qquad \text{…(A-1)}$$

$$\frac{A * Cl^{-}}{A^{-}} = 10^{-pK_2} \qquad \text{…(A-2)}$$

From A-1 & A-2 we can express A as a function of A^{2-}:

$$\frac{A * (Cl^{-})^2}{A^{2-}} = 10^{-(pK_1 + pK_2)} \qquad \text{...(A-3)}$$

Platinum balance

$$A_0^{\,2-} = A^{2-} + A^{-} + A \qquad \text{…(A-4)}$$

Chloride balance

$$4A_0^{\,2-} = 4A^{2-} + 3A^{-} + 2A + Cl^{-} \qquad \text{…(A-5)}$$

Subtracting A-4 from A-5

$$3A_0^{\,2-} = 3A^{2-} + 2A^{-} + A + Cl^{-} \qquad \text{…(A-6)}$$

Dividing by A^{2-} and multiplying by $(Cl^{-})^2$

$$3\frac{A_0^{\,2-} * (Cl^{-})^2}{A^{2-}} = 3(Cl^{-})^2 + 2\frac{A^{-} * (Cl^{-})^2}{A^{2-}} + \frac{A * (Cl^{-})^2}{A^{2-}} + \frac{Cl^{-} * (Cl^{-})^2}{A^{2-}} \text{ 、} \qquad \text{…(A-7)}$$

A-1, A-2 and A-3 in A-7

$$3\frac{A_0^{\,2-} * (Cl^{-})^2}{A^{2-}} = 3(Cl^{-})^2 + 2 * 10^{-pK_1} * Cl^{-} + 10^{-(pK_1 + pK_2)} + \frac{(Cl^{-})^3}{A^{2-}} \qquad \text{…(A-8)}$$

Rearranging the expression as a function of A^{2-}

$$A^{2-} = \frac{(3A_0^{\,2-} - Cl^-) * (Cl^-)^2}{3(Cl^-)^2 + 2 * 10^{-pK_1} * Cl^- + 10^{-(pK_1 + pK_2)}} \quad \text{...(A-9)}$$

A-1 in A-9

$$A^- = \frac{(3A_0^{\,2-} - Cl^-) * (Cl^-) * 10^{-pK_1}}{3(Cl^-)^2 + 2 * 10^{-pK_1} * Cl^- + 10^{-(pK_1 + pK_2)}} \quad \text{…(A-10)}$$

A-3 in A-9

$$A = \frac{(3A_0^{\,2-} - Cl^-) * 10^{-(pK_1 + pK_2)}}{3(Cl^-)^2 + 2 * 10^{-pK_1} * Cl^- + 10^{-(pK_1 + pK_2)}} \quad \text{...(A-11)}$$

Multiplying A-4 by four and then subtracting A-5 from the result

$$Cl^- = A^- + 2A \quad \text{...(A-12)}$$

A-10 & A-11 in A-12 and rearranging the polynomial equation

$$3(Cl^-)^3 + 3 * 10^{-pK_1} * (Cl^-)^2 + (3 * 10^{-(pK_1 + pK_2)} - 3A_0^{\,2-} * 10^{-pK_1}) * Cl^- - 6A_0^{\,2-} * 10^{-(pK_1 + pK_2)} = 0 \quad \text{...(A-13)}$$

The initial concentration of precursor salt (K_2PtCl_4) that is symbolized with ‘pA0’ in Figure 5.1 is symbolized with A_0^{2-}

APPENDIX B

Table B-1: Electronic energies with ZPE correction (E_0), enthalpies and free energies of reaction (kcal/mol) for the formation of $(PtCl_4^{2-})(H_2O)_{n+1}$ according to the reaction $(PtCl_4^{2-})(H_2O)_n + (H_2O)_2 \rightarrow (PtCl_4^{2-})(H_2O)_{n+1} + H_2O$. Note: n=0-3

n	Configuration	ΔE0	ΔH	ΔG	
0	1A	-12.2	-12.0	-10.0	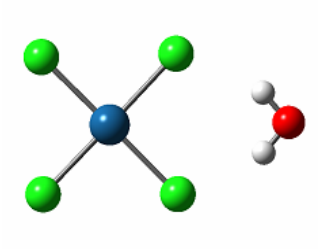
1	2A	-11.1	-10.9	-8.8	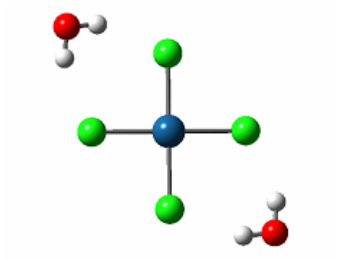
1	2B	-8.4	-8.4	-6.0	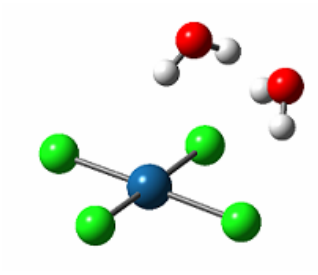
2	3A	-9.7	-9.8	-6.4	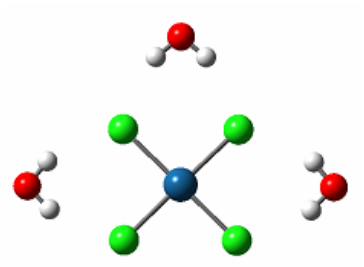
2	3B	-6.2	-6.9	-2.1	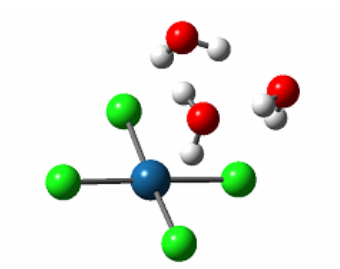

Table B-1. Continued

n	Configuration	ΔE0	ΔH	ΔG	
3	4A	-8.6	-7.6	-9.0	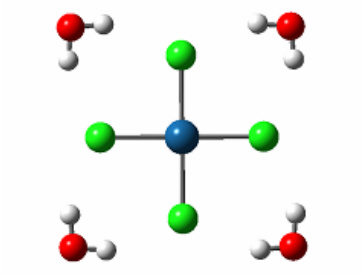
3	4B	-7.5	-7.3	-6.8	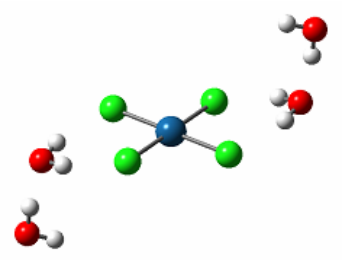
3	4D	-8.0	-8.3	-4.3	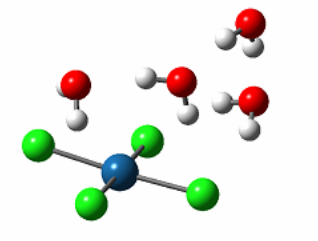
3	4F	-5.2	-5.4	-2.0	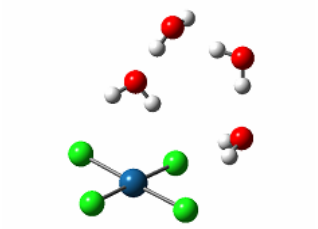
3	4I	-10.4	-11.6	-4.7	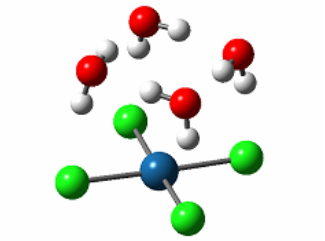

Table B-2: Electronic energies with ZPE correction (E_0), enthalpies and free energies of reaction (kcal/mol) for the formation of $(PtCl_3(H_2O)^-)(H_2O)_{n+1}$ according to the reaction $(PtCl_3(H_2O)^-)(H_2O)_n + (H_2O)_2$ ➔ $(PtCl_3(H_2O)^-)(H_2O)_{n+1} + H_2O$. Note: n=0-3

n	Configuration	ΔE0	ΔH	ΔG	
0	1A	-5.1	-4.7	-3.3	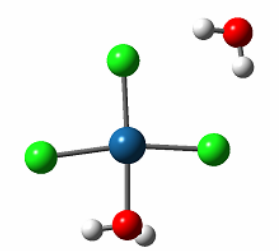
0	1B	-7.9	-8.3	-4.2	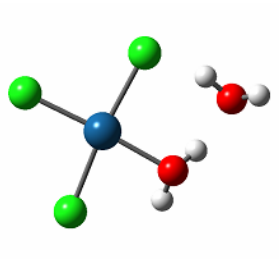
1	2A	-4.0	-3.5	-2.7	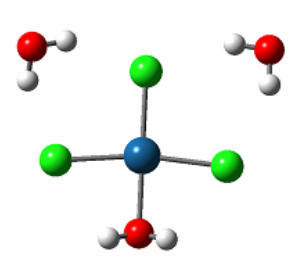
1	2B	-5.7	-5.8	-2.9	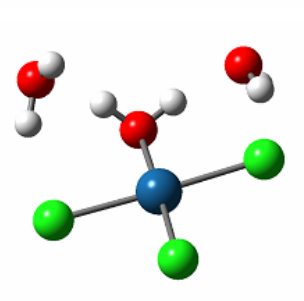
1	2C	-8.0	-8.1	-4.9	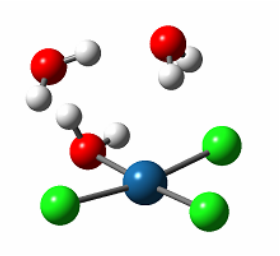

Table B-2. Continued

n	Configuration	ΔE0	ΔH	ΔG	
2	3A	-7.8	-8.1	-4.4	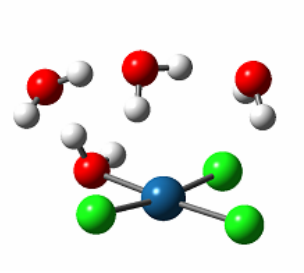
3	4A	2.1	3.4	1.3	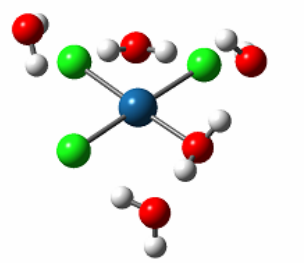
3	4B	1.0	1.0	3.8	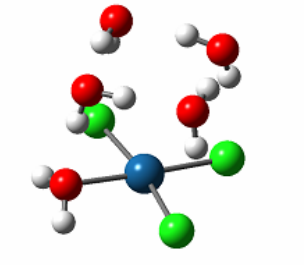
3	4C	-0.6	0.2	0.2	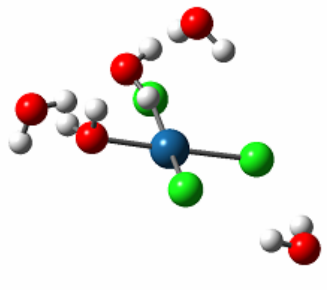

Table B-3: Electronic energies with ZPE correction (E_0), enthalpies and free energies of reaction (kcal/mol) for the formation of (*cis*-$PtCl_2(H_2O)_2)(H_2O)_{n+1}$ according to the reaction (*cis*-$PtCl_2(H_2O)_2)(H_2O)_n$ + $(H_2O)_2$ ➔ (*cis*-$PtCl_2(H_2O)_2)(H_2O)_{n+1}$ + H_2O. Note: n=0-3

n	Configuration	ΔE0	ΔH	ΔG	
0	1A	1.5	2.3	2.0	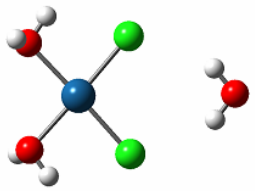
0	1B	-6.8	-7.1	-4.3	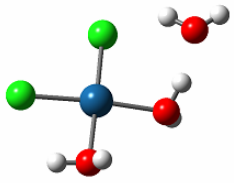
0	1C	-4.0	-3.9	-1.9	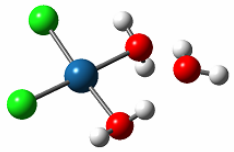
1	2A	0.9	1.9	2.0	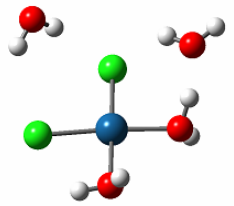
1	2B	-7.3	-7.3	-4.9	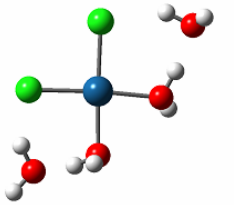
1	2C	-5.4	-5.6	-2.4	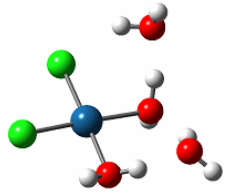

Table B-3. Continued

n	Configuration	ΔE0	ΔH	ΔG	
2	3A	-4.4	-4.6	-0.9	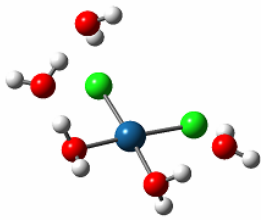
2	3C	-3.8	-4.0	-0.2	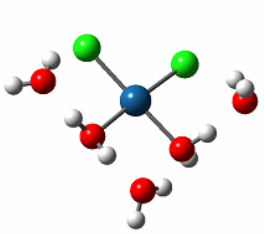
3	4A	-7.6	-8.0	-3.2	
3	4C	1.5	2.2	1.7	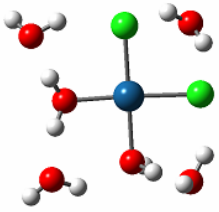
3	4E	-6.9	-6.9	-4.3	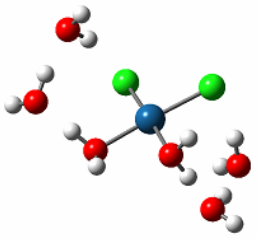

Table B-4: Electronic energies with ZPE correction (E_0), enthalpies and free energies of reaction (kcal/mol) for the formation of (trans-$PtCl_2(H_2O)_2)(H_2O)_{n+1}$ according to the reaction (*trans*-$PtCl_2(H_2O)_2)(H_2O)_n$ + $(H_2O)_2$ ➔ (trans-$PtCl_2(H_2O)_2)(H_2O)_{n+1}$ + H_2O. Note: n=0-3

n	Configuration	ΔE0	ΔH	ΔG	
0	1A	-9.7	-9.9	-6.6	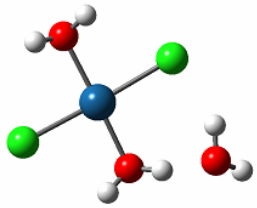
1	2A	-6.3	-6.2	-3.7	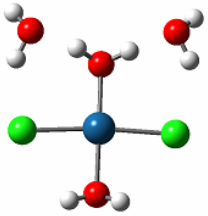
1	2B	-8.9	-9.1	-5.6	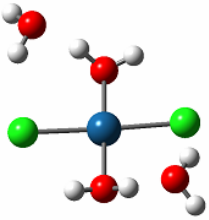
2	3Z	-4.7	-4.5	-2.8	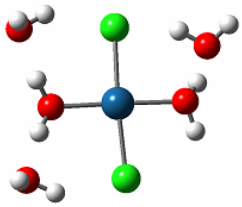
2	3A	1.6	1.7	3.8	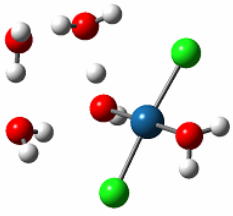

Table B-4. Continued

n	Configuration	ΔE0	ΔH	ΔG	
2	3B	-0.2	0.3	0.8	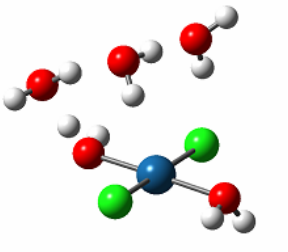
2	3C	-3.3	-3.7	0.5	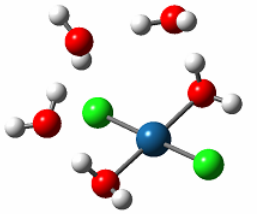
2	3D	3.1	3.8	4.4	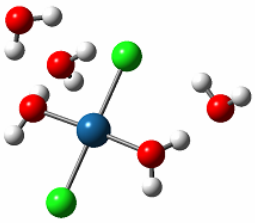
3	4A	-4.3	-4.9	0.2	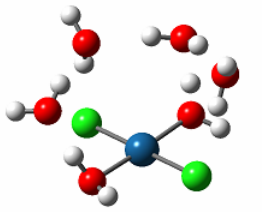
3	4Z	-6.3	-5.5	-5.7	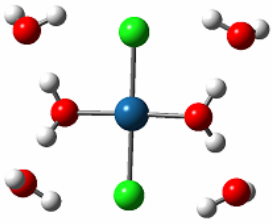

APPENDIX C

Table C-1: Electronic energies with ZPE correction (E_0), enthalpies and free energies of reaction (kcal/mol) for hydration of species B (according to this equation: $B(H_2O)_n + (H_2O)_2 \Longrightarrow B(H_2O)_{n+1} + H_2O$) as a function of n (number of water molecules in the reactant)

Species B	n	ΔE_0	ΔH	ΔG
K^+	0	-14.4	-13.6	-14.4
	1	-11.4	-10.7	-11.4
	2	-9.5	-8.8	-9.7
	3	-7.4	-6.6	-6.8
Cl^-	0	-9.7	-9.9	-10.8
	1	-8.4	-8.6	-6.4
	2	-6.6	-5.9	-7.1
	3	-6.2	-6.2	-4.2
OH^-	0	-24.6	-25.1	-24.3
	1	-17.0	-16.9	-16.0
	2	-14.1	-14.2	-12.4
	3	-9.1	-9.6	-5.6
$PtCl_4^{2-}$	0	-12.2	-12.0	-10.0
	1	-11.1	-10.9	-8.8
	2	-9.7	-9.8	-6.4
	3	-8.6	-7.6	-9.0
$PtCl_3(H_2O)^-$	0	-7.9	-8.3	-4.2
	1	-8.0	-8.1	-4.9
	2	-7.8	-8.1	-4.4
	3	-0.6	0.2	0.2
cis-$PtCl_2(H_2O)_2$	0	-6.8	-7.1	-4.3
	1	-7.3	-7.3	-4.9
	2	-4.4	-4.6	-0.9
	3	-7.6	-8.0	-3.2
trans- $PtCl_2(H_2O)_2$	0	-9.7	-9.9	-6.6
	1	-8.9	-9.1	-5.6
	2	-4.7	-4.5	-2.8
	3	-4.9	-4.7	-2.5

APPENDIX D

Table D-1: Selected bond distances (in angstroms) and dihedral angles (in degrees) for Fragment-[$PtCl_3^-$] structures where fragment: single site, single branch or outer pocket. In the third column, Pt-X, indicates Pt-N for sites N3 and N2, and Pt-O for sites O and OH. Pt-A1, Pt-A2 and Pt-A3 are Pt-Cl bond distances. Pt-A3 is the Pt-Cl *trans* to Pt-X. When two dihedral angles are shown they correspond to each branch in the pocket. When only one is shown, they correspond to one branch, except for Pt-N2 where such angle corresponds to the dihedral in N-methyl-acetamide (NMA). N3: tertiary amine N, N2: secondary amide N, O: amide O, OH: terminal group OH, CN2: methylene carbon neighbor to N2

		Bond distance (Å)				Dihedral Angle (degrees)	
Site	Fragment	Pt-X	Pt-A1	Pt-A2	Pt-A3	O=CN2-N2-H	O=CN2-N2-H
N3	$N(CH_3)_3$	2.20	2.40	2.42	2.36		
N2	NMA[a]	2.18	2.38	2.42	2.34	134.4	
OH	CH_3OH	2.17	2.38	2.42	2.32		
O	NMA[a]	2.14	2.39	2.40	2.33	177.4	
N3	DF27	2.21	2.38	2.42	2.35	178.9	
N2	DF27	2.18	2.37	2.42	2.34	137.5	
OH	DF27	2.19	2.39	2.40	2.32	177.9	
O	DF27	2.13	2.38	2.41	2.33	178.0	
N3	DF41	2.22	2.37	2.42	2.36	177.5	176.2
N2	DF41	2.18	2.36	2.42	2.34	135.1	174.0
OH	DF41	2.17	2.40	2.37	2.32	175.3	176.4
O	DF41	2.14	2.43	2.37	2.33	174.4	176.9

[a]NMA: n-methyl-acetamide

Table D-2: Selected bond distances (in angstroms) and bond angles (in degrees) for I1, TS and I2 configurations arising from the LER between Pt(II) complexes and the tertiary amine site (N3) of $N(CH_3)_3$. Atoms labeled as Y and Z are in the same plane as atom N as represented in Figure D-1*

		Bond distances					Bond angles		
Species	Config	Pt-N	Pt-A1	Pt-A2	Pt-A3	Pt-A4	N-Pt-Y	Y-Pt-Z	Z-Pt-N
$PtCl_4^{2-}$	I1	5.60	2.42	2.42	2.42	2.41			
	TS	2.73	2.41	2.41	3.09	2.39	141.6	144.8	73.6
	I2	2.20	2.40	2.42	>>>	2.36			
$PtCl_3(H_2O)^-$	I1	3.93	2.39	2.41	2.33	2.16			
	TS	2.93	2.37	2.41	2.32	2.59	135.1	154.3	70.2
	I2	2.20	2.40	2.41	2.36	3.51			
cis-$PtCl_2(H_2O)_2$	I1	3.80	2.31	2.33	2.12	2.17			
	TS	2.77	2.31	2.33	2.47	2.18	131.1	157.1	71.8
	I2	2.15	2.33	2.37	3.58	2.18			
trans-$PtCl_2(H_2O)_2$	I1	3.87	2.38	2.37	2.10	2.04			
	TS	2.72	2.38	2.37	2.34	2.14	132.4	154.8	72.8
	I2	2.09	2.38	2.39	3.80	2.13			

* Note: For $PtCl_4^{2-}$, A1-A4 are Cl^-; For $PtCl_3(H_2O)^-$, A1-A3 are Cl^- and A4 is H_2O. For *cis* and *trans*-$PtCl_2(H_2O)_2$, A1 and A2 are Cl^- and A3 and A4 are H_2O. The transition state structure is a five-member distorted tbp-like structure (See Figure D-1): Y and Z are atoms located in the trigonal plane as well as N (tertiary amine) is. Pt is found at the center of the transition state complex. N is the entering ligand and Z the leaving ligand

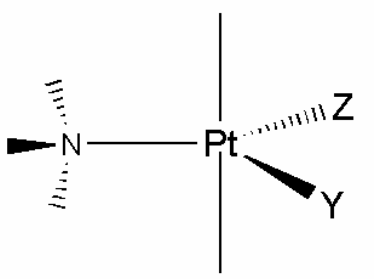

Figure D-1: Trigonal-bipyramidal-like transition state (TS) structure. Note: Atoms Z and Y correspond to Tables D-2 and D-8

Table D-3: Electronic energies with ZPE correction (E_0), enthalpies and free energies of reaction (kcal/mol) for the formation of DF41-X (X = $PtCl_4^{2-}$) according to the NCB reaction DF41-H_2O + X ➔ DF41-X + H_2O

Configuration	ΔE_0	ΔH	ΔG	
1A	-33.2	-31.7	-32.6	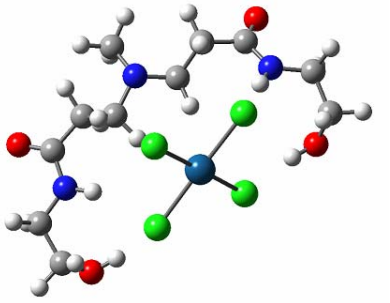
1B	-36.1	-34.9	-33.2	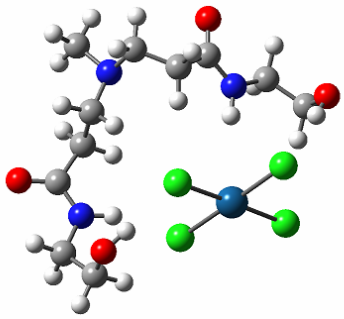
1D	-26.1	-25.0	-22.7	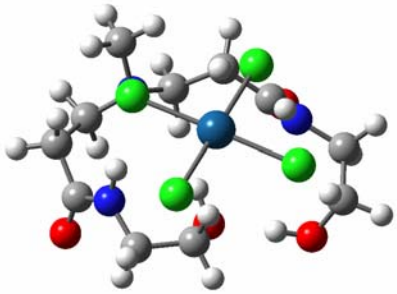
1F	-33.6	-32.4	-31.4	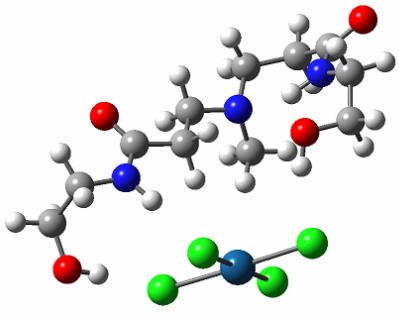

Table D-4: Electronic energies with ZPE correction (E_0), enthalpies and free energies of reaction (kcal/mol) for the formation of DF41-X (X= $PtCl_3(H_2O)^-$) according to the NCB reaction DF41-H_2O + X ➔ DF41-X + H_2O

Configuration	ΔE_0	ΔH	ΔG	
C1	-4.3	-3.3	-1.7	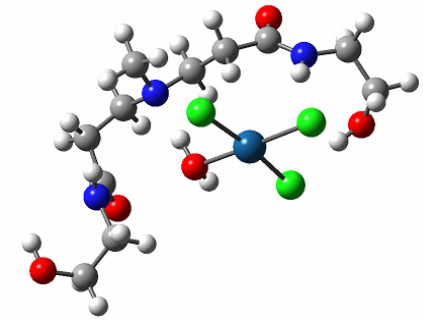
Z1	-5.6	-3.8	-4.5	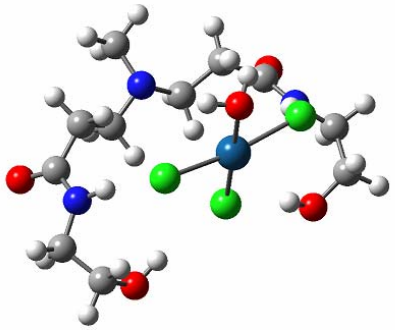
CF2B	-6.9	-5.9	-3.8	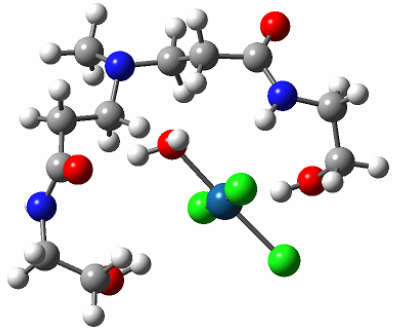
J	-4.4	-3.1	-2.5	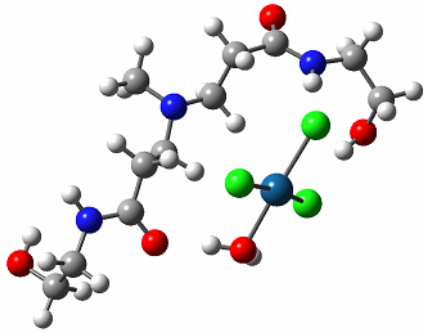

Table D-4. Continued

Configuration	ΔE_0	ΔH	ΔG	
E	-8.5	-7.6	-5.1	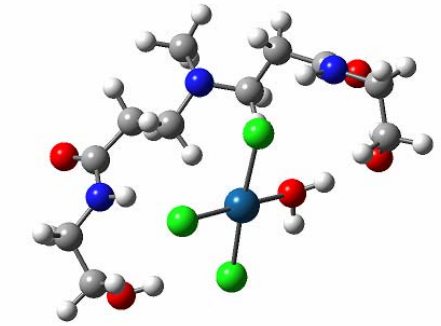
B5AC	-9.3	-8.0	-8.2	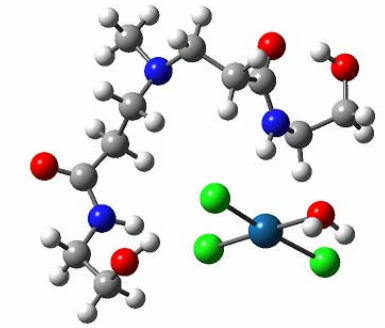
AAB	-11.3	-10.5	-7.7	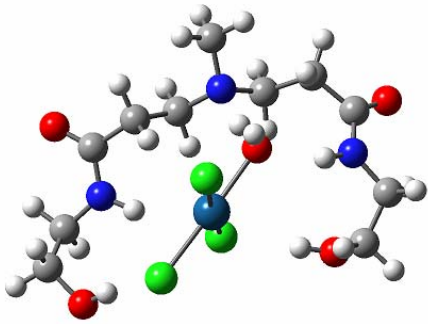
BC	-11.6	-10.8	-7.7	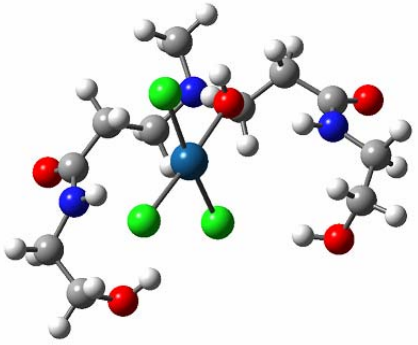

Table D-5: Electronic energies with ZPE correction (E_0), enthalpies and free energies of reaction (kcal/mol) for the formation of DF41-X (X= *cis*-$PtCl_2(H_2O)_2$) according to the NCB reaction DF41-H_2O + X ➔ DF41-X + H_2O

Configuration	ΔE_0	ΔH	ΔG	
1A	-8.9	-8.6	-5.6	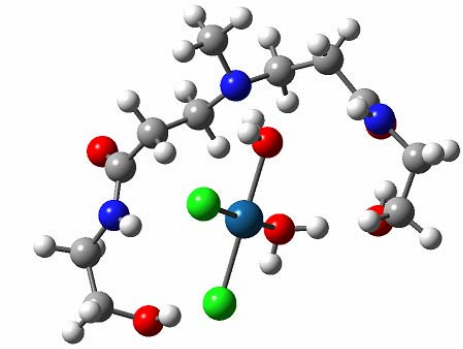
Y6	-9.2	-9.2	-4.1	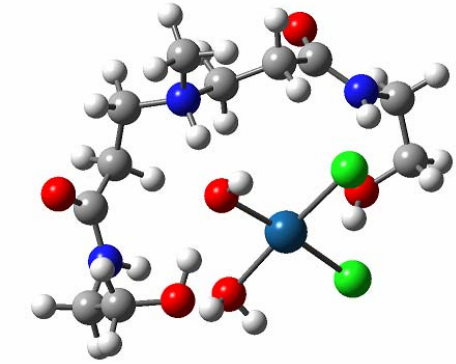
CF	-5.4	-4.9	-2.3	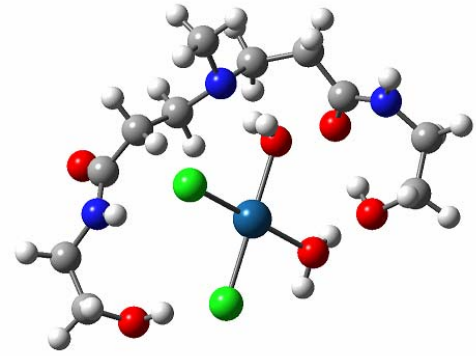

Table D-5. Continued

Configuration	ΔE_0	ΔH	ΔG	
B1D	-5.2	-4.5	-1.8	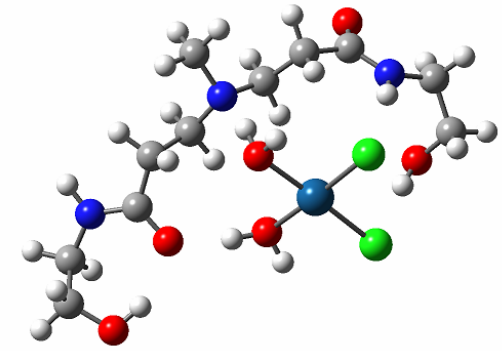
BE	-5.1	-4.5	-1.0	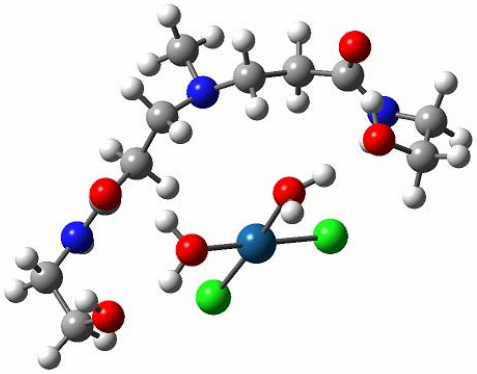
X1C	-10.1	-10.1	-5.2	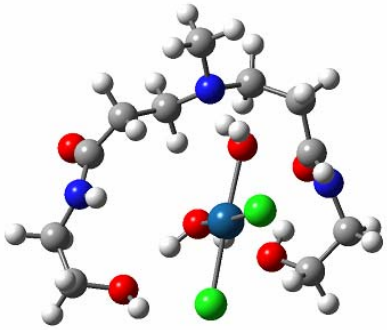

Table D-6: Electronic energies with ZPE correction (E_0), enthalpies and free energies of reaction (kcal/mol) for the formation of DF41-X (X= *trans* -$PtCl_2(H_2O)_2$) according to the NCB reaction DF41-H_2O + X ➔ DF41-X + H_2O

Configuration	ΔE_0	ΔH	ΔG	
BB	-11.8	-11.1	-7.7	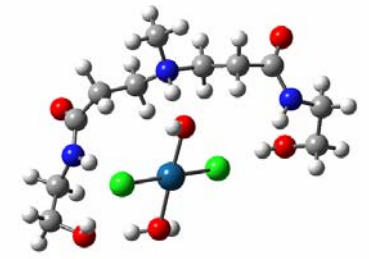
CB	-10.1	-9.4	-6.1	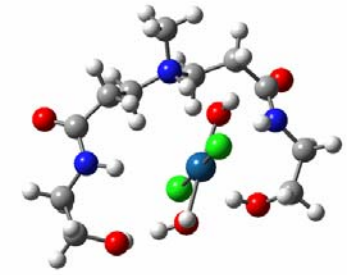
Y7	-8.8	-8.1	-4.5	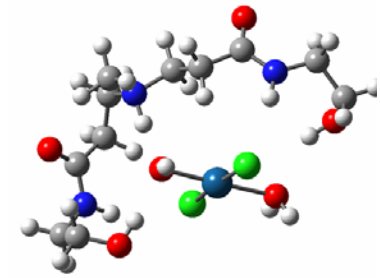
Z2E1	1.0	2.1	3.6	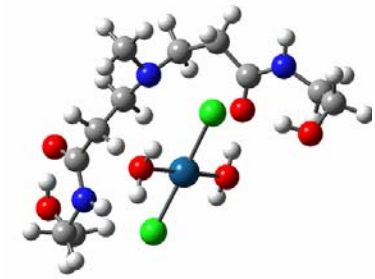
CoY	-11.5	-10.7	-8.2	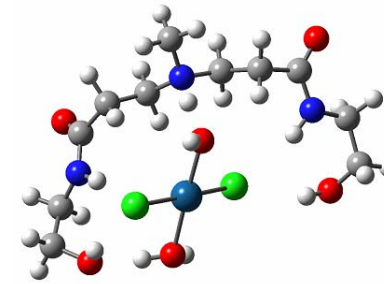

Table D-7: Selected bond distances (in angstroms) for DF41-X structures (where X = $PtC'_xD'_x$) of tables D-4 to D-7. Note: For $PtCl_4^{2-}$, A1-A4 are Cl^-; For $PtCl_3(H_2O)^-$, A1-A3 are Cl^- and A4 is H_2O. For *cis* and *trans*-$PtCl_2(H_2O)_2$, A1 and A2 are Cl^- and A3 and A4 are H_2O

Species	Conf.	Pt-N	Pt-A1	Pt-A2	Pt-A3	Pt-A4
$PtCl_4^{2-}$	1A	4.63	2.39	2.41	2.41	2.39
$PtCl_4^{2-}$	1B	5.72	2.42	2.39	2.40	2.40
$PtCl_4^{2-}$	1D	5.17	2.39	2.40	2.42	2.43
$PtCl_4^{2-}$	1F	5.07	2.41	2.41	2.39	2.41
$PtCl_3(H2O)^-$	C1	4.04	2.40	2.38	2.33	2.14
$PtCl_3(H2O)^-$	Z1	4.86	2.38	2.39	2.33	2.16
$PtCl_3(H2O)^-$	CF2B	5.70	2.40	2.37	2.32	2.16
$PtCl_3(H2O)^-$	J	4.41	2.41	2.37	2.34	2.15
$PtCl_3(H2O)^-$	E	4.71	2.39	2.39	2.33	2.15
$PtCl_3(H2O)^-$	B5AC	5.76	2.38	2.38	2.32	2.16
$PtCl_3(H2O)^-$	AAB	4.06	2.39	2.38	2.33	2.16
$PtCl_3(H2O)^-$	BC	4.00	2.38	2.40	2.33	2.15
cis-$PtCl_2(H_2O)_2$	1A	3.98	2.33	2.33	2.13	2.13
cis-$PtCl_2(H_2O)_2$	Y6	4.01	2.33	2.36	2.15	2.09
cis-$PtCl_2(H_2O)_2$	CF	4.18	2.33	2.33	2.15	2.12
cis-$PtCl_2(H_2O)_2$	B1D	3.84	2.33	2.33	2.13	2.13
cis-$PtCl_2(H_2O)_2$	BE	4.44	2.33	2.33	2.13	2.14
cis-$PtCl_2(H_2O)_2$	X1C	4.25	2.33	2.34	2.13	2.12
trans-$PtCl_2(H_2O)_2$	BB	3.83	2.38	2.39	2.13	2.01
trans-$PtCl_2(H_2O)_2$	CB	4.05	2.35	2.41	2.11	2.02
trans-$PtCl_2(H_2O)_2$	Y7	3.99	2.38	2.38	2.14	2.01
trans-$PtCl_2(H_2O)_2$	Z2E1	4.19	2.38	2.37	2.09	2.05
trans-$PtCl_2(H_2O)_2$	CoY	3.87	2.38	2.39	2.13	2.01

Table D-8: Selected bond distances (in angstroms) and bond angles (in degrees) for I1, TS and I2 configurations arising from the LER between Pt(II) complexes and the tertiary amine site (N3) of DF41. Atoms labeled as Y and Z are in the same plane as atom N as represented in Figure D-1*

Species	Config	Bond distances					Bond angles		
		Pt-N	Pt-A1	Pt-A2	Pt-A3	Pt-A4	N-Pt-Y	Y-Pt-Z	Z-Pt-N
$PtCl_4^{2-}$	I1	5.72	2.42	2.39	2.40	2.40			
	TS	2.85	2.41	2.38	2.40	3.06	137.1	127.5	95.5
	I2	2.21	2.42	2.39	2.38	7.03			
$PtCl_3(H_2O)^-$	I1	5.70	2.37	2.40	2.32	2.16			
	TS	2.82	2.37	2.41	2.34	2.63	141.6	145.3	72.6
	I2	2.20	2.37	2.43	2.36	4.58			
cis-$PtCl_2(H_2O)_2$	I1	4.25	2.33	2.34	2.12	2.13			
	TS	3.70	2.32	2.30	2.09	3.56	162.4	124.2	53.1
	I2	2.18	2.35	2.38	2.13	3.89			
trans-$PtCl_2(H_2O)_2$	I1	4.32	2.39	2.37	2.05	2.09			
	TS	2.64	2.41	2.36	2.13	2.49	129.3	149.8	80.9
	I2	2.11	2.42	2.38	2.12	3.87			

* Note: For $PtCl_4^{2-}$, A1-A4 are Cl^-; For $PtCl_3(H_2O)^-$, A1-A3 are Cl^- and A4 is H_2O. For *cis* and *trans*-$PtCl_2(H_2O)_2$, A1 and A2 are Cl^- and A3 and A4 are H_2O. The transition state structure is a five-member distorted tbp-like structure (See Figure D-1): Y and Z are atoms located in the trigonal plane as well as N (tertiary amine) is. Pt is found at the center of the transition state complex. N is the entering ligand and Z the leaving ligand

Table D-9: Electronic energies with ZPE correction (E_0), enthalpies and free energies of reaction (kcal/mol) for the formation of DF41-B according to the NCB reaction DF41-H_2O + B ➔ DF41-B + H_2O

Species B	ΔE_0	ΔH	ΔG
K^+	-36.1	-34.1	-40.5
$K\text{-}(H_2O)^+$	-39.9	-39.4	-37.4
$K\text{-}(H_2O)_2^+$	-34.6	-34.4	-31.0
Cl^-	-31.6	-30.6	-36.2
OH^-	-62.8	-63.2	-62.3
$PtCl_4^{2-}$	-36.1	-34.9	-33.2
$PtCl_3(H_2O)^-$	-11.6	-10.8	-7.7
cis-$PtCl_2(H_2O)_2$	-10.1	-10.1	-5.2
trans-$PtCl_2(H_2O)_2$	-11.8	-11.1	-7.7

VITA

Francisco Tarazona Vasquez received his Bachelor of Science degree in chemical engineering with honors from the Universidad Nacional de Ingeniería, Lima, Perú in 2002. He entered the graduate program in chemical engineering at the University of South Carolina in August 2002 where he joined Dr. Balbuena's research group. Since then, he has worked in the area of computational chemistry. He received his PhD in chemical engineering at Texas A&M University in December 2007.

Mr. Tarazona Vasquez may be reached at 3122 TAMU, Artie McFerrin Department of Chemical Engineering, College Station, TX 77843. His email address is francisco.tarazona@chemail.tamu.edu